ELECTROCHEMICAL IMPEDANCE MODELLING OF THE REACTIVITIES OF DENDRIMERIC POLY(PROPYLENE IMINE) DNA NANOBIOSENSORS

Omotayo Ademola Arotiba

A thesis submitted in partial fulfilment of the requirements for the degree of Doctor Philosophiae in the Department of Chemistry, University of the Western Cape.

Supervisors

Professor Emmanuel I. Iwuoha

Professor Priscilla G.L. Baker

November 2008

KEYWORDS

Electrochemical Impedance Modelling of the reactivities of Dendrimeric Poly(propylene imine) DNA Nanobiosensors

Omotayo Ademola Arotiba

keywords

Electrochemical DNA biosensor

Poly(propylene imine)

Dendrimer

Metallodendrimer

Gold nanoparticle

Electrochemical Impedance Spectroscopy

Nickel (II) salicylaldimine metallodendrimer

Glassy Carbon Electrode

Biosensor

Nanobiosensor

ABSTRACT

Electrochemical Impedance Modelling of the reactivities of Dendrimeric Poly(propylene imine) DNA Nanobiosensors

O. A. Arotiba

PhD Thesis, Department of Chemistry, University of the Western Cape November 2008

In this thesis, I present the electrochemical studies of three dendrimeric polypropylene imine (PPI) nanomaterials and their applications as a platform in the development of a novel label free DNA nanobiosensor based on electrochemical impedance spectroscopy. Cyclic voltammetry (CV), differential pulse voltammetry (DPV), square wave voltammetry (SWV) and electrochemical impedance spectroscopy (EIS) techniques were used to study and model the electrochemical reactivities of the nanomaterials on glassy carbon electrode (GCE) as the working electrode. Size and morphological information were obtained from scanning electron microscopy (SEM). The nanomaterials used or prepared were: (i) a novel generation two nickel (II) salicylaldimine metallodendrimer, (ii) Generation four (G4) PPI – gold nanoparticle composite and (iii) G1 to G3 PPI.

GCE was modified with the metallodendrimer by drop coating. Electrochemical interrogations showed that the metallodendrimer was conducting; electroactive in phosphate buffer solution with two reversible redox couples at $E^{0\prime}$ = +200 mV and $E^{0\prime}$ = +434 mV and catalysed $Fe(CN)_6^{3-/4-}$ redox reaction. As a

biosensor platform using amino modified 21 mer DNA probe, EIS profiles showed decrease in charge transfer resistance (R_{ct}) in phosphate buffer saline solution (PBS) and increase in R_{ct} in $Fe(CN)_6^{3-/4-}$ redox probe on hybridisation with target DNA. The biosensor developed on the metallodendrimer platform was sensitive enough to detect as as low as 5 nM target DNA.

A nanocomposite of G4 PPI and gold nanoparticle was co-electrodeposited on GCE using CV from an electrolyte solution containing the G4 PPI and $HAuCl_4$. Field emission SEM results confirmed the co-deposition of PPI (which was linked to the carbon electrode surface by C-N covalent bonds) and AuNP with size ca 60 nm. Voltammetric experiments showed that the platform (GCE/PPI-AuNP) was conducting and exhibited reversible electrochemistry ($E^{0\prime}$ = 235 mV) in pH 7.2 PBS due to the PPI component which showed a reversible electrochemistry when in solution. The redox chemistry of PPI was pH dependent and involves a two electron, one proton process, as interpreted from a 28 mV/pH value obtained from pH studies. The charge transfer resistance (R_{ct}) from the EIS profiles of GCE/PPI-AuNP monitored with $Fe(CN)_6^{3-/4-}$ redox probe, decreased by 81% compared to bare GCE. The conductivity (in PBS) and reduced R_{ct} (in $Fe(CN)_6^{3-/4-}$) values confirmed PPI-AuNP as a suitable electron transfer mediator platform for voltammetric and impedimetric DNA biosensor. The DNA probe was effectively wired onto the GCE/PPI-AuNP via Au-S linkage and electrostatic interactions. The nanobiosensor responses to target DNA which gave a dynamic linear range of 0.01 - 5 nM in PBS and a detection limit of 3.45×10^{-10} M, was based on the changes in R_{ct} values using $Fe(CN)_6^{3-/4-}$ redox probe.

In a similar electrodeposition method, G1 PPI (and also G2 and G3 PPI for comparison) of size ca 50 nm, was prepared. The dendrimer exhibited a reversible one electron electrochemistry ($E^{0\prime}$ = 212 mV) both in solution and when used as platform. The dendrimer immobilised effectively the probe DNA through electrostatic adsorption. The G1 platform nanobiosensor hybridisation response to target DNA Hybridisation based on R_{ct} data (from EIS) gave a detection limit of 6.6 x 10^{-10} M. The biosensor was also able to discriminate non complementary and base mismatch DNA targets.

DECLARATION

I declare that "Electrochemical impedance modelling of the reactivities of dendrimeric poly(propylene imine) DNA nanobiosensors" is my own work, that it has not been submitted before for any degree or assessment in any other university, and that all the sources I have used or quoted have been indicated and acknowledged by means of complete references.

Omotayo Ademola Arotiba November 2008

Signature _____

DEDICATION

I dedicate this thesis to

My wife

Adeola Abisola Arotiba
(Asunke)

&

Daughter

Zion Ewaoluwa Arotiba

ACKNOWLEDGEMENTS

God Almighty - I acknowledge God as the One behind all my successes. I am not an achiever but a receiver. Thank you my Lord Jesus for giving me the strength and wisdom through the Holy Spirit to complete this work.

Family - I thank my wife (Adeola) who stood with me through all the rough times. I love and praise you. My daughter (Zion), thank you for coming to spice up my life. I am also indebted to my parents **Chief Omotayo Arotiba and Mrs Margaret Arotiba** (Olori) for the price they paid to get me to where I am today. Big thanks to my brothers - Tunde, Gbenga and Muyiwa who believed in me. Kudos to my in-laws especially 'Mummy Adeola', Grand Ma, Daddy Adalumo and Uncle Agbo for their support.

Spiritual Family: Rev. Samson Ajetomobi, Pastor Bode Orekoya. The Men of Issachar Vision, Christ Image Assembly and Joy in Belhar fellowship. Segun and Tope Oludipe, Pastor Tim, Pastor Oduwole and wife, Bro. Kenneth Kirabo. Thank you all for your support.

Supervisors: - I am grateful to my supervisors Professor Emmanuel Iwuoha and Prof. Priscilla Baker for their academic guidance and kindness.

SensorLab: Colleagues - Evelyn, Sarah, Joseph, Nikkie, Jasmina, Fanelwa, Combs, Abdo, Zello, Takalani, Shanniel, Peter. Postdocs: Anna, Amir and Tesfaye. Seniors: Dr. Nazeem, Dr. Mangaka.

Organometallic research group - Professor Mapolie and Rehana Malgas-Enus (PhD colleague) who are the brains behind the nickel metallodendrimer synthesis, thanks for giving me your product to work with.

Chemistry Department Staff - Especially Prof. Farouk Ameer, the Chairperson.

Friends – Dr. Niyi Isafiade, Segun Akinyemi and Dr. Richard Akinyeye – for giving me the lead to getting this PhD admission. Dr. Tobi (of Zululand), Dr. Gabila, Betrand, Babajide, Omotola. Belhar neighbours: Carol, Vincent, Amy, Dylan, Jennie, Lorna.

National Research Foundation of South Africa (NRF) - for funding my PhD programme.

LIST OF PUBLICATIONS

1. **Arotiba, O.A.;** Ignaszak, A.; Malgas, R.; Al-Ahmed, A.; Baker, P.G.L.; Mapolie, S.F.; Iwuoha, E.I. An electrochemical DNA biosensor developed on novel multinuclear nickel(II) salicylaldimine metallodendrimer platform. *Electrochimica Acta* **2007,** *53*, 1689-1696.
2. **Arotiba, O.A**; Owino, J.H.O.; Songa, E.A.; Hendricks, N.; Waryo, T.T.; Jahed, N.; Baker, P.G.L.; Iwuoha, E.A. An Electrochemical DNA Biosensor Developed on a Nanocomposite Platform of Gold and Poly(propyleneimine) Dendrimer. *Sensors* **2008,** *8*, 6791-6809.
3. **Arotiba O.A**.; Owino, J.H.O.; Baker, P.G.L.; Iwuoha, E.I. Electrochemical impedimetry of electrodeposited poly(propylene imine) dendrimer monolayer. *Physical Chemistry Chemical Physics* In Press
4. **Arotiba O.A**.; Songa E.A. Owino, J.H.O.; Waryo, T.T.; Baker, P.G.L.; Iwuoha, E.I. An Electrochemical DNA biosensor developed on a generation one poly(propylene imine) dendrimer nanoplatform. *Analyst* In Press

CONTENTS

LIST OF FIGURES

LIST OF TABLES

LIST OF ABBREVIATIONS

EIS	Electrochemical Impedance Spectroscopy
EDB	Electrochemical DNA Biosensor
PPI	Poly(propylene imine)
AuNP	Gold nanoparticles
G4 PPI-AuNP	Generation 4 poly(propylene imine) –gold nanoparticle
CV	Cyclic voltammetry
DPV	Differential Pulse Voltammetry
SWV	Square Wave Voltammetry
I_{pa}	Peak anodic current
I_{pc}	Peak cathodic current
$E^{0'}$	Formal potential
E_{pa}	Peak anodic potential
E_{pc}	Peak cathodic potential
R_{ct}	Charge transfer resistance
PBS	Phosphate Buffer Saline
ΔE_p	Difference in potential peak potentials
D_e	Diffussion coefficient
GCE	Glassy Carbon Electrode

CHAPTER 1

INTRODUCTION

1.1 Background

Analysis or detection of pathogens, chemical and biological pollutants, disease strain are of utmost importance for prevention, monitoring, therapy and the general well being of our world. There has never been a time to pay attention to the health of the planet than now. Increased scientific and technological activities are taking their negative tolls and these are evident in the increase in environmental pollution, disease vulnerability, new disease strain and a lot more health disorders. The production of chemical and biological warfare has led to increase in terrorism. The world has become a small village with increase in human - human interaction and mobility. For example a disease strain found in a particular country, in no time crosses international and intercontinental borders. Increase and diversity in the trade of food and agricultural produce have made some disorders or germs ubiquitous. The border quarantine systems are becoming inefficient in handling the volumes of samples which leads to a lot of economic losses due to perish. Genetic testing in the clinical, forensics and biomedical field in general is becoming a popular and useful tool in solving problems.

The existing classical methods of analysis are very costly, time consuming, laboratory borne, need a lot of expertise in their operation and sometimes suffer from low detection limit. There is therefore need to quest for cheaper, faster, easier to use, low power consuming, miniaturizable, user friendly,

and on site analytical device as suitable complements or substitute for these classical methods.

Over the years, scientists have come to the realisation that biological systems and biomolecules such as enzymes, antibody and deoxyribonucleic acid (DNA) possess excellent intrinsic ability in their recognition of foreign substances with high reactivity, sensitivity, specificity and selectivity. This unparalleled features provided by nature has become a sort of inspiration to researchers, hence science is now returning to nature and harnessing its power to find solution to our everyday challenges - confirming the saying "if you can't beat them, you join them". This paradigm constitutes the underlying philosophies of the science and technology of biosensors – a multi disciplinary field involving chemistry, biochemistry, biotechnology, bioengineering, material science and nanotechnology.

A biosensor is an analytical devise that incorporates a bioreceptor (such as DNA, enzyme, antibody) onto a transducer surface and in the presence of analyte, produces measurable signals (due to a bio-recognition event) that are proportional to the analyte concentration. Since the pioneering work of Professor Leland C. Clark in 1956 [1], biosensor technology has undergone dramatic improvement and are now envisaged to be a meet to the draw backs of classical analytical techniques or protocols and revolutionise detection science. Among the various analytical techniques used in biosensor technology, electrochemical method stands out because of its relatively low cost and miniaturisability [2].

True to its purpose, electrochemical biosensors (and biosensors in general) have recorded success in the analytical world. The market size for worldwide

biosensors at year-end 2003 was about $7.3 billion, and the projection of growth to about $10.8 billion in 2007 with a growth rate of about 10.4% was feasible [3, 4] indicating the relevance and practicability of this field of research. The revolution that glucose biosensor brought to the monitoring of sugar level in diabetics is worthy on mentioning and to date, the commercial market for glucose monitoring continues to be the major share of about 85% [5]. Biosensors have also been used in the analysis of toxins, pollutants, diseases, genetically modified food, and in many other environmental, foods, biomedical and explosive detection applications [6-9]. Of interest in my thesis are electrochemical DNA biosensors which take advantage of the versatility of DNA chemical and biochemical reactions.

1.2 Problem Statement and Research Motivation

Despite the successes recorded by biosensors, there still remain challenges of finding a suitable immobilisation layer upon which the biomolecule (DNA in this case) will perform its biorecognition event to the optimum. The task of molecular diagnostics, drug screening, monitoring of differential gene expression and forensic analysis which generate a huge amount of genetic information have raised the need for DNA biosensors in order to decentralize DNA testing [10]. In 1999, there were about 200 companies working in the area of biosensor and bioelectronics worldwide [5]. As at 1999, none of those companies was from Africa and to date, there is no thriving biosensor and bioelectronics company in South Africa and Africa at large. Out of the over 200 companies, only some are still in the core business [5]. Most of these 'some' still rely on the old technology

and are still sticking to glucose biosensors. This shows that there is dearth of practicable ideas, discoveries and innovations upon which companies will thrive.

Compared to enzyme biosensors and immunosensors, there is still a scarcity of DNA biosensors available in the market and/or under research and development despite DNA's relative ease of synthesis, high stability and highly specific biological recognition [11]. One of the causes of this draw back is the challenge of finding a suitable immobilisation layer. The quest for suitable immobilisation material, technique and transducing material (electrode) have become the challenge of electrochemists in designing highly sensitive (low detection limit), biocompatible, single-use or multi-use, *in vitro* or *in vivo* biosensors. In electrochemical DNA biosensors (EDB), the immobilisation layer should be biocompatible, effectively adsorb the DNA and sensitive enough to interpret accurately the electronics of the bio-recognition event. Therefore optimum biosensor performance greatly depends on the nature of the immobilisation layer or matrix and chemistry (or technique) of immobilisation [2, 12, 13]. There is need to develop novel platforms using suitable materials for better biosensor performance and that which lends itself to mass production and commercialisation.

In recent times, a new class of materials called dendrimers have emerged. Dendrimers are now being extensively used in clinical or pharmaceutical applications especially in the field of non viral gene delivery and drug research with remarkable results [14-17]. Dendrimers physiochemical properties resemble those of protein and have been shown to be very compatible with DNA [18]. Dendrimer's biocompatibility with DNA and its ability to work even *in vivo*

(which is a more complicated system) by carrying gene or drug to the intended target organ with great prospect, suggests a unique DNA – dendrimer interaction which can also be exploited in electrochemical DNA biosensor. The use of dendrimer in EDB design is just at its infancy. A chart to illustrate this is presented in chapter 2. To the best of my knowledge, the use of dendrimeric poly(propylene imine) nanomaterial in electrochemical DNA biosensor design has not been reported.

1.3 Aim and Objectives

1.3.1 Aim

To electrochemically model the reactivities of dendrimeric nanomaterial composites and apply them as platforms in the development of a novel electrochemical DNA nanobiosensor with good performance for alternative faster, cheaper, more user friendly, miniaturisable gene analysis device.

1.3.2 Objectives

The following are the research objectives outlined:

- Quest for suitable or prospective materials for immobilisation layer.
- Electrochemical characterisation and impedance modelling of the material in solution and as electrode modifier.
- Surface characterisation using scanning electron microscopy.
- Electrochemical characterisation and impedance modelling of the biosensor and its hybridisation response.

1.4 The Thesis Statement

Dendrimeric poly(propylene imine) and its composites should have suitable electrochemical properties that make them applicable as electrochemical DNA biosensor platforms for good sensor performance.

1.5 Rationale behind the choice of biosensor component

The platform materials used in developing the DNA biosensor are DNA, PPI dendrimer, PPI –gold nanoparticle composite, and metallodendrimer

Though poly(propylene imine) PPI (reviewed in chapter 2) is among the most popular types of dendrimer, it is relatively less studied when compared to polyamidoamine (PAMAM). PPI is commercially available and safe to handle. It has found application in gene and drug research [17]. PPI and its metallodendrimer have the following characteristics which are similar to that of DNA:

- Highly branched globular Polymers
- Macromolecule
- Biocompatibility
- Conducting and electroactive
- 3-D structure
- Nano-structured
- Response to pH
- Large number of tunable surface group
- Behaves as micelles

Gold nanoparticle (which is also reviewed in chapter 2) also possesses the following properties which make them DNA friendly:

- Excellent Biocompatibility
- High conductivity
- Bimolecular nanoscopic wires
- Enhances electrode surface area and DNA immobilisation
- Enhances orientation of biomolecules

It is therefore hypothesised that the use of these materials either individually or as a composite will have a synergic effect when combined with DNA for better sensor performance.

1.6 Brief overview of Chapters

This thesis is broken down into seven chapters.

- Chapter one presents a general introduction, motivation, thesis statement and research aim and objectives.
- Chapter two introduces the scope of the literature review and the review in detail.
- Chapter three is on the methods. This chapter features the list of materials used, the research design and methods. A theoretical treatise of the analytical techniques used is also presented. The experimental consists of a general section that explains procedures common to the work in general, and those peculiar to each milestone covered.
- Chapter four to six: This thesis comprises of various milestone of which some have been published. A chapter is allocated to each of the milestone.

Chapter four to six consist of these results with a sub conclusion at the end of each chapter. The distinctive feature in the result chapters is the immobilisation layer material used. Nickel (II) salicylaldimine metallodendrimer, generation four (G4) PPI - gold nanocomposite and generation one (G1) PPI make up chapter four to six respectively.

- Chapter seven is on the general conclusion, recommendation and future work.

CHAPTER 2

LITERATURE REVIEW

2.1 Introduction

This chapter is an elaborated follow up of chapter one. The main focus of this review is on electrochemical DNA biosensors (EDB) developed on nanomaterial platform of dendrimer composites. The trend that led to this recent biosensor approach will be discussed briefly. The scope of this review can be summarised as follows:

- Brief review on Biosensor and market shares
- DNA as an electronic nanomaterial suitable for biosensor design
- Electrochemical DNA Biosensor, its principle and types
- Electrochemical DNA biosensors based on EIS
- Challenges in EDB
- Immobilisation platforms layers and chemistry in EDB
- Nanoparticles and nanocomposite in EDB
- Gold nanoparticle
- Dendrimer, metallodendrimer and its use as EDB platform
- Uses of Electrochemical DNA Biosensor

2.2 Biosensors

2.2.1. Definition and classifications

As defined earlier in the background (section 1.1), a biosensor is an analytical device that incorporates a bioreceptor onto a transducer surface and in

the presence of analyte, produces measurable signals that are proportional to the analyte concentration owing to a biorecognition event that took place. This signal can result from a change in proton concentration, light emission, absorption or reflectance, mass change, electron flow etc. The signal is converted by a transducer into a measurable response such as current, potential, temperature change, mass change, optical and so on [19]. Biosensors exploit the excellent selectivity, specificity and reactivities of immobilised biomaterials with their substrates.

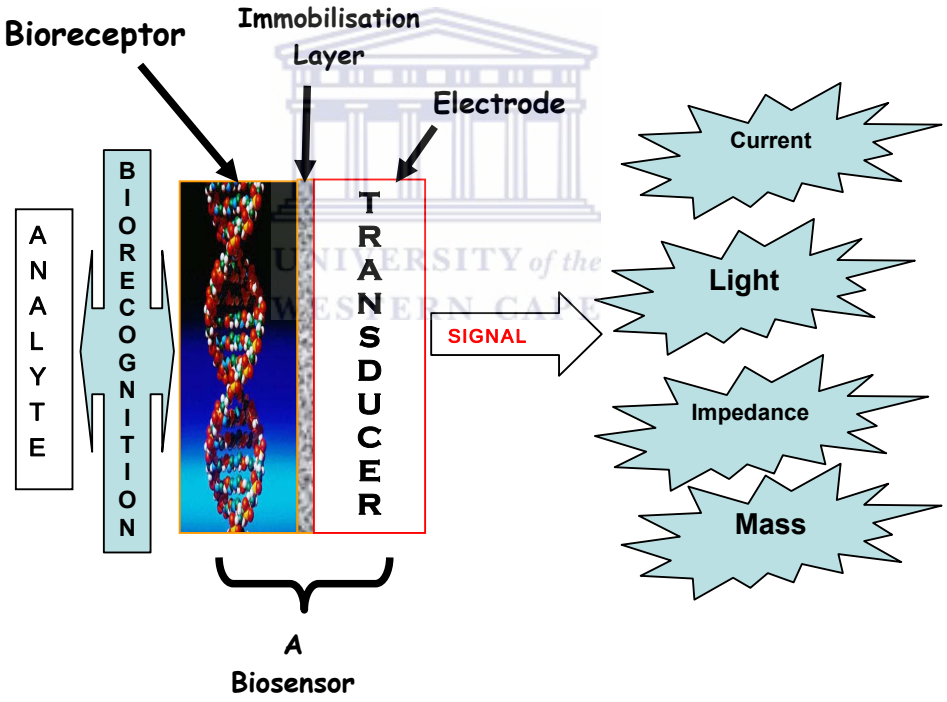

Figure 2.1 A schematic picture of a biosensor

The history of biosensor began with glucose monitoring and can be dated as far as 1956 through the work of Professor Leland C. Clark. He used an enzyme called glucose oxidase in a dialysis membrane over an oxygen probe and this devise was called then an enzyme electrode [1]. The enzyme electrode was used in the determination of glucose. Updike *et al* [20] developed an enzyme using electrochemical procedure to design a model that uses glucose oxidase immobilised on a gel to measure the concentration of glucose in biological solutions and in the tissues *in vitro*. The term biosensor emerged from bio-selective sensor [21].

Biosensors can be classified based on the bioreceptor, transduction methods, and sometimes the biorecognition principle. Bioreceptors are the key to specificity for biosensor technology. They are responsible for the biorecognition event which may be catalytic oxidation or reduction of the substrate or binding of the analyte of interest to the sensor for measurement. Common bioreceptors used are enzymes [6, 22-25], antibody [26, 27], DNA [2, 28], whole cell [29] and of recent, aptamers. Transduction methods used in biosensor include electrochemical, optical, surface plasmon resonance (SPR), thermal, piezoelectric, Quartz crystal microbalance (QCM) [30] and cantilever [31-33]. Electrochemical method of transduction constitutes more than half of the literature on biosensor [21]. The two broad classification of biosensors based on biorecognition principle are catalytic biosensors typical of enzyme bioreceptors and affinity biosensors typical of antibody and DNA. Therefore, a biosensor with electrochemical transduction method and DNA as a bioreceptor can be called DNA biosensor (based on bioreceptor) or affinity biosensor (based on biorecognition principle) or

electrochemical DNA biosensor (based on both the bioreceptor and transducer) - the name used in this writing. Other biosensors can be named immunosensor (antibody bioreceptor), enzyme biosensor and glucose oxidase sensor (using the specific name of the enzyme biomaterial).

2.2.2 Market share

In a study by Fuji-Keizai USA, Inc., 2004 [34], the market size for worldwide biosensors at year-end 2003 was about $7.3 billion, and the projection of growth to about $10.8 billion in 2007 with a growth rate of about 10.4% was feasible. Though it cannot be certainly indicated that the 2007 target was met, but these figures show that the projection and market share of biosensor is huge. Biosensor market can be divided into four sectors, namely medical, environmental, food, and military, with medical applications being the dominant player [35]. Ninety percent of sales come from glucose-detecting biosensors for medical applications. One can be sceptical about practicability of biosensors judging from the comparison between the huge volume of publications on biosensor and the actual biosensor in the market. However increase in market share, need for on site diagnosis and advances in nanotechnology are good enough to drive further commercialization of biosensors. In their review, Luong *et al* [5] gave an analysis of the various hurdles that must be crossed from the lab to the field in biosensor technology. Starting from the Yellowsprings instruments (YSI), the first company to commercialize glucose sensor in 1975 based on the idea of Clark and Lyons, Luong *et al* gave a comprehensive survey and list of the companies that are still actively involved in biosensor related products. Other than

the popular glucose sensor business, companies such as Affymetrix, Biacore international AB (GE health care), Applied biosystems and HTS biosystems, Neogen Corporation all deal with affinity type biosensor that is DNA and antibody. The websites of these companies are others can be found in the review [5]. The sales figures of these companies depict the profitability in biosensor technology business. Alocilja and Radke [35] centred their market survey on pathogens and food safety so as to create awareness and a sense of urgency for design of biosensors suitable for such environment. Long assay time is the major challenge posed by the classical methods when it comes to pathogen detection in foods and agricultural products. This time lag translates into economic loss thus; analytical devices such as biosensors are needed for speedy and accurate analysis. In this review, the economic importance of pathogens was highlighted with financial figures to show the opportunities therein for biosensor. For more information on the biosensor market, the following articles may be contacted [36-38].

2.3 DNA

Deoxyribonucleic acid, DNA, has been an object of intense study from various fields. In its molecular uniqueness, versatility and applicability lay the strength of EDB. Recent studies have been unveiling DNA's electronic, conductive and nano-size characteristic. These properties have contributed to the milestone covered in EDB development and are potentials which will no doubt aid in electrochemical DNA Biosensor's performance and miniaturisation in the near future.

DNA or nucleic acids occupy a position of central importance in biological systems [39] and its detection forms the basis of many applications in molecular diagnostics. To date, DNA studies and applications are based on the chemistry that arose from the DNA structural elucidation by Watson and Crick [40, 41]. The primary structure of DNA consists of phosphodiester-linked nucleotide units that contain a 2' –deoxy-D-ribose and an aromatic nucleobase. The resulting polynucleotide has a 5' → 3' polarity with both a negatively charged sugar-phosphate backbone and an array of hydrophobic nucleobases, which are responsible for the assembly and maintenance the double helix secondary and tertiary nucleic structure. DNA is a complex double-chained helical biopolymer that consists of repeating units of four nucleotide bases (or simply bases): adenine, guanine, cytosine, and thymine. These four nucleotide bases represent the "genetic alphabet" and the sequences of base-pairs along the length of the DNA molecule comprise a biochemical vocabulary which encodes the genetic information essential to life processes. The pairing of the bases is antiparallel, complementary and specific: adenine is always paired with thymine, and cytosine is always paired with guanine as seen in Fig. 2.2 [42]. In biochemical shorthand, the base-pairs are represented as A-T (adenine-thymine) and G-C (guanine-cytosine). It is estimated that there are about 3 billion base-pairs in the human genome - the term used to describe the total hereditary material in the 46 chromosomes. The absolute specificity of base-pairing also provides a mechanism through which "parent" DNA molecules can be copied to form identical "daughter" DNA molecules in the process of reproduction. The mechanism, known as replication (as opposed to duplication), is possible because

the two sides of the parent DNA molecule are complementary rather than identical [43]. The two complementary single strands in double helix DNA are bound together by hydrogen bonding and can be broken down (denature) by heat or high pH. Single strand DNA (ssDNA) will bind with high specificity to its complementary DNA in a process called hybridisation. DNA analysis of all sorts ranging from gene expression to forensics depend on this selective hybridisation of single stranded DNA (ssDNA) with its complementary ssDNA to form double stranded DNA (dsDNA). Conventional methods based on DNA hybridisation principle are Southern blotting [44], Northern blotting [45], denaturing gradient gel electrophoresis [46] and micro array-based gene analysis [47].

Over the last 25 years DNA application has transcends biology or genetics into material science and nanotechnology and DNA computation. Nanotechnology is motivated by the fact that at atomic or molecular level, a lot of manipulations and possibilities are possible because "there is plenty of room at the bottom" as Richard Feyman said about 50 years ago [48]. Owing to the discoveries that species made of interlocked molecular components are suitable for the bottom up approach in nanotechnology [49], DNA is now being regarded as one of the most promising molecules as the scaffold for molecular nanotechnology and nanoelectronics which includes electrochemical DNA biosensor, DNA computing and nanomachines [50-52]

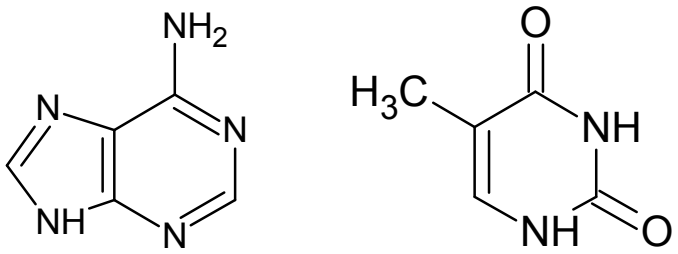

Adenine

Thymine

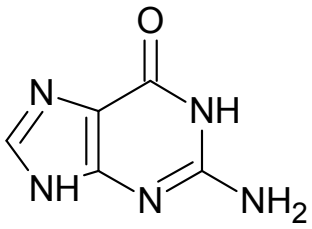

Guanine

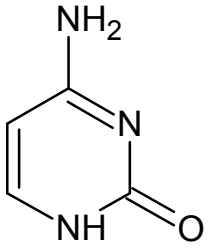

Cytosine

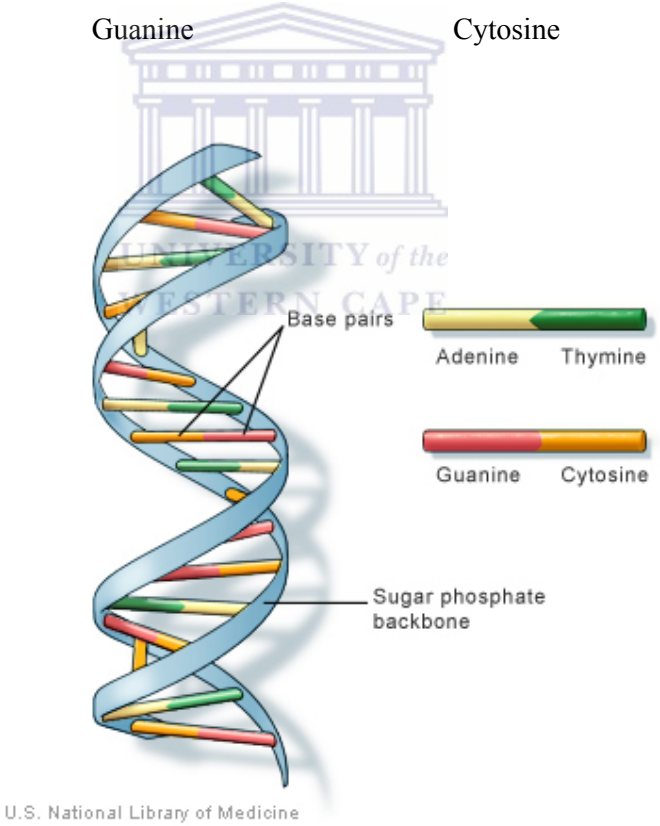

Figure 2.2 chemical formulas of the four DNA bases and the schematic structure of double stranded DNA showing the complemetary bases and phosphate backbone
[dsDNA source: http://ghr.nlm.nih.gov/handbook/illustrations/dnastructure.jpg]

DNA is a unique nanomaterial with a diameter of about 2 nm, with short structural repeats of about 3.4 – 3.6 nm and persistent length of around 50 nm. Its excellent self assembly "bottom up" properties are related to its intrinsic molecular recognition (highly predictable sequence-dependent properties), nanosize, electronic and conducting properties. DNA has thus been used by Seeman and co-workers [53]; and other scientist [54-57] as nanomachines, nanorobotics, and other various uses.

From electronic point of view, DNA has the special double helix structure with π electron cores of well-stacking bases for the use of long distance (e.g., 200 A °) and one-dimensional charge transport [58]. The conductivity and/or electron transport capabilities of DNA have been a topic of interest. Various researchers including pioneers such as Kelly, Boon and Barton [59-62], Fink and C Schönenberger [63] and others [64-67] have shown that DNA charge-transfer characteristics can be explained on the basis of the two most fundamental processes for electron transfer in extended electronic systems, which are coherent tunnelling and diffusive thermal hopping. The authors explained that DNA's ability to undergo electron transfer and its conductivity are due to its ability to adopt different structures along the molecule as well as the polyelectrolyte character of the double helix, which may lead to the flow of positively charged counter ions along the negatively charged phosphate backbone. It thus appears that electrons and holes are indeed able to shuttle along a single DNA molecule over a distance of a few nanometres. While most of these views are based on the bases (i.e. guanine, cytosine, adenosine and thymine) in DNA, electron delocalization in the conducting band through the phosphate backbone has also

been proposed [68]. In electrochemical DNA biosensor, the nanoscopic, conducting or electronic properties of DNA are important for signal generation which are usually in the form of current, charge transfer resistance, capacitance.

2.4 Electrochemical DNA Biosensor: Principles and types

DNA biosensor exploits the excellent selectivity, specificity and reactivities of deoxyribonucleic acid (DNA). It converts the Watson–Crick base pair recognition event into a readable analytical signal. A basic DNA biosensor is designed by the immobilisation of a single stranded oligonucleotide (probe) on a transducer surface to recognize its complementary (target) DNA sequence via hybridisation or using the DNA probe to detect other analytes (carcinogens, drugs, mutagenic pollutants, etc.) with binding affinities for the structure of DNA. The DNA duplex formed on the electrode surface is known as a hybrid [69]. When these events are converted into an analytical signal by the electrochemical transducers, they are referred to as Electrochemical DNA Biosensors [70].

The concept of Electrochemical DNA Biosensors was first introduced by Millan and Mikkelesen in 1993 [71] when he used tris(2,2'-bipyridyl)cobalt(III),$Co(bpy)_3^{3+}$ as an electroactive intercalators. In recent years there has been an increase in the use of nucleic acids as a tool in the recognition and monitoring of many compounds of analytical interest. EDB belongs to the class of affinity biosensor unlike their enzyme counterparts which is catalytic. Electrochemical biosensors are becoming more preferred than other transduction method because of :

(a) low cost and direct signal measurement. Since the 'natural' signal during hybridisation is electronic in nature, EDB lends itself to direct measurement using low cost electrochemical equipments.

(b) ease of miniaturisation The ease and possibilities of producing different kinds of electrodes through advances microelectronics allows downscale of EDB to smaller size – miniaturisation.

Electrochemical DNA biosensors can be divided into different classes depending on the object of classification. Broadly speaking EDB, based on the signal generation or reporting route, can be divided into two (i) Label and (ii) label free EDB. Five different pathways can be identified for electrochemical detection of DNA hybridisation. The first four are directly obtained from a review by Kerman *et al* [69] and the fifth added by the thesis author

(1) A decrease/increase in the oxidation/reduction peak current of the label, which selectively binds with dsDNA/ssDNA, is monitored.

(2) A decrease/increase in the oxidation/reduction peak current of electroactive DNA bases such as guanine or adenine is monitored.

(3) The electrochemical signal of the substrate after hybridisation with an enzyme-tagged probe is monitored.

(4) The electrochemical signal of a metal nanoparticle probe attached after hybridisation with the target is monitored.

(5) Electrochemical (usually impedance or voltammetric) change in direct signal obtained from the probe and hybrid on a suitable platform.

Pathways one to four are applicable to labelled EDB and pathways two and five are applicable to label free EDB.

2.4.1 Labelled EDB

A label is an electroactive substance (other than DNA) that forms a chemical association with either ssDNA or dsDNA and whose electrochemical signal is dependent on the extent of hybridisation. Labels used in EDB fall under these two categories- (i) intercalators with dsDNA (ii) affinity for ssDNA and enzyme labels. Some labels are capable of inserting themselves into the grooves of the dsDNA thereby enhancing the redox signal; such substances are called intercalators. For intercalation to occur, dsDNA usually "opens up" or unwinds a little and this may affect the structure of DNA hence some intercalators can be carcinogenic. Other labels simply have affinity for ssDNA for example methlylene blue. For intercalating labels, the hybridised biosensor is inserted into a solution containing the intercalator and its electrochemical signal measured. However, for ssDNA binder, the label will first be attached to the probe (ssDNA) before the hybridisation. The signal observed for the hybrid is expected to be lower than that of the probe. For example, in MB assay, the probe modified electrode is dipped into the solution containing MB. Reduction of MB to leucomethylene blue LB is monitored usually from 0 to -600 mV using CV or DPV. The peak is expected to reduce after dsDNA is formed. The reduction in the peak is proportional to the amount of dsDNA hybridised [72]. Kelly and Barton are pioneers in the use of MB an electroactive indicator. Erdem *et al* [73], in another novel approached used MB for the electrochemical detection of short DNA sequences related to the hepatitis B virus using a carbon paste electrode. In their study, they found out that the DPV current response of ssDNA with MB was far greater than that of dsDNA with MB. The enhancement is as a result of better

interaction between MB and the guanine residue of the ssDNA. This difference in current signal was used as a measure of hybridisation. In dsDNA, reduction in MB peak is observed because the guanine bases in ssDNA has been firmly bound to the cytosine bases [74]. Other labels such as ethidium bromide, daunomycin [70], Hoechst [75-77]; several metal complexes such as cobalt phenanthroline, cobalt bipyridine and ruthenium bipyridine; anticancer agents such as echinomycin have been used labelled EDB. Radioisotope labels such as ^{125}I, ^{32}P or ^{33}P have also been shown to be very efficient and highly sensitive and would have been a well explored route if not for the associated problems of safety, stability, waste disposal and high cost which have greatly deterred their exploitation. These problems motivated the quest for alternative routes [69]. Enzyme labels involve the labelling of the target DNA or the probe with electroactive enzymes. For example, indirect labelling using enzyme tag such as HRP [78], bilirubin oxidase [79] and gold nanoparticle labels have also been reported.

The following are usually the demerit associated with label approach: The designs of biosensors are aimed at keeping it as simple as possible but the use of label indicators complicates the biosensor design [80]. Labelling a molecule can have immense effect on its binding properties thereby constituting an error in the read out. It may be more expensive, requires more time and handling can be more complicated [81].

2.4.2 Label free

In the label free approach, the electrochemical signal observed is solely due to the electrochemical, and electronic or surface properties changes of the immobilised ssDNA or dsDNA as it interacts with another target molecule be it DNA or otherwise. The two approaches as stated earlier are (1) monitoring the decrease/increase in the oxidation/reduction peak current of electroactive DNA bases such as guanine or adenine and (2) electrochemical (usually impedance or voltammetric) change in direct signal obtained from the probe and hybrid on a suitable platform. The following allow the approach in the second point above:

(a) The electronic and ionic conductivity of DNA is enhanced after hybridisation because dsDNA is more conducting than ssDNA [59, 82] hence current change can be directly measured or the flow of counter-ions in and out of the DNA modified electrode surface can serve as a measure of the extent of hybridisation.

(b) DNA is an anionic molecule because of its negatively charged phosphate backbone. When ssDNA hybridises with its complementary ssDNA target, the dsDNA formed has higher anionic density. This anionic charge can create a resistance to the electron exchange of electroactive specie present in the solution.

(c) And lastly, the binding effect i.e. ssDNA to dsDNA, alters the dielectric properties and thickness of the biosensing layer and these translate to change in the double layer properties.

Thus properties such as current, capacitance, resistance, dielectric constant etc can be measured.

The earliest form of label free EDBs are those that apply the oxidation of guanine. The motivation to study DNA oxidative damages and DNA-drug interaction led to the study of the electrochemical behaviours of DNA bases. It is logical that damage to any of these bases will alter its electrochemical response. The various ways that DNA can be damaged was reviewed by Palacek and co workers [83]. Emil Palacek can be given the credit for his pioneering work in the electrochemical study of DNA bases [83, 84]. The electrochemistry of DNA bases – Guanine, Adenine, Thymine and Cytosine have been studied and found to be 0.7 V, 0.96 V, 1.16 V and 1.31 V respectively according to Oliveira-Brett *et al* [85]. The electrochemistry of guanine is mostly preferred to other bases because it has the lowest oxidation potential which will limit the electrochemistry of other unwanted molecules or interference. Guanine also undergo a one electron reaction with oxidants, hydroxyl radicals alkylating agents, transition metal complexes and some interesting response related to cancer [86]. Double stranded DNA is usually immobilised on the electrode surface. The molecule or drug of interest is allowed to interact with the DNA modified electrode and then the electrochemical response of any of the residue (usually guanine) will be measured. The result obtained is compared to that which has no target interaction for necessary interpretation. Using carbon based electrodes, Oliveira-Brett *et al* have used their long term understanding of the electrochemistry of DNA bases to study various DNA-drug or DNA-molecule interaction [87-90]. Marcini and co workers have used similar technique based on guanine oxidation to study the interaction

between a panel of antiproliferative metallo-drugs and double-stranded DNA immobilised on screen-printed electrodes as a model of the analogous interaction occurring in solution using square wave voltammetry [91].

Apart from the oxidation of DNA bases, measurements due to electrical surface changes have emerged. From the listed points in a - d above, an electrochemical technique that is sensitive to interfacial changes will be a good choice. This is why transduction using electrochemical impedance spectroscopy (discussed in greater details in chapter three) now dominates label free EDB reports. At this point, I will like to mention that label free biosensors based on hybridisation are argued to have lower detection limit and suffer from interferences due to non specific binding. This may not be a demerit if the intention of the biosensor is qualitative or semi quantitative. Qualitative means that the biosensor should be able to detect the infectious gene in the sample and semi quantitative means to be able to show that the present targets are in a range that is dangerous to health. These features are sufficient for point of care and most on-site environmental applications where quick diagnoses are needed. Label free EDB should be able to answer these questions: “Is there E coli in this sample? Are disease markers for cancer, hepatitis etc present? Are there signals for biological warfare chemicals?” If the answer to these questions is “yes”, a major problem has been solved because immediate decisions and actions can be taken to save life and the environment. The samples can then be subjected to more rigorous analytical test that can answer exactly how much, that is quantitative.

To allay the problem of sensitivity, most of the EDB that are label free use nanoparticle to amplify the electronic signal of the DNA. The reasons for the use of nanoparticle are not far fetched: 'Wires' in the dimension similar to the size of DNA are needed to hop or transport charge onto the electrode surface. Materials that will allow suitable immobilisation and provide DNA with large surface area and high conductivity are needed. Nanoparticles will be considered shortly.

2.5 Impedimetric DNA biosensors

Electrochemical impedance spectroscopy (EIS) provides detailed information on interfacial kinetics as it relates to capacitance and electron transfer resistance changes or changes in electrical properties at the modified electrode surface. Thus EIS is more suitable for affinity biosensors. Label free EDBs that use EIS signals are sometimes called impedimetric biosensors [92]. EIS have been used in the study and modelling of DNA/DNA hybridisation kinetics [93] and this demonstrates that this technique is sensitive to the interfacial electrical changes that accompany DNA biorecognition event. In EIS, impedance Z is given as a ratio of the applied voltage to its current response. There is usually a phase shift φ in between the voltage (or current) applied and current (or voltage) response. If the interfacial electrochemistry involves an electroactive specie, it is termed faradaic impedance and charge transfer resistance, R_{ct}, is mostly used as the reporting impedance element. On the other hand, if the interfacial electrochemistry is in the absence of electroactive specie, it is called non faradaic

impedance. EIS measurement in EDB can be done in either of these two ways (i) faradaic measurement of the charge transfer resistance R_{ct} over a wide frequency range and (ii) non faradaic measurement of impedance or capacitance at single frequency. Some biosensor designs use EIS as a characterisation tool at different stages but not to report the final DNA target responses [94, 95]. Such biosensor cannot be termed impedimetric.

2.5.1. Faradaic Impedance EDB based on charge transfer resistance change

This approach constitutes the majority in impedimetric DNA biosensor. For charge transfer resistance, the biomolecular probe i.e. DNA is immobilised on the electrode. The probe modified electrode is characterised in the presence of an electroactive substance (redox probe) in the electrolyte. An equimolar mixture of ferro and ferric cyanide ($Fe(CN)_6^{3-/4-}$) is most common. A bias dc potential which corresponds to the formal potential of the redox probe is applied along with the ac excitation potential, which is usually 10 mV (or less to maintain linearity), over a large range of frequency (100 kHz to 10 mHz). The resultant impedance is measured as charge transfer resistance R_{ct}. R_{ct} changes as DNA anionic density or modified electrode electrical surface changes owing to the hindrance to the flow of electron (or charge) of the redox probe at the surface of the DNA probe modified electrode. Charge transfer resistance is obtained from data fitting using an equivalent circuit. A typical Randle's equivalent circuit with its corresponding faradaic impedance plot (Nyquist or complex plane plot) is shown in Fig. 2.3. R_{ct} usually increases as target DNA concentration increases.

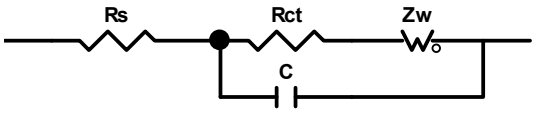

(a)

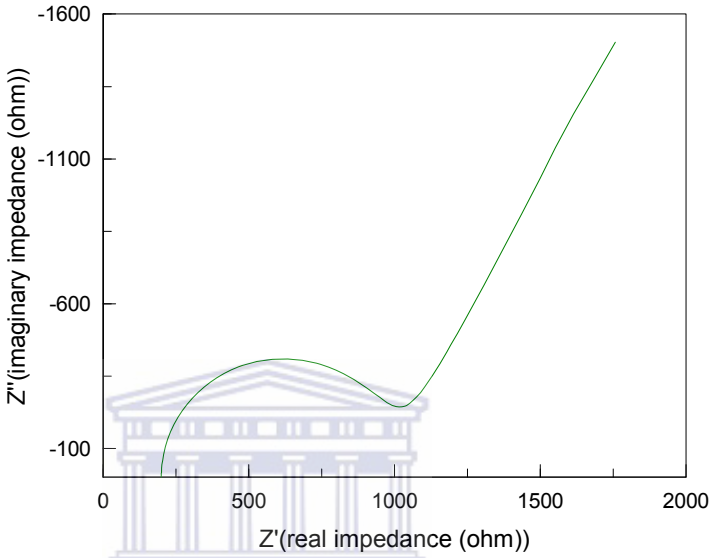

(b)

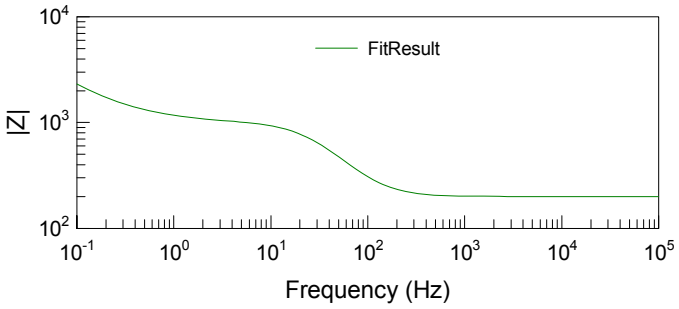

(c)

Figure 2.3 A typical faradaic electrochemical impedance graph (a) Ranlde's equivalent circuit (b) Nyquist plot (c) Bode plot

Bonanni *et al* [96-98] have used R_{ct} as the analytical parameter in the presence of $Fe(CN)_6^{3-/4-}$ redox probe in some of their EDB design. In their avidin –biotin immobilisation chemistry format, Bonani *et al* developed an impedimetric DNA biosensor using normalised R_{ct} (i.e. R_{ct} target DNA – R_{ct} blank) in [97] the

presence of $Fe(CN)_6^{3-/4-}$ redox probe. The detection limit of 5.1 pmol obtained in this avidin –biotin format was improved to 11.8 pmol [98] when Streptavidin-coated gold nanoparticles were used though the impedance protocol remained the same.

Charge transfer resistance was used to report the electrochemical responses of novel functionalized pyrroles, 3-pyrrolylacrylic acid (PAA), 5-(3-pyrrolyl) 2,4-pentadienoic acid (PPDA), and 3-pyrrolylpentanoic acid (PPA) in $Fe(CN)_6^{3-/4-}$ redox. These polymers were then used as immobilisation layers for a label free DNA biosensor design. A detection limit of 0.5 nM and a good selectivity were obtained based on R_{ct} [99].

Kafta *et al* [100] describes a faradaic impedimetric EDB where gold electrode was used to immobilise a thiolated DNA probe. The system was optimised by blocking the residual sites on the gold electrode with mercaptobutanol. Charge transfer resistance in the form of the ratio of the charge transfer resistance for the redox conversion of the ferri/ferrocyanide system between the situations of hybridised and denaturated sensor surface was chosen as analytical parameter. R_{ct} was also used to study the binding effect of fully complementary target and base mismatch. A new concept of binding the hybridised biosensor with a negatively charged molecule such as rose Bengal was introduced. Obviously R_{ct} increased after such binding. Urea was used for denaturation and a short assay time of 15 min per hybridisation cycle was reported.

In an attempt to avoid the traditional blocking (sometimes called backfilling) of the residual gold surface after SH-DNA immobilisation, Keighley *et al* [101], co-immobilised thiolated oligonucleotides and mercaptohexanol at different ratios on gold electrode. In the presence of $Fe(CN)_6^{3-/4-}$ redox probe, R_{ct} was used to compare the two approaches i.e. co immobilisation and backfilling. They found out that some discrepancies such as DNA orientation, surface homogeneity and defects in SAM resulted in the difference in the results of the two routes. For this, they claimed that co-immobilisation gives better reproducibility.

2.5.2 Non Faradaic Impedance EDB based on single frequency impedance or capacitance

In non faradaic approach, the modulus of impedance |Z| from Bode plot, real or imaginary impedance, and capacitance can be measured. The point of single frequency from which the impedance data will be obtained is carefully chosen. Usually this is the point at which the overlaid impedance responses show a consistent and measurable differential trend or optimum signal. Some authors refer to this as capacitance measurement because it is done in the absence of a redox probe and the impedance depends more on the imaginary impedance which is a measure of the capacitance. The Bode plot is a more familiar representation in this case. Non faradaic approach monitors the change in dielectrics at the DNA/electrolyte interface as a result of immobilisation and hybridisation. If a wide range of frequency is used, capacitance is most often measured using the double layer charge capacitance (see Fig. 3.9) or the constant phase element

(discussed in chapter 3). Capacitance has been observed to decrease as target DNA concentration increases. This observation is logical because the thickness DNA on the electrode surface is expected to increase after hybridisation. This increase reduces the capacitance according to equation 2.1

$$C = \frac{\varepsilon_0 \varepsilon A}{d} \qquad \textbf{eqn. 2.1}$$

Where $C, d, \varepsilon_0, \varepsilon, A$ represent capacitance, thickness, dielectric constant of vacuum, dielectric constant of the immobilisation layer (material) and electrode area respectively.

Biosensors based on this approach are sometimes called capacitive biosensors. If capacitance value is the interest, faradaic current (which can occur if the immobilisation layer is electroactive e.g. polyaniline) is reduced to the minimum. This is done by adding an insulating layer before DNA immobilisation [92]. I feel this may jeopardise the immobilisation chemistry envisaged between the redox polymer and ssDNA, therefore applying a dc potential outside the formal potential of the immobilisation layer is recommended. In fact varying dc potential can help to study the behaviour of the biomolecule (especially if it is charged) with respect to change in electric field [102]. Sometimes the thickness and dielectric changes are not proportional thus making it difficult to correlate capacitance with target DNA concentration resulting in poor reproducibility of measurements. Ma *et al* [103] used self assembled monolayer to immobilise thiol modified DNA probe onto the surface of a gold electrode. The DNA hybridisation was monitored using the electrical double layer capacitance at a single frequency

of 100 Hz. The authors conceded to the fact that this approach was difficult to reproduce. Weng *et al* developed an EDB on boron-doped diamond (BDD) electrode and used impedance at a single frequency of 10 Hz to detect complementary target DNA of a concentration as low as 10^{-9} g/ml. The concentration range was determined from a plot of relative impedance versus log of target DNA concentration. The impedance change could discriminate non complementary target too [104]. Using a platinum thin film as microelectrode, Hong *et al* [105] observed that the addition of DNA molecule increased the capacitance and reduce the dielectric at low frequency. This observation is consistence with the equation above - a dielectric loss will increase capacitance. On a salinised silicon chip electrode, Barney and co workers [106], developed a DNA biosensor. Capacitance change was measured at a single frequency. Their choice of frequency was based on the point at which the system models a near capacitor behaviour by using phase angle that is closest to 90°. They observed that the biosensor sensitivity was inversely proportional to the thickness of the insulating layer. A thin immobilisation layer was necessary for such approach.

Recently, Hassen *et al* [107] used impedance method to report the performance of an electrochemical DNA biosensor based on magnetic nanoparticles for human immunodeficiency virus (HIV) and hepatitis B virus (HBV) detection. Their format involved a smart blend of biotin- streptavidin binding and magnetic nanoparticles signal enhancement. The values of real impedance at a frequency of 100 mHz was used to characterize the hybridisation response. A detection limit of 50 pmol and 160 pmol were obtained for the HBV and HIV biosensor respectively.

The calibration curve for electrochemical impedance response is usually obtained from the plot of charge transfer resistance (which can also be normalised) or capacitance or impedance against concentration. From this plot, the linearity of the biosensor response is calculated. The linear range is the range in which the impedance response remains directly proportional to the concentration or logarithm of the concentration. The sensitivity is the slope obtained from the best line of fit in the linear range. The most used statistical approach for the determination of the detection limit is multiplying the standard deviation of the impedance signal obtained from blank measurements (i.e. solution void of target DNA under the same hybridisation condition) by three, and then divide this value obtained by the slope or sensitivity. That is, detection limit = $3\sigma / slope$ where for blank measurement minimum sampling, n, should be three (n=3)

2.6 Challenges in EDB

Rechnitz *et al* in 1977 [108], immobilised a whole cell microorganism (*Streptococcus faecium*) onto an ammonia gas sensing membrane and a linear response in the range of 5 x 10^{-5} to 1 x 10^{-3} M was obtained. Though this detection range may be considered poor today, but in this report, the importance of immobilisation layer was emphasised. They identified that putting bioreceptors such as DNA, enzymes and even whole cell in their natural environment will optimise biosensor performance. To date, creating that natural environment remains a challenge. In electrochemical DNA biosensors, the immobilisation layer should be biocompatible, effectively adsorb the DNA and sensitive enough to interpret accurately the electronics of the bio-recognition event. Therefore,

optimum biosensor performance greatly depends on the nature of the immobilisation layer or matrix, chemistry (or technique) of immobilisation [2, 12, 13] and hybridisation signal generation route. The challenge lies in getting the most suitable immobilisation layer for the best sensor result. The quest for such suitable immobilisation material, technique and transducing material (electrode) in the design of highly sensitive (low detection limit), biocompatible, single-use or multi-use, *in vivo* or *in vitro* biosensors is ongoing. My dissertation is a way to meet this challenge.

The two routes usually adopted to optimize the immobilisation of biomolecules are chemical modification of the substrate [109] and biological functionalisation of the biomolecule [110], both of which determine the immobilisation chemistry. In their study, Fausto Lucarelli *et al* [28] and Sassolas *et al* [111] demonstrated how the functionalisation of oligonucleotides improves their immobilisation chemistry and hence the performance of the DNA biosensors. On the other hand, the modification of electrodes or substrates using nanomaterials such as metal-oxide nanoparticles [112, 113] and polymers [114] are now emerging. A general look at the immobilisation chemistry and immobilisation layers common in DNA biosensor is presented in the next section.

2.7 Immobilisation layers and chemistry

DNA probes employed in EDB are usually between the ranges of 18 to 42 mer. According to biologists or biochemists, a minimum of 18 base DNA length is needed to express or identify a gene - the reason for the lower limit of 18. From the words of Sasolass *et al*, “the achievement of high sensitivity and selectivity

requires minimization of nonspecific adsorption and stability of immobilised biomolecules. The control of this step is essential to ensure high reactivity, orientation, accessibility, and stability of the surface-confined probe and to avoid nonspecific binding" [111]. This statement stresses the importance of a suitable immobilisation layer. The attachment relationship between the probe DNA biomolecule and the immobilisation layer is the immobilisation chemistry. The literature is littered with a myriad of immobilisation layers which include the electrode itself (that is bare electrode surface) which can be carbon, gold, platinum, indium tin oxide, silicon, boron dopped diamond etc. Other than bare electrodes, the following materials are used – conducting polymers (polyaniline and polypyrrole as the most common), hydrogel, sol-gel matrix, carbon paste, screen printed film, lipid membrane, molecular imprinted polymers (MIPs) and most recently dendrimers. A review on the use of polymers as immobilisation layer has been recently reported [115]. While dendrimers are nanomaterials by nature, the recent trend in literature towards improved sensor performance, is the synthesis of nanostructured derivatives of these polymers [116] or using them as composite with nanomaterials such as gold nanoparticle, carbon nanotubes etc

The following immobilisation types are found generally in the literature: physical adsorption, self assembly monolayers, entrapment, crosslinking and covelent adsorption. These immobilisation chemistries are peculiar to certain electrodes. A summary of the chemistry that exists between these immobilisation layers and probe ssDNA is summarised below.

2.7.1 Physical Adsorption

Adsorption is the simplest form of DNA immobilisation. Adsorption can either be physical or electrostatic. In either case, the DNA probe is not modified or functionalised in any way and use of other reagents are ousted. The anionic phosphate backbone of DNA usually provides the premise for this immobilisation method.

Potentiostatic or controlled potential can be used to immobilise DNA onto the transducer surface. In this case, a certain potential (usually +500 mV for glassy carbon electrode) is applied to a GCE in the presence of the probe DNA in the electrolyte. The +500 mV confers a positive charge on the GCE (or modified GCE) and this will drive and attach the DNA molecules onto the GCE surface. Another form of electrostatic adsorption is to drop-coat the probe DNA on a cationic immobilisation layer and adsorption takes place over a longer period of time. Some simply dip the electrode into the DNA solution for immobilisation. Dıaz-Gonzalez *et al* [117], in their development of DNA biosensor for severe acute respiratory syndrome (SARS) virus, immobilised unmodified 30-mer DNA on a polylysine modified screen printed carbon electrode (SPCE). The applied potential was +500 mV and the immobilisation time was 2 minutes. The short probe immobilisation time is an advantage of this method as compared to self assembly monolayers of several hours. The immobilisation of dsDNA on SPCE at similar potential for the determination of toxicant in water using guanine oxidation peak has been reported [118]. Physical adsorption without the application of potential has also been reported [119].

One of the draw backs in this is that during washing after probe immobilisation, it is likely to wash out the bound probe along with the unbound because of the weak force of adsorption. Gentle washing can be done to avoid this. But what exactly is *gentle*? It is relative. What if the washing is too gentle not to remove the unbound DNA? The biosensor world has a lot of these relative arguments.

2.7.2 Physical entrapment

This method is usually applied where the immobilisation layer includes a polymer which can be electropolymerised. Wang *et al* [120] entrapped ssDNA probe into the matrix of polypyrrole polymer on glassy carbon electrode and used the changes in the electrical properties of the polypyrrole polymer to monitor DNA hybridisation changes. The authors demonstrated through this approach, that DNA probes can serve as counter anions during the electropolymerisation of pyrrole and still retains its ability to hybridise. Since then many scientists have followed this route with different modifications. Xu *et al* [121] entrapped a 24-mer DNA into the matrices of polypyrrole by polymerising pyrrole monomer in the presence of the DNA probe (as dopant) on carbon nanotube modified electrode. EIS was used to determine the polymeric impedance changes as a result of hybridisation and a detection limit of 5 x 10^{-11} M was achieved. Ricardi and co workers [122] linked DNA probe to a sequential electropolymerisation of a self doped pyrrole, 2,5-bis(2-thienyl)-N-(3-phosphorylpropyl)pyrrole (pTPTC3-PO3H2) on a polypyrrole-modified electrode by forming a bidentate complex between Mg^{2+} and an alkyl phosphonic acid group of the polymer. The negative

charge of the phosphate group on the DNA represents an electrostatic barrier for the chloride anion moving in and out of the inner polypyrrole layer during electrochemical cycling of the modified electrode. This increase in negative charge at that barrier due to formation of the double helix during hybridisation was used to monitor the DNA hybridisation event.

Thompson *et al*. [123] had earlier reported the idea of using Mg^{2+} to link the phosphoric group on the DNA probe to phosphoric acid residue on the polymer. They investigated the modulation of the ion-exchange kinetics of a polypyrrole film with DNA biorecognition event by exploiting the discovery that electrostatic binding of Mg^{2+} to the phosphate groups provides significant stabilisation of the double-helical structure [124]. This approach pushes the DNA off the polymer surface and allows a higher degree of freedom and orientation. Another approach different from DNA polymer doping involves the impregnation of the probe DNA into the electrode material directly [125]. Carbon paste electrode is used for this purpose. A fresh probe DNA surface is exposed by polishing the electrode.

Electropolymerisation of polymers such as polypyrrole [126], polyaniline [27] and other conducting polymers usually take place in acidic medium which is unfavourable for DNA. Thus, the DNA may lose some of its bioactivity or get damaged due to harsh pH condition. Also, the orientation of the DNA cannot be ascertained and steric hindrance to the on coming target is bound to occur – the reason for the approach by Thompson *et al* [123]. Nevertheless, this approach has produced results.

2.7.3 Covalent attachment

Covalent attachment involves the formation of a bond between the ssDNA probe and the surface of the electrode or modified electrode. The probe DNA is sometimes modified or functionalised with the desired end group so as to effect the covalent attachment onto the electrode. Some covalent attachments are peculiar to the nature of the electrode material. The common electrode used in EDB are carbon and gold while others include indium tin oxide (ITO), platinum and boron doped diamond. Reviews on the use of these electrode types have been reported [28, 127-129]. Some commonly used covalent immobilisation methods are presented below.

2.7.3.1 Avidin-biotin attachment

Biotin is a small molecule that attaches with very high affinity to avidin binding sites (K_a = 1 x 10^{15} M^{-1}). This value is nearly equal to that of a covalent bond. In lieu of avidin, streptavidin or neutravidin is also employed due to more binding sites. The protocol here involves the modification or functionalisation of both the probe DNA with biotin (biotinylated DNA) at the 5′ end and the electrode with streptavidin. The ensued tetravalent covalent bond of streptavidin-biotin is very stable and can weather a wide range of pH and temperatures [86]. The coupling of biotinylated DNA onto an avidin surface was employed by Arora *et al* [130]. In their approach, polypyrrole-polyvinyl sulfonate (PPy-PVS) modified electrode was used as the platform for the avidin activation. Since avidins are proteins, the presence of non-specific binding sites may hamper the sensitivity of such biosensor assay [86].

2.7.3.2 Carbodiimide covalent binding

Carbodiimides are commonly used to modify proteins on their carboxylate groups and have been applied to DNA biosensor immobilisation layer. Carbodiimides can be used either alone or in combination with amines to create new amide bonds off the carboxyl. This mechanism in bioconjugate system has been explained [131]. This approach is more common with carbon electrodes. The two reagents used to activate carbodiimide chemistry are 1-ethyl-3-(3-dimethylaminopropyl) carbodiimide (EDC) and N-hydrosulfosuccinimide (NHS) and is sometimes written as Carbodiimide/N-hydroxy-succinimide (EDC/NHS) binding. While an amino modified DNA is used to form an amide bong with the activated carboxyl group.

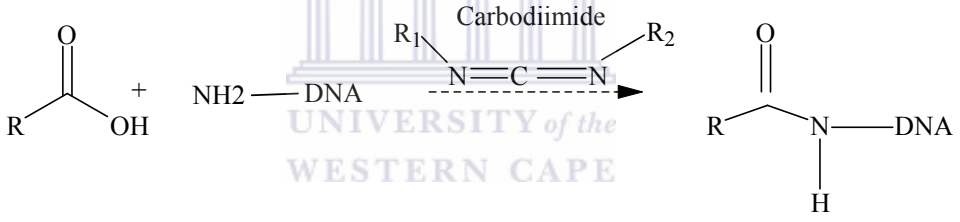

Figure 2.4 A simple reaction scheme showing the immobilisation of amino modified probe DNA based on carbodiimide chemistry

Milan and Mikkelsen used carbodiimide chemistry to attach DNA deoxyguanine residue to a glassy carbon electrode surface which has been activated by 1-[3-(dimethylamino)propyl]-3-ethylcarbodiimide hydrochloride and N-hydroxysulfosuccinimide [71]. This binding involves the displacement of the –OR residue formed from the cross linking reaction EDC/NHS by the nitrogen from the amino group in the probe DNA to form an amide bond. For amide to be formed there must be a way of activating a carboxylic functional group onto the GCE. The use of 4-aminobenzoic acid (ABA) can thus be appreciated in this

regard [132]. Other recent reports on carbodiimide immobilisation chemistry can be found in this reference [95].

2.7.3.3 Thiol linkage

This involves the covalent bond between sulphur and gold - Au-S. This Au-S chemisorption is usually done using a thiol modified DNA on either a gold electrode [100] or gold nanoparticle (AuNP) deposited on another electrode material such as glassy carbon electrode [94]. The thiolated DNA is dropped on the gold electrode or gold nanoparticle modified electrode and is allowed to self assemble over a period of time. Self assembled monolayer (SAM) is when a layer consists of a molecule of another substance. This technique is used for 'couples', such as gold and thiol, with high binding affinity. For thiolated DNA as an example, the SH-DNA is dropped on the gold surface and binds on the gold surface with the liberty of its natural orientation (external forces are excluded). The excess SH-DNA molecules will be washed away leaving (supposedly) a monolayer. After DNA binding of this sort, some sites of unbound gold may still be available for target DNA to bind unto - this is called non specific binding. To minimise this effect, the residual gold site is blocked (or passivated) with another agent which will not interfere in DNA biorecognition. 6-Mercapto-1-hexanol (MCH) [133] and 4-mercapto-1-butanol (MCB) are commonly used. MCB takes the advantage of the stabilisation of SAMs by matching the C_6 of the SH group on the 5′ end of the DNA that is inherently incorporated in synthesis [134, 135]. Li *et al* [136] used a sol gel immobilisation layer to construct an EDB on a gold electrode. The sol gel film prepared from 3-Mercaptopropyltrimethoxysiloxane

(MPTMS) and 3-glycidoxypropyltrimethoxysiloxane (GPTMS) precursors was covalently attached through SAM onto the gold electrode surface through Au-S linkage. Amino functionalized probe ssDNA was immobilised onto the sol gel matrix through epoxide/amine coupling reaction. The biosensor gave a detection limit of 10^{-10} M.

2.8 Nanomaterials in DNA biosensors

Electrochemical DNA biosensor has high potentials in DNA diagnostic applications which include genetics, pathology, criminology, pharmacogenetics, food safety and many other fields [137]. According to the words of Joseph Wang: "To continue these advances, to exploit these opportunities, and to move DNA diagnostics out of the central laboratory, future devices must link high performance (particularly high sensitivity and selectivity), with high speed, miniaturization, and low cost. The realization of such powerful devices requires innovative efforts, coupling fundamental biological, chemical and material sciences" [138]; indeed material science has played a critical role. The advent of nanotechnology has brought a lot of innovations into the field of biosensor. Microelectronics, related micro-electromechanical system (MEMS), and biotechnology are being interwoven to produce devices such as miniaturised arrays of electrodes, lab on a chip and lately microcantilevers which use more of optical and piezo-resistive signals as read outs.

Nanomaterials, based on size similarities with DNA and other bioreceptors are now used to modify electrode or the biomolecules directly for biosensor optimisation. The major features of nanostructures as regards biosensors are their

catalytic properties, large surface area, compatibility with biomolecules and high conductivity. Notable among such materials are carbon nanotubes, metal nanoparticles, metal oxide nanoparticles, quantum dots, magnetic beads, polymer nanotubes or nanostructure [138], and most recently dendrimer. Nanomaterials are either used alone or in combination to produce a nanocomposite. In electrochemical DNA biosensor, nanomaterials form an excellent, biocompatible immobilisation interface for signal amplification.

Carbon nanotubes (CNT) which was first synthesised by lijima in 1991 [139] and gold nanoparticles are the most widely used nanoparticles in biosensing [140]. In a review [141], on the role of CNT in electroanalytical chemistry, the authors present quite a comprehensive list the applications of CNT, CNT as composite, CNT modified electrodes and immobilisation layer and the target molecule of interest. CNTs are a new allotrope of carbon originated from the fullerene family, behaving like microcrystals with molecular dimensions [142]. Like other nanomaterials, CNTs guarantee a very large active surface area, high porosity and reactivity [115]. Other reviews on nanomaterials in electrochemical biosensor can be consulted [10, 137, 138, 143, 144]. Nanobiosensor is now being used as the name for a biosensor developed using nanomaterial platform or nanomaterial modified electrodes.

2.9 Gold nanoparticles related EDB

The synthesis of gold nanoparticles (also called colloidal gold) can be divided into two: chemical synthesis and electrochemical synthesis. There are varieties of AuNP chemical synthesis. The general chemical synthesis involves

the reduction of gold salt or acid ($HAuCl_4$) from Au^{3+} to Au^0. Owing to the high surface energy of theAu^0 formed, aggregation of the AuNP occurs. To avoid this, that is to stabilise the AuNP formed, the surface are passivated or capped with other substances. Examples of reducing agents are sodium citrate [109], and sodium borohydride [145]. Examples of capping agents are sodium citrate and dendrimer [146, 147]. Electrochemical preparation of gold nanoparticles (AuNP) is mostly carried out by electrodeposition using constant potential of – 200 mV for a chosen time from a solution of $HAuCl_4$ [148]. Sometimes, already chemically synthesised gold nanoparticles AuNP or colloidal gold is allowed to self assemble on a pre-treated electrode [109, 149]. Varieties of gold nanoparticles synthesis are discussed in these reviews [150, 151].

Gold nanoparticles are known to exhibit excellent biocompatibility and high conductivity. They act as biomolecular nanoscopic wires that create large electrode surface areas that suitably orient DNA molecules for optimal immobilisation, and have been used to chemisorb thiolated DNA onto electrode surface [150, 152-157]. Gold nanoparticles' high conductivity, promotes direct electron transfer between protein (and other biomolecules) and the electrode. Zhang *et al* [149] attached AuNP onto GCE through sulfhydryl-terminated monolayer for the immobilisation of haemoglobin without the aid of an electron mediator. The bio-activity of the haemoglobin was retained and it exhibited a detection limit of 9.1×10^{-7} M towards hydrogen peroxide. This report clearly illustrates AuNP biocompatibility and its ability to wire biomolecule. AuNP was able to reach into the iron haem group of the protein haemoglobin to enhance its electrochemistry. Other works demonstrating the excellent biocompatibility,

conductivity and signal amplification efficency of AuNP have been recently reported. These include the detection of cytochrome c with detection limit of 6.7 x 10-10 M [158]; AuNP/polyaniline nanotube membranes on the glassy carbon electrode toward the recognition of Phosphinothricin acetyltransferase (PAT) gene sequence, existing in some transgenic crops with detection limit of 3.1 x 10^{-13} M [148]; combination of AuNP with CNT in the development of sensor for baebene cancer [159]; and others. Other reports on DNA biosensors based on the use of AuNP can be consulted [160, 161].

2.10 Dendrimers

The first answer to why nanomaterials became a choice in biosensor design is simply because the biomolecules themselves are nanomaterials. It is good to always remember the following about biosensor:

- The whole idea emanated from nature
- It is all about mimicry of nature i.e. mimicry of biomolecules such as DNA, enzymes etc.
- It is making nature do what it does best in the natural biological environment in another environment
- It is all about making the biomolecules 'comfortable' in the new environment by various 'deceptive' tactics such as optimum pH, temperatures, and use of biocompatible materials.

A look at the diagram in Fig. 2.5 shows the relative size of materials.

Dendrimers are not the first class of materials to be considered for biomimicry. Cyclodextrin, cyclophanes have been attempted but their draw back

lies in the inability to create the sort of nanoenvironment present in protein [162]. Higher molecular weight polymers could not 'reach out' into the active sites of the biomolecules which are, in nature, usually located within a large matrix of molecular weight that may reach a thousand, and to make it more complex, some of these matrices are hydrophobic in nature.

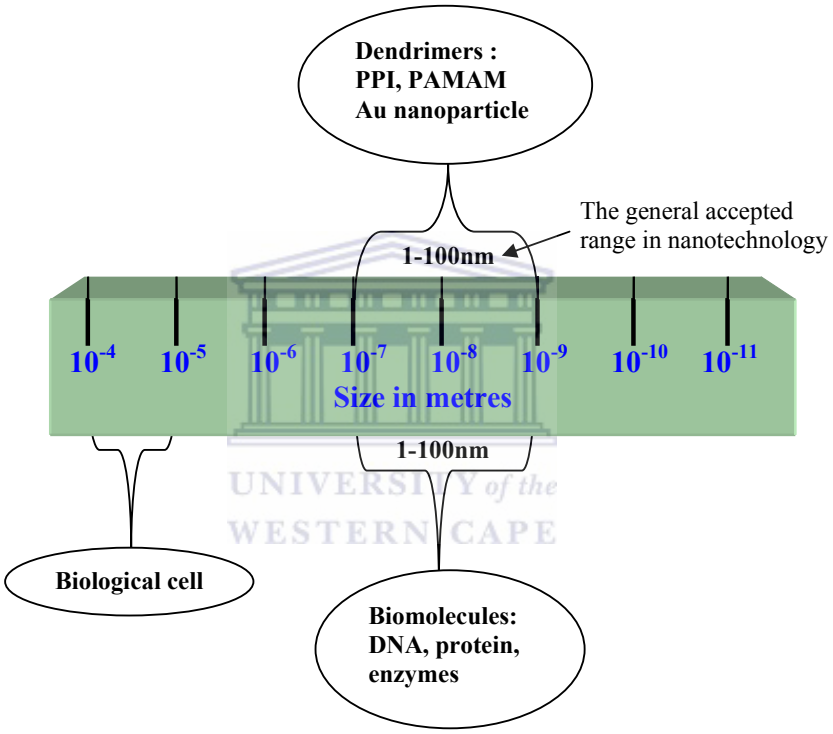

Figure 2.5 A sketch of a comparison between the size of dendrimer and biomolecules**.**

This is where the term 'molecular wiring' (especially in enzymes) sprouted from. Materials of like size and excellent conductivity are thus needed to reach out into this hidden active site responsible for the biochemistry of interest. One will agree with Liang and Fretchet [162] that no other synthetic material available offers the degree of control that exists within dendrimers and biological molecules. Dendrimers are the closest synthetic analogues of small enzymes (and DNA) in

terms of size, functional complexity, and structural precision. The dendritic architecture actually originated from nature. Boas *et al* [163] listed various natural examples such as tree leaves and root; the bronchioles and alveoli in the lungs; the wall gecko's feet hair (satae) etc. It is no wonder why nature welcomes dendrimer (as seen in host-guest), *mimicry* is the word!

The field of dendrimers have been advanced through the works of various brilliant scientists. A summary of pioneers and milestones in dendrimer history obtained from Frontier Scientific, Inc. [164] is presented below. (Note some of the references are omitted and interested reader may consult the Frontier scientific website)

P. J. Flory – Evidence for Branched-Chain Macromolecules – 1941 – 1942 (Nobel 1974) [165]

J.-M. Lehn – Stepwise Strategies for Synthesis of Marcocyclic Rings – 1973 (Nobel 1987)

F. Vögtle – Cascade Synthesis – 1978 [166]

R. G. Denkwalter – Lysine-dendrimer Patent – 1981 27, 28, 29

G. R. Newkome – First Modular Dendrimer Synthesis, First Reference to Unimolecular Micelles – 1985 [167]

D. A. Tomalia – First High-Generation Dendrimers based on Linear Monomers – 1985 [168]

J.-M. Fréchet – First Convergent Synthesis – 1990 [169]

P. G. DeGennes – First Theoretical Study on Dendrimers – 1983 (Nobel 1991)

J. S. Moore – Phenylacetylene Dendrimers – 1991

Wörner, Mülhaupt, De Brabander-van den Berg, Meijer – Improved Vögtle' Procedure and Later Developed the Dendritic Box – 1993 [170, 171]

S. Masamune – Silicone-based Dendrimers – 1990

J. –P. Marjoral – Phosphorous-based Dendrimers – 1994

S. Zimmerman – Self-Assembly of Dendrimers – 1995

A. D. Schlüter – Dendronized-Polymers – 1995

V. Balzani – Metallodendrimers – 1989 [172]

D. Seebach – Chiral Dendrimers – 1993 50

R. H. E. Hudson – DNA-based Dendrimers – 1993 [173]

Dendrimers are synthetic three-dimensional macromolecules with a well-defined, highly branched and globular shaped molecular structure [174]. The term dendrimer is derived from Greek - 'dendra and 'meros' meaning tree and part respectively. The architecture of dendrimer comprises of central core (C), branched unit (B) and surface group (S). Another way to describe this three-level architecture is the inner core, the branches and the periphery. The term generation in dendrimer nomenclature represents the repeating monomer units or it is the number of branching points (or focal points) when going from the core towards the dendrimer surface. With *generation* written as G, a dendrimer with one monomer repeating unit (or branch) is labelled G1, while G4 dendrimer has four monomer repeating units etc. G0 is sometimes used to refer to the core of the dendrimer. Other dendrimer terms or nomenclature as reported by Boas *et al* are:

> *Shell*: The dendrimer shell is the homo-structural spatial segment between the focal points and the "generation space". The "outer shell" is the space between the last outer branching point and the surface. The "inner shells" are generally referred to as the dendrimer interior.
> *End-group* is also generally referred to as the "terminal group" … Dendrimers having amine end-groups are termed "amino-terminated dendrimers".

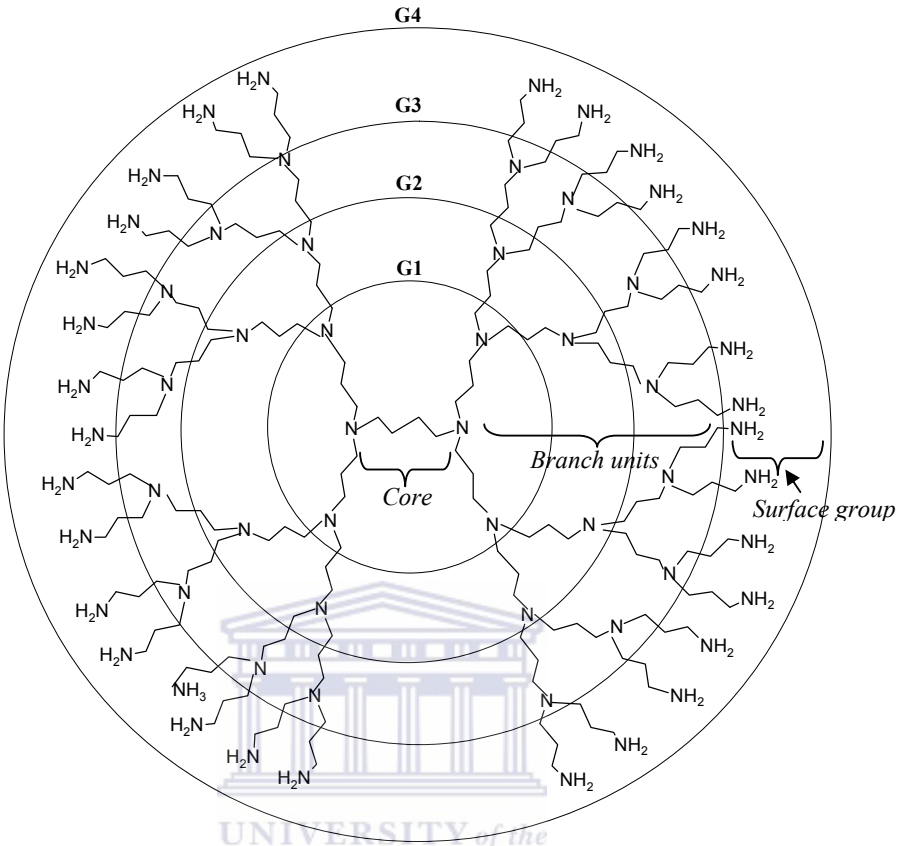

Figure 2.6 A typical dendrimer (poly(propylene imine)) with four generations

There are two approaches to dendrimer synthesis: the divergent approach and the convergent approach. Vogtle *et al* [166] pioneered the initial divergent synthesis method (which they called cascade approach) upon which most dendrimers are now based. Tomalia *et al* were the first to introduce the name dendrimer [168]. The convergent approach was pioneered by Frechet [174, 175]. poly(amidoamine) (PAMAM) [168] and Poly(propylene imine) (PPI) are among the most common class of dendrimers, but PAMAM is more widely studied. Because molecular size and generation of dendrimers are increased stepwise via the repetition of a reaction sequence, their size and structure are highly

controllable and their molecular weight distribution is generally very narrow [176].

Poly(propylene imine) dendrimers are sometimes called ‘‘DAB-dendrimers’’ where DAB refers to the core structure which is usually based on DiAminoButane. POPAM is also sometimes used to describe Poly(propylene imine) dendrimers. POPAM stands for POly (Propylene AMine) [163]. The pioneer scientists in the synthesis of PPI are Wörner, Mülhaupt, de Brabander-van den Berg and Meijer [170, 171]. Their approach was an improvement of Vogtle's cascade procedure. The average diameter and the number of amino end group in G1 to G4 poly(propylene imine) are presented in Table 2.1 [177, 178].

Table 2. Some properties of generation 1-4 Poly(propylene imine) dendrimer

Properties	**G1**	**G2**	**G3**	**G4**
Molecular weight	317	773	1687	3514
Number of NH_2 end group	4	8	16	32
Diameter (nm)	1.22	1.79	2.36	3.12

A dendrimer is called metallodendrimer when a metal is incorporated into its structure. The metal incorporation can be at the dendrimer core, or at the terminal or in between the branches [179]. Balzani [180-182] and Newkome [183, 184] and their co workers led the way into the incorporation of metal ions into dendritic architecture. I believe one of the motivations for metallodendrimer synthesis is catalysis. Again, this is a lesson from nature – most enzymes such as cytochrome P450 [23, 185, 186]; and some proteins (metalloproteins) such as haemoglobin [187]; owe their activities to metal centres. Dendrimers and metallodendrimers

have been applied for various uses. The scope of this review is limited dendrimer/metallodendrimer and its relationship with biological molecules. Therefore the reader may consult the following literatures for extensive information on dendrimer synthesis and other applications [179, 188-194]. Also in the journal *Topics in Current Chemistry*, published by SpringerLink, the following volumes (with year in bracket) are dedicated to dendrimer: 196 (1998), 210 (2000), 212 (2001), 217 (2001), 228 (2003).

2.10.1 Dendrimers in gene and drug delivery

One of the most fascinating uses of dendrimer is in the biomedical environment as gene or drug carriers. In a review by Svenson and Tomalia [195], various applications of dendrimer as biomemetric proteins, nanoscale containers, gene transfection agent, drug delivery agent, imaging agent, nanoscoffolds and even as nano-drugs were discussed. In fact this application motivated me to developing a dendrimeric nanobiosensor. The understanding of diseases at genetic level and its therapy has been progressive in the biomedical arena since the human genome-sequencing project was completed [196]. Gene therapy is a broad term that encompasses any strategy to treat a disease by introducing an exogenous gene, gene segments, or oligonucleotides into cells of an affected person [197]. It aims at delivering DNA, RNA, or antisense sequences that alter gene expression within a specific cell population, thereby manipulating cellular processes and responses. The gene delivery researches are already yielding commercial products and a clinical result of note is the approval of the first commercial gene therapy for the treatment of patients suffering from head and neck cancers [198]. The

application of dendrimers in drug delivery is based also on host guest supramolecular chemistry. The drugs are encapsulated into the void nanoscopic space of the dendrimer. Covalent and non covalent attachments to drugs have also been exploited [199].

The two vectors used in gene delivery are viral and non viral. “Viruses have sections of their genome removed to make them replication deficient, allowing the insertion of genes encoding for therapeutic proteins. The limited space available in the viral genome combined with expensive production requirements and major safety issues related to over-reaction of the immune system have inspired the development of alternative non-viral strategies” [196]. Other shortcomings of viral vectors such as mutations in the host leading to carcinogenesis, toxic immunological reactions, long-term effect of the integrated transgene of the virus in the host have been highlighted along with real life clinical examples [197]. Owing to these viral vectors draw back, non viral vectors are becoming an alternative source. The non viral approach is based on electrostatic interaction between anionic nucleic acid and the cationic synthetic vector which will complex and condense the DNA into nanoparticles. Some examples of such synthetic cationic non viral vectors include cationic lipids or polymers. Names such as lipoplex, polyplex, or dendriplex have been given to the resulting nanoparticle depending on the vector type [200]. It has been shown that dendrimers molecules are actually part of the supramolecular assembly when used to in the delivery of DNA [15]. The DNA/dendrimer supramolecular assemblies which are complexed by protonation are prerequisite to gene delivery. The

mechanism involved in polycation (which includes PPI dendrimer) has been highlighted [197].

PPI dendrimer among others, have been shown to have low toxicity in a wide range of mammalian cells. PPI have the ability to condense DNA of bases 600 and above into nanoparticles [201]. Using total intensity light scattering, electron microscopy and atomic force microscopy techniques, Chen *et al* [202] demonstrated that DNA of shorter strands (usually called oligonucleotide or simply DNA as used in this thesis) can also form nanoparticles with PPI. Recently, PPI are able to form dendrosomes. Dendrosomes are novel, vesicular, spherical, supramolecular entities, containing entrapped dendrimer–DNA complex, possessing negligible hemolytic toxicity, higher transfection efficiency and better *in vivo* acceptability. The potentials of PPI dendrosomes in genetic immunization against hepatitis B was explored by Dutta *et al* [203]. Reviews that deal with the use of dendrimers especially PPI and PAMAM in biological systems have been reported.

Dendrimers can be said to be DNA friendly because of their nanoscopic size, cationic nature, host guest supramolecular efficiency, biocompatibility, nano-engineering possibilities, multiple attachment sites etc in gene delivery application. With the numerous applications of dendrimers in gene and drug delivery *in vitro* and *in vivo*, one will expect the same myriads of application in the field of DNA biosensor. But the contrary is observed! Fig. 2.7 presents a survey (carried out 15 November 2008) of literatures from 2000 to date. The keyword search “electrochemical DNA biosensor and dendrimer” returned an average of three journals which included one of our papers [82]. The keyword

"*DNA biosensor* and *dendrimer"* returned only eight. The dearth of literature observed is an index of the relevance of this thesis. The figure also shows that electrochemical DNA biosensor based on impedance is relatively new when compared to the keyword "electrochemical DNA biosensor" within the same year range which gave over a thousand references.

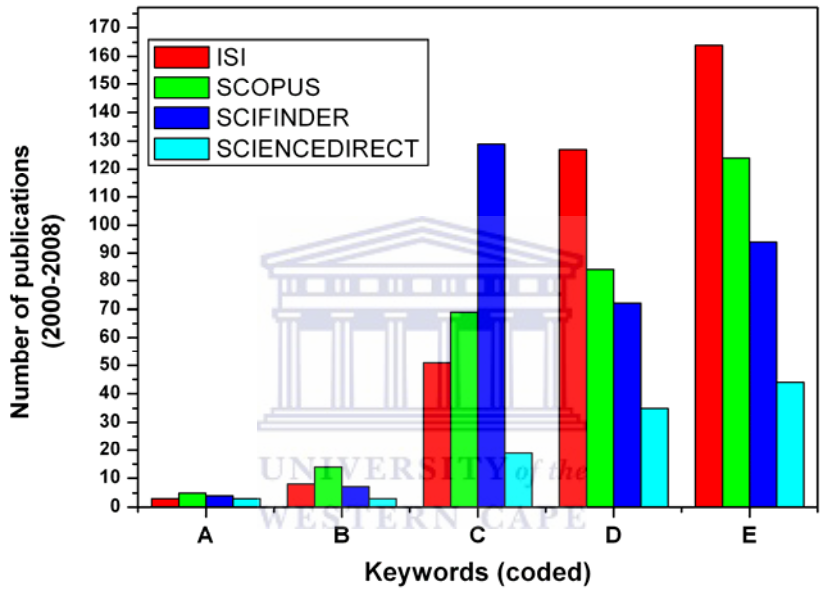

Figure 2.7 Survey of published literature on electrochemical DNA based on dendrimer Keyword code: A = electrochemical DNA biosensor and dendrimer, B = DNA biosensor and dendrimer, C = biosensor and dendrimer, D = electrochemical DNA biosensor, and impedance, E = DNA biosensor and impedance

2.10.2 Dendrimers in Electrochemical DNA biosensor

To the best of my knowledge, poly(propylene imine) dendrimer, either in its pristine form or as a nanocomposite, has not been used as an immobilisation layer in the design of an electrochemical DNA biosensor. But its commercially available counterpart PAMAM has been used in this regard. It seems that the application of dendrimer as an immobilisation layer began in 2001 with Worhle

and co workers [204, 205] at the Institute of Organic and Macromolecular Chemistry, University Bremen, Bremen, Germany. Their work however was not based on electrochemical transduction but fluorescence. PAMAM was cross linked on a glass substrate and DNA was immobilised. In 2002, Benters *et al* (Wohrle's group) [205] designed a DNA biosensor for the discrimination of single nucleotide polymorphisms using G4 PAMAM as a dendritic linker on a glass substrate. PAMAM dendrimer was drop coated on a pre-treated glass substrate and a combination of glutaric anhydride and *N*-hydroxysuccinimide were used to activate the PAMAM. Carbodiimide chemistry was used to immobilise amino modified DNA probe. This dendrimer functionalised surface gave the best hybridisation and regeneration results when compared to other surfaces prepared in the absence of dendrimer but the same carbodiimide chemistry. This report though not based on impedance transduction is among the early use of dendrimer immobilisation layer for DNA.

Aixue Li *et al* [206] were the first to report the use of dendrimer (PAMAM) in the design of an electrochemical impedimetric DNA biosensor in 2006. The immobilisation procedure involved a series of chemistries: Self assembled monolayer of thiol linkage onto the gold electrode using 2-aminoethanethiol created a free amino end on the gold electrode. Glutaraldehyde was then used to create a formyl end upon which PAMAM was deposited and crosslinked. The PAMAM modified layer was again functionalised with glutaraldehyde and amino modified probe ssDNA was finally linked using carbodiimide linkage. Faradaic impedance in the presence of $Fe(CN)_6^{3-/4-}$ redox probe was used to monitor the hybridisation. Using a simple Randle's equivalent

circuit for fitting, a calibration plot of change in change transfer resistance versus logarithm of target DNA was obtained. They found out that the presence of dendrimer improved immobilisation capacity and efficiency and obtained a linear range of 10^{-11} to 10^{-8} M with detection limit of 3.8 x 10^{-12}. Despite the complexity of their immobilisation procedure, a good result was obtained demonstrating the advantage of dendrimer in biosensor design.

In contrast to Aixue Li's label free format [206], a labelled EDB was recently (March 2008) published by Wei-Jie *et al* [207] using G1 PAMAM as immobilisation layer. *N*-Hydroxysulfosuccinimide (NHS) and 1-[3-(dimethylamino) propyl]-3-ethylcarbodiimide hydrochloride (EDC) cross linking was carried out on a glassy carbon electrode and using carbodiimide chemistry PAMAM was covalently attached by drop coating. An unmodified probe ssDNA was immobilised on the PAMAM modified GCE using electrostatic physical adsorption. Hybridisation signal was monitored by differential pulse voltammetry using MB as the electroactive indicator. A detection limit of 1 x 10^{-9} M was obtained.

While the approached used by Auxie Li and Wei-Jie are plausible, other simpler electrode modification technique such as adsorption, electrodeposition can be explored. The use of dendrimer and dendrimer nanocomposite other than PAMAM will be a worthwhile endeavour; and these I have attempted in this thesis.

Outside the sphere of electrochemical DNA biosensor, Zhang and Hu [208] reported an electrochemical biosensor using PPI and gold nanoparticle (which they called nanoclusters) as an immobilisation layer for the assembly of

myoglobin layer-by-layer films on a glassy carbon electrode. The PPI-AuNP nanoclusters (which I call nanocomposite) gave excellent catalytic and better immobilisation properties when compared with PAMAM and myoglobin modified GCE.

2.11 Uses of Electrochemical DNA Biosensors

EDB is not only seen as a prospective analytical tool but has found application in environmental, food, agriculture, medical and warfare domains. In the area of environmental monitoring, Mascini and co workers [209] reported an electrochemical DNA biosensor for the detection of low-molecular-mass substances that are of environmental concern including polychlorinated biphenyls (PCBs) and aflaxtoxin. Other researchers have reported environmental biosensor systems for the detection of organophosphates in air, soil and water [8]; pesticides in soil [210] and water pollutants [211]. LaGier *et al* developed a biosensor for the detection of E coli which is a faecal indicator in water [9]. Tencaliec *et al* used EDB on screen printed electrode for the detection of toxicant in water samples. The results obtained showed a good correlation with another established method called ToxAlert®100 which is based on bioluminescence inhibition of Vibrio fischeri [118].

In the clinical or medical domain over 95% of its applications have been for infectious disease testing [212]. EDB for diseases such as hepatitis, human interleukine-2 gene [213], helicobacter pylori, a bacterium that can cause digestive illnesses, including gastritis, peptic ulcer disease, and possibly two types of stomach cancer [214], E. coli 0157:H7 disease marker [211] and many more.

Though most of these applications are still at the modelling phase there are some commercially available EDB [Kerman paper]. Toshiba's electrochemical DNA hybridisation detection system is called the GenelyzerTM [32]. GeneOhm Sciences developed an EDB that is used in the detection of single-nucleotide polymorphisms (SNPs) [215]

EDB has also been applied in food contaminants detection [216, 217] and in the area or warfare, explosives [7]; and chemical warfare agents [218].

CHAPTER 3

MATERIALS AND METHODS

3.1 Introduction

This chapter consists of the following:

- Materials: Information on all the materials used.
- Research design: A general overview of all the sequential steps taken in other to solve the thesis problem.
- Methodology: A more detailed presentation of the instrumental and experimental techniques,

Experimental procedures are written based on the result chapters. However procedures common to the dissertation as a whole is written under general experimental.

3.2 Materials

Ultra pure water (nuclease free) with resistivity 18.2 M using a Millipore Synergy water purification system was used in all solution preparation. All reagents were of analytical grade. A list of the materials used is presented in the table below:

Table 3.1 List and source of materials used

Material	Source	Other information
Ultra pure water	Millipore Synergy water purification system	Resistivity 18.2 MΩ
DNA sequences	Inqaba Biotechnical (Pty) Ltd, Cape Town, South Africa	Details of sequences are given in other chapters
Generation 1 PPI dendrimer	Sigma-Aldrich	Used as received
PPI dendrimer: G1, G2, G3, G4	SyMO-Chem, Eindhoven, Netherlands and Sigma-Aldrich.	Used as received
$HAuCl_4$	Sigma Aldrich	
Buffer components: Na_2HPO_4, KH_2PO_4, KCl,	Sigma Aldrich	
TE Buffer	Sigma Aldrich	
Redox probe: $K_3Fe(CN)_6$, $K_4Fe(CN)_6$	Sigma Aldrich	
Urea	Sigma Aldrich	
Nickel (II) salicylaldimine metallodendrimer	Organometallic lab, UWC	Details in Chapter 4
Glassy carbon electrode	BASi	
Ag/AgCl (3 M Cl^-)	BASi	
Pt auxiliary electrode	BASi	

3.3 Research Design

My thesis was designed to follow some sequential steps or cycles which were optimised over time. Electrochemical measurements were made after each of the preparative step to ascertain its conformity to *expected results*. Expected results, in this context, refer to results that were based on theory where applicable and/or on numerous repetitive measurements which enabled the prediction of a particular outcome. The broad research design can be summarised in the flow diagram below:

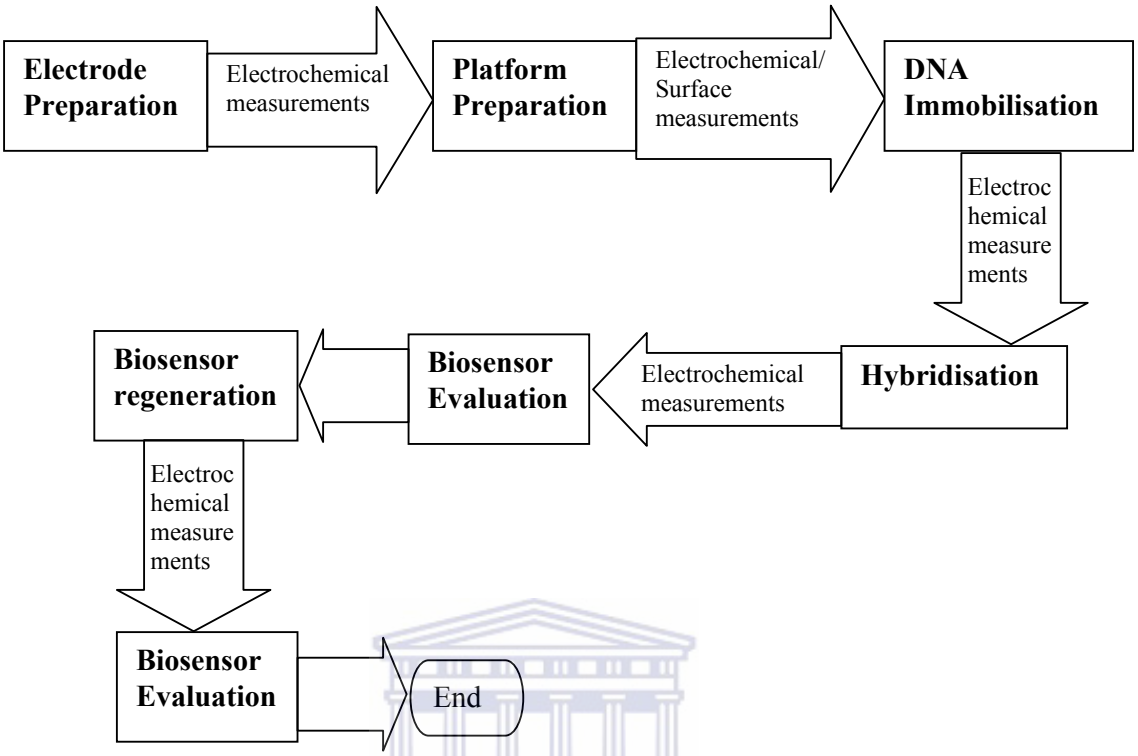

Figure 3.1 A flow chart of the research design

The above sequence involves:

1. **Electrode and solution preparation**
2. **Standardization of the glassy carbon electrode:** This involved the electrochemical measurements taken in order to ascertain the cleanliness of the electrode and also model its behaviour in the presence of blank electrolytes.
3. **Electrochemical measurements:** Voltammetric methods such as cyclic voltammetry (CV), differential pulse voltammetry (DPV), square wave voltammetry (SWV) and electrochemical impedance spectroscopy (EIS) were used at different stages to obtain relevant data towards the characterization of the platform and development of the biosensor.

4. **Preparation of the dendrimeric platform:** This can also be referred to as the electrode modification step. The two approaches used were drop coating and electrodeposition.
5. **Surface measurements:** Surface measurement was carried out using scanning electron microscopy
6. **Immobilisation**: Drop coating of the probe DNA onto the modified electrode was used.
7. **Hybridisation**: This involves bringing the biosensor (immobilised probe single stranded DNA) in contact with target single stranded DNA for the biorecognition called hybridisation to take place.
8. **Biosensor evaluation**: Measurement of response to target DNA, stability, linearity, sensitivity and detection limit.
9. **Regeneration:** This involved a process of denaturing or unwinding the double stranded DNA formed as a result of hybridisation and putting the biosensor to multiple uses.

3.4 Methodology

3.4.1 Electrode and solution preparation

Glassy carbon electrode was used throughout this work. The cleaning method used was predominantly mechanical polishing using alumina powder of size 1, 0.3 and 0.05 micron respectively followed by sonication in ethanol and water. Other information on the GCE used can be found at the manufacturer's website [219].

Solutions were prepared using general analytical procedures and formula such as equations 3.1 and 3.2 for preparation and dilution of solutions respectively.

$$mass = \frac{molar\ mass \times Molarity \times volume}{1000} \qquad \textbf{eqn. 3.1}$$

$$C_1V_1 = C_2V_2 \qquad \textbf{eqn. 3.2}$$

.

Details of other calculations necessary will be found in the experimental and result sections.

3.4.2 Standardization of the glassy carbon electrode

Electrode surface are bound to change after each experiment due to contamination from adsorbed species. To ensure reproducibility, electrochemical measurements are taken after each cleaning step. The cleaning is repeated until the surface can be said to be clean judging from the voltammetric data obtained in the respective electrolyte. In extreme cases, cathodic cleaning and even quick etching in piranha solutions (H_2SO_4: H_2O_2, 3:1) were used to ensure that the electrode surface was regenerated.

3.4.3 Voltammetry

Voltammetric techniques are characterised by the application of a potential E to an electrode and the monitoring of the resulting current i flowing through the electrochemical cell. In many cases the applied potential is varied or the current is monitored over a period of time t [220]. Thus, voltammetry can be broadly defined as the exploration of the three-dimensional space that relates

potential (*E*), current (*i*), and time (*t*) [221].The history of voltammetry began with polarography at the dropping mercury electrode (DME) as far back as 1922 through the experimental work of the Czech chemist Jaroslav Heyrovsky for which he received the 1959 Nobel prize. Heyrovsky could obtain information about the nature of the species in solution that were reduced at the mercury drop by measuring current while the potential of the electrode was changed. In 1925, Heyrovsky and Shikata [222] developed an automatic instrument to photographically record *i–E* curves and called it a polarograph. This term now means voltammetry at the DME. The polarograph was one of the first automated recording analytical instruments and ushered in the field of instrumental analysis [221].

At the onset, an electrochemical cell usually consists of a working electrode and reference electrode. The working electrode (WE) facilitates the transfer of electron to and fro the electrolyte while the reference electrode (RE) is used as a standard to indicate the potential of the working electrode. Using this two-electrode set up, it is extremely difficult for an electrode to maintain a constant potential while passing current to counter redox events at the working electrode. To solve this problem, a third electrode called auxiliary or counter electrode (AE) has to be introduced to pass or sink all the current needed to balance the current observed at the WE. Thus in a three electrode system, the RE only acts as a reference in measuring and controlling the working electrodes potential and at no point does any current pass through it. A three electrode electrochemical cell configuration was used in this research as depicted in Fig. 3.2

Figure 3. 2 A three electrode system electrochemical cell. WE = working electrode, RE = reference electrode and AE = auxiliary electrode

Since the pioneering work of Heyrovsky, voltammetry have undergone rapid improvement. The term "voltammetry" was first introduced in 1940 to describe experiments in which the current as a function of potential at a solid working electrode is measured [223] and this field of study has undergone tremendous changes to date. For more on the history of voltammetry the reader may consult a report by Bard and Zoski and the references therein [221]. The basic components of a modern electroanalytical system for voltammetry are a potentiostat, computer, the electrochemical cell. The following are among the leading manufactures of electrochemical workstations Bioanalytical Systems, CH Instruments, Eco Chemie, Zanher electrik, Radiometer, Brinkman Instruments (Metrohm) etc.

The general theory of voltammetry is based on the effect of the applied potential and the behaviour of the redox current which are described by several well-known laws. As summarised by Kounaves [220], the applied potential controls the concentrations of the redox species at the electrode surface $C_o^0 and\, C_R^0$ and the rate of the reaction k^0 as described by the Nernst or Butler–Volmer equations, respectively. In the cases where diffusion plays a controlling part, the current resulting from the redox process (known as the faradaic current) is related to the material flux at the electrode–solution interface and is described by Fick's law. The interplay between these processes is responsible for the characteristic features observed in the voltammograms of the various techniques. For a reversible electrochemical reaction (that is, a reaction so fast that equilibrium is always re-established as changes are made), which can be described by equation 3.3,

$$O + ne^- \Leftrightarrow R \qquad \textbf{eqn. 3.3}$$

The application of a potential E forces the respective concentrations of O and R at the surface of the electrode i.e. $C_o^0 and\, C_R^0$ to a ratio in compliance with the Nernst equation:

$$E = E^0 - \frac{RT}{nF} \ln \frac{C_R^0}{C_O^0} \qquad \textbf{eqn. 3.4}$$

Where R is the molar gas constant (8.314 J $mol^{-1}K^{-1}$), T is the absolute temperature (K), n is the number of electrons transferred, F = Faraday constant (96,485 $Cmol^{-1}$), and E^0 is the standard reduction potential for the redox couple. A change in the applied potential affects the ratio of C_R^0 / C_O^0 at the electrode

surface since it is at equilibrium, the ratio will adjust to satisfy the Nernst equation. A shift in the potential applied toward the negative will cause reduction while a positive shift will cause oxidation.

Apart from the actual electron transfer that occurs at the electrode interface, mass transport can also determine the faradiac current or general electrochemical rate. This is why we say an electrode process can be kinetic controlled or diffusion controlled. Diffusion, which is one of the means of mass transport (the others are migration and convection) is usually governed by Fick's law, which states that the flux of matter Φ is directly proportional to the concentration gradient and is given by

$$\Phi = -D_o\left(dC_o/dx\right) \qquad \textbf{eqn. 3.5}$$

Where D_o is the diffusion coefficient of O and x is the distance from the electrode surface. A more detailed treatise of this can be found in the bibliography.

Voltammetry has a variety of methods which include

- Potential sweep methods: linear and cyclic voltammetry
- Pulse methods: polarography, normal pulse voltammetry (NPV), differential pulse voltammetry and square wave voltammetry
- Controlled potential or current methods:
- Coulometry:

A brief overview of the predominating techniques used in this work will only be presented.

3.4.3.1 Cyclic Voltammetry

Cyclic voltammetry (CV) is one of the most widely used voltammetric techniques. In CV, the potential is ramped linearly at both forward and backward position at rates between 0.01–105 V/s, with the resulting current recorded as a function of potential (which is equivalent to recording current versus time). It is widely used for the study of redox processes, for understanding reaction intermediates, and for obtaining stability of reaction products. A typical CV plot is shown in Fig.3.3.

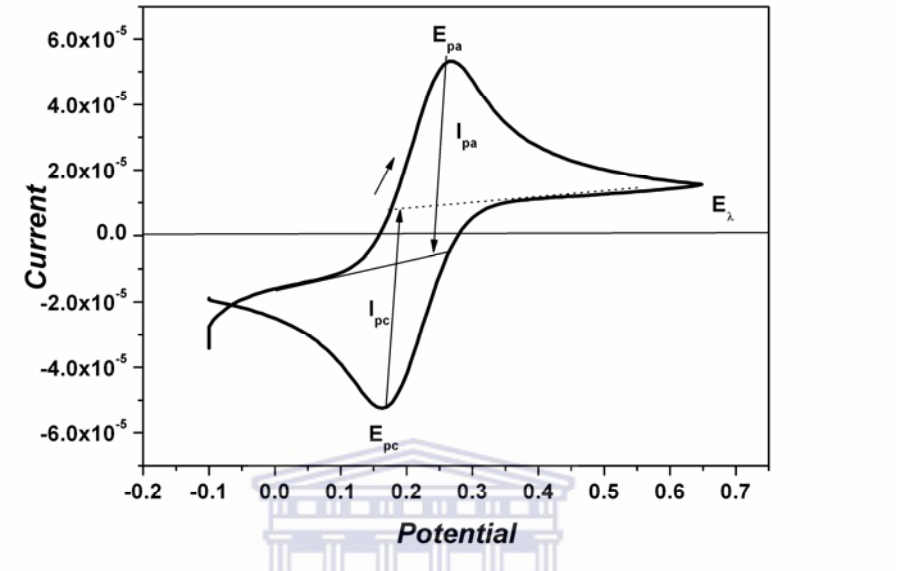

(a)

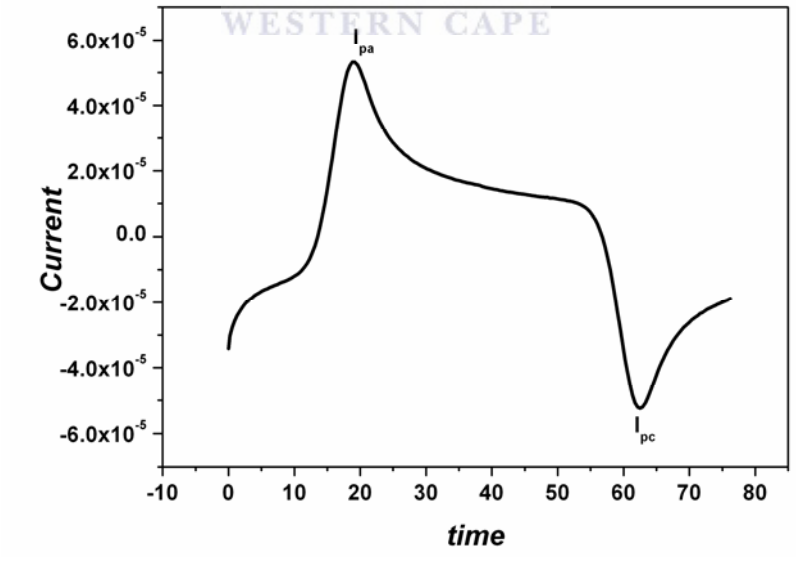

(b)

Figure 3. 3 A typical CV plot (a) Current versus potential curve (b) Current versus time curve.

In a reversible system, diffusion is the main mode of transport and semiinfinite linear diffusion conditions prevail. In cyclic voltammetry, the following are diagnostic of a reversible system $I_{p,a}/I_{p,c} = 1$

$\Delta E_p = 2.218\,RT/nF = 57/n\,mV\ at\ 298\,K$ and it is independent scan rate v.

Or $E_{p,a}\ and\ E_{p,c}$ are independent of v

$I_p \alpha v^{1/2}$ which is expressed by the Randles-Sevcik equation.

$$I_p = \left(2.69\times10^5\right)n^{3/2}AD^{1/2}v^{1/2}C \qquad \textbf{eqn. 3.6}$$

The scan rate defines the timescale of the experiment. For short timescales (high *v*), the diffusion-controlled current is increased over that for longer timescales (smaller *v*). This is due to the fact that the concentration gradient and the flux of educt to the electrode increase with increasing *v*. This relationship is used to prove diffusion control of the current as opposed to currents due to surface-bound or adsorbed redox. $\left|E_p - E_{p/2}\right| = 2\left|E_p - E_{1/2}\right| = 2.218\left(RT/nF\right)$

For a surface thin layer adsorption or strong adsorption:

$$I_p = \frac{n^2F^2}{4RT}vV[A]_{bulk} \qquad \textbf{eqn. 3.7a}$$

Where V is the volume of the thin layer

$$I_p = \frac{n^2F^2}{4RT}vA\Gamma_0 \qquad \textbf{eqn. 3.7b}$$

From the equation above, I_p is proportional to scan rate. For more details on cyclic voltammetry, these textbooks [224, 225] and other electrochemistry textbooks may be consulted

3.4.3.2 Differential Pulse Voltammetry (DPV)

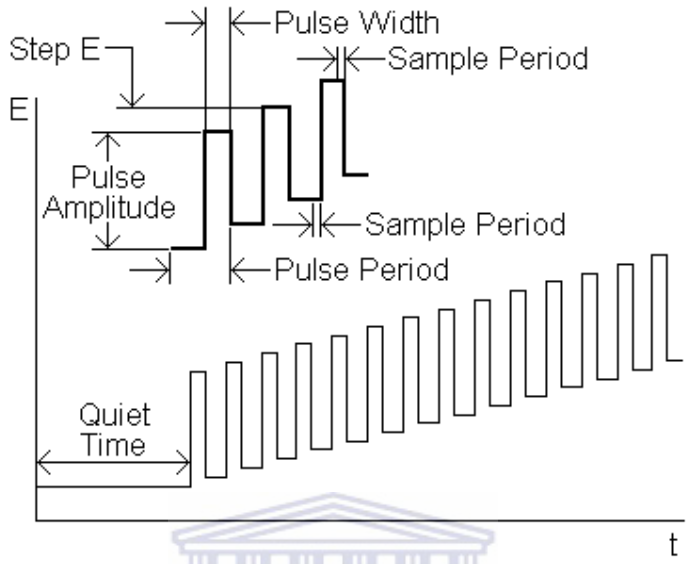

Figure 3.4 Potential wave form for Differential Pulse Voltammetry

DPV was originally applied for DME and was then called pulse polarography. The imposition of pulse potential increases the ratio of the charging (capacitive) and faradaic current as compared to that of linear sweep voltammetry. Therefore current flow is measured near the end of the pulse when the faradaic current has decayed, often to a diffusion-limited value and at this point, the charging current is insignificant. The potential wave form of DPV is shown in Fig. 3.4. For DPV in particular, the difference between two sampled currents is measured, registered just before the end of the pulse and just before pulse application as seen in the figure above. This gives the advantage of eliminating the capacitive or background current. The peak potential, E_p, for a reversible reaction is given as

$$E_p = E_{1/2} - \frac{\Delta E}{2} \qquad \textbf{eqn. 3.8}$$

Where $E_{1/2} = E^{0'} + \frac{RT}{nF}\ln\left(\frac{D_R}{D_O}\right)^{1/2}$ and ΔE is the pulse amplitude.

Another important parameter in DPV is the peak width at half height, $w_{1/2}$. For low values of ΔE or $\Delta E < (2RT/nF)$,

$$w_{1/2} = \frac{3.52RT}{nF} \qquad \textbf{eqn. 3.9}$$

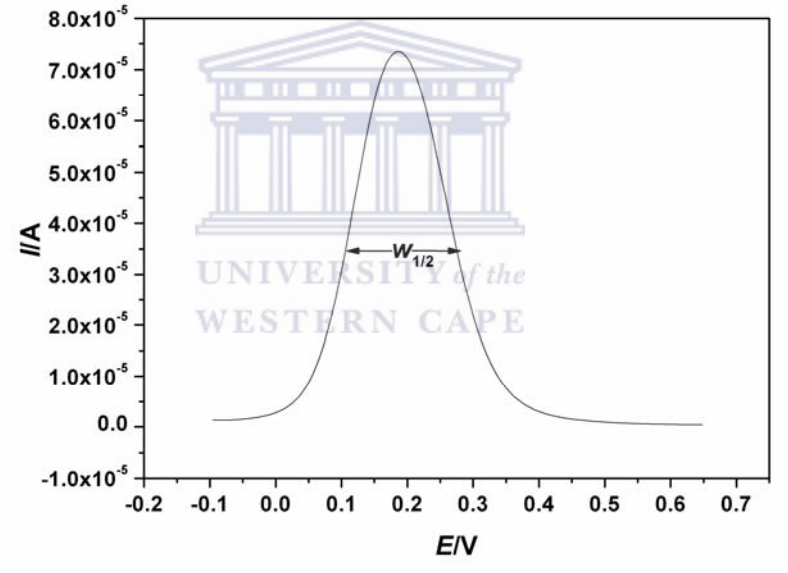

Figure 3. 5 A Differential pulse voltammogram showing the peak width at half height

And at 25 °C, the number of electron involved in a reaction, n, is 1, 2 and 3 for $w_{1/2}$ values of 90.4, 45.2 and 30.1 mV respectively. Owing to its better sensitivity, DPV can detect a faradaic current which is not observed in CV.

For quantitative purpose, the height of peak current is proportional to analyte concentration and amplitude ΔE according to Osteryoung-Parry equation given below

$$\Delta I_p = \frac{n^2 F^2 A}{4RT}\left(\frac{D}{\pi t}\right)^{1/2} C\Delta E \qquad \textbf{eqn. 3.10}$$

The term $\left(\frac{D}{\pi t}\right)^{1/2}$ implies that diffusion of analyte to the electrode is crucial for accurate determination of ΔI_p

3.4.3.3 Square Wave Voltammetry (SWV)

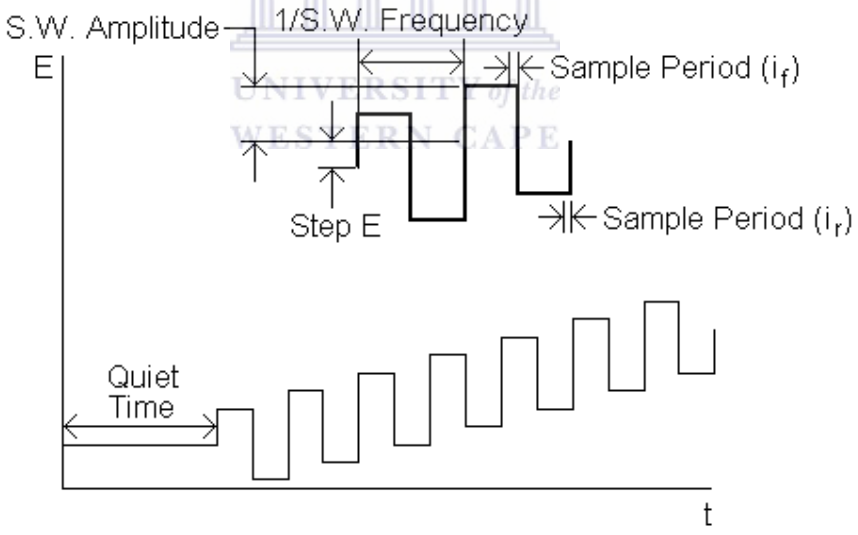

Figure 3. 6 Potential wave form for Square Wave Voltammetry

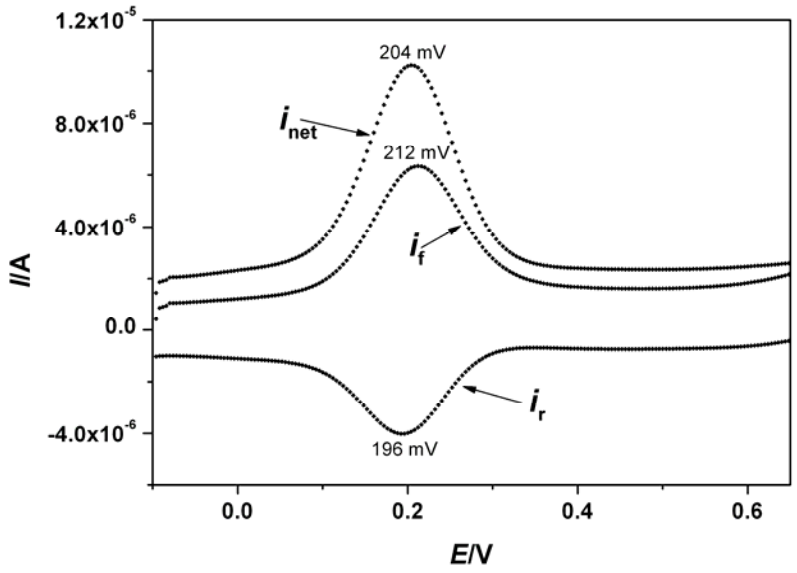

Figure 3.7 A square wave voltammogram showing the the forward (i_f), reverse (i_r) and net (i_{net}) currents

Though SWV was pioneered by Barker [226], it was the works of Osteryoung and co workers [227] that brought it to limelight. It has a slightly better sensitivity that DPV and can be used to study electrochemical processes at fast scan rates. The potential waveform (Fig. 3.6) consists of a square wave superimposed on a staircase. The current at the end of the forward pulse, i_f , and the current at the end of the reverse pulse, i_r, are both registered as a function of the staircase potential, which is midway between the potentials corresponding to the forward and backward potential steps as shown in Fig. 3.7 above. The difference, i_{net}, (i_f-i_r) is larger than each individual component in the region of the peak that is centred on the half-wave potential because i_f and i_r have opposite signs. This difference, effectively cancels the capacitive currents and thus higher scan rates are possible without background current interferences. This makes SWV a useful tool in kinetic study.

SWV is characterised by four parameters: square wave period, τ, pulse width, $t_p = \tau/2$, step height, ΔE_s and pulse height, ΔE_{sw}. The pulse width is related to the square wave frequency, $f = 1/(2t_p)$ and as the staircase step at the beginning of each cycle is ΔE_s it means that the effective scan rate is $\upsilon = \Delta E_s / 2t_p = f\Delta E_s$ .Peak Current is given by

$$\Delta i_p = \frac{nFAD_O^{1/2}C_O^*}{\pi^{1/2}t_p^{1/2}}\Delta\psi_p \qquad \textbf{eqn. 3.11a}$$

Experimentally, ΔE_s is usually kept constant while the frequency is varied. Therefore the equation above can be derived for frequency instead of pulse width, t_p, as seen below:

$$2f = 1/t_p \Rightarrow \sqrt{2f} = \sqrt{1/t_p} \Rightarrow 1.414 f^{1/2} = \left(\frac{1}{t_p^{1/2}}\right) \qquad \textbf{eqn. 3.11b}$$

$$\Delta i_p = \frac{nFAD_O^{1/2}C_O^*}{\pi^{1/2}}1.414 f^{1/2}\Delta\psi_p \qquad \textbf{eqn. 3.11c}$$

An approximate value can be obtained for $\Delta\psi_p$ from the dimensionless table, of $\Delta\psi_p$ vs. $n\Delta E_p$ *and* $n\Delta E_s$ [224].

Thus i_p *vs* $f^{1/2}$ is proportional and linear.

The experimental parameter chosen on Epsilon electrochemical workstation was ΔE_s (step E) = 4 mV and ΔE_p (amplitude) = 25 mV. Reading off these values from the $\Delta\psi_p$ table, a value of 0.47 can be estimated. Therefore the equation becomes

$$\Delta i_p = \frac{0.665nFAD_O^{1/2}C_O^*}{\pi^{1/2}} f^{1/2} \qquad \textbf{eqn. 3.12}$$

The lower detection limit of CV, DPV and SWV are 1 x 10^{-5}, 10^{-8}-5 x 10^{-8}, 1 x10^{-8} M respectively [225].

3.4.4 Electrochemical Impedance Spectroscopy

Macdonald, in his review [228], traced the foundation of electrochemical impedance spectroscopy (EIS) back to a scientist called Oliver Heaviside. Heaviside was the first person to define the term impedance. Electrochemical impedance spectroscopy is an excellent, non-destructive, accurate and rapid in-situ technique for examining processes occurring at electrode surfaces. A small amplitude ac (sinusoidal) excitation signal (potential or current), covering a wide range of frequencies, is applied to the system under investigation and the response (current or voltage or another signal of interest) is measured. This is in contrast to the 'usual' spectroscopic techniques where interactions of electromagnetic waves and materials are measured.

The measurement of impedance is only valid when the system is linear – thus the need for the small amplitude of the excitation signals in EIS. The measurement should be carried out without significantly disturbing the properties being measured. Due to the wide range of frequencies used, the complex sequence of coupled processes such as, electron transfer, mass transport, chemical reaction, etc. can often be separated and investigated with a single measurement. It is routinely used in electrode kinetics and mechanism investigations, and in the characterization of batteries, fuel cells, and corrosion phenomena [229]. It is also

widely applied in the characterization of semiconductors, organic films and very recently biosensors. The application of EIS in biosensor is relatively new [230].

A brief theory:

From Ohm's law

$$V = IR \qquad \textbf{eqn. 3.12}$$

Resistance is independent of frequency. AC current and voltage through a resistor are in phase with each other.

Suppose we apply a sinusoidal potential excitation. The response to this potential is an AC current signal containing the excitation frequency and its harmonics which is not in the same phase with the AC voltage. The resultant resistance in this case is called **Impedance** as expressed below

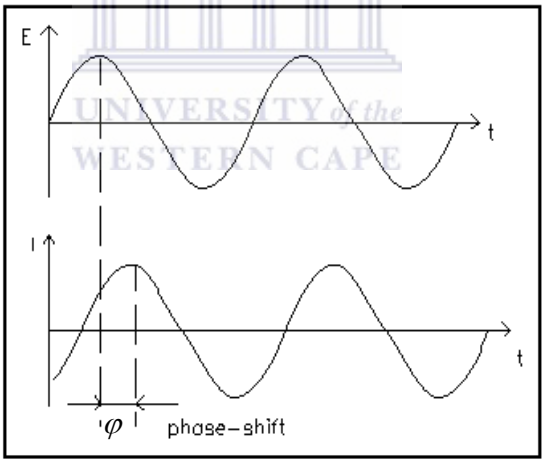

Figure 3.8 Impedance: Ac plot of voltage versus current showing the shift in phase

The system response on the application of a sinusoidal signal is given by

$$E = E_0 \sin(\omega t) \qquad \textbf{eqn. 3.13a}$$

$$i = I \sin(\omega t + \varphi) \qquad \textbf{eqn. 3.13b}$$

$$i(t) = \frac{E_0}{|Z|}\sin(\omega t + \varphi) \qquad \textbf{eqn. 3.14}$$

Where E_0 is the signal amplitude, ω = angular frequency $= 2\pi f$, f is the frequency and φ is the phase angle between the current and the potential. From equation 3.14, the current and the applied potential have the same frequency but it is phase shifted by and angle φ. Therefore the impedance of a system is the ratio of potential to current and has the unit of resistance.

$$Z = \frac{\dot{I}}{\dot{E}} \qquad \textbf{eqn. 3.15}$$

Using complex notation,

$$Z(j\omega) = Z' + jZ'' = R + \frac{1}{j\omega C} = R - j\frac{1}{\omega C} \qquad \textbf{eqn. 3.16}$$

The total impedance in an EIS measurement is the sum of the real impedance and imaginary impedance, while the modulus of the impedance $|Z|$ is given by:

$$|Z| = \sqrt{(Z')^2 + (Z'')^2} = \sqrt{R^2 + (1/\omega C)^2} \qquad \textbf{eqn 3.17a}$$

$$Z^* = Z' - jZ'' \qquad \textbf{eqn 3.17b}$$

The **resistance** R portion of the impedance is defined as the impedance to the flow of charge and it is frequency independent $Z^*(R) = Z' = R$ and $\varphi = 0$.

Z' is the real impedance which is plotted on the x axis in the Nyquist plot

The concept of double layer of charge on the electrode surface introduces another term called **capacitance**. The impedance of a pure capacitor is given as:

$$Z^*(C) = Z'' = {}^{1}\!/_{j\omega C} \qquad \textbf{eqn. 3.18}$$

Z'' is the imaginary impedance which is a measure of the **capacitance** and it is frequency dependent. $\varphi = -\pi/2$

While the phase angle φ is given by:

$$\tan\varphi = \frac{Z''}{Z'} = \frac{1}{\omega RC} \qquad \textbf{eqn. 3.19}$$

Admittance is the inverse of impedance and it is written as

$$Y = 1/Z \qquad \textbf{eqn 3.20a}$$

and

$$Y = jC\omega \qquad \textbf{eqn3.20b}$$

In EIS, data is usually presented in two major ways – the Nyquist (complex plane) plot and the Bode plot. Nyquist plot is a plot of imaginary impedance, Z", versus real impedance, Z'. The major draw back in this plot is that the frequency of each impedance point is not shown. However, frequency at some specific points of interest can be inserted for better interpretation. A typical Nyquist and Bode plots are shown in Fig. 3.9 and Fig. 3.10 respectively

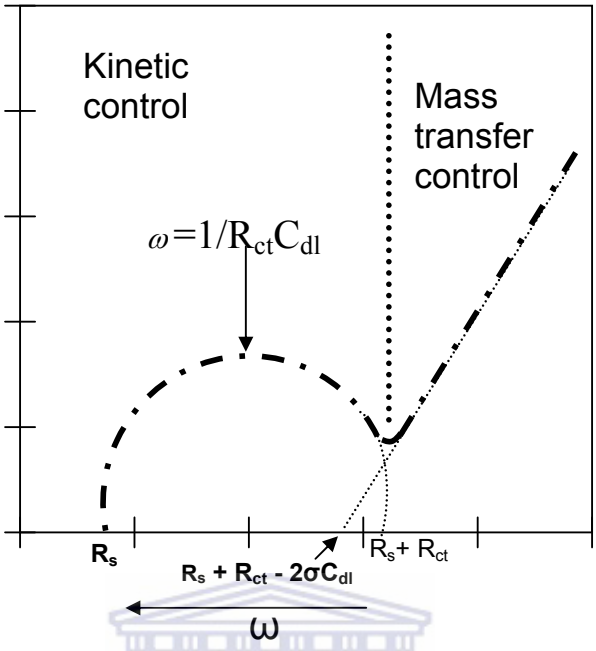

Figure 3.9 Electrochemical Impedance Spectroscopy: A Nyquist plot

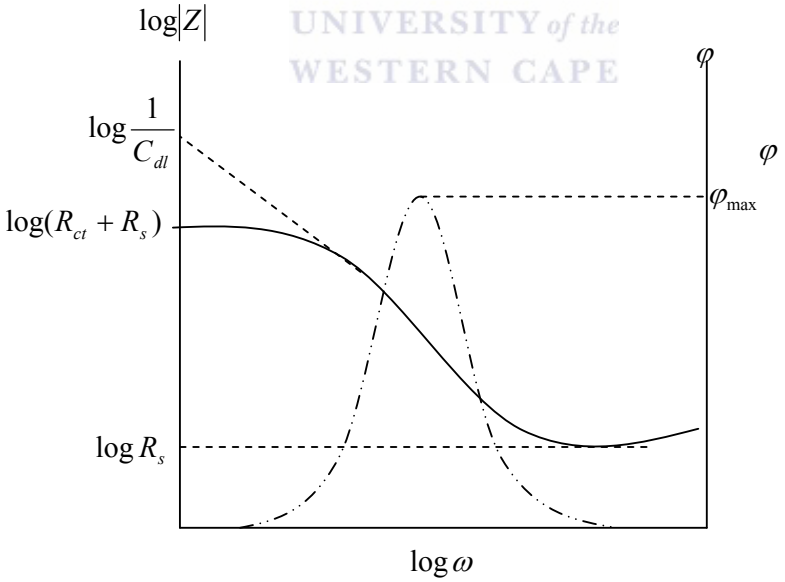

Figure 3.10 Electrochemical Impedance Spectroscopy: A Bode plot

Where R_s = solution resistance, R_{ct} is the charge transfer resistance, C_{dl} is the double layer capacitance. From the Nyquist plot above, the kinetics and the mass transport parts of the electrochemical reaction can be seen separately. The Bode plot gives direct information on the frequency and phase angle. The frequency at maximum phase is a useful parameter in determining the double layer capacitance as shown below:

$$\omega_{\phi \max} = \frac{(1 + R_{ct}/R_{sol})}{R_{ct}C_{dl}} \qquad \textbf{eqn. 3.21}$$

The electrical analogues of impedance measurement as represented by the Nyquist, Bode and also the admittance plot are presented below.

3.4.4.1 Electrical analogues of Impedance

(a) Resistance and Capacitance in series

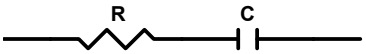

(a)

R = 500Ω and C = 1μF

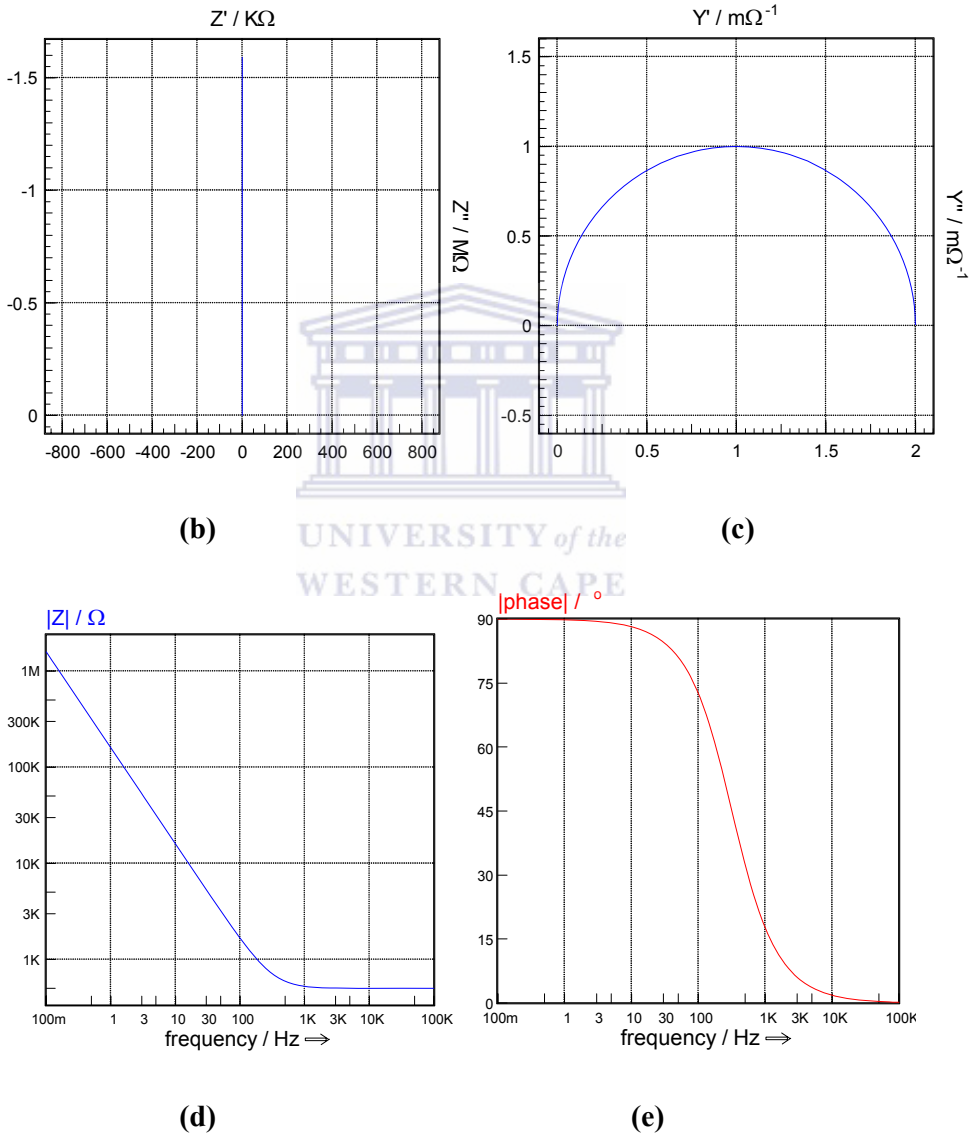

Figure 3.11 EIS graphical representations of Resistance and Capacitance in series (a) The circuit. (b) Nyquist. (c) Admittance. (d) Modulus of impedance (Bode). (e) Phase angle

The Nyquist (or complex plane plot), which is a plot of $Z''\,vs\,Z'$ consist of a straight line perpendicular to the real impedance axis. The impedance in this series connection is given by:

$$Z(j\omega) = R + \frac{1}{j\omega C} = R - \frac{j}{\omega C} \qquad \textbf{eqn. 3.22a}$$

While the magnitude of the impedance is

$$|Z| = \sqrt{R2 + \frac{1}{\omega^2 C^2}} \qquad \textbf{eqn. 3.22b}$$

And phase angle is

$$\varphi = \arctan\left(-\frac{1}{R\omega C}\right) \qquad \textbf{eqn. 3.22c}$$

The admittance of the Nyquist plot in R-C series is semicircle and is given by the equation:

$$Y(j\omega) = \frac{1}{Z(j\omega)} = \frac{R}{R - \frac{j}{\omega C}} = \frac{R}{R^2 + \frac{1}{\omega^2 C^2}} + \frac{j}{\omega C\left(R^2 + \frac{1}{\omega^2 C^2}\right)} \qquad \textbf{eqn. 3.22d}$$

A combination of Fig. 3.11d and e, that is impedance plot $|Z|\,vs\,\log freq$ and phase angle plot $\varphi\,vs\,\log freq$ gives the Bode plot. The impedance plot has only one bend or shoulder point which is characteristic of the system. The absence of the second bend/shoulder indicates the system has no charge transfer resistance or the charge transfer resistance is infinite. This circuit is usually used to for an ideally polarized electrode.

(b) Resistance and capacitance in parallel.

R = 500Ω, C= 1μF

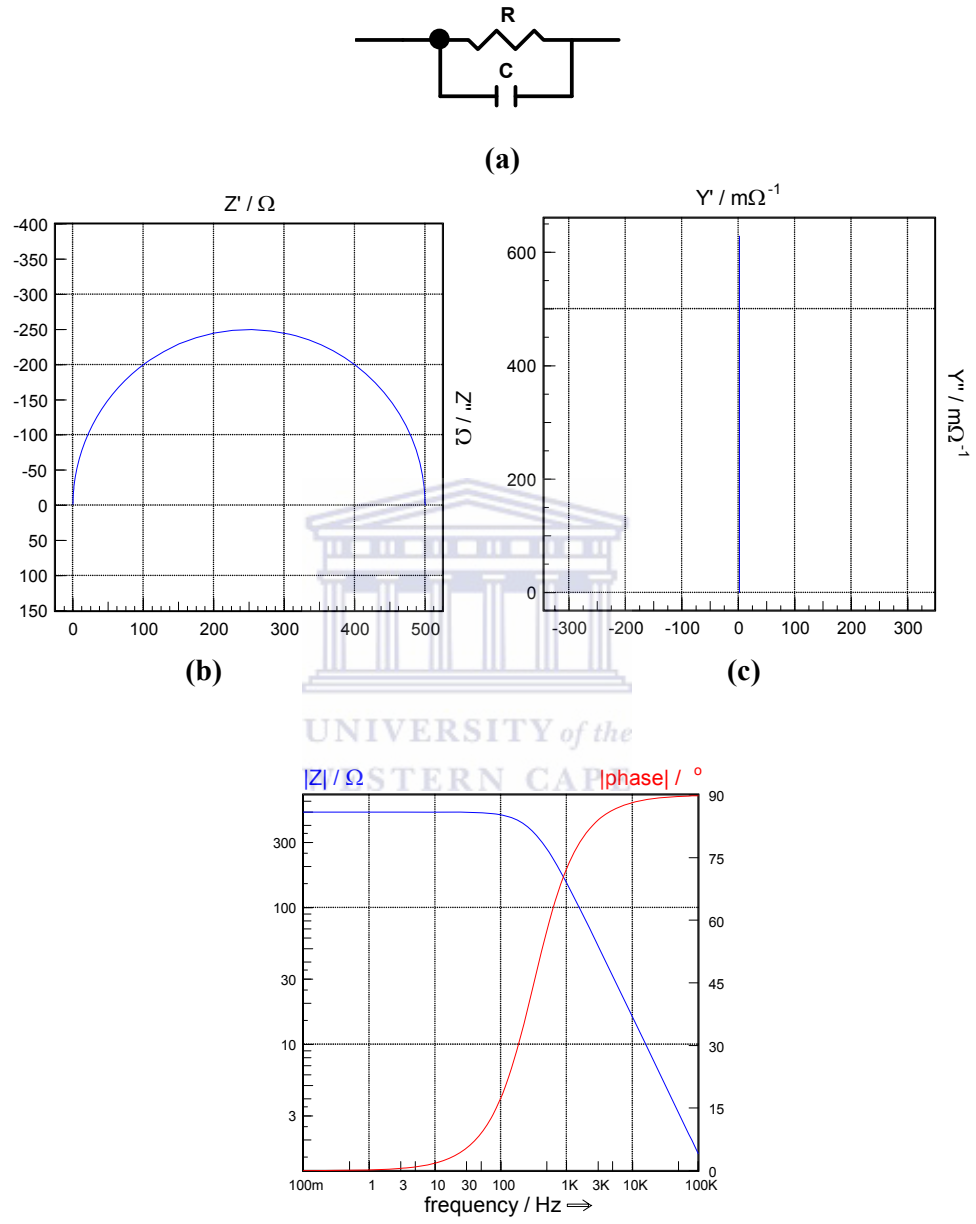

Figure 3.12 EIS graphical representations of Resistance and Capacitance in parallel (a) The circuit. (b) Nyquist. (c) Admittance. (d) Bode

The following equation is used to express the RC parallel circuit

$$Z(j\omega) = \frac{1}{\frac{1}{R} + j\omega C} = \frac{R}{1 + j\omega RC} = \frac{R}{1 + \omega^2 R^2 C^2} - \frac{j\omega R2C}{1 + \omega^2 R^2 C^2} \qquad \textbf{eqn. 3.23a}$$

It can be observed from the Nyquist plot that as frequency f or angular frequency $\omega = 0$, Z = R (R is simply the diameter of the semicircle). As $\omega \to \infty$ the impedance Z = 0.

Magnitude of impedance is

$$|Z| = \left(\frac{1}{R^2} + \omega^2 C^2 \right)^{-1/2} \qquad \textbf{eqn. 3.23b}$$

And the phase angle is

$$\varphi = \arctan(-R\omega C) \qquad \textbf{eqn. 3.23c}$$

In EIS, each RC constitute a time constant τ. That is $\tau = RC$. The frequency at maximum Z'' is given by

$$\omega_{\max} = 1/RC \qquad \textbf{eqn. 3.23d}$$

From the Bode plot, the frequency at the shoulder corresponds to that at the peak of the semicircle in the Nyquist plot.

The phase shift for RC in series and parallel are opposite. For series, as $\omega \to 0$, $\varphi = 90^0$, but for parallel, $\omega \to \infty$, $\varphi = 90^0$.

The admittance gives a straight line parallel to the imaginary impedance axis.

(c) Resistance in series with parallel RC circuit.

R_s = 50Ω, R_{ct} = 550Ω, C= 50μF

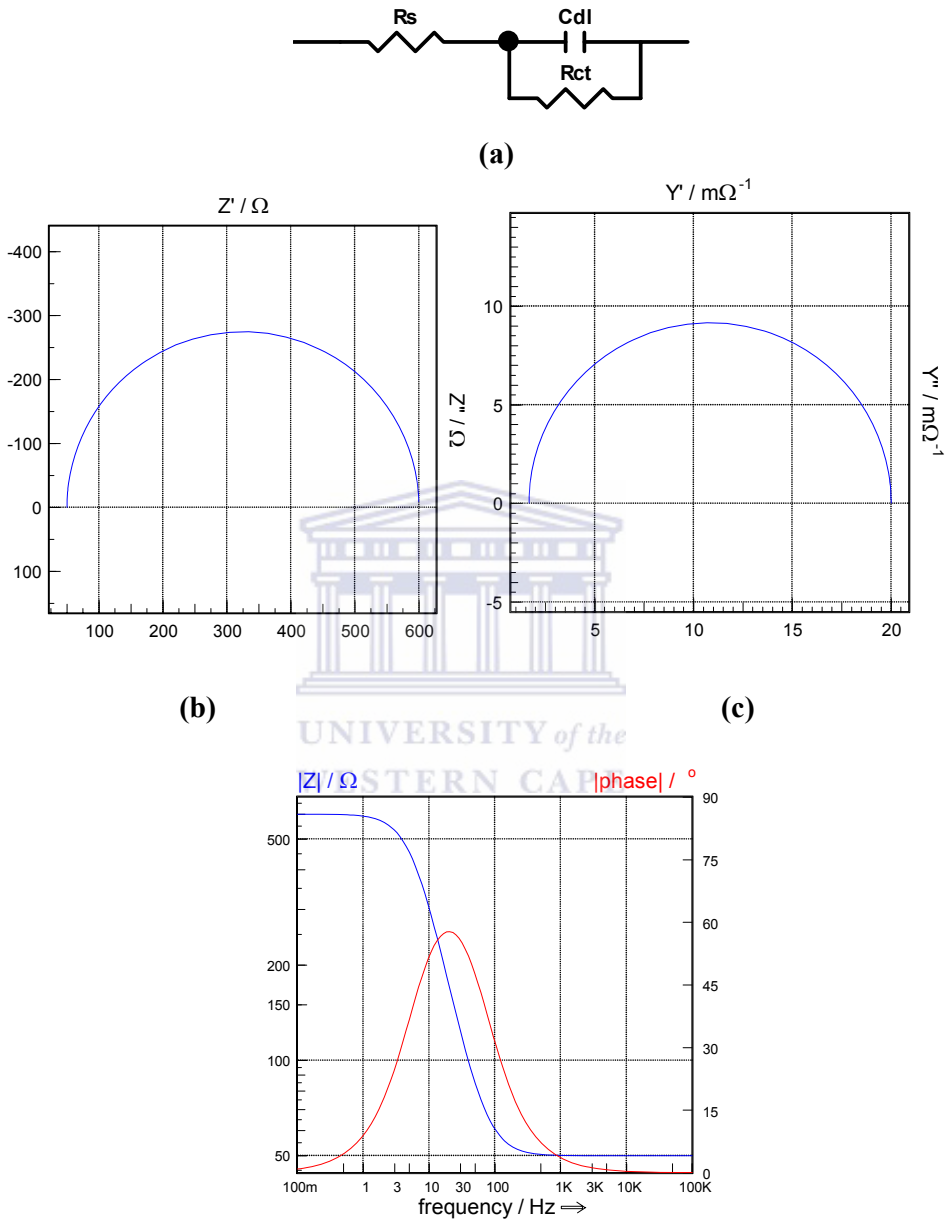

Figure 3.13 EIS graphical representations of Resistance in series with parallel RC. (a) The circuit. (b) Nyquist. (c) Admittance. (d) Bode

This circuit configuration (Fig. 3.13 and others below) introduces us to what is generally observed in an electrochemical cell. The difference between this circuit and the one discussed earlier is simply the introduction of solution resistance R_s. At the highest frequency or as $\omega \to \infty$, the impedance is R_s and at the lowest frequency or as $\omega \to 0$, the impedance Z becomes the sum of R_s and R_{ct}. The Bode plot now shows 2 shoulders. The distance between these two shoulders is the R_{ct} (see the Bode model in Fig.3.10). The capacitance in this case is called the double layer capacitance owing to the fact that some adsorption phenomena occur at the electrode surface.

The impedance is given by:

$$Z(j\omega) = R_s + \frac{1}{1/Rct + j\omega C_{dl}} \qquad \textbf{eqn. 3.24}$$

(d) The Randle's circuit

$R_s = 50\Omega$, $R_{ct} = 500\Omega$, C= 1μF and $Z_w = 2k\Omega^{-1/2}$

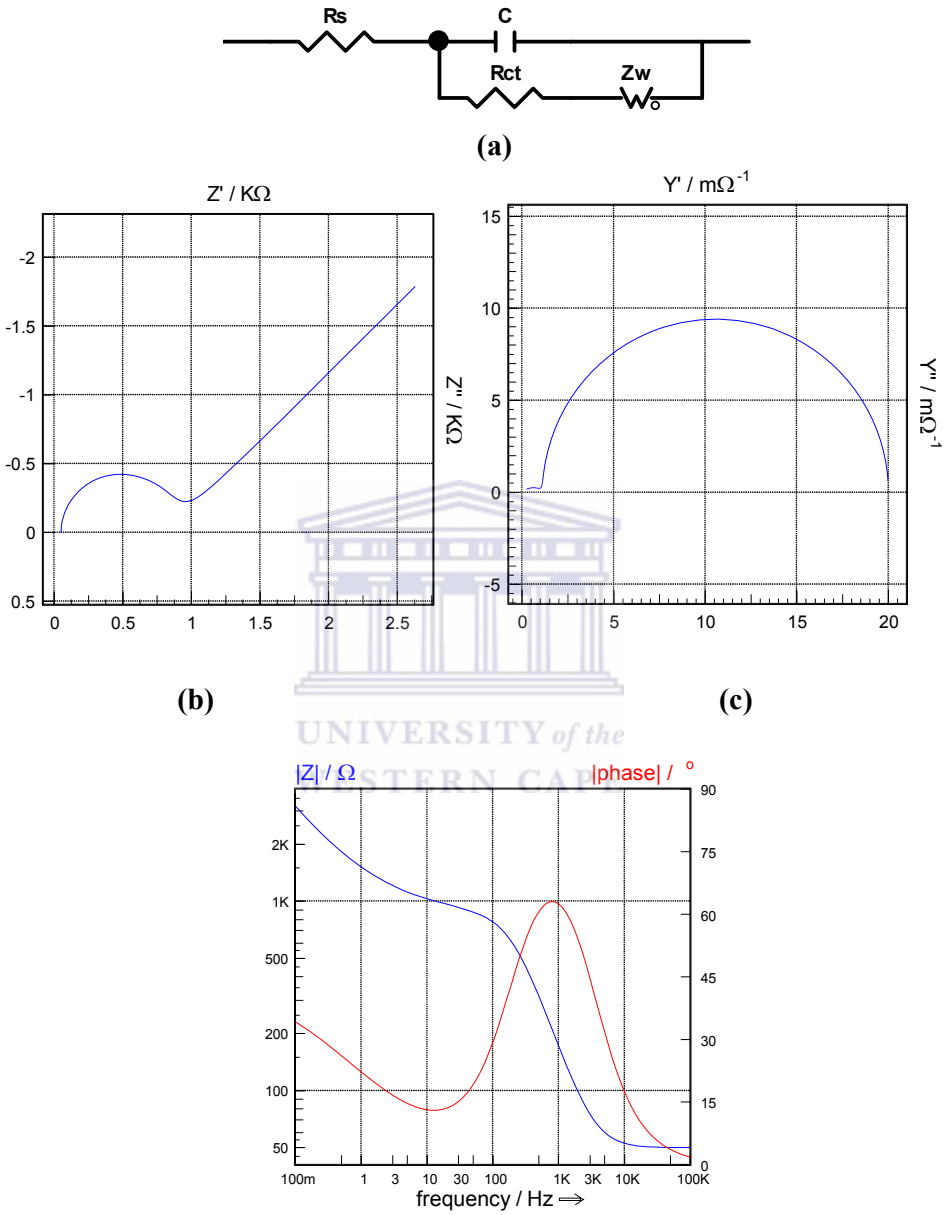

Figure 3.14 EIS graphical representations of a Randle's circuit. (a) The circuit. (b) Nyquist. (c) Admittance. (d) Bode

The inclusion of Warburg impedance (which will be discussed soon) distinguishes Fig.3.13 from. Fig.3.14. The features of the Nyquist plot has already been shown in Fig. 3.9. In the admittance plot, the straight line and semi circle in Nyquist are seen as a semi circle and a straight line respectively. Therefore the admittance plot can be used to model a Nyquist plot that is predominantly diffusion controlled.

(e) A two time constant circuit.

R_s = 238Ω, R1 = 250Ω, C1 = 10µF, R2 = 800Ω, C2 = 124µF

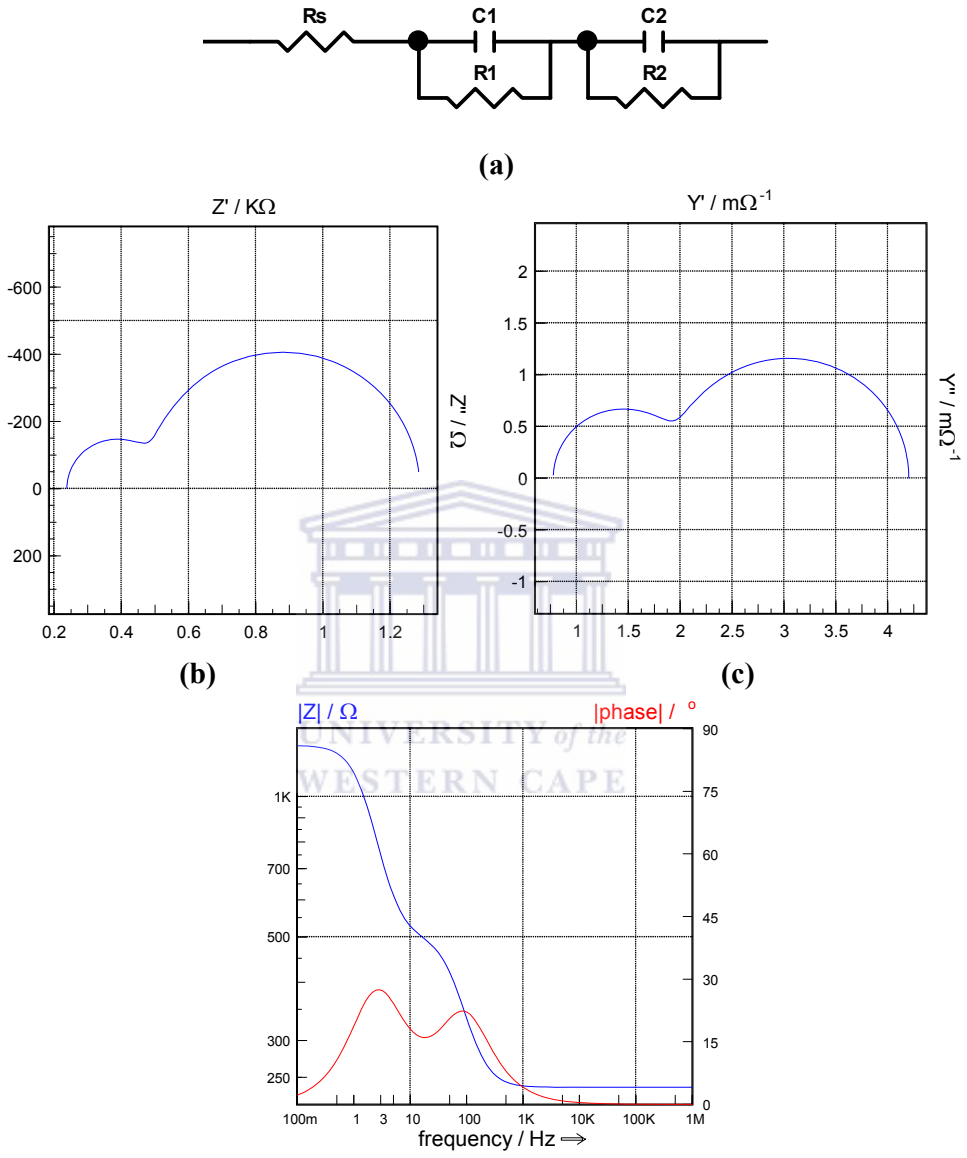

Figure 3.15 EIS graphical representations of two time constants. (a) The circuit. (b) Nyquist. (c) Admittance. (d) Bode

The two time constants is presented as two semicircles in the Nyquist, 2 phase angle peaks and three shoulders in the Bode plot. This indicates that two redox

reactions are occurring. This phenomenon was observed and discussed in chapter four.

3.4.4.2 Characteristics of a valid impedance Experiment

It is very important to validate an experiment before going ahead to interpret or fit the data. There are some certain conditions that must be obeyed for an impedance experiment to be valid. There are two general mathematical procedures which allow the verification of the impedance data. The first, called KK transform, was introduced by Kramers [231] and Kronig [232] and further developed by Bode [233]. It has now found application in EIS [234]. The other one is the Z-HIT transform used in the Zahner impedance software.

According to Lasia [235], for a valid EIS experiment, the following criteria must be met:

- **Linearity**: A system is linear when its response to a sum of individual input signals is equal to the sum of the individual responses…Electrochemical systems are usually highly nonlinear and the impedance is obtained by linearization of equations …For the linear systems the response is independent of the amplitude. It is easy to verify the linearity of the system: if the obtained impedance is the same when the amplitude of the applied ac signal is halved then the system is linear…
- **Causality**: The response of the system must be entirely determined by the applied perturbation, that is, the output depends only on the present and past input values. The causal system cannot predict what its future input will be. Causal systems are also called physically realizable systems. If the system is at rest and a perturbation is applied at $t = 0$, the response must be zero for $t < 0$. ..

- **Stability**: The stability of a system is determined by its response to inputs. A stable system remains stable unless excited by an external source and it should return to its original state once the perturbation is removed and the system cannot supply power to the output irrespective of the input. The system is stable if its response to the impulse excitation approaches zero at long times or when every bounded input produces a bounded output. Mathematically this means that the function does not have any singularities that cannot be avoided… The impedance measurements must also be stationary, that is, the measured impedance must not be time dependent. This condition may be easily checked by repetitive recording of the impedance spectra; then the obtained Bode plots should be identical.
- **Finiteness**: The real and imaginary components of the impedance must be finite-valued over the entire frequency range $0 < \omega < \infty$. In particular, the impedance must tend to a constant real value for $\omega \rightarrow 0$ and $\omega \rightarrow \infty$.

When the four conditions above are met, KK and Z-HIT transforms then hold. Depending on the section of your impedance, KK allows the calculation of the imaginary impedance from the real part using the equation below:

$$Z''(\omega) = -\frac{2\omega}{\pi}\int_0^{\infty}\frac{Z'(x)-Z'(\omega)}{x^2-\omega^2}dx \qquad \textbf{eqn. 3.25}$$

Other forms of KK transform and discourse can be found in this reference [235].

The ZHIT transform is a more recent integral approach which arguably gives a better validation than KK [236]. One advantage observed experimentally on the Thales Software by Zahner electric, is the shorter time used in its calculation. The

equation allows the calculation of the impedance data Z(f) from the Phase data φ(f)

$$\ln\left|H(\omega_0)\right| \approx const.\frac{2}{\pi}\int_{\omega_s}^{\omega_0}\varphi\ (\omega)d\ln\omega + \gamma.\frac{d\varphi(\omega_0)}{d\ln\omega} \qquad \textbf{eqn. 3.26}$$

3.4.4.3 Data Modelling and Equivalent circuit element

After data validation using the conditions and equations in the section above, the next step in impedance is to model the data. The simpler way to obtain electrochemical impedance spectroscopy parameters from a measurement is to model the electrochemical cell after an array of electrical components called the equivalent circuit (same as the circuits in section 3.4.4.1). The other way is to derive the transfer function from equations governing the kinetics of the electrochemical reaction. Modelling can be very challenging and deceptive since a model can be used for different impedance result and vice versa. This is seen as a drawback in the use of equivalent circuit modelling. A good understanding of the system in question is required. Some variations in experimental input such as potential, the raw data (good understanding of the Nyquist and Bode plots) and the expected electrochemistry should dictate ones model and not what you want it to be. Usually the errors observed for each circuit element can be a guide. Also SIM fitting software (Thales, Zahner) gives the significance of each element in the overall process. A very low significance may indicate the redundancy or absurdity of the element in question.

The fitting of data to a model is usually accomplished by a complex nonlinear least-squares (CNLS) program based on some intrinsic choice of

statistical weights methods depending on the software used. This is a nonlinear least-squares fit of the real and imaginary parts, or magnitude and phase-angle of the experimental impedance/admittance to a given model. In general, the sum of squares

$$S = \sum_{i=1}^{N} \left\{ w_i' \left[Z_i' - Z_{i,calc}' \right]^2 + w_i'' \left[Z_i'' - Z_{i,calc}'' \right]^2 \right\} \quad \textbf{eqn. 3.27}$$

must be minimized, where Z'_i and Z_i'' are the real and imaginary parts of the experimental impedances at the frequencies ω_i, $Z'_{i,calc}$ and $Z''_{i,calc}$ are the values calculated from a given model, w'_i and w_i'' are the statistical weights of the data, and the summation runs over all N experimentally used frequencies.

The CNLS fit must be initialised by some initial sets of values called seed values. Owing to the iterative nature of the algorithm this initial choice of the seed values are very important and they must lie relatively close to the real values, otherwise the CNLS method may become divergent. To get these seed values, a simpler model can first be used to determine some parameters which can then be fed into the more complex model. Also by the inspection of the Nyquist plot, seed values such as solution resistant, R_s and R_{ct} can be read from the real impedance axis (x axis). A rough capacitance value can be obtained using $\omega_{\max} = 1/R_{ct}C_{dl}$ or $Z'' = 1/j\omega C$ from the imaginary impedance.

Programs used in impedance modelling and fitting are easily available. Most companies manufacturing electrochemical workstation which includes Impedance module have their peculiar software. Some examples include Thales (Zahner), ZMAN (Zahner) Zview (Scribner Associates), Gamry etc.

The basic impedance or circuit elements used are shown in table below

Table 3.2 General Circuit elements

Circuit element	**Formula**	**Name**
R	$Z = R$	Resistance
C	$Zc = 1/j\omega C$ or $C = \varepsilon.\varepsilon_0 A/d$	Capacitane
CPE	$A_0(j\omega)^{-\alpha}$	Constance phase element (Psuedo capacitance)
W	$Zw = \sigma/\sqrt{j\omega}$	Warburg diffusion element

The solution resistance R_s is as a result of the finite conductance of the ions in the bulk electrolyte solution. The charge transfer resistance R_{ct} reports the interfacial charge transfer process that occurs at the electrode/electrolyte interface. It measures the reluctance to the flow of charge at the interface due to electrostatic repulsion or steric. R_{ct} can also be a measure of the energy or rate of the redox process. The magnitude of R_{ct} varies as the electrochemical process transits from irreversibility to reversibility.

Capacitance, usually the double layer capacitance in EIS can be modelled using the full capacitance C or the constant phase element CPE. C_{dl} models the double layer properties which includes thickness and dielectric. In real experiment, a value lower than $\pi/2$ is often observed owing to a microscopic roughness of the electrode, slow adsorption of ions and inhomogeneities of the adsorbed layer. In order to model this anomalous behaviour, the double layer capacitance is expressed in terms of the distributive element CPE given by

$$Z_{CPE} = A_0(j\omega)^{-\alpha} \qquad \textbf{eqn. 3.28}$$

Where A_0 and α are frequently independent parameter and $0 \le \alpha \le 1$. For α =1, CPE is an ideal capacitor; for α =0, CPE is an ideal resistor and for α =0.5, CPE is infinite Warburg impedance. CPE is observed as a depressed semi circle on the Nyquist plot as seen below

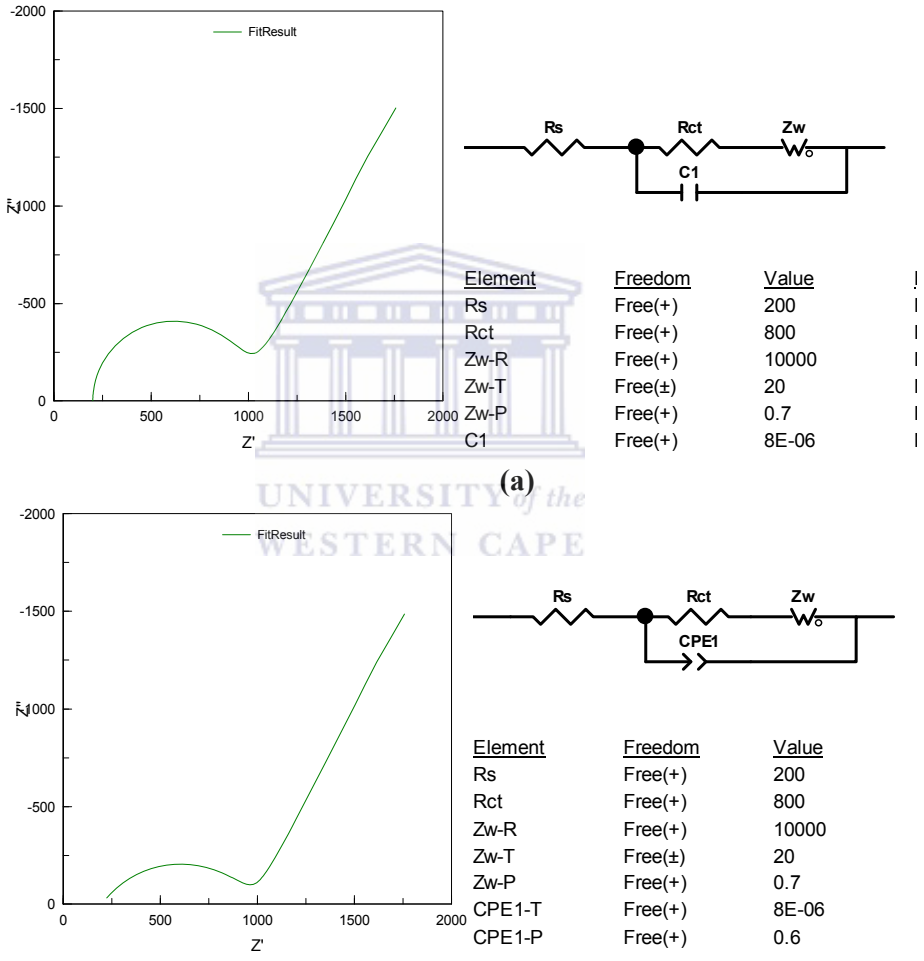

Figure 3.16 Observation of a depressed semi circle from simulated Nyquist plot with the equivalent circuit. (a) Pure capacitance. (b) Constance phase element

Another distributive element introduced by J R Macdonald [237] is the Warburg impedance used to describe the mass transport portion of an electrochemical reaction it is written as Z_w.

3.4.4.4 Faradaic Impedance

In the presence of electroactive specie, charge transfer at an electrochemical interface occurs at the end of a succession of more or less coupled elementary phenomena:

- transport of electroactive species in the bulk of the solution, often associated with chemical reactions in the bulk phase.
- adsorption of the electroactive species on the electrode
- electrochemical and chemical interfacial reactions.

Adsorption and reactions take place on the electrode surface, but mass transport is a homogeneous phase phenomenon. The aim of the electrochemist is to be able to study each elementary phenomenon in isolation from the others. Hence, a technique which is able to extract the data which allows these phenomena to be separated has to be used. Electrochemical impedance spectroscopy is the technique that allows such calculations.

The general model for faradaic impedance can be written in two ways: in terms of the total resistance Rs and capacitance Cs or in terms of charge transfer resistance R_{ct} and Z_w. It can also be explained in terms of Fig 3.17

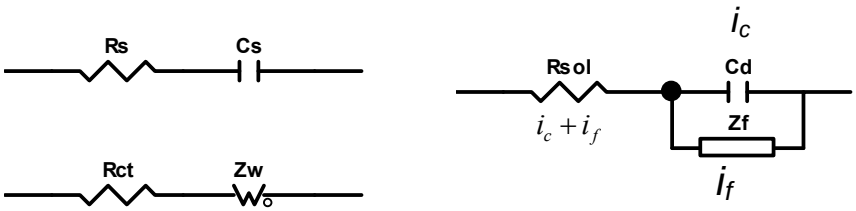

Figure 3.17 General equivalent circuit representation of a faradaic impedance process

Rs (resistive impedance) + **Cs** (capacitive impedance) = $\mathbf{Z_f}$ total faradaic impedance.

And $\mathbf{R_{ct}}$ = charge transfer resistance = Charge transfer Kinetics, Zw = Warburg impedance = Mass transfer effect.

$$Rs = R_{ct} + \sigma / \omega^{1/2} \qquad \textbf{eqn. 3.28}$$

$$C_s = \frac{1}{\sigma\omega^{1/2}} \qquad \textbf{eqn. 3.29}$$

Warburg impedance and coefficient

Since σω is common to equation 3.28 and 3.29, the total faradaic impedance can thus be written as

$$Z_f = R_{ct} + \left[\sigma\omega^{1/2} - j(\sigma\omega^{1/2})\right] \qquad \textbf{eqn. 3.30a}$$

The term in the square bracket represents the Warburg impedance Zw and thus can be written as

$$Z_f = R_{ct} + Z_w \qquad \textbf{eqn. 3.30b}$$

The modulus of the total faradaic impedance can be written as

$$\left|Z_f\right| = \sqrt{R_{ct}^2 + 2\sigma^2/\omega} \qquad \textbf{eqn. 3.31}$$

The term σ is called the Warburg coefficient and it can be calculated from equation 3.32.

$$\sigma = \frac{RT}{n^2F^2A\sqrt{2}}\left[\frac{1}{C_R\sqrt{D_R}} + \frac{1}{C_O\sqrt{D_O}}\right] \qquad \textbf{eqn. 3.32}$$

C_R, C_O, D_R, D_O are the concentration of the reduced and oxidized specie, and the diffusion coefficient of the reduced and oxidized respectively. For an adsorbed reversibly electroactive specie, $C_R = C_O \; and \; D_R = D_O$. σ can be used to obtain C_{dl} from Nyquist plot if it is possible to extrapolate the Warburg diffusion line to the x axis as shown in Fig .3.9. Equation 3.33 relates phase angle to σ:

$$\cot\phi = 1 + R_{ct}\sqrt{\omega}/\sigma \qquad \textbf{eqn. 3.33}$$

As can be seen from equation 3.28 and 3.29, Warburg impedance, Z_w consists of a resistance and a capacitance part. Since resistance is related to the real impedance while capacitance is related to the imaginary impedance, the Warburg impedance thus have both in-phase Z'_w and out of phase Z'' quantities i.e.

$$Z'_f = R_{ct} + \sigma\omega^{-1/2} \qquad \textbf{eqn. 3.34a}$$

$$Z''_f = -\sigma\omega^{-1/2} \qquad \textbf{eqn. 3.34b}$$

Therefore a plot of Z'_f and of $-Z''_f$ vs. $\omega^{-1/2}$ should give a slope σ and for both Z'_f and $-Z''_f$ and an intercept of R_{ct} for Z'_f as depicted in Fig. 3.18.

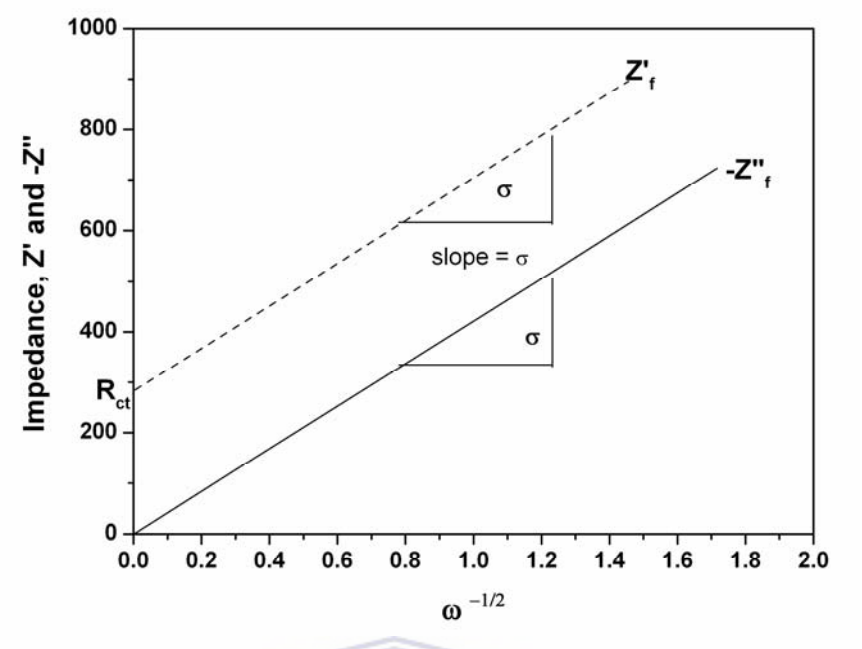

Figure 3.18 Determination of Warburg coefficient, σ, from a plot of impedance versus the iverse of the square root of radial frequency ($\omega^{-1/2}$)

σ is a useful parameter in determining the quality and swellings of coating

Charge transfer Resistance R_{ct}

For **reversible** reactions, the electron transfer is very facile and thus a semi circle may not be observed. In such a case, $R_s \approx R_{ct}$. The system is limited by mass transport because it is the slower step. Therefore in the Nyquist plot, a straight at 45 degrees to the real impedance axis will be observed. As the rate of electron transfer becomes slower as in the case of slower reactions or **quasi-reversible** reactions, R_{ct} will begin to evolve. It will get to a point at which the diameter of the semicircle (R_{ct}) becomes infinitely large as the reaction tends towards **irreversibility**.

A small ac potential is needed to maintain linearity in impedance measurement and it is usually not more than 10 mV. However, the value of dc

potential (bias potential) is supposed to be the equilibrium potential peculiar to the electroactive species. However, because fast electron transfer reactions have small over potential, and also the ease of using concentration rather than activity from experimental point of view, the formal potential is used. At equilibrium potential, the redox process is optimized and there is no net current. Such a choice is imperative so as to conform to some assumptions made in kinetic equations such as that of Butler-Volmer equation (3.35)

From Butller – Volmer equation

$$I(t) = nFA\left[k_a^0 C_R e^{\alpha nFE/RT} - k_c^0 C_O e^{-(1-\alpha)nFE/RT}\right] \qquad \textbf{eqn 3.35}$$

(I(t) = total current; n = number of electrons; F = Faraday constant; k_a and k_c = rate constant of anodic and cathodic reaction respectively; C_R and C_O = concentration of the reduced and oxidized specie on the electrode respectively; A = area of electrode and α = transfer coefficient).

At formal potential, using standard rate constant k^{Θ}, the term overpotential can be introduced. By differentiating this equation with respect to the potential, for a steady state value of the potential, we get:

$$R_{ct}^{-1} = \frac{n^2F^2}{RT} A\left[\alpha k_a^0 C_R e^{\alpha nFE/RT} + (1-\alpha) k_c^0 C_O e^{-(1-\alpha)nFE/RT}\right] \qquad \textbf{eqn. 3.36a}$$

$$R_{ct}^{-1} = \frac{nFI_o}{RT} \qquad \textbf{eqn. 3.36b}$$

$$Z_{Rct} = R_{ct} = \frac{RT}{nFI_o} \qquad \textbf{eqn. 3.36c}$$

I_o is the exchange current. R = gas constant, F = Faraday constant, n = number of electrons.

$$I_o = nFAk_{ct}[S] \qquad \textbf{eqn. 3.37}$$

K_{ct} is the charge transfer rate constant, [S] is the bulk concentration in mol/cm^3

3.5 General Experimental

3.5.1 Solutions

10 mM saline phosphate buffer solution (PBS) pH 7.2 containing Na_2HPO_4, KH_2PO_4 and 0.3 mM KCl was prepared. In the absence of 0.3 M KCl, the buffer is referred to as phosphate buffer. 5 mM (1:1) solution of $K_3Fe(CN)_6$ and $K_4Fe(CN)_6$ ($[Fe(CN)_6]^{3-/4-}$) was prepared in 100 mL of 10 mM phosphate buffer solution at pH 7.2. 100 μM of DNA stock was prepared in Tris-EDTA buffer (pH 8.00) and stored at -20 °C. Working DNA solutions were prepared by diluting the stock solution to the desired concentrations in phosphate buffer solution, stored at 4 °C and not used when older than 4 weeks. Hybridisation was done in phosphate buffer saline (PBS).

3.5.2 Electrochemical cell

A three electrode system was used to perform all electrochemical experiments. Glassy carbon electrode (GCE) with diameter 0.3 cm was used as the working electrode; platinum wire as the counter electrode, and Ag/AgCl (3M Cl^-) as the reference electrode. All solutions were de-aerated by bubbling argon through it for 5 minutes.

3.6 Experimental: Chapter 4

3.6.1 Material

Oligonucleotides (referred to as DNA) of 21 bases with the sequence below was Amino modified probe: NH_2-5′-GAGGAGTTGGGGGAGCACATT-3′

Complementary: 5′-AATGTGCTCCCCCAACTCCTC-3′

Nickel (II) salicylaldimine G2 metallodendrimer: The G2-metallodendromer was prepared using the generation 2, salicylaldimine ligand, DAB-$(salicyl)_8$. The synthesis of both the ligand and its nickel complex is described below [82, 238]:

3.6.2 Preparation of DAB-$(salicyl)_8$ ligand, L1

The commercially available amino functionalized polypropylene imine dendrimer, $DAB^{-}(NH_2)_8$ (0.5 g, 1.6 mmol) was added to dry toluene (10 ml) in a Schlenk tube, under nitrogen. Salicylaldehyde (1.56 ml, 12.8 mmol) was added to the solution and the mixture was allowed to stir for 72 hours at room temperature. The solvent was evaporated on a rotary evaporator yielding a yellow oily residue. The residue was dissolved in 20 ml of CH_2Cl_2 and the resulting solution extracted with water (5x30ml). The dichloromethane layer was dried over magnesium sulphate after which the latter was filtered off. The filtrate was evaporated under vacuum producing a yellow oil, yield, 80%.

Anal. Found : C, 71.87%; H, 8.28%; N, 11.76%. Calc. for $C_{96}H_{128}N_{14}O_8$;: C, 71.79%; H, 8.03%; N, 12.21%.

^{1}H NMR (200 MHz, $CDCl_3$) : δ1.31 (br s, 4H); 1.61 (m, 8H); 2.45 (br t, 4H); 2.32 (t, 8H; 3.60 (t, 8H); 2.39 (t, 16H), 2.61 (m, 16H), 3.61 (t, 16H), 7.39-7.53 (br m, 24H); 8.31 (s, 8H).

^{13}C NMR (50 MHz, $CDCl_3$) : δ24.1, 24.8, 30.1, 52.1, 52.2, 54.0, 57.3, 116.9, 118.7, , 131.1, 131.9, 161.2, 164.8;

IR (neat oil), ν(O-H) cm^{-1} : 3058(s), ν(C-N) 1664 cm^{-1} , ν(C-O) 1279 cm^{-1}.

MH^+ = 1607.13 (ESI-MS).

3.6.3 Synthesis of nickel metallodendrimer

The DAB-$(salicyl)_8$, G2 salicylaldimine ligand, **L1** (0.5 g, 0.31 mmol) was dissolved in ethanol (10 ml) in a round bottom flask, under nitrogen. Nickel acetate tetrahydrate (0.30 g, 1.24 mmol) was then added to the solution. The reaction mixture was refluxed for 24 hours under nitrogen. During this time a green solid precipitates out of solution. The precipitate was filtered by vacuum filtration and washed with ethanol, yielding green powder. The product was dissolved in dichloromethane and the solution filtered. The solvent was removed from the filtrate leaving a green solid which dried under vacuum. Yield, 80%

M.p. 210-215 °C (decomposition without melting).

Anal. Found: C, 58.04%; H, 6.25%; N, 7.08%. Calc. for $C_{132}H_{192}N_{14}O_8Ni_4 \cdot CH_2Cl_2$,

C, 58.77%; H, 6.24%; N, 6.79%.

IR (Nujol): ν(C=N) 1632cm^{-1}(s); ν(C-O) 1344 cm^{-1}(m). ESI Mass Spectroscopy: MH^+ *m/z* 1834.2

3.6.4 Solutions

10 mM PBS, 5 mM $Fe(CN)_6]^{3-/4-}$ and DNA stock were prepared as in section 3.5.1. 250 μL of 10 mM stock of the nickel metallodendrimer (Molecular mass = 1832.83 g mol^{-1}) was prepared in dichloromethane (DCM) solution.

3.6.5 Electrochemical measurements

All electrochemical (voltammetric) experiments were recorded with BASi 100B electrochemical work station (LG Fayette). For square wave voltammetry (SWV) measurements, amplitude of 25 mV and frequency of 15 Hz were applied. For all differential pulse voltammetry (DPV), pulse amplitude of 50 mV, sample width of 10 msec, pulse period of 200 msec were used. Electrochemical impedance spectroscopy (EIS) measurements were recorded with VoltaLab PGZ 402 (Radiometer Analytical France) at voltage amplitude of 10 mV and with frequency range from 100 kHz to 100 mHz.

3.6.6 Preparation of Dendrimer-modified electrode (GCE/Dendrimer) and biosensor

Glassy carbon electrode was first polished with 0.3 and 0.05 micron alumina powder rinsed with water and then sonicated in water for 4 minutes. Prior to modification with the dendrimer, a potential range where the electrode shows no electrochemistry (redox peaks) in the PBS was determined using cyclic voltammetry (CV) and SWV. The stability of this electrode in the chosen range was confirmed by EIS. The cleaned GCE was immersed in dichloromethane for 3 minutes, and then it was dried with argon. 8 μL of the dendrimer solution was

then drop coated on the GCE surface and allowed to dry under argon for at least 1 hour. The electrochemistry of the dendrimer-modified electrode was studied in PBS and ferrocyanide solutions using voltammetric and EIS techniques.

For the biosensor, the GCE/Dendrimer electrode was rinsed with PBS and then dried with argon. A 15 μL of 2 μM probe single strand DNA (ssDNA) solution was dropped on the modified electrode and was left to immobilize for 1hr in an oven at a temperature of 26 °C. The DNA biosensor thus prepared was rinsed with water and PBS successively to remove any unbound probe ssDNA. The biosensor was either used immediately or stored at 4 °C when not in use. The biosensor was characterised by voltammetry and EIS.

3.6.7 Detection of complementary DNA

10 μL of 5 nM of the target ssDNA was dropped on the biosensor surface and hybridisation was allowed to take place for 35 minutes in an oven at a temperature of 37 °C. The hybridised biosensor was washed thoroughly with water and PBS successively to remove unbound target ssDNA before measurement. The response of the biosensor to the target ssDNA was measured in PBS in the presence or in the absence of $[Fe(CN)_6]^{3-/4-}$ redox probe using voltammetry and EIS. For the second hybridisation, another 10 μL of the ssDNA target solution was dropped on the surface of the same biosensor as above. To denature, the hybridised biosensor was dipped into 50 mM NaOH for 5 min or in hot water (95 °C) for 10 min which is another method of denaturation. Electrochemical measurements were carried out after denaturation. For the purpose of total cleaning, the biosensor was simply rinsed in a DCM solution for

2 minutes to remove the metallodendrimer, and then the usual electrode cleaning procedure was carried out.

3.7 Experimental: Chapter 5

3.7.1 Materials

DNA 20mer sequence:

Probe: SH-5′-AAGCGGAGGATTGACGACTA-3′

Complementary: 5′-TAGTCGTCAATCCTCCGCTT-3′

Generation 4 (G4) poly(propylene imine) dendrimer (which was used as received) and $HAuCl_4$

3.7.2 Solutions

10 mM PBS and 0.1 M phosphate buffer; 5 mM $Fe(CN)_6^{3-/4-}$ and DNA stock were prepared as in section 3.5.1. For pH studies, 0.1M phosphate buffer solutions of pH ranging from 2 to 12 (corrected with HCl and NaOH) were prepared. Solutions of 6 mM G4 PPI (Molecular mass = 3514 g/mol) and 5 mM $HAuCl_4$ were prepared in water. 2 μM solution of thiolated DNA (SH-DNA) was prepared from stock. Prior to use, the disulphide bond of the SH-DNA probe was cleaved using dithiothreitol (DTT) as follows. 200 μL of 100 mM DTT was added to 100 μL of 100 μM solution of thiolated DNA (SH-DNA) and eluted twice using PBS according to the NAP^{TM}-10 column manufacturer's instructions. The concentration of the eluted SH-DNA was determined by nanodrop spectrophotometer.

3.7.3 Equipment and Apparatus

All voltammetric experiments were performed on an Epsilon (BASi) electrochemical workstation (LaFayette) with oxidative scan direction except stated otherwise. Square wave voltammetry (SWV) measurements were performed by applying an amplitude of 25 mV and frequency of 15 Hz. Differential pulse voltammetry (DPV) measurements were recorded using pulse amplitude of 50 mV, sample width of 10 msec, pulse period of 200 msec. EIS measurements were recorded with Zahner IM6ex Germany, at a perturbation amplitude of 10 mV within the frequency range of 100 kHz to 100 mHz. FE-SEM images were captured using a field emission electron microscope (JEOL- JSM 7500F) fitted EDAX CDU Leap Detector. DNA concentration was determined using nanodrop ND-1000 Spectrophotometer.

3.7.4 Preparation of GCE/PPI, GCE/AuNP and GCE/PPI-AuNP modified electrodes

For all electrodeposition processes, the GCE was mechanically polished with 0.3 and 0.05 micron alumina powder rinsed with water and then ultrasonicated in water for 4 minutes. The cleanliness of the surface was verified in PBS with potential range of -100 mV to +650 mV where no peak was expected. GCE/Au-NP was prepared by electrodepositing AuNP on clean GCE surface by cycling the electrode potential from -350 mV to +1000 mV for 10 cycles at 50 mV/s using 2.5 mM aqueous $HAuCl_4$ as the electrolyte. GCE/PPI was prepared as described for GCE/AuNP except that 3 mM PPI aqueous solution as electrolyte instead of $HAuCl_4$. The preparation of GCE/PPI-AuNP electrode system involved

the simultaneous cyclic voltammetric deposition of PPI and AuNP on a clean GCE from an argon-degassed electrolyte consisting of 6 mM PPI and 5 mM $HAuCl_4$ in a 1:1 v/v ratio. The GCE/AuNP, GCE/PPI and GCE/PPI-AuNP modified electrodes were rinsed with water and characterised by CV, SWV and EIS; and stored at 4 °C when not in use. However, Screen printed carbon electrode (SPCE) was used as substrate (under the same electrodeposition conditions) for FE-SEM measurements.

3.7.5 Immobilisation of probe DNA (GCE/PPI-AuNP/ssDNA) and hybridisation with target DNA (GCE/PPI-AuNP/dsDNA)

The GCE/PPI-AuNP/ssDNA nanobiosensor was prepared by dropping a 20 μL solution of 2 μM thiolated single strand probe DNA (or probe ssDNA) onto the surface of a previously argon-dried GCE/PPI-AuNP, and was left to immobilize for 3 h at 25 °C and then successively rinsed with water and phosphate buffer solution to remove any unbound probe ssDNA. The biosensor was stored at 4 °C when not in use. The biosensor was characterised by voltammetry and EIS in PBS and 5 mM (1:1) ferro/ferricyanide solution $Fe(CN)_6^{3-/4-}$, respectively.

The bio-recognition experiments, was carried out in 1 mL of PBS containing six different concentrations of complementary ssDNA (target ssDNA) ranging from 0.01 to 5 nM. For each hybridisation step (each target ssDNA concentration), the nanobiosensor (GCE/PPI-AuNP/ssDNA) was immersed in the target ssDNA solution for 45 min at 38 °C. The hybridised biosensor (i.e. GCE/PPI-AuNP/dsDNA) was washed thoroughly with water and phosphate

buffer solution to remove unbound target ssDNA before taking measurements. The impedimetric responses of the biosensor to the target ssDNA were measured in PBS using $Fe(CN)_6^{3-/4-}$ as the redox probe. However a single concentration of 0.05 nM complementary DNA was used to investigate the voltammetric response.

3.8 Experimental: Chapter 6

3.8.1 Materials

DNA 21mer sequence were as follows

Probe: 5′-GAGGAGTTGGGGGAGCACATT-3′

Complementary: 5′-AATGTGCTCCCCCAACTCCTC-3′

Non complementary: AACGTGTGAATGACCCAGTAT-3′

3 base mismatch: 5′-AATGTGGTCGCCCTACTCCTC-3′

Generation one G1 to G4 poly(propylene imine) dendrimer (used as received)

3.8.2 Solutions

10 mM PBS and 0.1 M phosphate buffer; 5 mM $Fe(CN)_6^{3-/4-}$ and DNA stock were prepared as in section 3.5.1. 10 mM G1 PPI in 0.1 M phosphate buffer was prepared from 86.26 mM (0.237g in 10 mL) stock. 6 M urea was used for denaturation.

3.8.3 Equipment and apparatus

All apparatus and equipment used are the same as in section 3.7.3

3.8.4 Studies of GCE/G1/PPI$_{sol}$, and GCE/G1PPI

CV and SWV experiments were carried out using clean bare GCE in the presence of blank 0.1 M phosphate buffer (without the dendrimer) and 10 mM G1 PPI in 0.1M phosphate buffer (PB) at different scan rates and frequencies within the potential window of -100 mV and 650 mV. EIS measurements were also taken in these two electrolytes (blank and G1 PPI) at different bias potentials from 100 mHz to 100 kHz. The electrode was labelled GCE/G1PPI$_{sol}$ for studies of PPI in solution. After electrodeposition, the GCE/G1PPI electrode was stored either at room temperature of at 4°C.

The electrodeposition of G1 PPI onto GCE was carried out using CV. The electrode potential was cycled from -100 mV to 1100 mV for 10 cycles at 50 mV/s scan rate in the 10 mM G1 PPI in 0.1 M phosphate buffer solution and labelled GCE/G1PPI. To confirm that the same electrooxidation step occur in other higher generations, 10 mM G2 and 5 mM G3 were prepared in 0.1 M phosphate buffer. CV and SWV experiments using the GCE/G1PPI electrode were carried out in 0.1 M PBS at potential window of -100 mV to 650 mV; while EIS was carried out in both PBS and $Fe(CN)_6]^{3-/4-}$ redox probe at different bias potentials.

Scanning electron microscopy was carried out using screen printed carbon electrode (SPCE) as the substrate instead of GCE. However the electrodeposition conditions were the same.

3.8.5 Immobilisation of probe DNA (GCE/G1PPI/ssDNA) and hybridisation

Immobilisation of the probe DNA onto the GCE/G1PPI electrode was carried out by dropping a 20 μL solution of 2 μM single strand probe DNA (or probe ssDNA) on the surface of a previously argon-dried GCE/G1PPI, and was left to immobilize for 5 hr at 25 °C and then successively rinsed with water and phosphate buffer solution to remove any unbound probe ssDNA. The biosensor was stored at 4 °C when not in use. The biosensor was characterised by voltammetry and EIS in PBS (voltammetry and EIS) and 5 mM (1:1) ferro/ferricyanide solution $Fe(CN)_6^{3-/4-}$ (EIS). The nanobiosensor was labelled GCE/G1PPI/ssDNA.

Hybridisation was carried out by immersing GCE/G1PPI/ssDNA in blank solution and target ssDNA solutions for 45 min at 38 °C. Blank measurements were carried out in three successive sessions in a 1 mL solution of 10 mM PBS void of DNA (labelled blank). For target ssDNA, a 1 mL solution of 10 mM PBS containing different concentrations of complementary ssDNA (target ssDNA) ranging from 0.01 to 5 nM was used for the hybridisation (labelled GCE/G1PPI/dsDNA). For each hybridisation step the hybridised nanobiosensor was washed with water and phosphate buffer solution respectively to remove unbound target ssDNA before taking measurements. The EIS responses of the nanobiosensor to the target ssDNA were measured in PBS and $Fe(CN)_6^{3-/4-}$ redox probe.

Denaturation was carried out using 6 M urea solution. The hybridised nanobiosensor (GCE/G1PPI/dsDNA) was immersed into the urea solution with gentle stirring for 25 minutes in total. Impedance measurement was carried out

using the denatured electrode (GCE/G1PPI/den). The denatured electrode was characterised by EIS.

CHAPTER 4

RESULTS AND DISCUSSION: An Electrochemical DNA Biosensor developed on a Novel Multinuclear Nickel (II) Salicylaldimine Metallodendrimer Platform

4.1 Introduction

The results discussed in this chapter stem from the experimental procedures outlined in **Chapter 3 section 3.5** (general experimental) and **section 3.6.** This chapter presents the result of my first quest for dendrimeric materials as a meet to the challenge in electrochemical DNA biosensor. Electrochemical characterization and immobilisation of a novel multinuclear Nickel (II) salicylaldimine metallodendrimer – a PPI derivative, and its suitability as an immobilisation layer in impedimetric and voltametric DNA biosensor is described for the first time in this report. The synthesis of this novel metallodendrimer and the most of the data presented here has been published [82, 238]. To give the reader an overview of the work carried out at this milestone of my PhD, a mini abstract is presented the following paragraph.

An electrochemical DNA biosensor (EDB) was prepared using an amino modified oligonucleotide of 21 bases (probe DNA) immobilised on a novel multinuclear Nickel (II) salicylaldimine metallodendrimer on glassy carbon electrode (GCE). The metallodendrimer was synthesized from amino functionalized polypropylene imine dendrimer, DAB-$(NH_2)_8$. The EDB was prepared by depositing probe DNA on a dendrimer modified GCE surface and left

to immobilize for 1 hr. Voltammetric and electrochemical impedance spectroscopic (EIS) studies were carried out to characterize the novel metallodendrimer, the EDB and its hybridisation response in PBS using $[Fe(CN)_6]^{3-/4-}$ as a redox probe at pH 7.2. The metallodendrimer was electroactive in PBS with two reversible redox couples at $E^{\circ\prime}$ = +200 mV and $E^{\circ\prime}$ = +434 mV; catalytic by reducing the E_{pa} of $[Fe(CN)_6]^{3-/4-}$ by 22 mV; conducting and has diffusion coefficient of 8.597×10^{-8} cm^2s^{-1}. From the EIS circuit fitting results, the EDB responded to 5 nM target DNA by exhibiting a decrease in charge transfer resistance (R_{ct}) in PBS and increase in R_{ct} in $[Fe(CN)_6]^{3-/4-}$ redox probe; while in voltammetry, increase in peak anodic current was observed in PBS after hybridisation, thus giving the EDB a dual probe advantage.

4.2 Dendrimer preparation

The metallodendrimer was prepared by complexing the multinuclear salicylaldimine ligand **L1** to nickel using nickel acetate as metal source. This results in the formation of a tetranuclear nickel salicylaldimine complex. The complex was isolated as a green solid which is stable in air and shows relatively high thermal stability, decomposing only around 210°C. The dendritic complex was characterised by IR spectroscopy, ESI-mass spectrometry and elemental analysis. The IR spectrum of the complex shows a band around 1632 $cm^{-1,}$ which is due to the ν(C=N) stretching frequency of the complexed salicylaldimine ligand. This band occurs at a lower wave number than the analogous band in the spectrum of the free ligand. Another distinguishing feature in the IR spectrum of the complex is the C-O vibration, which occurs at 1279 cm^{-1} in the Schiff base

ligand and shifts to ~1344 cm^{-1} upon complexation. The elemental analysis of the complex corresponds to a species in which a single molecule of dichloromethane is associated with the complex. Attempts to study the complex by NMR spectroscopy were not successful as only broad peaks were observed in the spectrum. This is indicative of paramagnetic metal complexes. The ESI mass spectrum of the complex which was recorded in DMSO solution confirms the proposed structure of the dendritic dendrimer in which four nickel centres are associated with the dendritic ligand. This means that the salicylaldimine functionalities on two dendrimer branches are associated with a single nickel centre [82, 238]. The detailed reaction scheme can be found in Malgas *et al* [238] however, the structure of the G2 multinuclear Nickel (II) salicylaldimine metallodendrimer is depicted in Fig. 4.1.

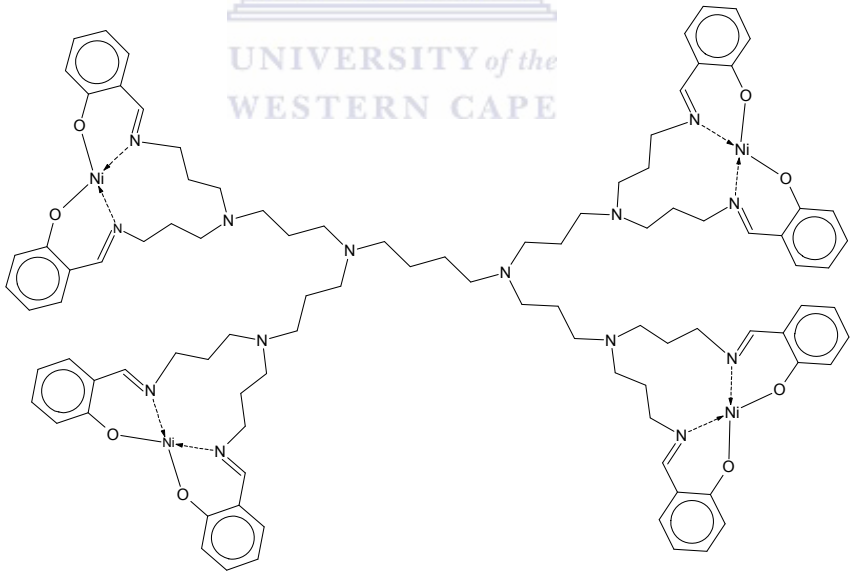

Figure 4.1 Structure of the G2 multinuclear Nickel (II) salicylaldimine metallodendrimer

4.3 Electrochemistry of the metallodendrimer in PBS and $Fe(CN)_6^{3-/4-}$solution

Prior to electrode modification, a safe potential region where bare GCE exhibits no noticeable redox electrochemistry in phosphate buffer solution was chosen in order to ascertain that the electrochemistry observed is due to the deposited metallodendrimer. A potential window between +650 mV to -100 mV was chosen to avoid the small anodic peak (amplified by SWV in the inset) observed in Fig 4.2, while +650 mV was chosen to avoid the oxidation of the DNA guanine base which at ca 700 mV [85] since our biosensor design does not involve the oxidation of any of the DNA bases.

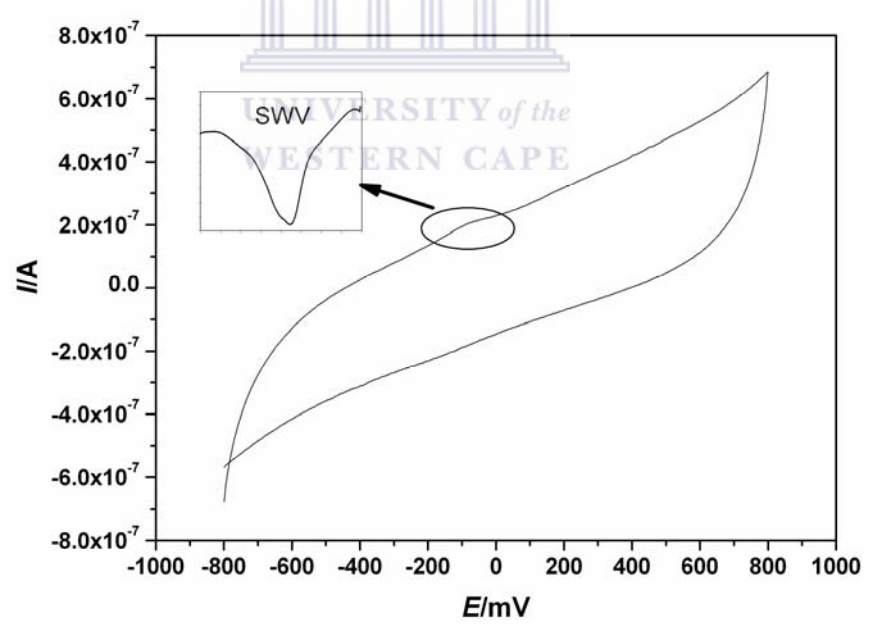

Figure 4.2 Cyclic voltammetry of bare GCE in 10 mM phosphate buffer saline solution at 20 mV/s scan rate

Fig. 4.3 shows the differential pulse voltammogram of the metallodendrimer immobilised on GCE at different scan rates between 20 mVs^{-1} to 50 mVs^{-1}. At 20 mVs^{-1} scan rate, the GCE/Dend shows two quasi-reversible redox couples. Both the cathodic and anodic DPV were run, but only the cathodic plots are shown. The Redox couple (labelled I) occurred at E_{pa} = +216 mV; E_{pc} = +183 mV; $E^{0'}$ = +200 mV; while the redox couple (labelled II) occurred at E_{pa} = +453 mV; E_{pc} = +415 mV; $E^{0'}$ = +434 mV. The redox couple I at formal potential +200 mV is assigned to the salicylaldimine ligand because the outer substituted salicylaldimine moiety of the dendrimer has conjugated bonds (and imine linkage as observed also in emaraldine) which probably allows electron movement along this chain, giving rise to a redox electron transfers. The presence of this couple at ca $E^{0'}$ = +200 mV and absence of a redox couple at $E^{0'}$ = +434 mV (and nowhere else within the potential window of -100 mV to +650 mV) when the voltammetry of the ligand was run before complexation with the metal, further supported this redox peak assignment. The redox couple II is assigned to the nickel electrochemistry. The peak at +453 mV corresponds to the oxidation of nickel ion from Ni^{II} to Ni^{III} while that at +415 mV corresponds to the reduction of nickel ion from Ni^{III} to Ni^{II}. Thus the metallodendrimer is electroactive. It is also conducting at both couples because current increase was directly proportional to scan rate with correlation coefficient (R^2) of 0.994; and there was little or no shift in formal potential at different scan rates. From the plot of peak cathodic/anodic peak current versus square root of scan rate, the electron diffusion coefficient D_e, a measure of how fast charge can be transported through the dendrimer layer, was calculated using Randle Sevcik equation and found to be 8.597×10^{-8} cm^2s^{-1}. This

reiterated the conductivity of the dendrimer and this value is comparable to those reported in literature for conducting polymers - D_e of 6.68×10^{-9} cm^2s^{-1} [239], 6.46×10^{-8} cm^2s^{-1} [240] and for dendrimer, 3.6×10^{-7} cm^2s^{-1} [241].

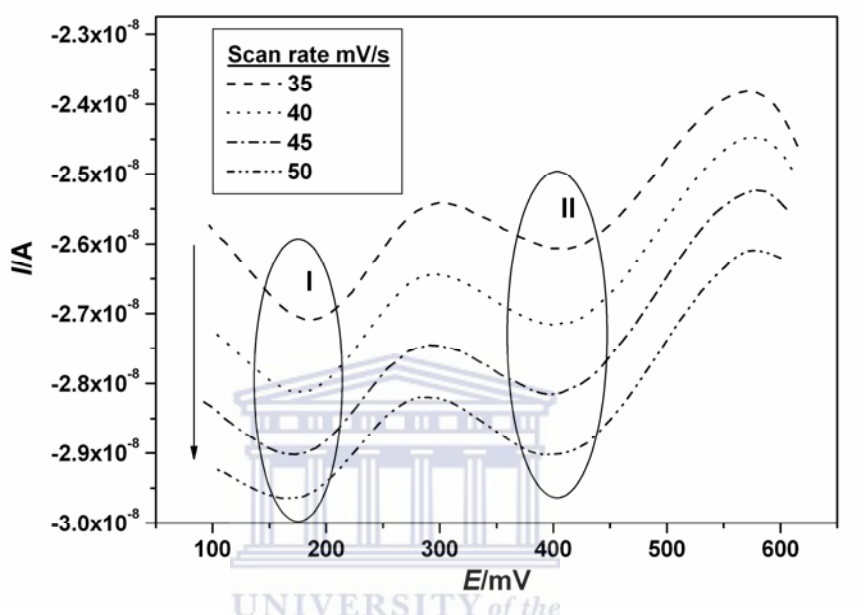

Figure 4.3 DPV of GCE/dend in 10mM PBS at increasing scan rate showing redox couple I and II.

DPV experiment (Fig. 4.4a), of bare GCE in the presence of $Fe(CN)_6^{3-/4-}$ redox probe, shows a reversible redox couple at +210 mV. An EIS experiment carried out to confirm this gave the lowest charge transfer resistance at +200 mV (Fig. 4.4 b and c) which is expected because at the voltammetric formal potential, electron exchange at the electrode interface is optimum. It can be said to be the point of maximum conductivity.

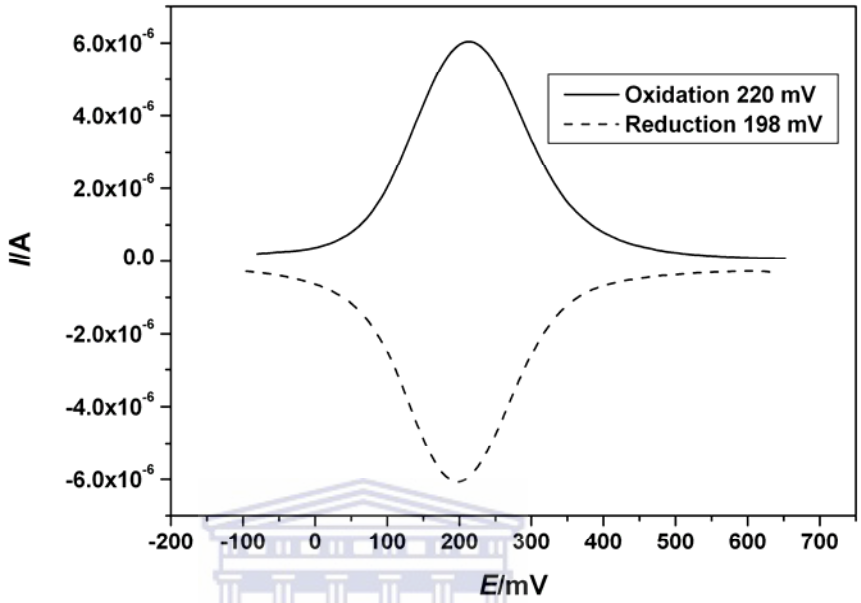

(a)

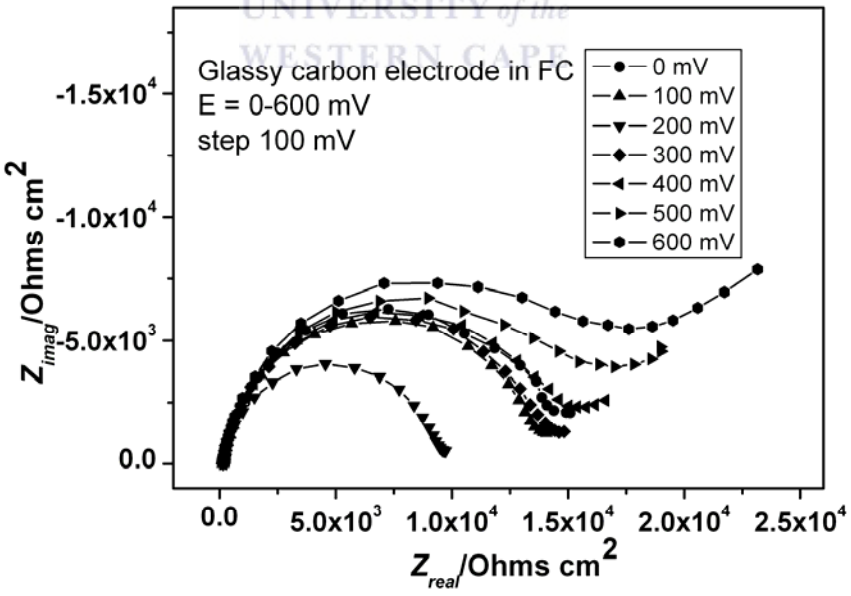

(b)

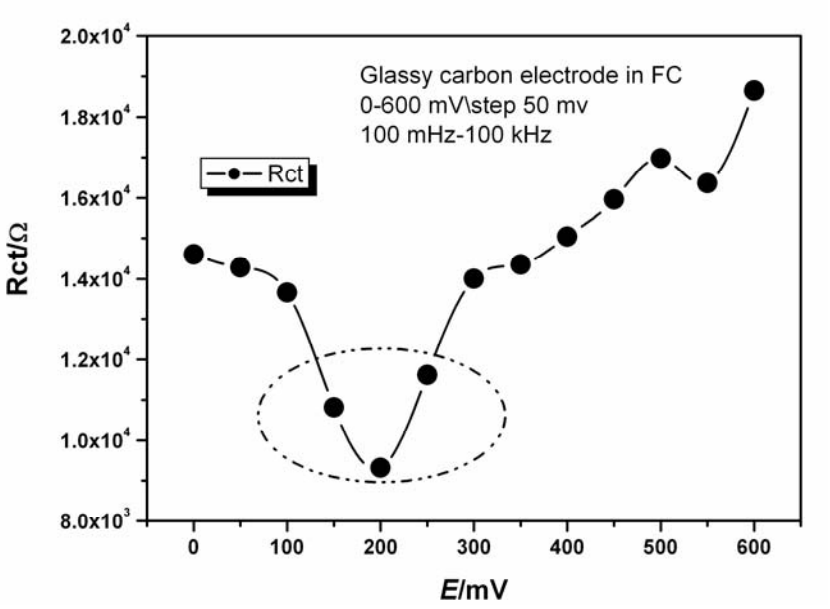

(c)

Figure 4.4 (a) DPV of bare GCE in 5mM $Fe(CN)_6^{3-/4-}$, pH 7.2 showing the reversible redox peaks. (b) Nyquist plot of bare GCE in $Fe(CN)_6^{3-/4-}$ at different potentials. (c) A plot of charge transfer resistance obtained from the fitting of the Nyquist versus potential

The complex plane plot of GCE in $Fe(CN)_6^{3-/4-}$ formed a background upon which further electrode modification results will be compared. After the GCE was modified with the dendrimer, the anodic and cathodic peak currents response in the presence of $Fe(CN)_6^{3-/4-}$, was slightly higher than unmodified or bare GCE. The observed current increase was as a result of the proximity between the formal potential +200 mV of the dendrimer in PBS (Fig. 4.3) and that of the $Fe(CN)_6^{3-/4-}$ at +210 mV which caused an overlap of current response from both the dendrimer and $Fe(CN)_6^{3-/4-}$. This formal potential coincidence may be exploited as a voltammetric signal amplifier in biosensor application or for another purpose. The $Fe(CN)_6^{3-/4-}$ electrochemistry still observed after dendrimer immobilisation, confirms that the dendrimer layer is conducting.

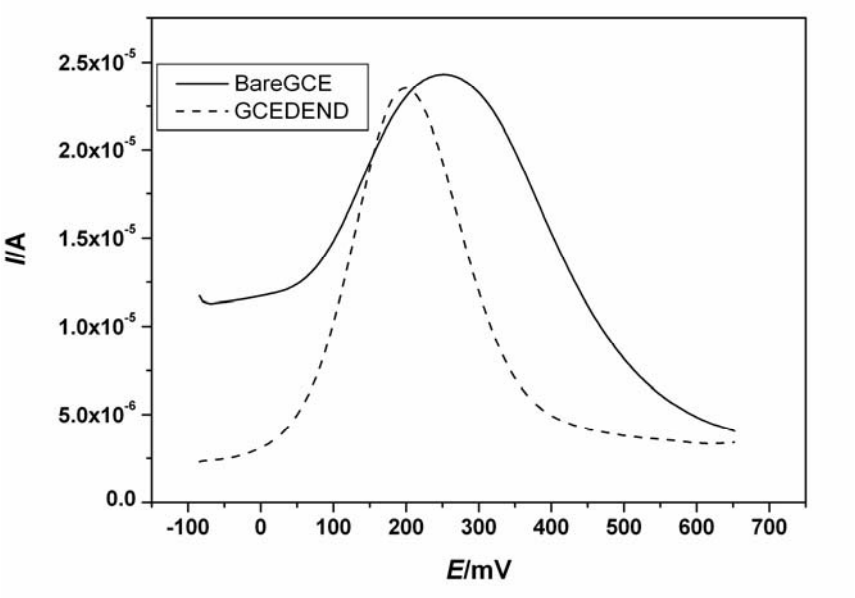

(a)

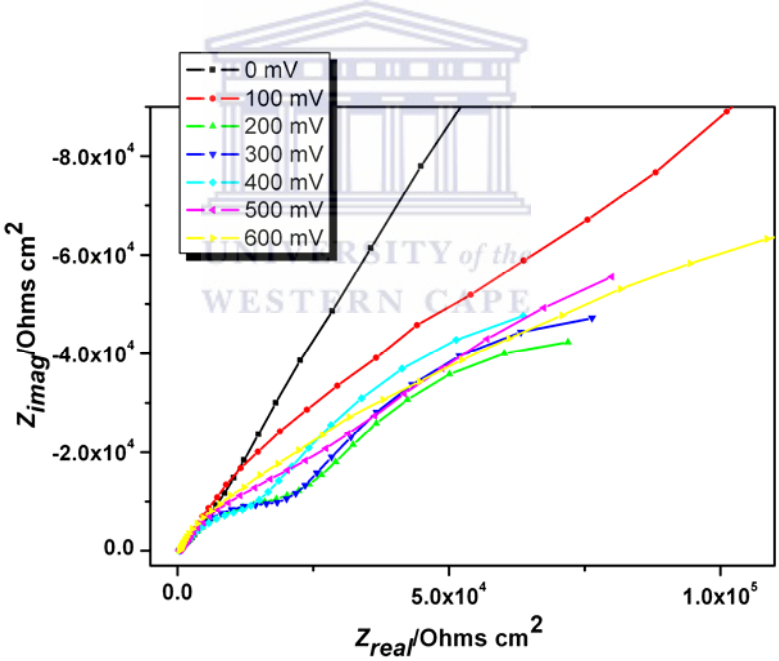

(b)

Figure 4.5 (a) SWV of bare GCE and GCE/dend in 5mM $Fe(CN)_6^{3-/4-}$, pH 7.2 showing the catalytic effect of the dendrimer and (b) Nyquist plot of GCE/dend in 5mM $Fe(CN)_6^{3-/4-}$ at 0–600 mV (100 mV steps).

From Fig. 4.5a, the dendrimer shows some kind of electrocatalytic effect towards the electrochemistry of $Fe(CN)_6^{3-/4-}$. With bare GCE, $Fe(CN)_6^{3-/4-}$ had E_{pa} of +220 mV but when the GCE was dendrimer modified (GCE/Dend), the E_{pa}

was lowered by 22 mV. The catalytic effect is explained by the reduced oxidation potential (potential is a form of energy) caused by the dendrimer. It is accepted that a catalyst generally lowers the activation energy of a chemical process. The EIS plot over the potential range of 0 mV and +600 mV (100 mV potential steps) in Fig. 4.5b shows that the metallodendrimer had lower R_{ct} between +200 mV and 500 mV with lowest R_{ct} at +200 mV. This is in accordance with the fact that the dendrimer itself has two redox processes which fall within this range and that the dendrimer is most conducting at +200 mV. At this potential, the dendrimer can be said to have maximum attraction to the $Fe(CN)_6^{3-/4-}$ which is an indication of a cationic material. This feature is an advantage as far as its intended application as immobilisation surface for DNA, which is an anionic macromolecule, is concerned. Thus for impedimetric measurements, +200 mV was chosen as the probing potential for the EDB.

4.4 DNA biosensor response to complementary DNA in PBS

Figures 4.6a and b show the electrochemical behaviour of the EDB when probe ssDNA was immobilised and its response to hybridisation. From the cyclic voltammetry (Fig 4.6a), the wave 'GCE/DEND' represents the response of the dendrimer modified GCE electrode. An increase in charge of about 5% was observed when the probe ssDNA was deposited on the modified electrode (as seen in wave EDB). When SWV was used (Fig 4.6b), the same phenomenon was observed at formal potential +200 mV (see wave GCE/DEND and EDB). It is known that ssDNA has a measure of conductivity [63] the reason for the small charge and not complete insulation of the dendrimer modified electrode surface.

Because DNA is anionic and the dendrimer cationic; an electrostatic DNA-metallodendrimer adsorption is expected. However, the DNA was amino modified because we speculate a coordinate covalent bond between the lone pair on the $-NH_2$ and the empty orbital in the Ni (II) ion centers. Ni^{2+} is known to exist in coordination numbers 4 and 5 in its compound [242]. The lone pair of electron on the amino group could probably bond on the axial position of the Ni^{2+} center (being the approach with least steric hindrance) thus changing its geometry from square planar to square pyramidal. In addition, the DNA can be entrapped (physical adsorption) within the 'pockets' of the metallodendrimer. Since one of the major reasons for new immobilisation layer/platform quest is for proper DNA probe adsorption, these three bonding routes (i.e. electrostatic, physical and coordinate covalent) may have synergic effect.

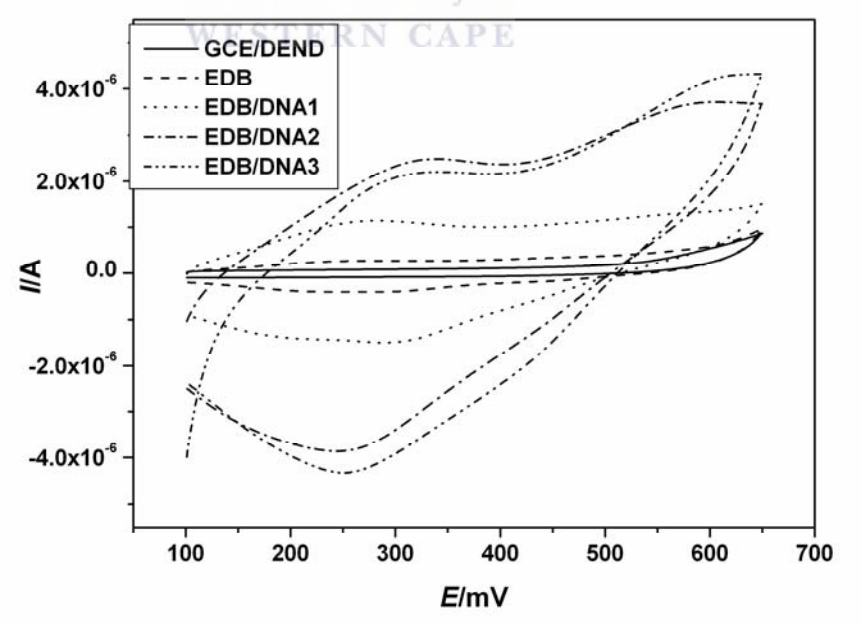

(a)

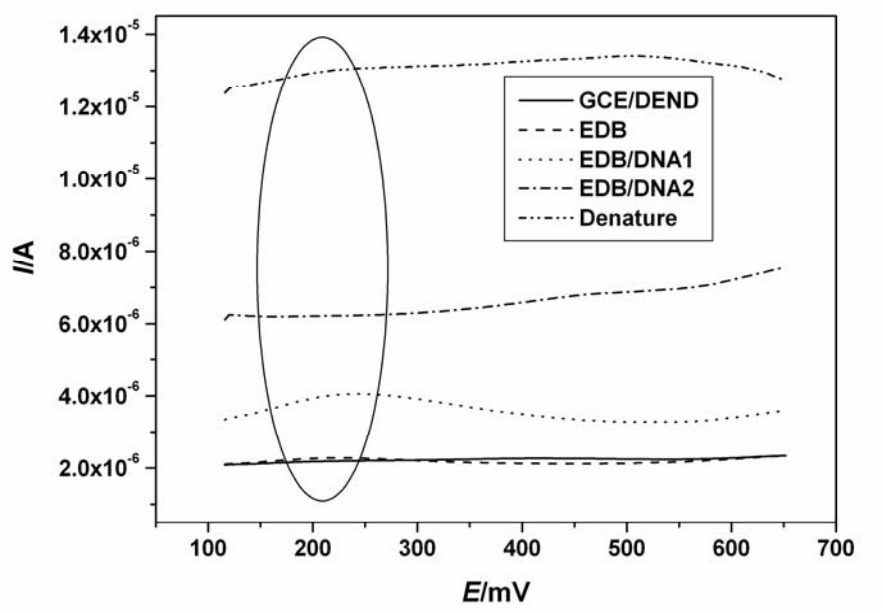

(b)

Figure 4.6 Voltammetric responses of the GCE/Dend, EDB, hybridisations and denaturation in PBS, pH 7.2. (a) CV at 20 mV/s scan rate (denaturation not shown); (b) SWV at 15 Hz, including denaturation

From both CV and SWV, there was a large increase in anodic current (~ 120%) after the EDB incubation with target ssDNA (see wave EDB/DNA1). This is in accordance with the fact that double strand DNA (dsDNA) (formed as a result of hybridisation) is more conducting than ssDNA [59, 243]. The current signal further increases on additional incubation of the same biosensor with target ssDNA (see wave EDB/DNA2) because more dsDNA was formed on the biosensor surface. But the third hybridisation EDB/DNA3 (shown only in Fig 4.6 a) gave signal that was not in agreement with the trend from EDB to EDB/DNA2. Immobilised ssDNA probe on the EDB must have been saturated (fully hybridised) with its complementary target ssDNA. Attempt to denature was not successful as seen in wave 'Denature" in Fig 4.6 b. At the dsDNA denaturing temperature of 95 °C, the dendrimer was unstable hence led to the degradation of

the biosensor platform. This was observed by visual inspection, as roughness on the surface of the GCE. Attempts to use NaOH for denaturing also failed. This behaviour suggests that this biosensor design favours single use.

EIS was also used to characterize the GCE/Dendrimer response to ssDNA probe immobilisation and hybridisation studies and the Nyquist plot results are shown in Fig. 4.7a. To obtain the electrical parameters, the impedance data was fitted using the circuit model (Fig. 4.7b) consisting of solution resistance R_s, Warburg impedance Z_w, charge transfer resistance R_{ct} and constant phase element CPE. The Warburg element suggests that the system is diffusion controlled [155] and it was introduced because of the straight line (at near angle 45°) observed at the low frequency region of the Nyquist plot (Fig. 4.7a). Table 4.1 shows the values of the fitting results of equivalent circuit. R_{ct} increased when the ssDNA probe was immobilised on the dendrimer matrix because of the poor conductivity of the probe ssDNA (voltammetry shows the same trend). Capacitance (CPE_{dl}) also increased because a new layer of charge has been concentrated on the dendrimer surface causing an increase in double layer thickness (see table 4.1).

For the first hybridisation (EDB to EDB/DNA1), R_{ct} decreased since dsDNA is more conducting than ssDNA (see table 1), this also agrees with the voltammetric result in Fig 5a and 5b. A similar trend was observed in the second hybridisation. The negative effect of denaturation in not reproducing the EDB impedance was also observed with the EIS as shown earlier with voltammetry.

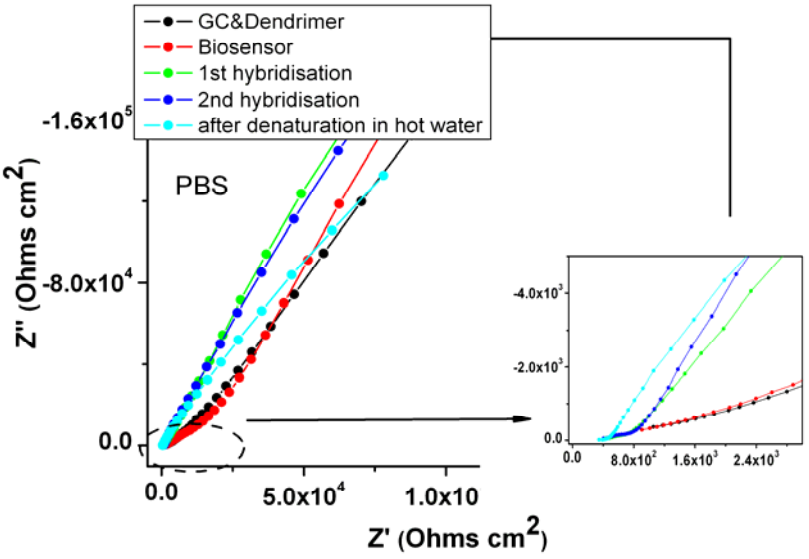

(a)

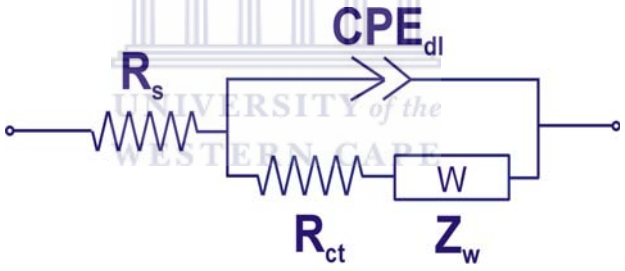

(b)

Figure 4.7 Impedance responses of the GCE/Dend, EDB, hybridisations and denaturation in PBS, pH 7.2. (a) Nyquist plot with inset for high frequencies; (b) circuit model for the impedance data fitting.

4.5 DNA biosensor response to complementary DNA in the presence of $Fe(CN)_6^{3-/4-}$ redox probe

Fig. 4.8a shows the Nyquist plot of the impedance measurement of the EDB in the presence of the redox probe. The biosensor behaves in a different way in the presence of redox probe. The two semicircles and absence of a straight line

at low frequency observed suggested that the system was not diffusion controlled (as in Fig. 4.7a) but electron transfer limited process which is caused by the introduction of the $Fe(CN)_6^{3-/4-}$ redox probe. Therefore, an equivalent circuit model (Fig. 4.8b) consisting of R_s, R_1 and R_2, CPE_1 and CPE_2 was used for fitting where R_s is solution resistance, R_1 and R_2 are charge transfer resistances and CPE_1 and CPE_2 are constant phase element. CPE was used because of the in-homogenous surface roughness. Moreover, it also gave a better fit than full capacitance. A similar circuit has been proposed by Wensha Wang *et al* [244] and Gu *et al* [243]. Bonanni A *et al* [96] also proposed the same circuit but they immobilised DNA directly on graphite epoxy composite electrode.

R_1, CPE_1 and R_2, CPE_2 correspond to the first and second semicircles or time constant respectively. Since both R_1 and R_2 may mean R_{ct}, it is still quite unclear which one should be the better analytical parameter to measure the extent of hybridisation or target DNA concentration. However, I propose R_1 as a more probable parameter for the following reasons: (1) Since R_s measures the solution resistance, R_1 and CPE_1 should correspond to the layer that forms interface with the solution and this is the DNA/solution interface. This is also observed in the first semicircle for the +200 mV curve in Fig. 4.5b which depicts the dendrimer/$[Fe(CN_6)]^{3-/4-}$ interfacial kinetics. (2) Hybridisation causes the thickness *d* of the DNA layer on the dendrimer surface to increase and this will lead to decrease in capacitance, C as shown in equation 4.1 (ε and ε_0 are dielectric constant of the electrode surface and dielectric constant of vaccum respectively).

$$C = \frac{\varepsilon\varepsilon_0}{d} \qquad \textbf{eqn. 4.1}$$

And from Table 4.2, CPE_1 reduced after hybridisation while CPE_2 showed no significant change. (3) The insignificant change in CPE_2 after hybridisation suggests that it measures the GCE/Dendrimer interface (which is not affected by hybridisation) and may also be the space charge capacitance peculiar to the dendrimer referred to by Huiru Gu *et al* [243]. The value of CPE_2 is also higher than the corresponding CPE_1 which is expected if it is a measure of the dendrimer double layer.

This increase in R_1 is contrast to that observed in the presence of PBS. Though dsDNA is more conducting, it has a higher negative charge density than ssDNA because there are more negatively charged phosphate backbones. Increase in dsDNA concentration on the EDB surface resulted in increased negativity and this repelled the bulky $Fe(CN)_6^{3-/4-}$ anion [155]. This repulsion factor far outweighs the conductivity factor as seen PBS (without $Fe(CN)_6^{3-/4-}$). The repulsion prevented charges from passing from the bulk through the dendrimer to the transducer hence the increase in R_1. This also gave rise to the semicircles which means that the interfacial electron kinetics due to the DNA/$Fe(CN)_6^{3-/4-}$ is the limiting factor. R_2 values also showed the same increase trend.

Error for the fitting of each element in electrical equivalent circuit was between 0.7% to 8% for the EIS data obtained in PBS and $Fe(CN)_6^{3-/4-}$. However, the average error obtained for the R_{ct} (Fig 4.7a) and R_1 (Fig 8a), which are the measuring parameters for the target DNA, was ca 5%.

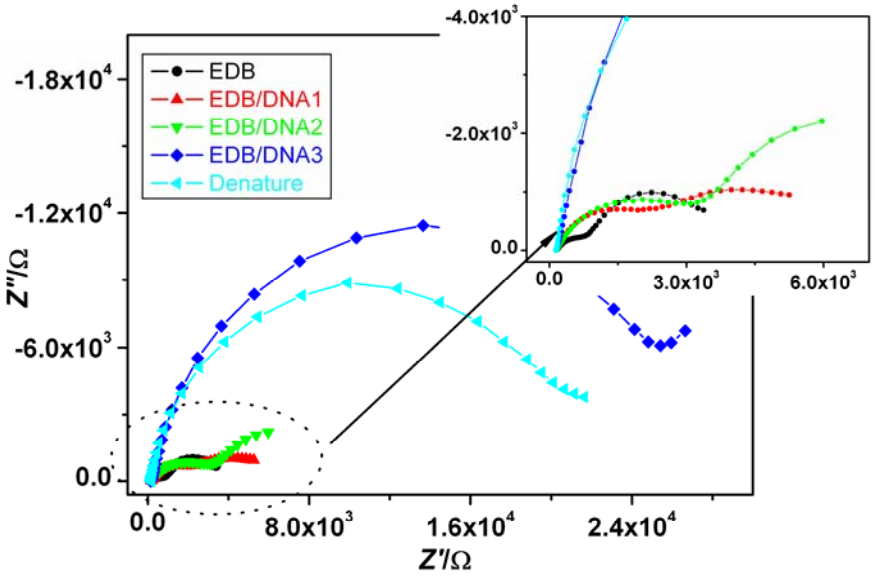

(a)

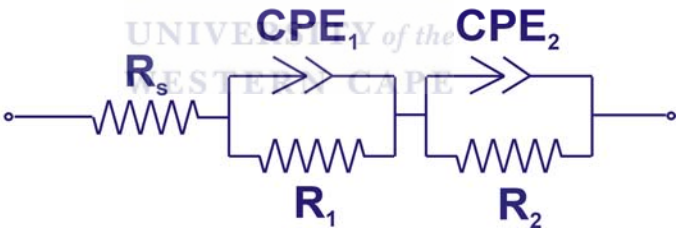

(b)

Figure 4.8 Impedance response of the GCE/Dend, EDB, hybridisations and denaturation in $Fe(CN)_6^{3-/4-}$ redox probe pH 7.2. (a) Nyquist plot with inset for high frequencies; (b) circuit model for the impedance data fitting.

Table 4.1: The electrical parameters obtained from the circuit fitting of the biosensor response to hybridisation from Fig 4.7a

Circuit Parameters	GCE/DEND	Biosensor	1st hybridisation	2nd hybridisation
Rs (Ω)	907.9	939.3	469.7	386.3
R_{ct} (Ω)	4073	1575.3	584.6	600
Z_w (Ω)	9.3E5	8.9E5	1.11E6	2.66E6
CPE_{dl}	1.15E-6	3.57E-6	2.84E-6	1.43E-7

Table 4.2: The electrical parameters obtained from the circuit fitting of the biosensor response to hybridisation from Fig 4.8a.

Circuit Parameters	Biosensor	1st hybridisation	2nd hybridisation
R_s (Ω)	166.7	139	154
R_1 (Ω)	670	1685	2898
CPE_1	1.44E-5	2.86E-6	8.70E-6
R_2	3022	4954	9198
CPE_2	1.07E-4	1.07E-4	2.56E-4

4.6 Sub conclusions

The novel metallodendrimer possesses suitable characteristics that are applicable for electrochemical DNA biosensor design. It is electroactive with two reversible redox couples, conducting and electro catalytic in the presence of $Fe(CN)_6^{3-/4-}$ anion when immobilised on GCE surface. It also adsorbs DNA strongly because the biosensor retained its activity after series of electrochemical measurements except after denaturation. The EDB gave measurable charge transfer resistance response to a 10 µL of 5 nM target DNA. The EDB is suitable for single use purpose.

CHAPTER 5

RESULTS AND DISCUSSION: An Electrochemical DNA Biosensor developed on a Nanocomposite Platform of Gold and Poly(Propyleneimine) Dendrimer

5.1 Introduction

The results discussed in this chapter stem from the experimental procedures outlined in **Chapter 3 section 3.5** (general experimental) and **section 3.7.**

In chapter 4, it was observed that the metallodendrimer gave two redox peaks. The electroactivity observed in the dendrimer matrix apart from that of the nickel metal encouraged a further probe of the behaviour of the PPI matrix itself. Could PPI be electroactive? A higher generation PPI (if electroactive) has more pockets available for host-guest interaction with DNA. Thus G4 PPI was chosen for investigation.

The two routes usually adopted to optimize the immobilisation of biomolecules are chemical modification of the substrate and biological functionalisation of the biomolecule [110], both of which determine the immobilisation chemistry. Functionalisation of DNA has been shown to improve immobilisation [28, 111] because the group attached provides the desired chemistry and hence enhances the performance of DNA biosensors. On the other hand, the modification of electrodes or substrates using nanomaterials has been reviewed in chapter 2. In this study, the functionalisation of both the

immobilisation platform and the DNA was performed with the aim of improving the biosensor response characteristics. For an overview of this milestone, a mini abstract is provided in the paragraph below.

An electrochemical DNA nanobiosensor was prepared by immobilisation of a 20mer thiolated probe DNA on electrodeposited generation 4 (G4) poly(propyleneimine) dendrimer (PPI) doped with gold nanoparticles (AuNP) as platform, on a glassy carbon electrode (GCE). Field emission scanning electron microscopy results confirmed the co-deposition of PPI (which was linked to the carbon electrode surface by C-N covalent bonds) and AuNP ca 60 nm. Voltammetric interrogations showed that the platform (GCE/PPI-AuNP) was conducting and exhibited reversible electrochemistry ($E^{\circ\prime}$ = 235 mV) in pH 7.2 phosphate buffer saline solution (PBS) due to the PPI component. The redox chemistry of PPI was pH dependent and involves a two electron, one proton process, as interpreted from a 28 mV/pH value obtained from pH studies. The charge transfer resistance (R_{ct}) from the electrochemical impedance spectroscopy (EIS) profiles of GCE/PPI-AuNP monitored with ferro/ferricyanide ($Fe(CN)_6^{3-/4-}$) redox probe, decreased by 81% compared to bare GCE. The conductivity (in PBS) and reduced R_{ct} (in $Fe(CN)_6^{3-/4-}$) values confirmed PPI-AuNP as a suitable electron transfer mediator platform for voltammetric and impedimetric DNA biosensor. The DNA probe was effectively wired onto the GCE/PPI-AuNP via Au-S linkage and electrostatic interactions. The nanobiosensor responses to target DNA which gave a dynamic linear range of 0.01 - 5 nM in PBS was based on the changes in R_{ct} values using Fe(CN)63-/4- redox probe.

The thought of using a nanocomposite platform of PPI and AuNP was provoked by the similar characteristics among PPI, AuNP, and DNA. A synergic effect favourable to the biosensor performance can be obtained from such a platform. The PPI in the nanoplatform therefore is expected to (i) house the DNA through the nanoscopic pockets of the G4 PPI, (ii) mediates charge flow, while the AuNP will (iii) assists in anchoring and wiring the DNA (iv) amplify signal owing to its excellent conductivity. This is depicted in figure 5.1. Some of the results obtained in this investigation has been published [245].

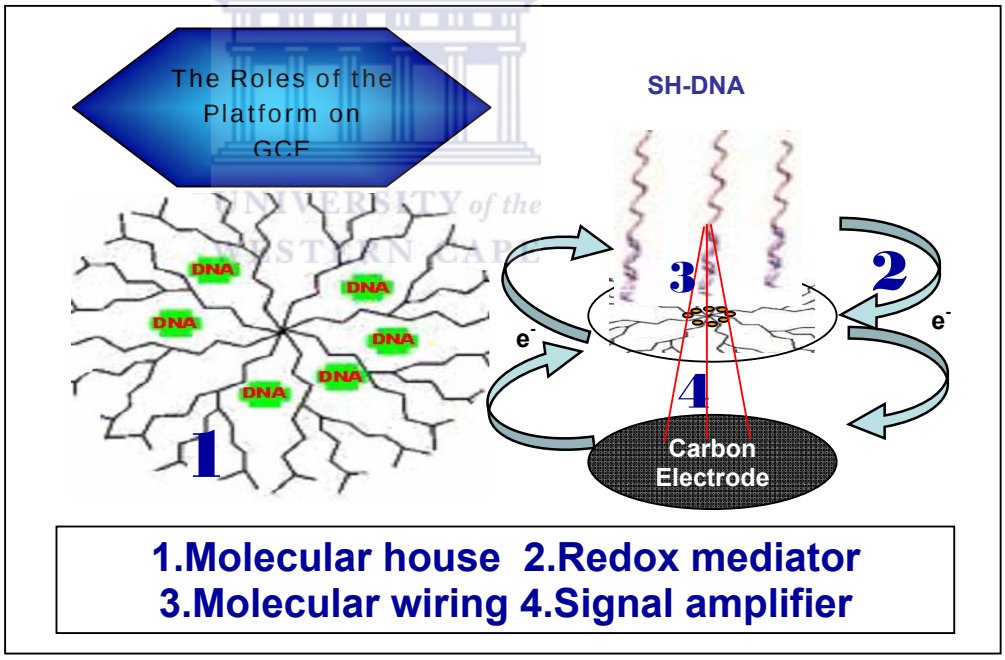

Figure 5.1 A schematic sketch of the roles of the nanocomposite platform in the electrochemical DNA biosensor.

5.2 Morphology and Voltammetric behaviour of GCE/PPI-AuNP

Fig. 5.2a to d show the FE-SEM images of the blank SPCE, SPCE/AuNP, SPCE/PPI and SPCE/PPI-AuNP respectively. An average size of 60 nm AuNP can be observed deposited on the surface of the SPCE in Fig. 5.2b (compare with blank SPCE in Fig. 5.2a). Fig 5.2c confirmed the attachment of PPI onto the carbon surface as seen as a globular growth on the SPCE. At the point of measurement, Fig 5.2d exhibited a reflectance not observed in Fig. 5.2c as a result of the AuNP which was co-deposited. The diameter of G4 PPI is about 3.12 nm [177] and has been known to be flexible thus in Fig. 5.2d, PPI appears to cluster around the AuNP because it is smaller in size. The nanocomposite has higher particle size than the separate components. However; the morphology of the PPI-AuNP is similar to that of PPI only (Fig. 5.2c). As a further proof of the presence of AuNP in Fig. 5.2d, energy-dispersive x-ray analysis (EDAX) of the sample gave 4.95 weight percent of gold relative to carbon and other elements present. TEM image of GCE/PPI-AuNP gave a smaller AuNP size of about 30 nm (result not shown) and this suggests that the roughness of the electrode (substrate) has effect on the distribution and particle size of AuNP.

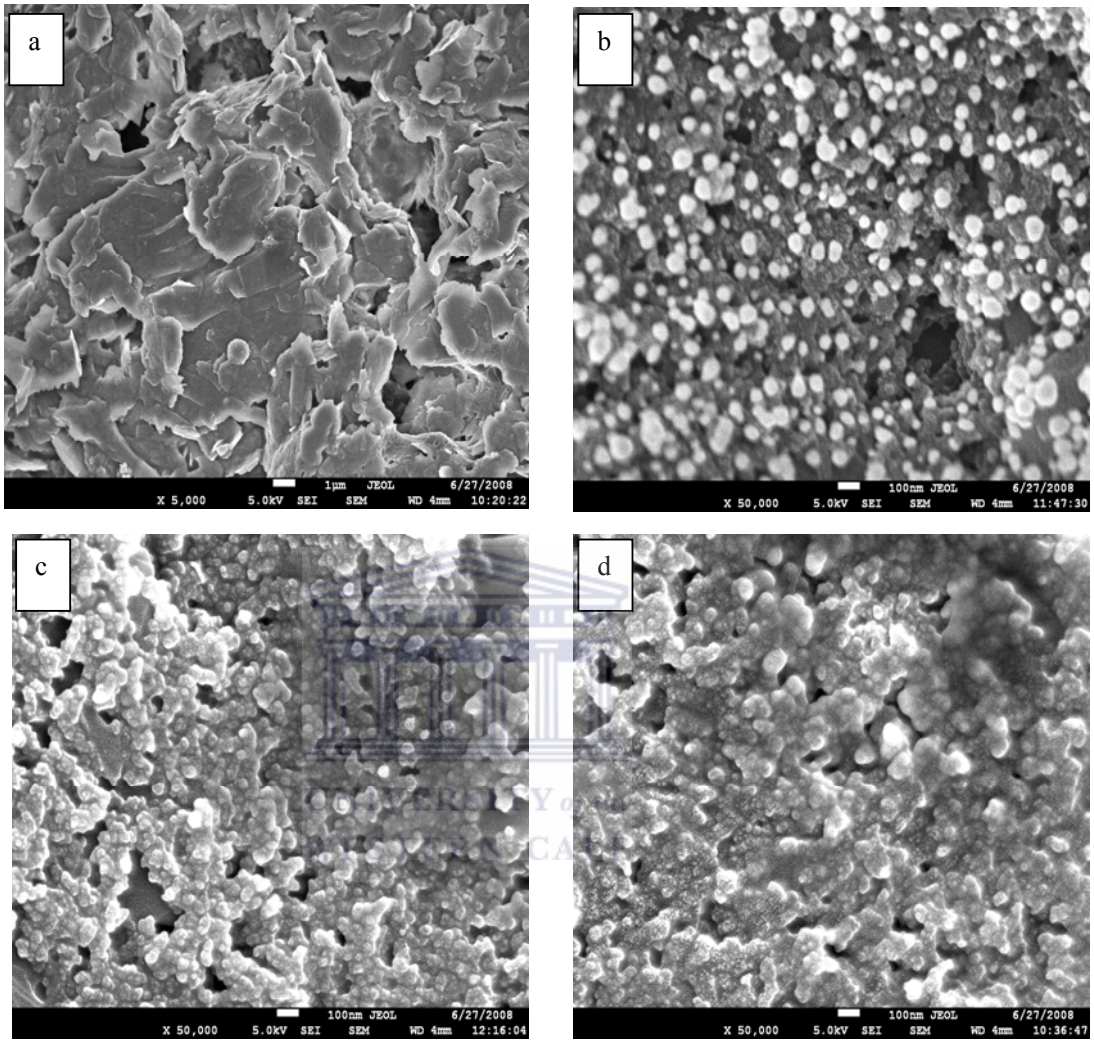

Figure 5.2 FE-SEM images on screen printed carbon electrodes (SPCE) (a) blank SPCE. (b) SPCE/AuNP. (c) SPCE/PPI (d). SPCE/PPI-AuNP

The chemical (covalent) modification of GCE using either aliphatic or aromatic primary amine to form C-N bond has been in use for quite a while and its mechanism involves the formation of amine cation radical [246-248]. This reaction mechanism has been known not to occur with tertiary amine. [247]. G4 PPI consists of peripheral primary amines and internal tertiary amine. Thus the

same chemistry should apply in the attachment of the peripheral primary amines (and not the internal tertiary amines) of PPI (Fig.5.3a) onto the GCE (also SPCE for SEM) surface at a potential of ca 1000 mV where electrooxidation of primary amines occurs [247]. Fig. 5.3b shows the CV during the electrodeposition process. It can be observed that for PPI, the electrooxidation step which is evident in the first cycle took place at about 680 mV which is 300 mV lower than other primary amines recorded in literature. The cyclic voltammetric deposition of PPI and AuNP on the GCE, therefore, involves the formation of amine linkages between PPI and GCE while the AuNP were simultaneously deposited with the PPI using the -200 mV potential.

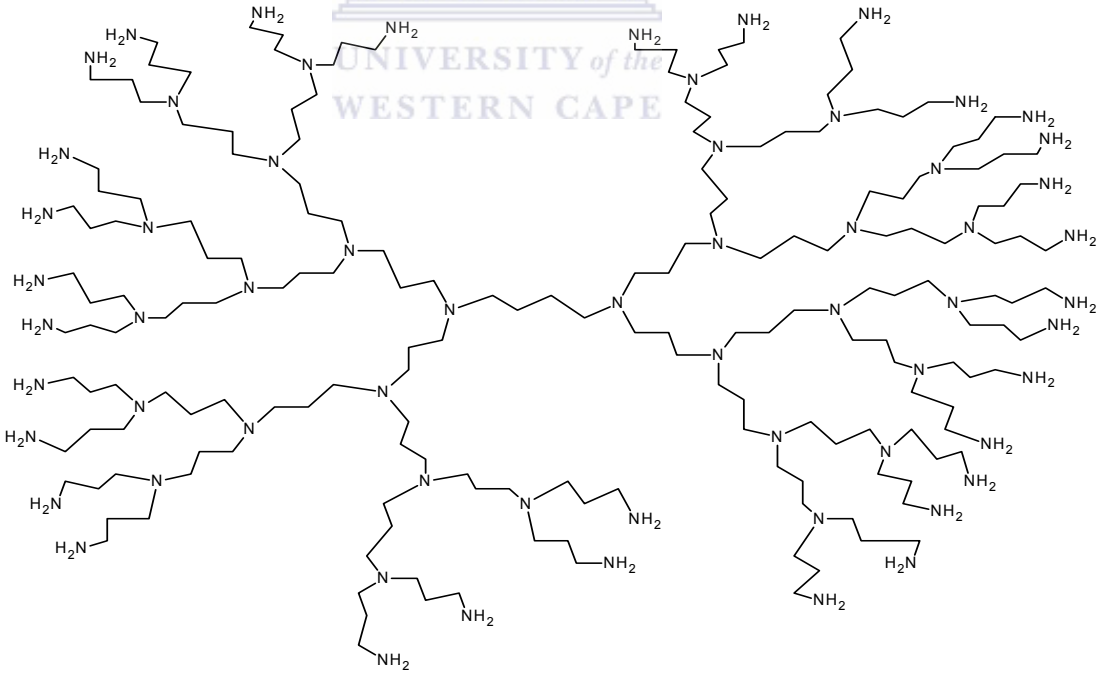

(a)

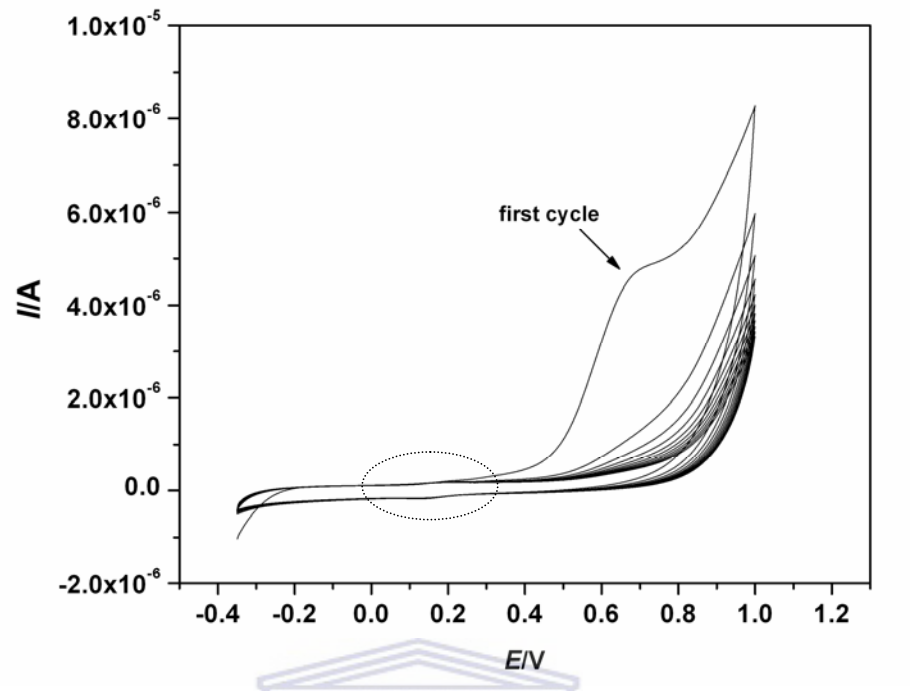

(b)

Figure 5.3 (a) Structure of G4 Poly(propylene imine) dendrimer showing the peripheral primary amine and internal tertiary amine. (b) Electro co-deposition of PPI and AuNP onto GCE surface at 50 mV/s from 1100 mV to -200 mV

Figure 5.4a, compares the electrochemical behaviour of GCE/PPI-AuNP (dotted line) against the bare GCE (solid line) in PBS. The PPI-AuNP composite film exhibited reversible electrochemistry characteristic of surface adsorbed species with formal potential $E^{0\prime}$ = 233 ± 5 mV for 6 different measurements demonstrating the good reproducibility of the composite platform. To ascertain the species responsible for the reversible peaks, PPI and AuNP were deposited alone as shown in Fig. 5.4b and 5.4c respectively. In Fig 5.4b, 3 mM PPI in PBS solution exhibited a quasi reversible electrochemistry; and when it was electrodeposited, the anodic and cathodic potential peaks separation became less. However, the formal potential shifted anodically by ca 10 mV when PPI was electrodeposited. In Fig 5.4c, where only AuNP was deposited on GCE, no peaks

were observed. This meant that the pair of peaks observed in Fig. 5.4a was due to the PPI component of the nanocomposite. The reversibility of the electrochemical oxidation/reduction occurring within the PPI-AuNP nanocomposite platform was confirmed by the ratio of anodic (I_{pa}) to cathodic (I_{pc}) peak currents which was calculated to give 0.992. Also, the anodic and cathodic square wave voltammograms gave approximately the same peak potential values (see Fig. 5.4d). In addition, the integration of the anodic and cathodic CV peaks from Fig. 5.4a (wave GCE/PPI-AuNP) gave charges of 528.1 nC and -524.7 nC, respectively, which are the same within experimental error.

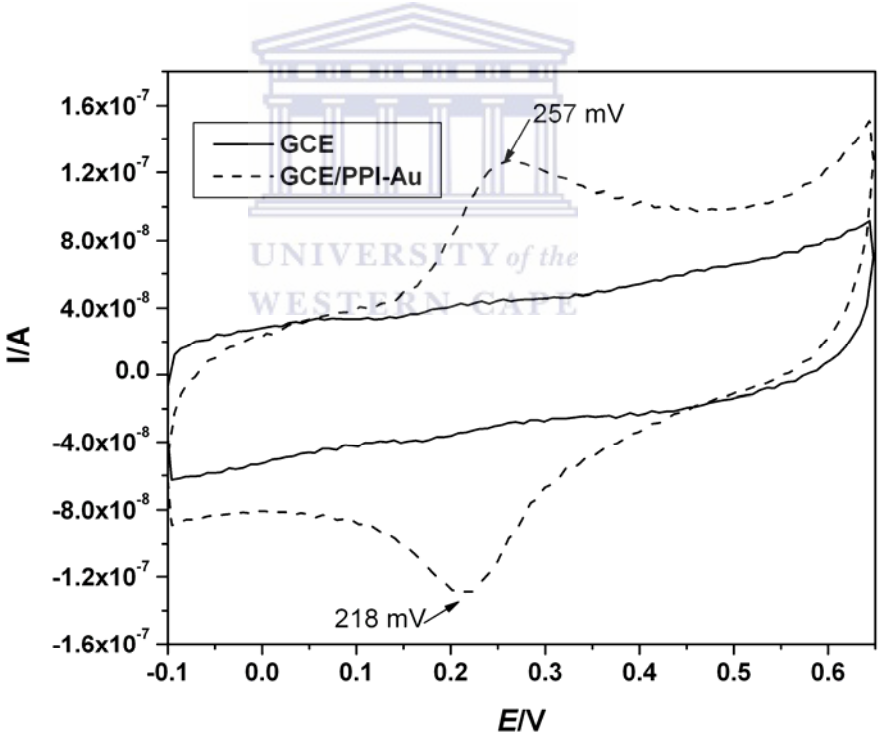

(a)

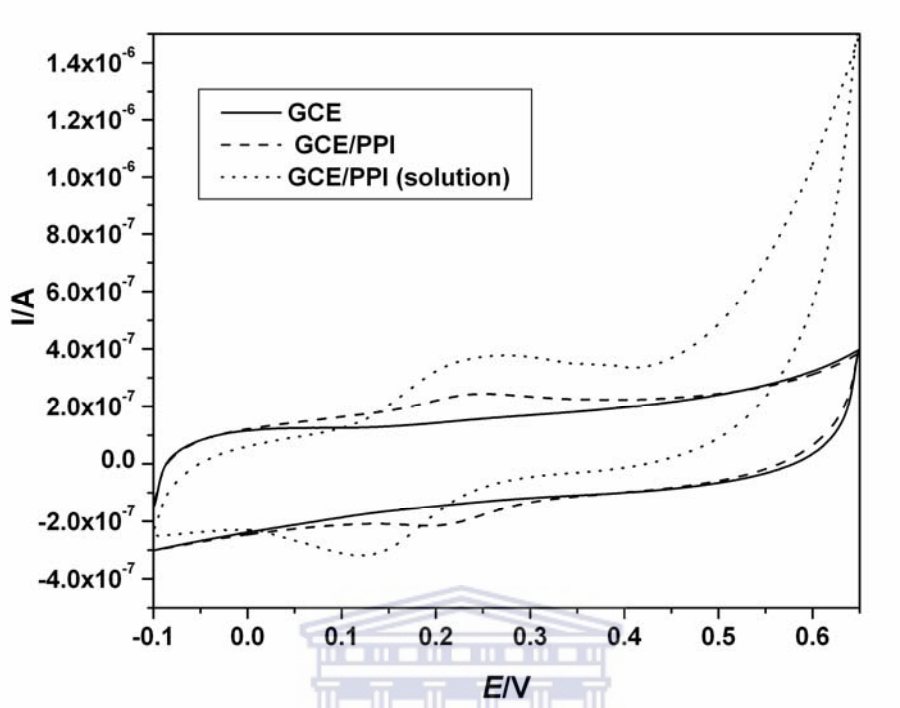

(b)

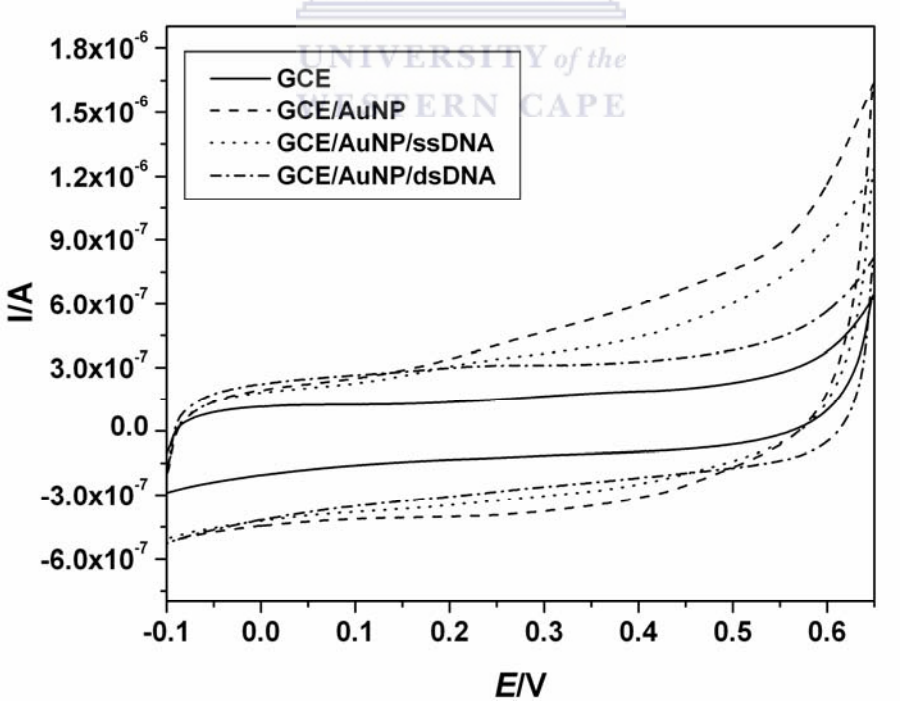

(c)

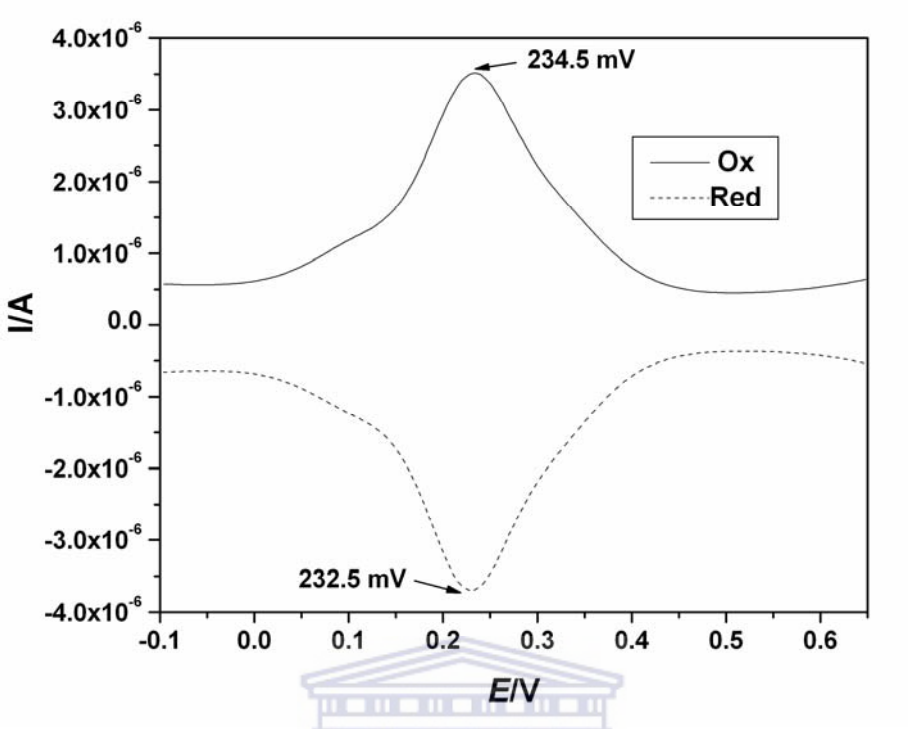

Figure 5.4 (a) CV of GCE and GCE/PPI-AuNP in PBS from -100 mV to 650 mV at 20 mV/s. (b) CV of 3 mM PPI solution on GCE and GCE/PPI. Background electrolyte is 10 mM PBS. (c) CV of GCE and GCE/AuNP with ssDNA and dsDNA in PBS. (d) Oxidative and reductive square wave voltammograms of GCE/PPI-AuNP in PBS

Fig. 5.5a shows the CV of GCE/PPI-AuNP at different scan rates in PBS. From this figure, (i) the currents increased with increase in scan rate with no shift in potential, (ii) I_{pa} was proportional to scan rate and (iii) a plot of I_{pa} versus scan rate showed linearity with correlation coefficient of 0.9978 (Fig 5.5b). It can thus be deduced that the platform was conducting and exhibited a reversible electrochemistry characteristic of surface adsorbed specie because I_{pa} versus scan rate was linear [249]. Ideally, for surface adsorbed specie, E_{pa} should be the same as E_{pc}. However, the ΔE of ca 30 mV observed here may be as a result of

diffusion of electrons along the PPI matrix and this value suggests a two electron system. The fact that there was no shift in potential and the I_{pa}/I_{pc} remained unity also showed the stability of the PPI-AuNP platform in PBS.

In order to investigate the surface concentration of the deposited G4 PPI, the charge passed at any of the scan rates in Fig. 5.5a was calculated by integrating the anodic or the cathodic faradaic current using equation 5.1 or 5.2. A charge of ca 0.7698 μC was obtained.

$$Q = \frac{1}{\nu}\int i\,dE \qquad \textbf{eqn. 5.1}$$

$$Q = \int_{t_0}^{t_1} i\,dt \qquad \textbf{eqn. 5.2}$$

Equation 5.1 is used if the cyclic voltammogram is an $i\,vs\,E$ plot while eqn. 5.2 is used for $i\ vs\ t$ plot.

Proof:

$Scan\,rate, \nu = \frac{dE}{dt}$ (a). Therefore $dt = \frac{dE}{\nu}$ (b)

Put (b) into $Q = \int_{t_0}^{t_1} i\,dt$ and take out the constant $1/\nu$

$$Q = \int_{t_0}^{t_1} i\,\frac{dE}{\nu} \qquad \Rightarrow Q = \frac{1}{\nu}\int i\,dE$$

A surface concentration, Γ, of 1.12 x 10^{-10} mol/cm^2 was obtained using equation 5.3, where Q = 0.7698 μC, A = 0.071cm^2.

$$Q = nFA\Gamma \qquad \textbf{eqn. 5.3}$$

This value indicates that the electrodeposited dendrimer was a monolayer.

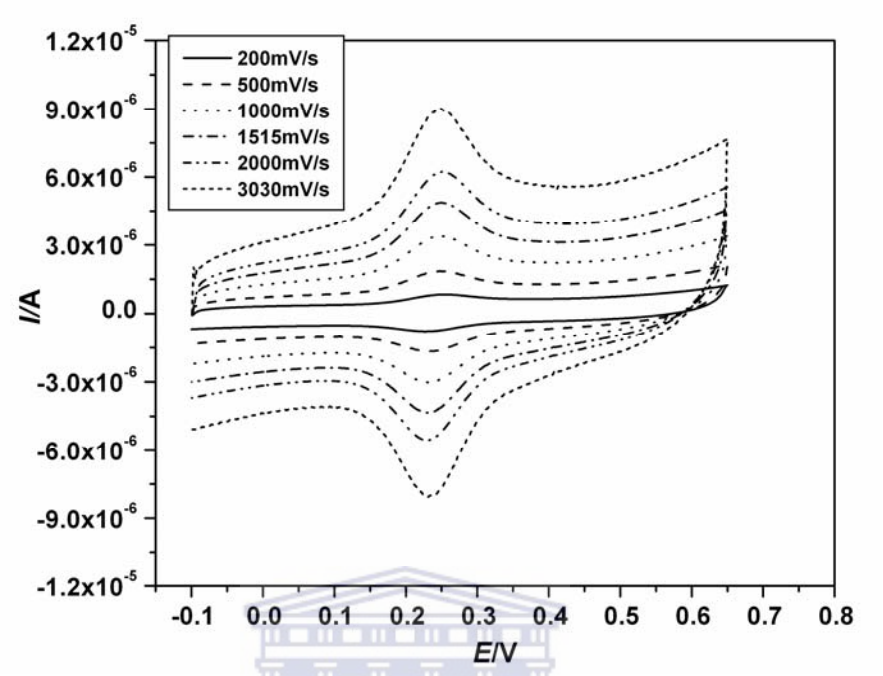

(a)

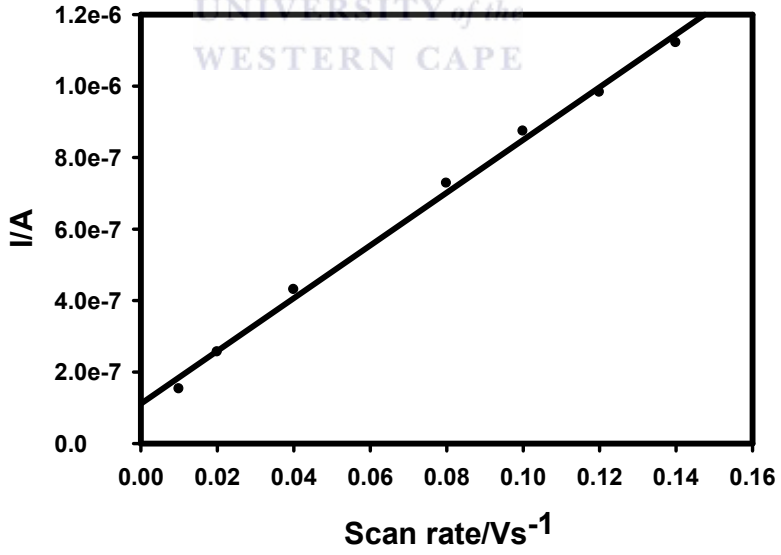

(b)

Figure 5.5 (a) CV of the GCE/PPI-AuNP in PBS as a function of scan rate (b) Scan rate dependence of I_{pa} plot

5.3 pH studies of GCE/PPI

The PPI on the electrode consists of secondary and tertiary amine molecules which are responsible for its reaction. PPI are positively charged (cationic) polyelectrolyte in their protonated form. The ionization behaviour of PPI has been studied using potentiometry and NMR. These studies [250, 251] revealed that PPI can be protonated to a degree of 2/3. For more insights into the number of electron(s) and proton(s) involved in the electrochemistry of immobilised PPI, effect of variation in pH on its voltammetric response was studied in PBS. From the CV (Table 5.1) and SWV (Table 5.1 and Fig. 5.6) data, it can be inferred that the optimum pH for the PPI's reversibility and conductivity is ca 7.

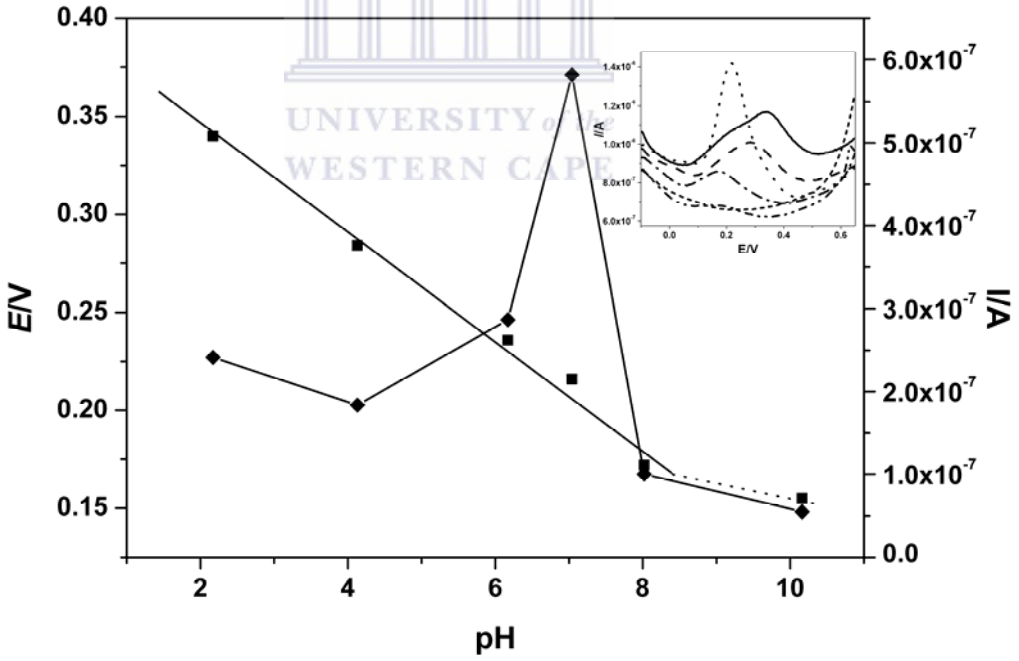

Figure 5.6 A plot of E_{pa} (▪) and I_{pa} (♦) vs pH obtained from square wave responses (inset) of GCE/PPI in phosphate buffer solution at different pH

Fig. 5.6 shows the plot of E_{pa} and I_{pa} vs pH obtained from SWV (Fig. 5.6 inset). E_{pa} shifted cathodically (to lower values) as pH increased from 2 to 8 (Fig. 5.6 solid line (▪)) following the relationship $E_{pa} = 399.97 - 0.028pH$ (and $E^{\circ'} = 425.74 - 0.030pH$ for CV). The 28 mV per pH unit, which is close to the Nernstian value of 29.5 mV (59/n for n =2), showed that the redox mechanism of PPI involves a two electron, one proton process [252]. Above the pH of 8.5 there was deviation from this relationship and the electrochemistry was completely quenched at pH 12. From this response to pH, it can be inferred that the electrochemistry of the nanocomposite is facile only when the dendrimer is moderately protonated. The pKa of tertiary amine is ca 10 (pKb = 4) thus, the common rules (derived from Henderson-Hasselbach equation) which states that (i). at $pH \leq pKa - 2$ the substance exist mostly in its associated or protonated form and (ii) at $pH \geq pKa + 2$ the substance exist mostly in its dissociated or deprotonated form, supports our observation. The dendrimer can be thought to be practically completely protonated up to the pH of 8.5 and below and totally deprotonated above pH 12. The pH dependence of PPI observed agrees with Koper and co-workers [253] who carried out ^{15}N-NMR study of PPI using Ising model. They observed variation in chemical shift of tertiary nitrogen with pH as a result of protonation which vary in degrees from shell to shell in a two step mechanism.

Table 5.1 Potential parameters obtained from the response of GCE/PPI to pH in 0.1 M phosphate buffer solution (Fig. 5.6) using both CV and SWV at 100 mV/s

pH	E_{pa} (mV) CV [SWV]	E_{pc} (mV) CV	$E^{0\prime}$ (mV) CV	ΔE (mV) CV
2.17	388 [340]	336	362	52
4.13	320 [284]	270	295	50
6.17	249 [236]	213	231	36
7.04	223 [216]	201	212	22
8.02	211 [172]	149	180	62
10.16	-[155]	186	-	-
12.00	-	-	-	-

5.4 Electrochemical Impedance spectroscopy of GCE/PPI-AuNP

Charge transfer resistance (in form of a semi circle) was not observed in the complex plane plot of the GCE/PPI-AuNP in PBS (Fig. 5.7a). This observation is expected for reversible system where the charge transfer is very facile (as seen in the high scan rates of 3000 mV in Fig. 5.5a) hence $R_{ct} \approx R_s$. Thus EIS also confirmed the reversible electrochemistry of PPI-AuNP as discussed with voltammetry. Also, total impedance (in PBS) of GCE/PPI-AuNP was remarkably lower than that of bare GCE confirming the presence of a conducting layer. Fig. 5.7b shows the complex plane impedance behaviour of GCE/PPI-AuNP electrode system in $Fe(CN)_6^{3-/4-}$ redox probe while Table 5.2 shows the equivalent circuit (Fig. 5.7b inset) parameters of GCE/PPI-AuNP at 200 mV. The E°′ and lowest R_{ct} of $Fe(CN)_6^{3-/4-}$ redox chemistry on GCE [82] and GCE/PPI-AuNP occurred at ca 200 mV, hence the choice of 200 mV as the bias potential in

the EIS studies. The $Fe(CN)_6^{3-/4-}$ redox probe exhibited kinetic control and diffusion controlled electrochemistry at high and low frequency respectively at the PPI-AuNP interface. Complex phase element, CPE, was used in the model because the semi circle observed was depressed, the phase angle observed in the measurement was less than 90° (not shown) and CPE is also appropriate to model the non ideal behaviour of the inhomogeneous electrode surface. Solution resistance, R_s, was used to model the electrolyte resistance at high frequency when the double layer capacitance is very small and the charge transfer kinetics is just at the onset. Charge transfer resistance, R_{ct}, corresponding to the diameter of the semicircle in Fig. 5.7b and was used to model the resistance of the $Fe(CN)_6^{3-/4-}$ redox probe at the electrode surface. At a sufficiently low frequency, diffusion controlled process becomes limiting and this was modelled by Warburg impedance (Z_w).

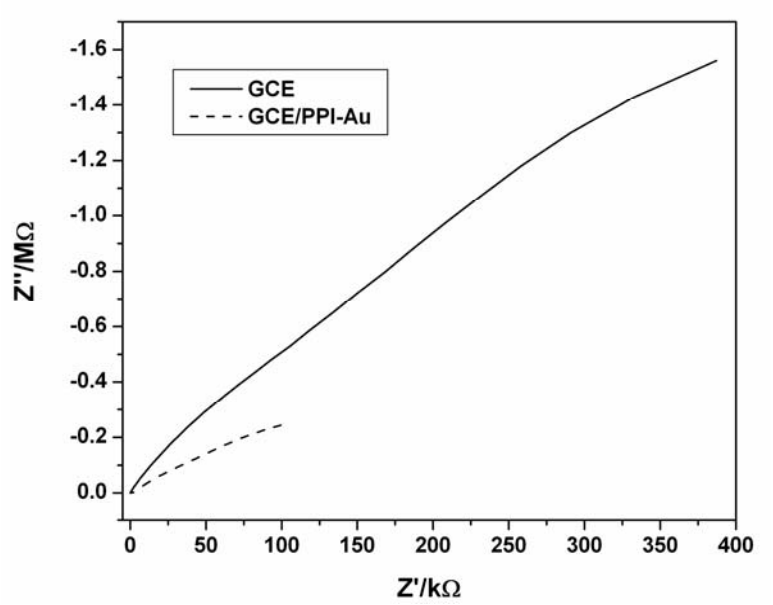

(a)

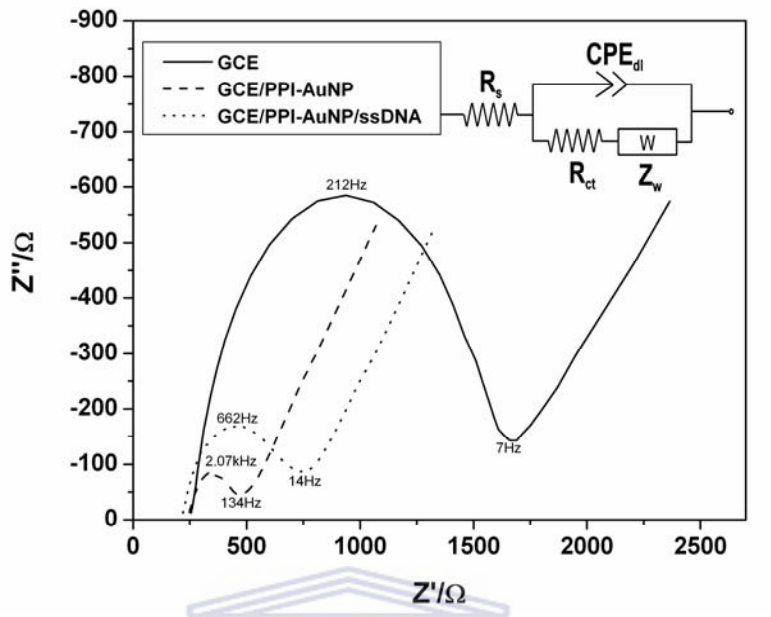

(b)

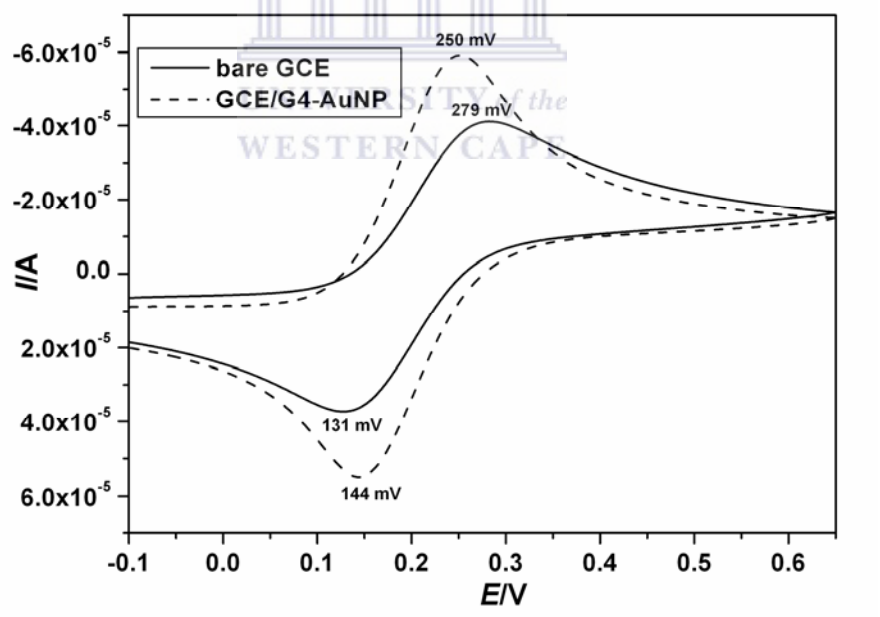

(c)

Figure 5.7 (a) Nyquist plot of bare GCE and GCE/PPI-AuNP in PBS. (b) Nyquist plot of GCE, GCE/PPI-AuNP and GCE/PPI-AuNP/ssDNA in 5 mM $Fe(CN)_6^{3-/4-}$ redox probe. (c) CV of bare GCE and GCE/PPI-AuNP in $Fe(CN)_6^{3-/4-}$

From Fig. 5.7b, R_{ct} for GCE/PPI-AuNP decreased by 81% compared to that of the bare GCE. The positively charged (cationic) platform (AuNP is Au^0) attracted the negatively charged $Fe(CN)_6^{3-/4-}$ to its surface and facilitated the electron exchange for $Fe(CN)_6^{3-/4}$. The result showed that the redox kinetics of $Fe(CN)_6^{3-/4-}$ was faster when GCE was modified with PPI-AuNP and this makes the platform more suitable for biosensor redox mediation in the presence of $Fe(CN)_6^{3-/4-}$ redox probe. The decreased R_{ct} also suggests the improved conductivity. The GCE/PPI-AuNP platform enhanced the electrochemistry of $Fe(CN)_6^{3-/4-}$ by the noticeable reduction in formal potential from 148 mV to 106 mV and increased faradiac current as seen in Fig 5.7c. The PPI-AuNP can be said to have catalytic effect on the rate of the charge transfer kinetics or the faradaic process of the redox probe. This can be shown by calculating the time constant of the faradaic process using the frequency (ω_{max}) at the maximum imaginary impedance according to equations 5.4 and 5.5 [249]:

$$\omega_{max} = \frac{1}{R_{ct}C_{dl}} \qquad \textbf{eqn. 5.4}$$

$$\tau = R_{ct}C_{dl} \qquad \textbf{eqn. 5.5}$$

where C_{dl} = double layer capacitance; τ = time constant; $\omega_{max} = 2\pi f$

From Table 5.2, for the bare GCE, R_{ct} = 1348 Ω, $\omega_{max} = 2\pi x 212 Hz$ Therefore C_{dl} = 0.557 μF and τ = 7.508 x 10^{-4} s rad^{-1}. For GCE/PPI-AuNP, R_{ct} = 251.2 Ω, $\omega_{max} = 2\pi x 2.07 kHz$. Therefore C_{dl} = 0.306 μF and τ = 7.687 x 10^{-5} s rad^{-1}. The time constant calculated showed that the faradaic process of the $Fe(CN)_6^{3-/4-}$ probe is one order of magnitude faster on the PPI-AuNP modified GCE than bare GCE

thus confirming its catalytic properties. The exchange current i_0 which is a measure of the rate of electron transfer expressed in current was also calculated using equation 5.6:

$$R_{ct} = \frac{RT}{nFi_0} \qquad \textbf{eqn. 5.6}$$

i_0 = 1.905 x 10^{-5} A and 1.022 x 10^{-4} A for GCE and GCE/PPI-AuNP respectively, where R = 8.314 $JK^{-1}mol^{-1}$, F = 96 486 $Cmol^{-1}$, and n =1. A higher exchange current, which means increase in the rate of electron transfer, was observed at the modified GCE. GCE/PPI in the presence of $Fe(CN)_6^{3-/4-}$ also behaved in a similar way to GCE/PPI-AuNP but the R_{ct} was larger and the catalytic effect observed above was not as pronounced. Thus some possible reasons for the catalytic effect (increase in reaction rate) observed at the GCE/PPI-AuNP/$Fe(CN)_6^{3-/4-}$ interface are (i) nanostructured nature of the electrode surface (ii) the enhanced surface area and conductivity due to AuNP, and (iii) increase in $Fe(CN)_6^{3-/4-}$ flux to the electrode surface due to the electrostatic attraction between the cationic platform and the anionic $Fe(CN)_6^{3-/4-}$. Similar effect of improved electrochemical properties of $Fe(CN)_6^{3-/4-}$ using AuNP has been reported [254]. The ability of the PPI-AuNP platform to catalyse Fe^{3+}/Fe^{2+} redox reaction is a promising feature for redox mediation in enzymes which have $Fe^{2+/3+}$ at the haem group. This catalytic effect was observed during the EIS measurements. It took 56 s to reach the 7 Hz (low frequency end of the charge transfer resistant) for GCE, whereas it took 29 s to reach 134 Hz frequency for GCE/PPI-AuNP.

Table 5.2 The EIS parameters obtained from the circuit fitting of Fig. 5.7b.

Circuit element	R_s (Ω)	R_{ct} (Ω)	CPE (nF)	Z_w
GCE	258	1348	463	699
GCE/PPI-AuNP	236	251	434	617
GCE/PPI-AuNP/ssDNA	212	528	468	604
Average Error	6.88	2.97	8.31	2.47

5.5 The voltammetric responses of the biosensor

Apart from AuNP enhancing the R_{ct} of $Fe(CN)_6^{3-/4-}$ [254], AuNP was also incorporated into the composite for the purpose of connecting the thiolated probe ssDNA to the GCE surface via Au-S linkage [150, 156]. The probe immobilisation effectiveness would also be improved by an electrostatic attraction between the cationic platform and anionic DNA probe. Figure 5.8a presents the cyclic voltammetric responses of the bare GCE, GCE/PPI-AuNP (the platform), GCE/PPI-AuNP/ssDNA (the biosensor) and GCE/PPI-AuNP/dsDNA (the hybridised biosensor). The biosensor stability monitored over a period of 30 days shown in Fig. 5.8b, indicates effective adsorption of the probe DNA on the PPI-AuNP platform.

As can be seen in Fig.5.8a, there was a 36% attenuation of the anodic peak current (I_{pa}) of GCE/PPI-AuNP after the immobilisation of the target ssDNA. However, the I_{pa} increased by 20% after exposing the resulting DNA biosensor to 0.05 nM target ssDNA (hybridisation). This phenomenon may be attributed to the electrical or charge transportation properties of DNA. Various researchers [59, 63-66], have shown that DNA charge-transport or transfer characteristics can be

explained on the basis of the two most fundamental processes for electron transfer in extended electronic systems, which are coherent tunnelling and diffusive thermal hopping. Furthermore, DNA's ability to undergo electron transfer and its conductivity are due to its ability to adopt different structures along the molecule, as well as the polyelectrolyte character of the double helix. These may lead to the flow of positively charged counter ions along the negatively charged phosphate backbone, with electrons and holes appearing to shuttle along a single DNA molecule over a distance of a few nanometres.

While most of these views are based on the bases (i.e. guanine, cytosine, adenosine and thymine) in DNA, electron delocalization in the conducting band through the phosphate backbone has also been proposed [68]. Based on these theories of DNA behaviour, the electrochemical responses of the GCE/PPI-AuNP after probe ssDNA immobilisation and hybridisation with target ssDNA can be attributed to the possibility of charge transfer between the cationic PPI and DNA base stacks and/or anionic backbone. Though DNA is not electroactive at +230 mV unlike the G4 PPI (Fig. 5.4), its 2-deoxyriboso-5-phosphate backbone, with PPI provides a supramolecular setting in which protons can be delocalised over a wider space and their contribution could be under potential control. Earlier studies [255] have shown that PPI can be an efficient hydrogen donor. It can therefore be speculated that DNA's conductivity allowed certain degree of protonation of PPI (Fig. 5.8c). Also the fact that electron or charge is able to tunnel through the DNA base stack can also lead to a delocalized electron flow between the DNA and PPI molecules. The increase in the number of the more conducting guanine-cytosine

(G-C) base pairs as a result of the formation of dsDNA is responsible for the increased current when the biosensor was hybridised.

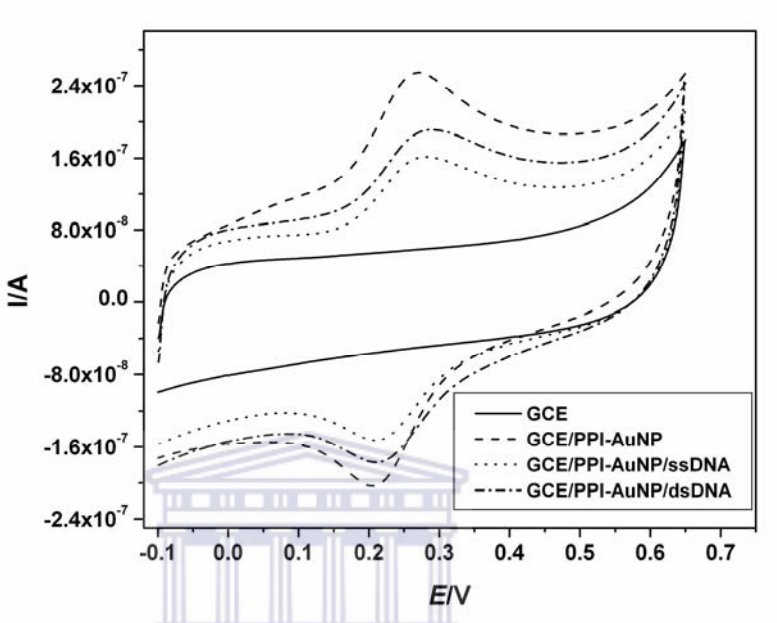

(a)

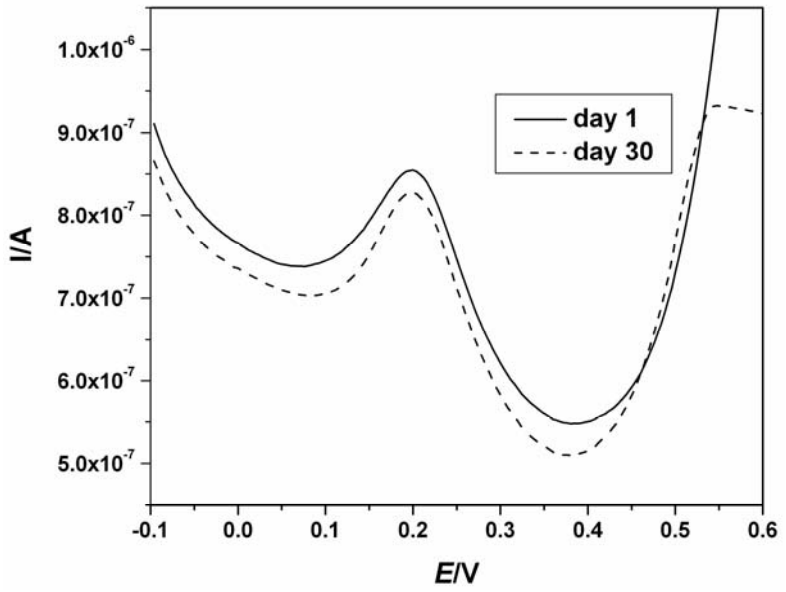

(b)

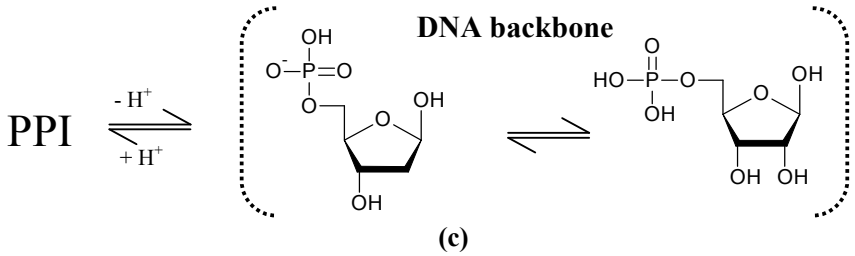

Figure 5.8 (a) CV of GCE/PPI-AuNP/ssDNA (developed with 2 μM thiolated ssDNA) and GCE/PPI-AuNP/dsDNA (i.e. response to 0.05 nM DNA target ssDNA) in PBS at 20 mV/s. (b) Differential pulse voltammograms of GCE/PPI-AuNP/ssDNA biosensor in PBS when stored for 30 days. (c) Proposed charge transfer scheme between the PBS electrolyte, DNA and PPI-AuNP.

5.6 Impedimetric responses of the biosensors

During the analysis of the spectra in Fig. 5.7b, it was observed that R_{ct} increased by 276.4 Ω (Table 5.2) when the probe DNA was immobilised. The reason for this is that the negatively charged phosphate backbone of the single strand DNA attached to the platform repels the anionic $Fe(CN)_6^{3-/4-}$ redox probe. As shown in Fig. 5.9a, after the pairing up (hybridisation) with target ssDNA, the anionic density of the resultant GCE/PPI-AuNP/dsDNA further increased the barrier for interfacial electron transfer because of the double strands formed. The dsDNA formed further repelled the negatively charged $Fe(CN)_6^{3-/4-}$ redox probe and thus increased the R_{ct} [256]. Kramers Kronig transform (eqn. 5.7) was used to validate the impedimetric responses shown in Fig.5.9c. This integral equation allows the imaginary impedance, Z″, to be calculated from the real impedance, Z′, data. The experimental and calculated imaginary impedance show very good correlation.

$$Z''(\omega) = -\frac{2\omega}{\pi}\int_0^{\infty}\frac{Z'(x)-Z'(\omega)}{x^2-\omega^2}dx \qquad \textbf{eqn. 5.7}$$

The impedance spectra in Fig. 5.9a were fitted to the equivalent circuit in Fig. 5.7b (inset) where the parallel R_{ct} and CPE were used to model the combination of the three layers, namely, the platform, probe DNA and target DNA. As explained earlier, the absence of a second semi circle is due to the fast redox of chemistry of the platform. Hence the R_{ct} of $Fe(CN)_6^{3-/4-}$ reports the DNA/ $Fe(CN)_6^{3-/4-}$ interfacial kinetics. Table 5.3 shows the values obtained from the circuit fitting. Fitting errors were less than 1% for R_{ct} which was chosen as the analytical parameter and less than 10% (not shown) for other circuit elements.

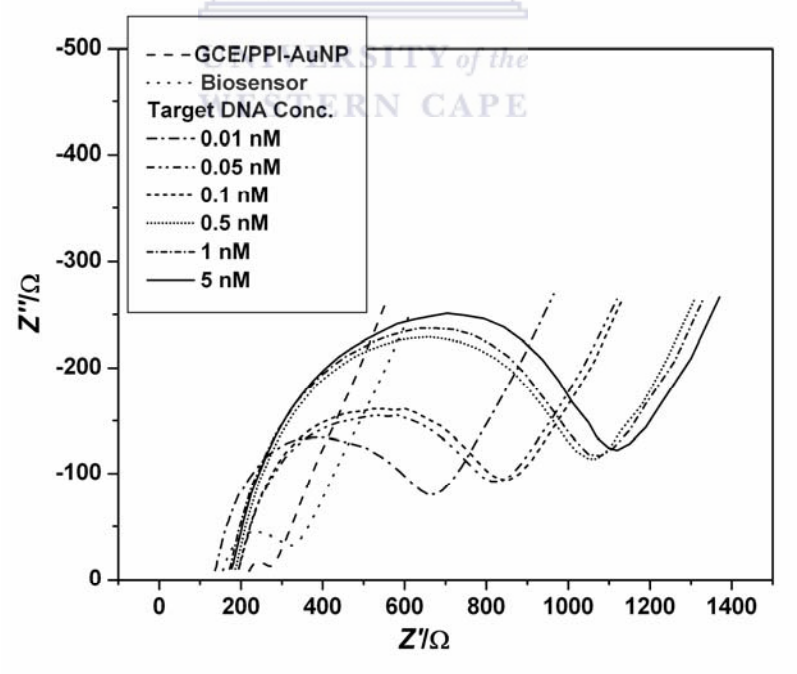

(a)

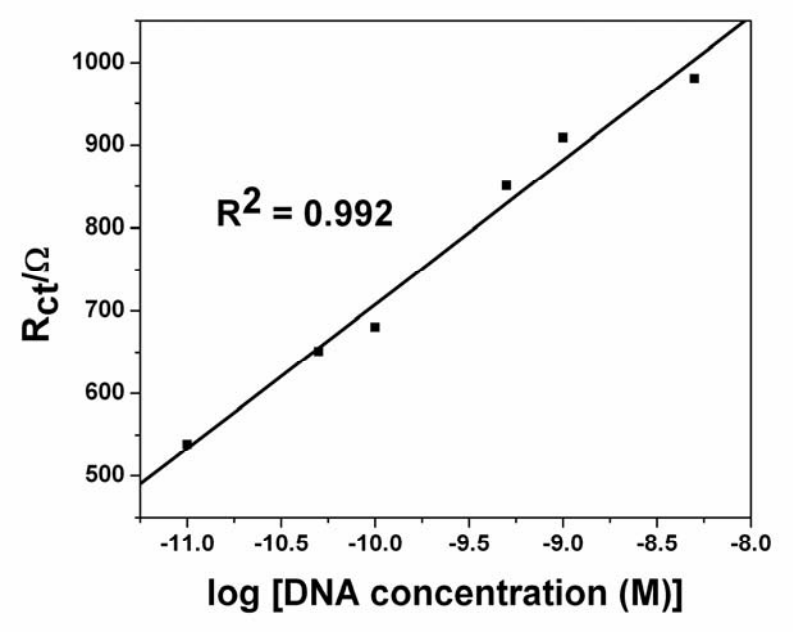

(b)

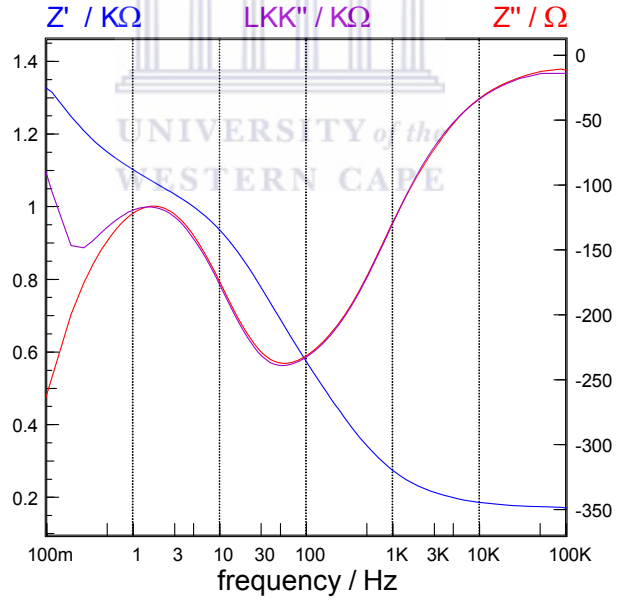

(c)

Figure 5.9 (a) Nyquist plots of the biosensor responses to 0.01 nM to 5 nM of target DNA in the presence of $Fe(CN)_6^{3-/4-}$ redox probe (b) The calibration curve obtained using Rct versus logarithm of concentration. (c) Kramer-Kronig (KK) plot for data validation. Z′ (blue line) is the experimental real impedance; LKK″(lilac line) is imaginary impedance calculated with the Kramer-Kronig equation; and Z″ (red line) is the experimental imaginary

Fig. 5.9b shows the calibration plot of the DNA biosensor. A correlation coefficient, $R^2 = 0.992$ and a sensitivity of 1.56×10^{11} Ω/M were obtained. With a standard deviation of $\sigma = 19.3$ for three blank hybridisation measurements, the detection limit calculated was 3.45×10^{-10} M using $3\sigma/slope$.

Table 5.3 EIS parameters of GCE/PPI-AuNP/dsDNA obtained from Fig.5.9a.

Target DNA conc. (nM)	**0.01**	**0.05**	**0.1**	**0.5**	**1**	**5**
log (Target DNA conc. (nM))	-11	-10.3	-10	-9.3	-9	-8.3
R_{ct} (Ω)	538.3	651.2	680.5	850.4	908.8	981
Error (R_{ct})	0.43	1.24	0.93	0.6	0.36	0.53
R_s (Ω)	127.4	183	182.9	176.4	161.8	167.4
CPE (nF)	852	871.3	850.5	802.7	830	812.8
Z_w	301.3	286.2	286.7	288.5	282.9	285.1

5.7 Sub Conclusions

A new method of modifying GCE with poly(propylene imine) dendrimer and gold nanoparticle nanocomposite and exploiting their properties for immobilisation of ssDNA was developed. The GCE/PPI-AuNP nanocomposite platform exhibited reversible electrochemistry, good conductivity, pH sensitivity and excellent catalytic properties toward $Fe(CN)_6^{3-/4-}$ redox probe. This DNA biosensor was highly sensitive; to the extent that it was able to amperometrically detect target DNA concentrations as low as 0.05 nM in PBS Using impedimetric detection techniques, the biosensor had a dynamic linearity of 10^{-12} to 10^{-9} M for target DNA ($R^2 = 0.992$), and a detection limit of 3.45×10^{-10} M. The obtained values

compare well with the best reported in literature for impedrimetric DNA biosensors [157, 243]. This study also showed that owing to the favourable biomolecular immobilisation properties of dendrimers and the possibility of modifying their inner core, the PPI-modified GCE can also be applied in enzyme and antibody biosensors.

CHAPTER 6

RESULTS AND DISCUSSION: An Electrochemical DNA Biosensor developed on a Generation One Poly(Propylene Imine) Dendrimer Nanoplatform

6.1 Introduction

This chapter presents the results obtained from electrochemical preparation, characterization and application of generation one poly(propylene imine) dendrimer (G1 PPI) as a nanobiosensor platform. The experimental procedures leading to the results have been explained in **Chapter 3 section 3.5** (general experimental) and **section 3.8.**

The biocompatibility of poly(propylene imine) with DNA has been demonstrated in its application in gene and drug delivery [15] and also in its DNA binding studies [257] without the use of gold nanoparticle (AuNP). Therefore, a platform without AuNP was investigated. The previous chapter established G4 PPI to be electroactive and since G1 also contain amine group prone to protonation [253], a similar electrochemistry may be observed. G1 PPI was characterised i) in solution (GCE/G1PPI$_{sol}$), ii) as electrodeposited (GCE/G1PPI) and iii) as platform for DNA biosensor (GCE/G1PPI/DNA). Apart from the electrodeposition of G1 PPI, G2 and G3 were deposited in order to see any unique pattern. The G1 platform was electroactive and the detection limit of the biosensor was 6.6 x 10^{-10} M.

6.2 Electrochemical behaviour of generation one PPI in solution (G1 PPI_{sol})

6.2.1 Voltammetry

Fig 6.1a and 1b show the CV and SWV of bare GCE in PBS versus bare GCE in 10 mM G1 PPI respectively. No redox chemistry was observed for GCE in PBS within the potential window chosen. However, in the presence of 10 mM G1 PPI, a redox couple at E_{pa} = 242 mV and E_{pc} = 182 mV with formal potential $E^{0'}$ = 212 mV is observed for CV. While the overlapped oxidative and reductive SWV peaks gave a $E^{0'}$ = 211 mV. This shows that G1 PPI is electroactive. Similar electroactive behaviour has been observed with G4 PPI and this observation further confirmed that PPI can behave as electroactive materials at the shown potential.

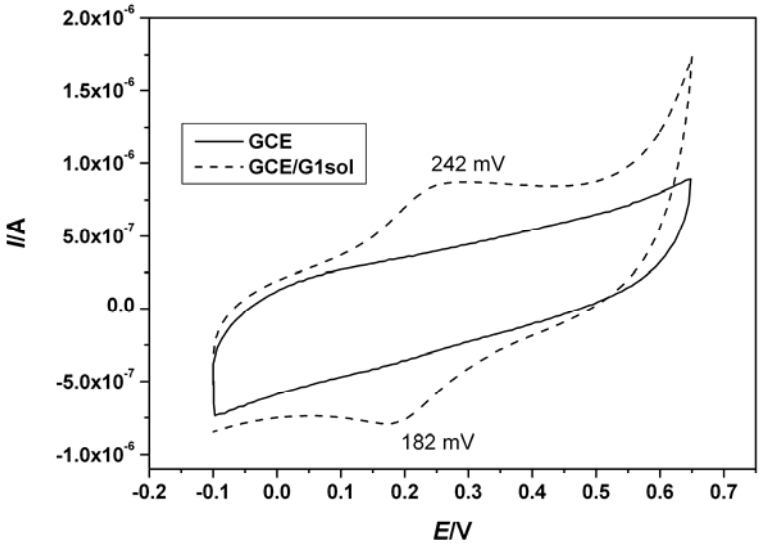

(a)

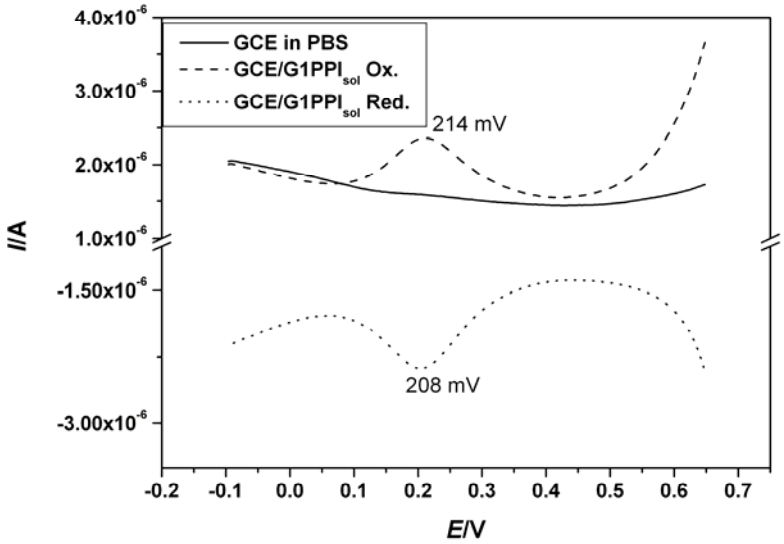

(b)

Figure 6.1 Voltammetry of 10 mM G1 PPI in solution on a bare GCE. (a) CV and (b) SWV overlaying the oxidation and the reduction peak

From Fig. 6.1 and 6.2, the following deductions, which are diagnostic of a reversible reaction, can be seen: Fig. 6.1: Ip_c / Ip_a is 0.9, the formal potential $E^{0'}$ from the CV and SWV is ca 210 mV and is located midway the two potentials. Fig. 6.2:

E_{pa} and E_{pc} are independent of scan rate.

$\Delta E = 60\,mV$ Hence number of electron, n = 1 as obtained from ($\Delta E\left(E_{pa} - E_{pc}\right) = {}^{59}\!/_{n}\, mV$).

$Ip_a / Ip_c \approx 1$ at most scan rate and Ip versus $\nu^{1/2}$ is linear with correlation coefficient of 0.9994.

These confirm that the electrochemistry of $G1PPI_{sol}$ is a reversible one electron process.

From Fig. 6.2 a and b, the diffusion coefficient calculated from CV using the Randle Sevcik equation (eqn. 6.1) gave 7.5 x 10^{-10} cm^2s^{-1} as shown below:

T = 25°C, R = 8.314 $Jmol^{-1}K^{-1}$ and F = 96486 $Cmol^{-1}$ C = 1 x 10^{-5} mol/cm^3, n = 1, A = 0.071 cm^2 and slope = 5.23 x 10^{-6}.

$$I_p = \left(2.69\times10^5\right)n^{3/2}AD^{1/2}v^{1/2}C \qquad \textbf{eqn. 6.1}$$

Therefore:

$$\frac{I_p}{v^{1/2}} = slope = 5.23\times10^{-6} = \left(2.69\times10^5\right)\times1\times0.071\times\left(1\times10^{-5}\right)\times D^{1/2}$$

$$\frac{I_p}{v^{1/2}} = slope = 5.23\times10^{-6} = 0.191\times D^{1/2}. \rightarrow \left(\frac{5.23\times10^{-6}}{0.191}\right)^2 = D_e = 7.5\times10^{-10}\ cm^2s^{-1}$$

From Fig. 6.2 c and d, the diffusion coefficient using the slope = 4.264 x 10^{-7} was also calculated from

$$\Delta i_p = \frac{0.665nFAD_O^{1/2}C_O^*}{\pi^{1/2}}f^{1/2} \qquad \textbf{eqn. 6.2}$$

(See section 3.4.3.3 for how this equation was derived)

D_e obtained was 2.75 x 10^{-10} cm^2s^{-1}. This value is close to that obtained from CV suggesting that the derived equation is a fair SWV analogue of Randle sevcik equation. The diffusion coefficients calculated cannot be judged as low or high because dendrimer are a novel class of macromolecule and such data are very few. However, the D_e obtained is not that different from reported value of 6.68×10^{-9} cm^2 s^{-1} [239] for polyaniline. Abruna [241] calculated diffusion coefficient of a PAMAM which has been functionalised with redox active species and obtained a value of 3.6×10^{-7} cm^2 s^{-1}. The G1 PPI used here was not functionalised and thus we have no good basis for comparison. Even Abruna noted discrepancies in the

voltammetric D_e and judged the value to be too low. Until more kinetic data on pristine dendrimer evolve, these values can serve as reference points. Protonation effect which does not occur uniformly on the shell and core may be a reason for the 'low' diffusion coefficient.

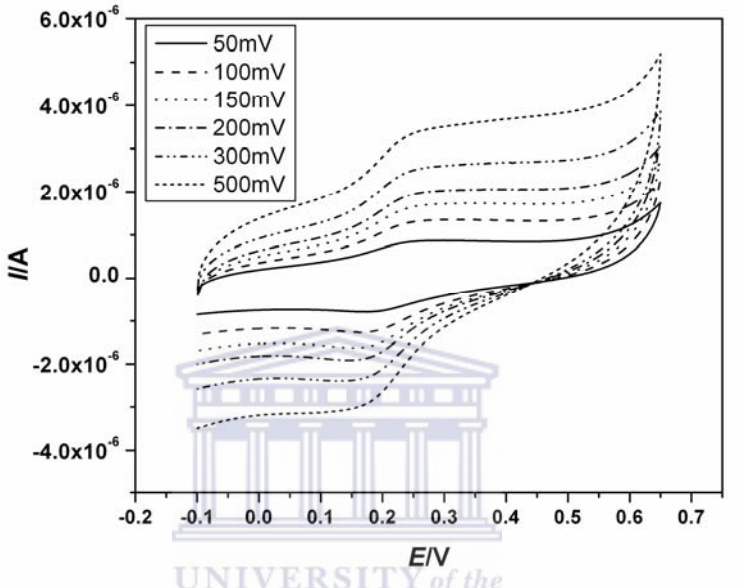

(a)

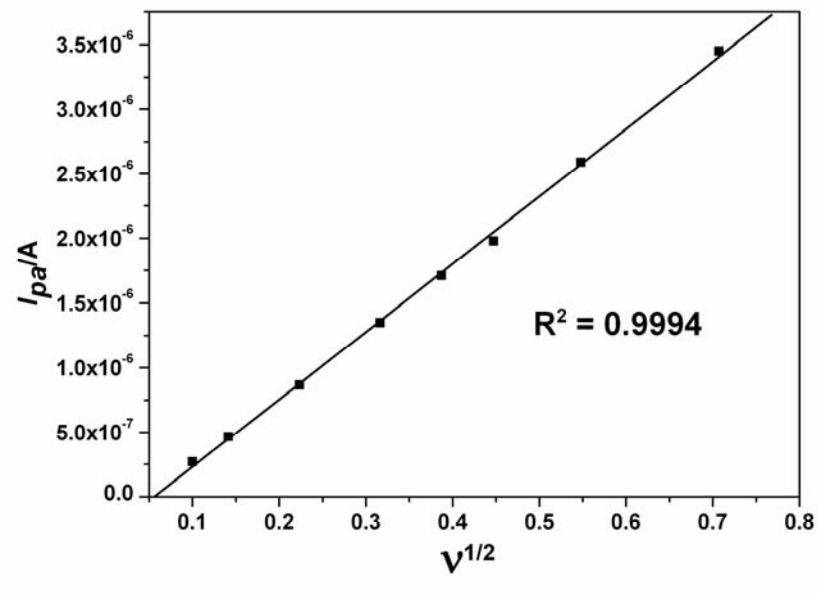

(b)

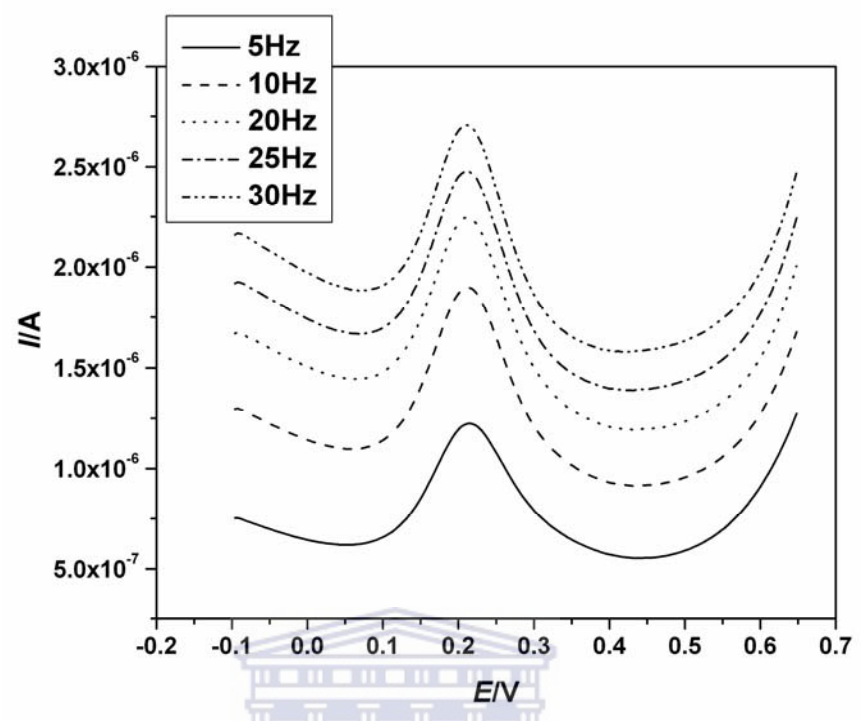

(c)

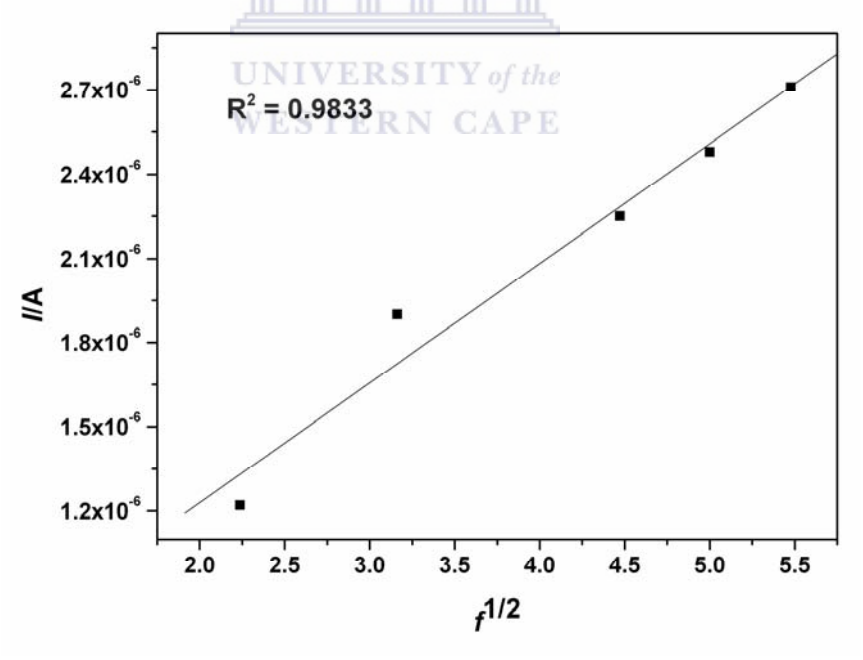

(d)

Figure 6.2 Voltammetry of 10 mM G1PPI in 0.1 M PBS. (a) CV at different scan rates. (b) Randles Sevcik plot (c) SWV at different frequencies. (d) a plot of current versus $f^{1/2}$.

6.2.2 Electrochemical Impedance Spectroscopy (EIS)

EIS Nyquist plane plot of G1 PPI_{sol} (Fig 6.3) gave the least real and imaginary impedance at 200 mV which further supports the formal potential obtained from voltammetry. The experimental data obtained was validated using KK (eqn. 6.3) and Z-HIT (eqn. 6.4) transforms. The KK equation allows the imaginary impedance, Z″, to be calculated from the real impedance, Z′; while Z-HIT calculates the impedance data |Z|(f) from the phase data φ(f) data. The results are shown in Fig 6.4 a (KK) and b (Z-HIT). It has been shown that Z-HIT transform offers a more reliable result than KK [236]. Therefore Z-HIT transform will be used henceforth. In Fig. 6.4 a, there is a good correlation between the experimental Z′ data (red) and KK calculated data (lilac). Fig. 6.4b, also shows a good correlation between the experimental absolute impedance |Z| data (red) and Z-HIT calculated data (lilac). Thus the data obtained were at steady state and therefore credible.

$$Z''(\omega) = -\frac{2\omega}{\pi}\int_0^{\infty}\frac{Z'(x)-Z'(\omega)}{x^2-\omega^2}dx \qquad \textbf{eqn. 6.3}$$

$$\ln\left|H(\omega_0)\right| \approx const.\frac{2}{\pi}\int_{\omega_s}^{\omega_0}\varphi\,(\omega)d\ln\omega + \gamma.\frac{d\varphi(\omega_0)}{d\ln\omega} \qquad \textbf{eqn. 6.4}$$

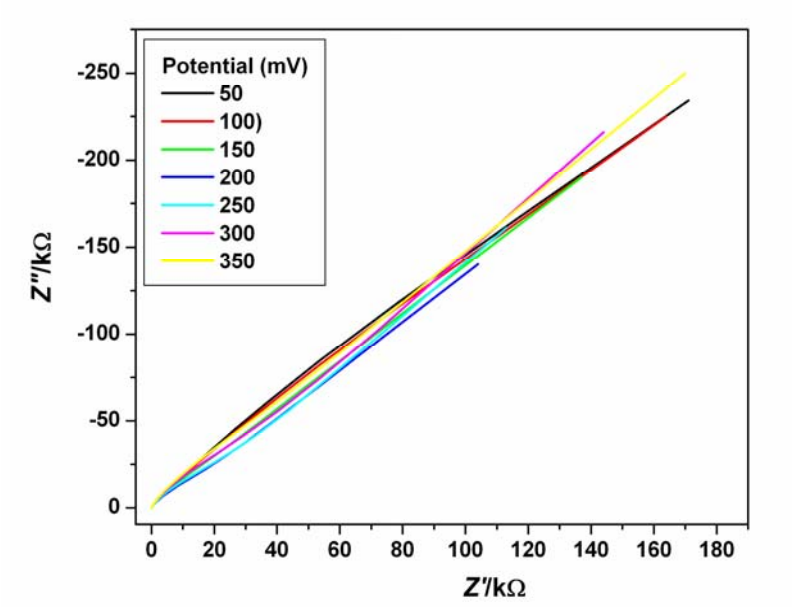

Figure 6.3 Nyquist plot of 10 mM G1 PPI in 0.1 M PBS at different potentials.

The absence of semi circle (complex plane plot) and the R_{ct} portion in the bode plot (Fig. 6.4 b, ZHIT) suggested that the electron transfer kinetics of G1 PPI is very fast and the time scale was too fast to be noticed as charge transfer resistance.

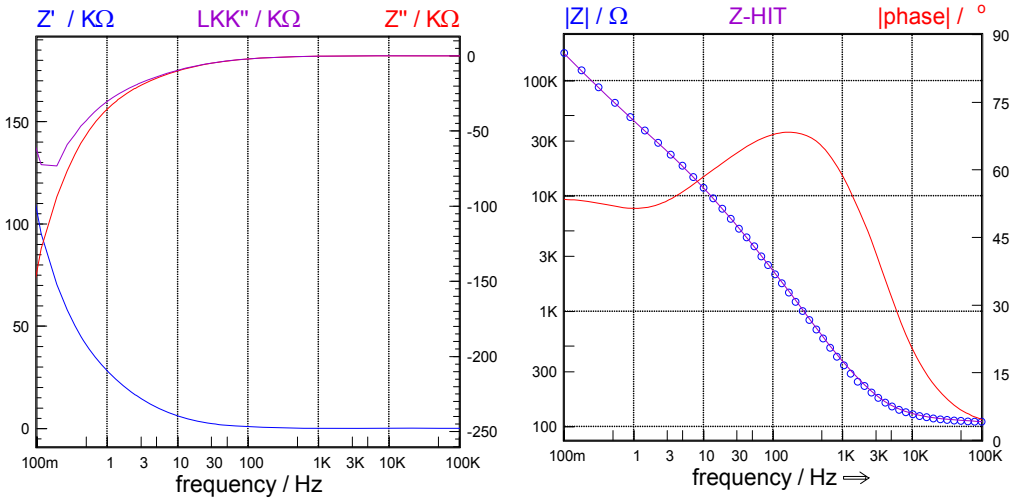

Figure 6.4 (a) KK transform of experimental data from Fig. 6.3. experimental Z′ (blue), experimental Z″ (red), KK calculated Z″ (lilac). (b) Z-HIT plot. Experimental phase φ (red), experimental |Z| (blue circles) calculated |Z| (lilac)

The impedance of GI PPI in solution was dominated by diffusion process as seen in Fig. 6.3. The Warburg coefficient, σ, is usually calculated using the equation:

$$Z'_f = R_{ct} + \sigma\omega^{-1/2} \qquad \textbf{eqn. 6.4a}$$

$$Z''_f = -\sigma\omega^{-1/2} \qquad \textbf{eqn. 6.4b}$$

Equation 6.4a expresses Warburg coefficient as a function of the real impedance where charge transfer resistant R_{ct} dominates. The value of σ from this equation is usually computed at the lower frequency end where the effect of R_{ct} diminishes. However, owing to the fast electron transfer reaction of the dendrimer in solution, R_{ct} could not be observed, thus an estimate of σ will be computed from equation

6.4b. A plot of the imaginary impedance $-Z''$ versus $\omega^{-1/2}$ should give a linear plot passing through the origin as shown in Fig. 6.5

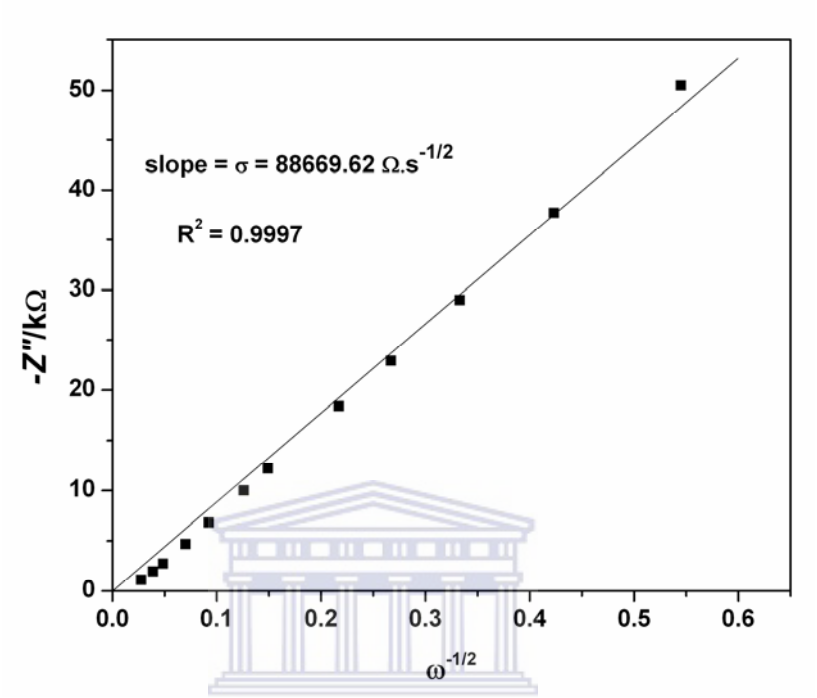

Figure 6.5 Determination of Warburg coefficient from a plot of imaginary impedance versus the inverse of the square root of radial frequency.

Diffusion coefficient can be calculated using the σ from equation 6.5a

$$\sigma = \frac{RT}{n^2F^2A\sqrt{2}}\left[\frac{1}{C_R\sqrt{D_R}} + \frac{1}{C_O\sqrt{D_O}}\right] \qquad \textbf{eqn. 6.5a}$$

It is assumed that $C_R = C_O = C^*$ and $D_R = D_O = D_e$, therefore equation 6.5a simplifies to:

$$\sigma = \frac{RT}{n^2F^2A\sqrt{2}}\left[\frac{2}{C^*\sqrt{D_e}}\right] \qquad \textbf{eqn. 6.5b}$$

With all other parameters remaining the same (as used in the voltammetric determination) and $\sigma = 8.87\times10^4\ \Omega s^{-1/2}$, D_e was found to be $3.57\times10^{-11}\ cm^2s^{-1}$.

There is therefore a fair comparison between the diffusion coefficient obtained from CV and EIS within the limits of the assumptions made and experimental error.

6.3 Electrodeposition of G1 PPI (GCE/G1PPI)

Surface characterization was done using similar method in chapter 5. Fig. 6.6a to c represent the blank SPCE, the electrodeposited G1 PPI at 50, 000 and 100,000 thousand magnification respectively. A uniform globular growth of G1 PPI of ca 50 nm size is observed. A higher magnification, would have given a better estimate of a smaller size at higher magnification; unfortunately the SEM used for this particular analysis could not produce excellent images at higher magnification unlike the FE SEM used in chapter 5. However the intention of the SEM is to confirm electrodeposition, morphology and see if the size is below 100 nm.

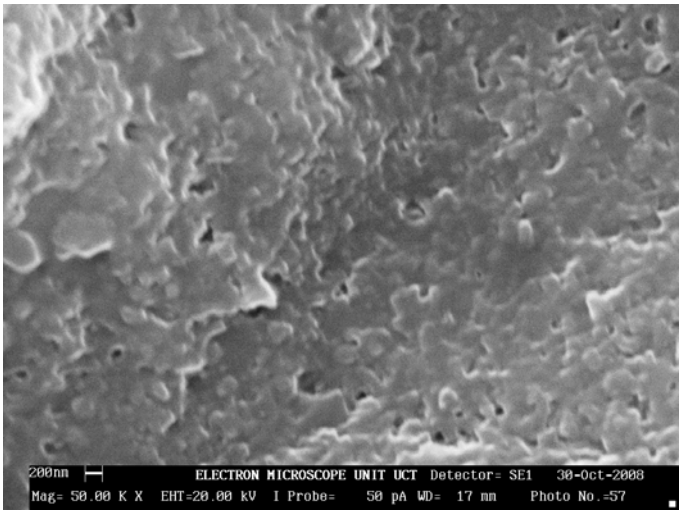

(a)

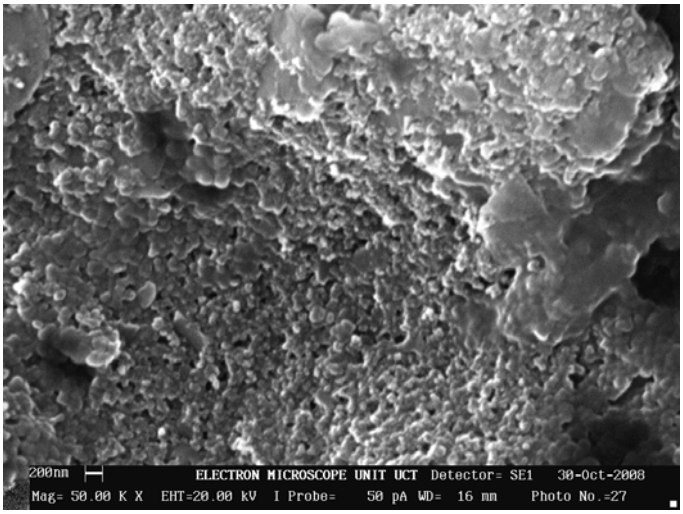

(b)

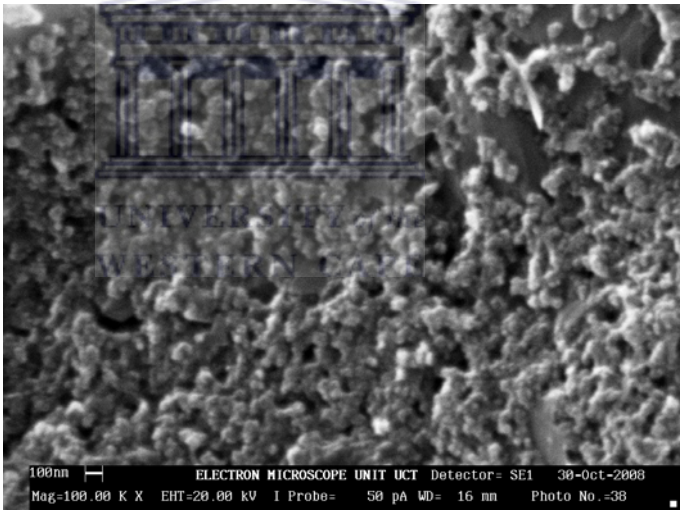

(c)

Figure 6.6 SEM images of electrodeposited G1 PPI onto SPCE. (a) blanc (b) G1 at 50k magnification, (c) G1 at 100k magnification

G1 PPI was linked to the GCE via electrooxidation of primary amine onto carbon forming C-N bond. Electrooxidation of free primary amine have been used to modify GCE [247]. The most common is the use of 4-aminobenzoic acid (4-ABA) which is covalently grafted on a glassy C electrode (GCE) by amine cation radical formation during the electrooxidation [258]. The primary amine in G1 PPI

(Fig. 6.7) was attached via this well established amine cation radical formation. The first cycle in Fig 6.8 shows the electrooxidation/free radical formation peak which occurred at ca 700 mV. Subsequent cycles did dot show any increase in current or film growth. This means that there was no polymerization but just a deposition and the multi cycle was just to ensure maximum coverage of the GCE surface. The portion highlighted by a circle in the Fig. 6.8 shows the onset of the electroactive response even during the electrodeposition. The electroactive behaviour is peculiar to PPI and not as a result of impurity. To ascertain this and also to observe the trend in PPI electrodeposition, G1 to G3 PPI (G4 was shown in chapter 5) from both sigma Aldrich and SyMO-Chem, were used. It can be observed from Fig. 6.8a to c that the voltammogram obtained are alike. The first scan peak due to the cationic radical formation is seen at ca 700 mV for all. Also a redox couple around 200 mV can be observed.

It was observed that immediately after electrodeposition, the electrode voltammetric signal was unstable when run in PBS. This variability in faradiac response was solved by a step I call ‘equilibration’. After every electrodeposition, the GCE/G1PPI is left either at room temperature or at 4°C temperature to ‘equilibrate’ for a minimum of 5 hrs. Then voltammetry is repeated in PBS until the signal remains steady (Fig. 6.9). The electrode was only used after a stable signal was ensured i.e. after the equilibration procedure.

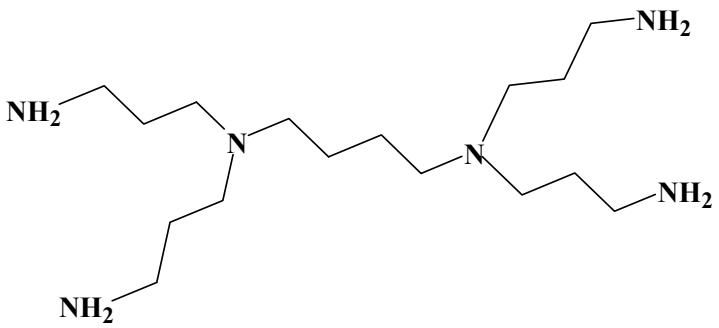

Figure 6.7 Structure of Generation 1 poly(propylene imine)

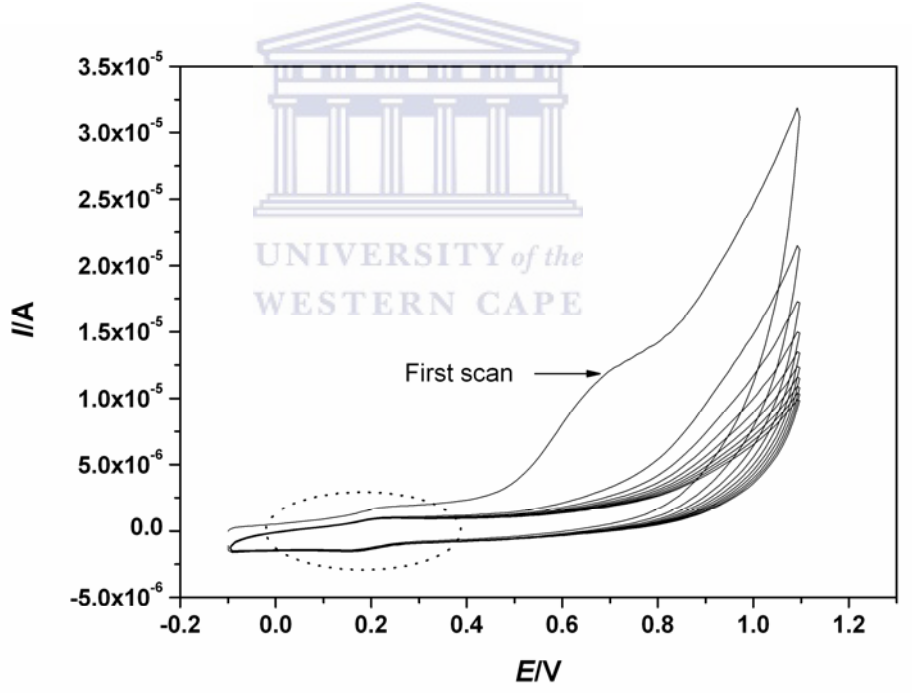

(a)

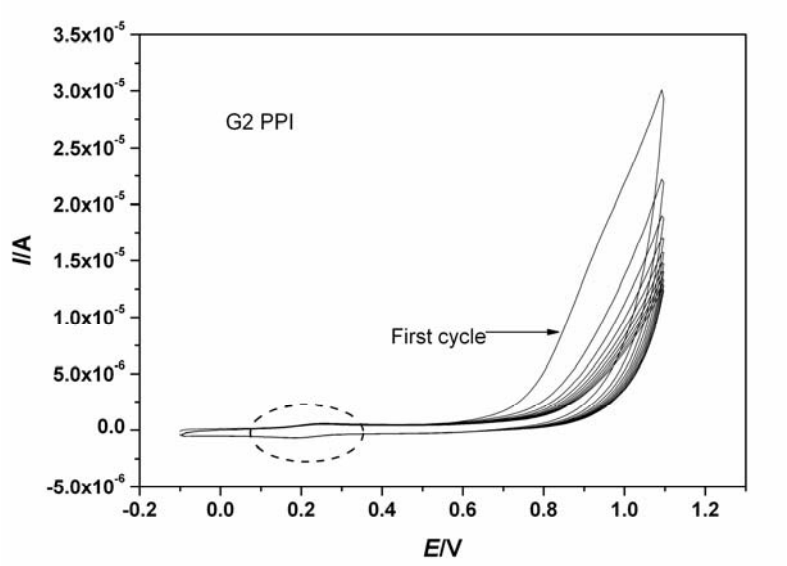

(b)

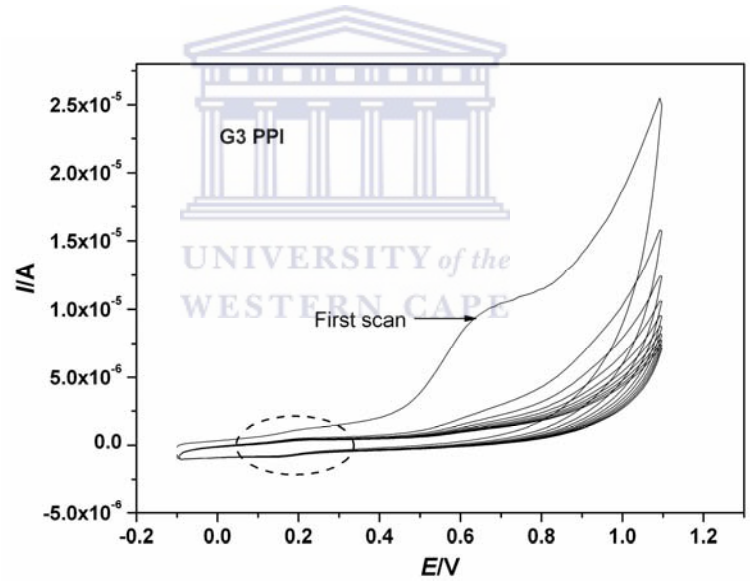

(c)

Figure 6.8 Electrooxidation of PPI onto GCE from a 0.1 M phosphate buffer solution. (a) 10 mM G1. (b) 10 mM G2. (c) 5 mM G3

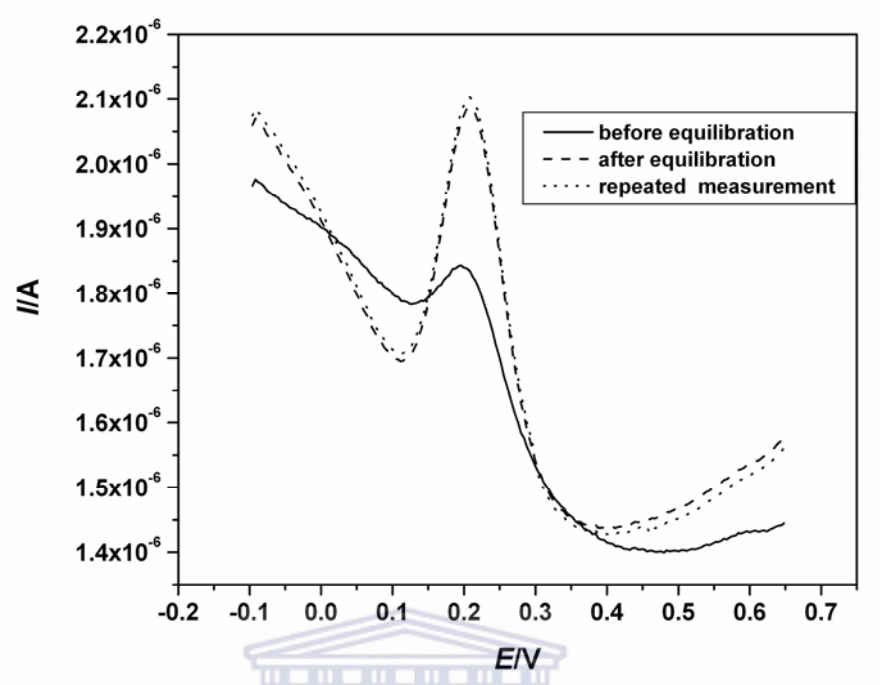

Figure 6.9 The equilibration step: Repeated measurements of the SWV of GCE/G1PPI in PBS after electrodeposition.

6.4 Electrochemistry of GCE/G1PPI in PBS

The CV obtained after deposition (Fig.6.10) was similar to that of the solution (Fig. 6.1a) with formal potential $E^{0'}$ of 220 mV. It appears that E_{pa}, E_{pc} and $E^{0'}$ of GCE/G1PPI shifted anodically in comparison to GCE/G1PPI$_{sol}$. A similar shift was observed for G4 PPI. The exact reason for this is not known but it may be due to the difference in the energy level or reactivity of G1 PPI in solution and G1 PPI deposited. There is no free primary amine in the electrodeposited PPI because it has been used for the C-N bonding. Thus, the outermost shell comprises of secondary amine and the influence of the primary amine shell in the protonation or electrochemical mechanism is altered. From Fig. 6.10 and 6.11, it can be observed that there is no significant shift in E_{pa} and E_{pc} as

scan rate changes. For a reversible reaction, $\Delta E\left(E_{pa} - E_{pc}\right) = {}^{59}\!/_{n}\, mV$ and ΔE = 250 -190 = 60, thus n = 1. The peak current ratio, $Ip_a / Ip_c = \left(0.743/0.727\right)\mu A \approx 1$. A plot of anodic (or cathodic) peak current I_p versus scan rate (Fig. 6.11b), when CV of GCE/G1PPI was characterised in PBS at different scan rate (Fig 6.11), was linear with correlation coefficient of 0.992. This linearity is characteristic of surface bound or adsorbed specie as expected from equation 6.6. Fig. 6.10 and 6.11 also show that the deposited G1 PPI is electroactive and undergoes a reversible one electron system for the same reasons in section 6.1. The electroactive behaviour is as a result of the protonation of the amine of the dendrimer [250, 251, 259].

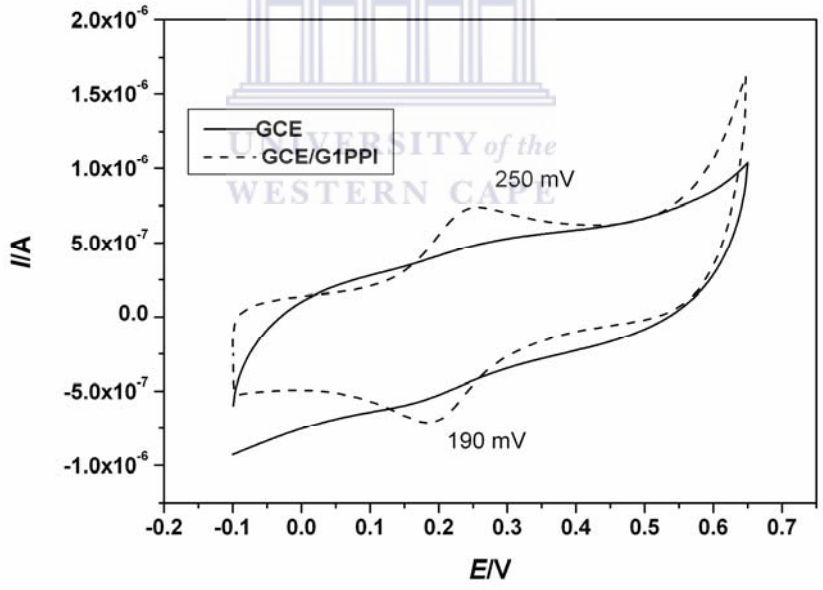

Figure 6.10 Cyclic voltammetry of electrodeposited GCE/G1PPI in PBS

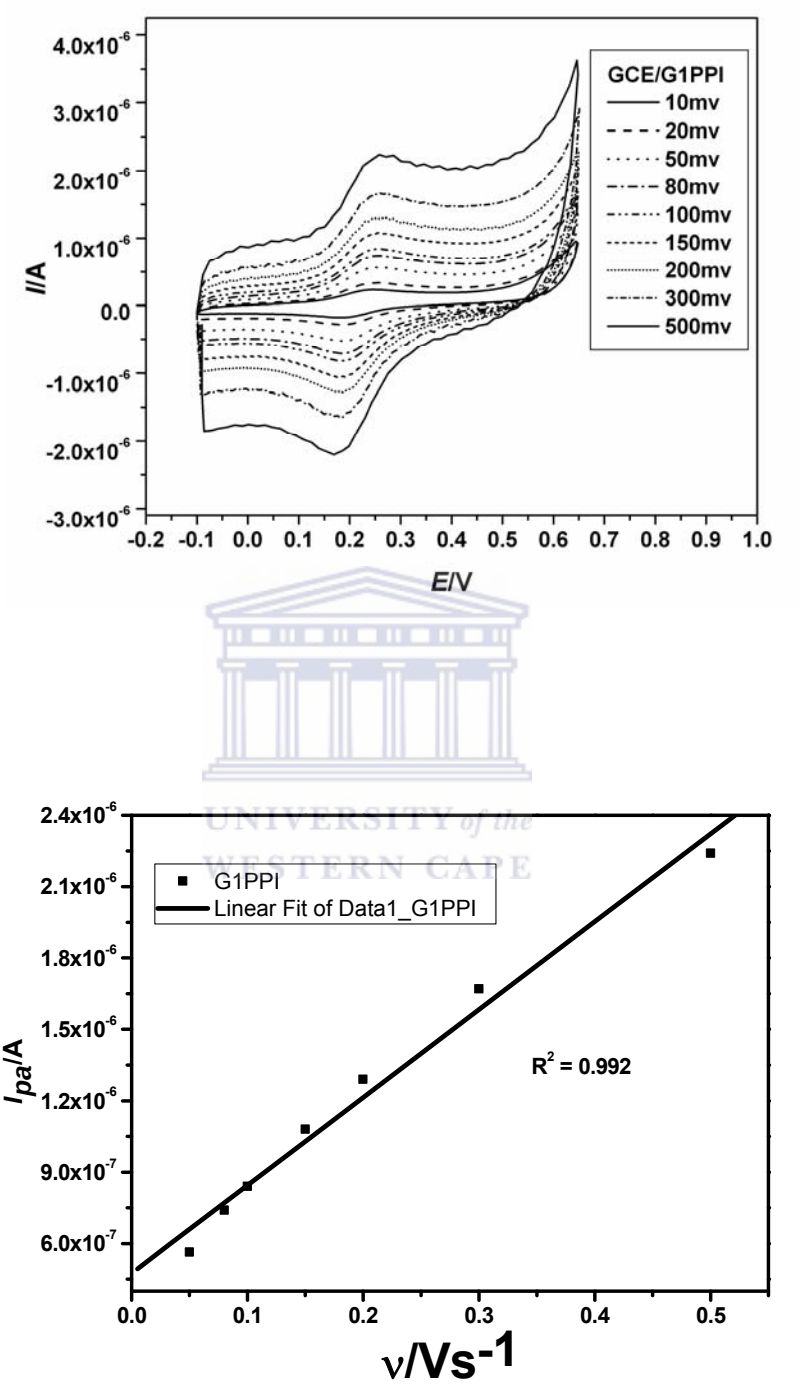

Figure 6.11 (a) Cyclic voltammetry of GCE/G1PPI at different scan rates in PBS. (b) Randle's plot

$$i_p = \frac{n^2 F^2}{4RT} \nu A \Gamma^* \qquad \textbf{eqn. 6.6}$$

The surface concentration of the deposited G1PPI was calculated using the following equations as follows:

$$Q = \int i \, dt \qquad \textbf{eqn. 6.7a}$$

$$\Gamma = \frac{Q}{nFA} \qquad \textbf{eqn. 6.7b}$$

The faradaic charge passed (wave GCE/G1PPI (Fig.6.10)) = 5.826 μC and surface concentration = 8.504 x 10^{-10} mol/cm^2. Thus the concentration of PPI falls into the monolayer region. This supports the CV obtained from the deposition where no film growth was observed after the first cycle.

The Nyquist plot in Fig. 6.12 compares the impedance response of the generation one PPI modified GCE (GCE/G1PPI) at different potential with that of bare GCE in PBS. While the Bode plot in Fig. 6.13, compares bare GCE with GCE/G1PPI in PBS at 200 mV. These figures show that GCE/G1PPI's conductivity and impedance were least at 200 mV (green solid line in Fig. 6.12). The impedance data was fitted using the equivalent circuit in Fig 6.12b

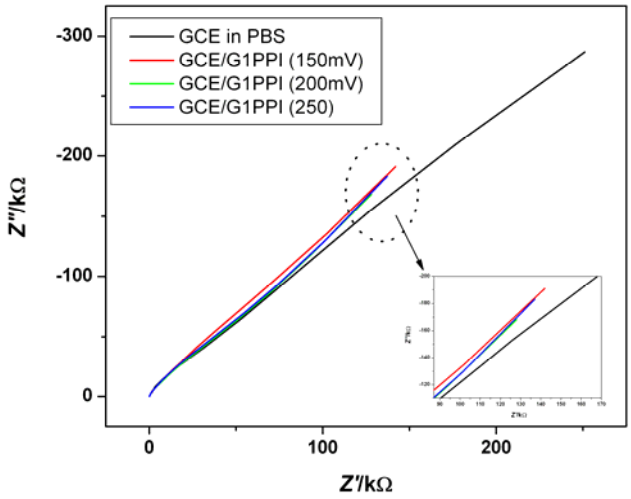

(a)

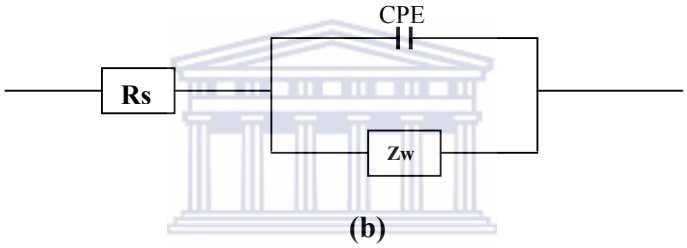

(b)

Figure 6.12 (a) Nyquist plot of GCE/G1PPI at different bias potential in PBS. (b) The equivalent circuit

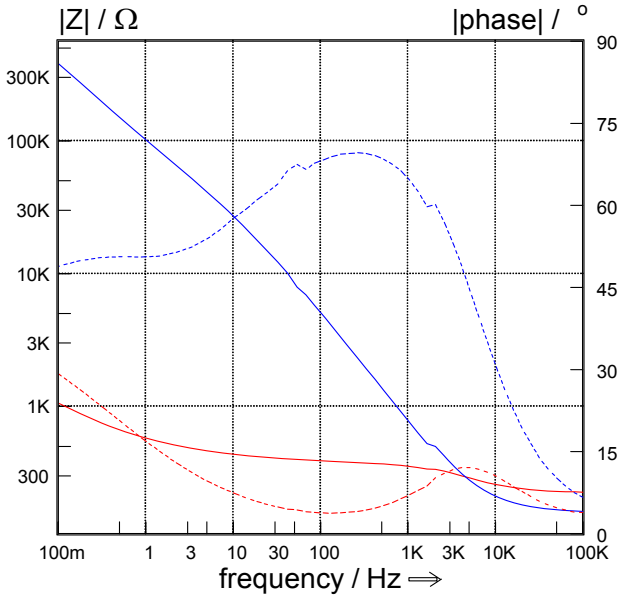

Figure 6.13 Bode plot of GCE/G1PPI at 200 mV in PBS

As discussed earlier, R_{ct} could not be noticed because of the speed of the electron transfer, hence for this system, $R_s \approx R_{ct}$. Since the kinetics is fast, the process is diffusion controlled and this is depicted by the 45° Warburg impedance line. Constant phase element was used to model the capacitance. Fig 6.14 compares the raw experimental data with the fitted data using the equivalent circuit, while table 6.1 shows the fitting parameters obtained with the errors.

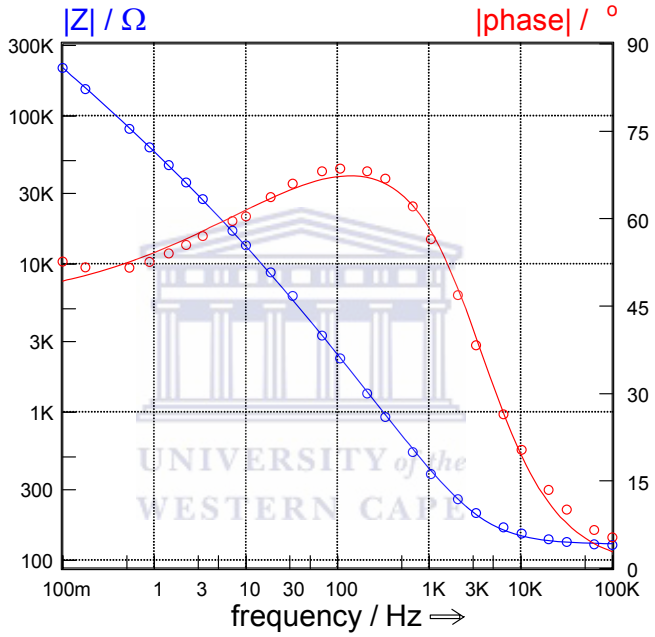

Figure 6.14 Bode plot of the overlay of the experimental data (red and blue circles) and the fitted data (red and blue line) raw data from the equivalent circuit fitting

Table 6.1 The EIS fitting values obtained from GCE/G1PPI in PBS.

Circuit element	GCE	GCE/G1PP1			
		150 mV	200 mV	250 mV	Average error (%)
Rs (ohm)	157.7	127.5	128.5	128.6	4.74
CPE (nF) [α]	165.9	391.5	378.6	375	6.44
Zw ($k\Omega/s^{1/2}$)	307.9	219.6	188.2	205.5	6.23

The increase in the double layer or the presence of a film is indicated by the increase in capacitance after electrodeposition. The lowest value of Warburg impedance was that of GCE/G1PPI (200 mV) depicting the condition of best diffusion of ions or charge through the platform.

6.5 Electrochemistry of GCE/G1PPI in $Fe(CN)_6^{3-/4-}$ redox probe

Prior to electrodeposition of G1 PPI onto GCE, EIS measurement of bare GCE in $Fe(CN)_6^{3-/4-}$ redox probe was taken (Fig. 6.15a) and the equivalent circuit in Fig . 6.15b was used to fit the data.

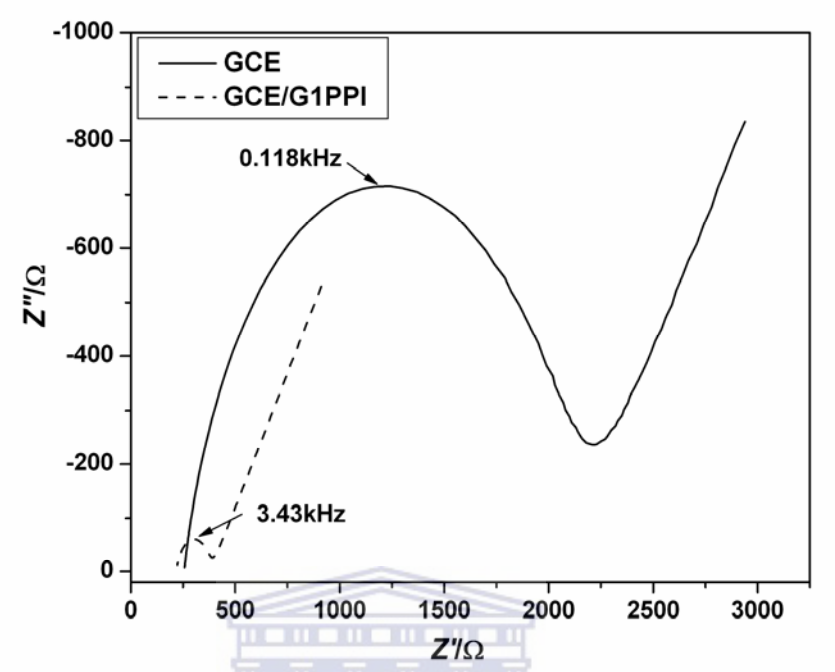

(a)

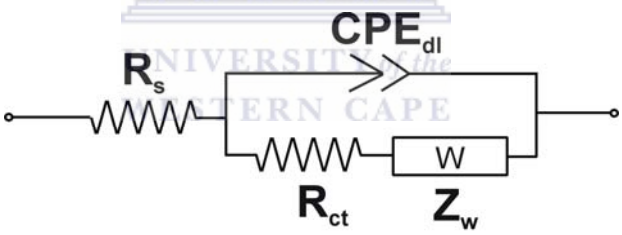

(b)

Figure 6.15 (a) Nyquist plot of bare GCE and GCE/G1PPI in $Fe(CN)_6^{3-/4-}$ redox probe (b) Equivalent circuit used for fitting all EIS data in the presence of $Fe(CN)_6^{3-/4-}$ redox probe

The choice and explanation of this circuit model has been discussed in Chapter 5. Fig. 6.16a to d show the experimental and fitted data obtained from bare GCE and GCE/G1PPI in $Fe(CN)_6^{3-/4-}$, while Fig.6.16 e and f show the Z-HIT check of the impedance results obtained from both GCE and GCE/G1PPI. The quality of this

circuit model is obvious and the Z-HIT check confirms the credibility of the impedance data.

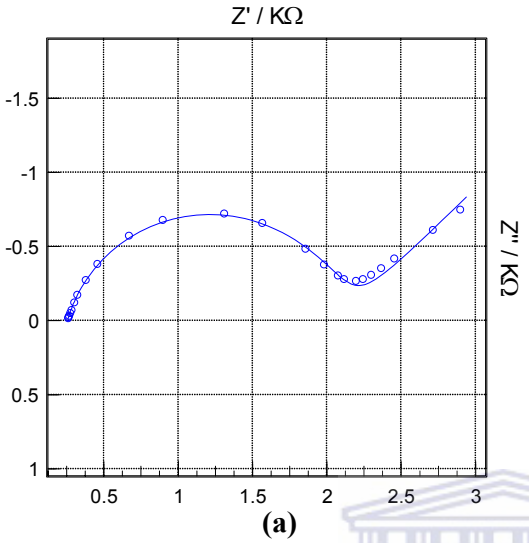

(a)

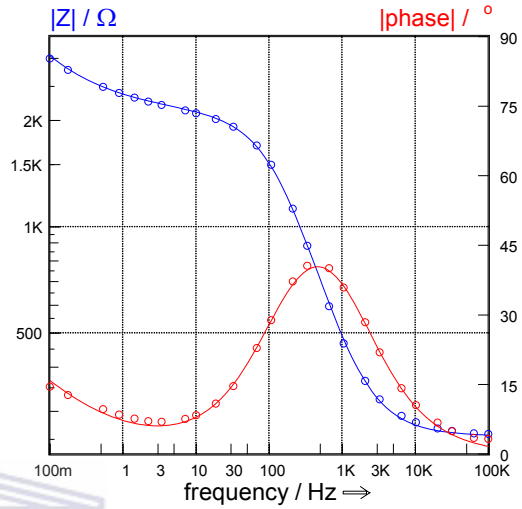

(b)

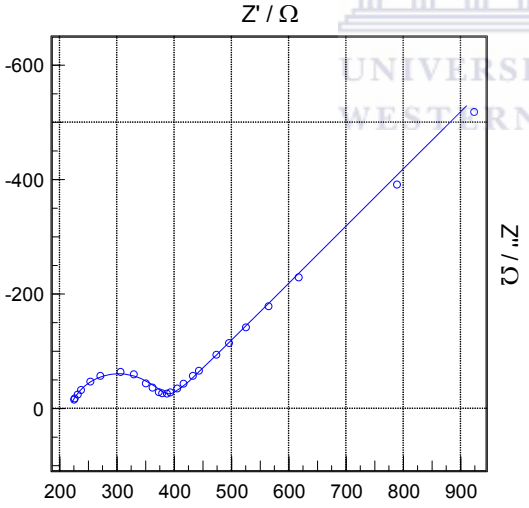

(c)

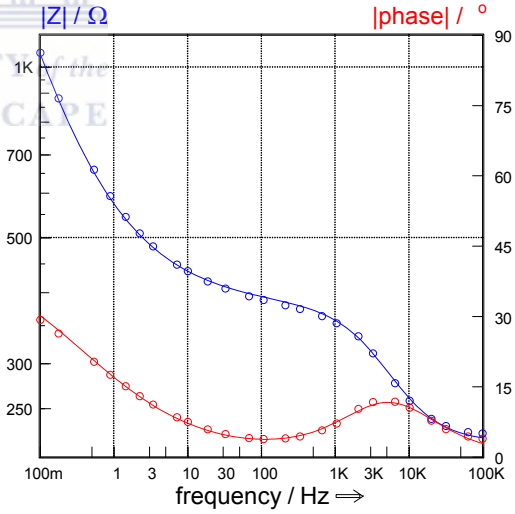

(d)

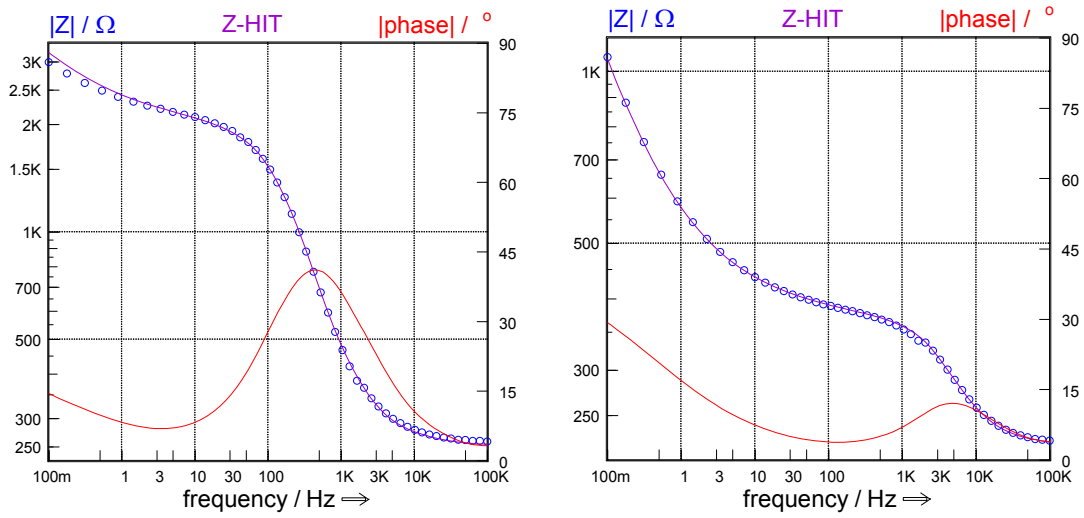

(d) **(e)**

Figure 6.16 EIS in $Fe(CN)_6^{3-/4-}$ (a) Nyquist overlay of experimental (circles) and fitted (line) data of GCE. (b) Bode overlay of experimental (circles) and fitted (line) of GCE. (c) Nyquist overlay of experimental (circles) and fitted (line) data of GCE/G1PPI. (d) Bode overlay of experimental (circles) and fitted (line) of GCE/G1PPI. (e) Z-HIT check for GCE. (f) Z-HIT check for GCE/G1PPI.

Table 6.2 EIS fitting values from Fig. 6.16.

Circuit element	GCE	GCE/G1PPI
Rs (Ω)	254.8	217
R_{ct} (Ω)	1865	165.4
CPE (nF)	460.7	335.3
Zw (kΩ/$s^{1/2}$)	928.1	593.3
Phase shift $\lvert\varphi\rvert$	40.36	11.6

Surface coverage, θ of the G1PPI can be estimated from the above figure using

$$\theta = 1 - \frac{R_{ct}^{Dend}}{R_{ct}^{Bare}} \qquad \textbf{eqn. 6.8}$$

It should be noted that the G1 PPI is cationic while $Fe(CN)_6^{3-/4-}$ is anionic, hence attraction rather than repulsion exists between them. This is the reason why the surface coverage formula is inverted. Using the R_{ct} values from Table 6.2, $\theta =$ 0.91 i.e. percentage coverage is 91%. The may be improved upon if scan rate of deposition is changed.

The frequency at maximum imaginary impedance of the semicircle, can be used to obtain useful kinetic parameters such as time constant (cycle life) τ, exchange current i_0, and heterogeneous rate constant k_{et} [225]. All these kinetic parameters express the speed at which the $Fe^{2+} \Leftrightarrow Fe^{3+} + e -$ electron transfer occurs. These values were calculated as shown:

$$\omega_{\max} = \frac{1}{R_{ct}C_{dl}} \qquad \textbf{eqn. 6.7}$$

$$\tau = R_{ct}C_{dl} \qquad \textbf{eqn. 6.8}$$

$$R_{ct} = \frac{RT}{nFi_0} \qquad \textbf{eqn. 6.9}$$

$$i_o = nFAK_{et}C \qquad \textbf{eqn. 6.10}$$

The values of these kinetic parameters are presented in Table 6.3, where $\omega_{\max} = 2\pi f$, C_{dl} is double layer capacitance; τ = time constant; C is bulk concentration of $Fe(CN)_6^{3-/4-}$ = 5 x 10^{-6} mole/cm^3. The frequency values were taken from Fig. 6.15

Table 6.3 Effect of G1 PPI platform on the kinetics of $Fe(CN)_6^{3-/4-}$

Kinetic parameters	GCE	GCE/G1PPI
ω_{max} **(rad/s)**	741.42	21551.33
τ **(s/rad)**	1.35×10^{-3}	4.64×10^{-5}
i_0 **(A)**	1.38×10^{-5}	1.55×10^{-4}
k_{et}	4.02×10^{-4}	4.52×10^{-3}

The cycle life of the redox reaction of $Fe(CN)_6^{3-/4-}$ at the dendrimer interface is over an order of magnitude faster than on bare GCE/solution interface. A similar trend is observed for exchange current and heterogeneous rate constant at the two interfaces. The Bode plots also show remarkable differences in the electrochemistry of GCE/ $Fe(CN)_6^{3-/4-}$ and GCE/G1PPI/ $Fe(CN)_6^{3-/4-}$ interfaces with maximum phase angle shift of 41° (f = 419.5 Hz) to 12° (f = 5.156 kHz) respectively. Equation 6.11, is a measure of R_{ct} and C_{dl} if $\omega_{\phi max}$ is known. As seen in my case, R_{ct} decrease after electrodeposition i.e. GCE/G1PPI, can be observed as increase in $\omega_{\phi max}$.

$$\omega_{\phi max} = \frac{(1 + R_{ct}/R_{sol})}{R_{ct}C_{dl}} \qquad \textbf{eqn. 6.11}$$

It can thus be deduced that the G1 PPI platform catalysed the redox reaction of $Fe(CN)_6^{3-/4-}$.

6.6 Immobilisation of probe ssDNA

The probe ssDNA was immobilised on the GCE/G1PPI platform via physical and electrostatic adsorption. The cationic and anionic nature of PPI and DNA respectively created the electrostatic attraction. Dendrimer has been shown

to encapsulate or bind effectively with DNA or gene in the biomedical field of gene and drug delivery. This ability to encapsulate DNA was exploited in the immobilisation step coupled with the electrostatic force of attraction. Fig. 6.17 shows a marked reduction in square wave faradaic peak (GCE/G1PPIssDNA) after immobilisation. A small peak in the same potential region, can however still be observed for GCE/G1PPIssDNA. This peak reduction resulted from the poor conductivity of ssDNA. Which deter the flow of charged into the PPI matrix. The reduced current is an indicator of immobilisation.

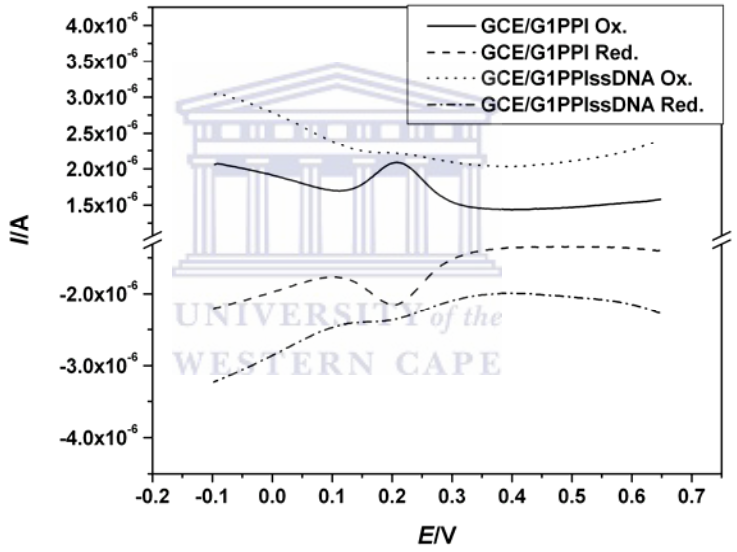

Figure 6.17 Square wave voltammogram showing the effect of probe immobilisation.

The Nyquist plot in Fig. 6.18a shows the behaviour of the immobilised ssDNA probe in the presence $Fe(CN)_6^{3-/4-}$ redox probe. Charge transfer resistance R_{ct} increased because of the repulsion between the anionic ssDNA and anionic $Fe(CN)_6^{3-/4-}$ which hinders the flow of charge or ion onto the platform [82, 98, 100, 245, 256]. The presence of ssDNA obviously slows down the electron

kinetics of the $Fe(CN)_6^{3-/4-}$. The data obtained after immobilisation was again verified using Z-HIT (Fig. 18b) and a good correlation was observed.

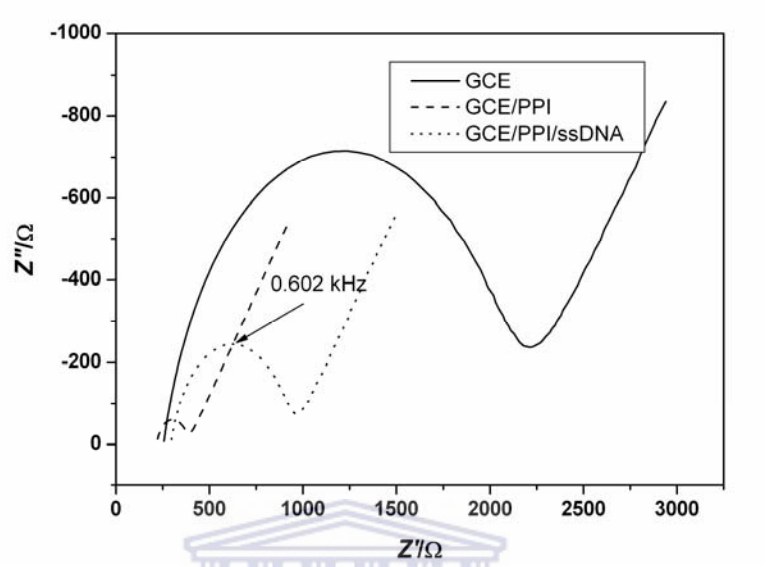

(a)

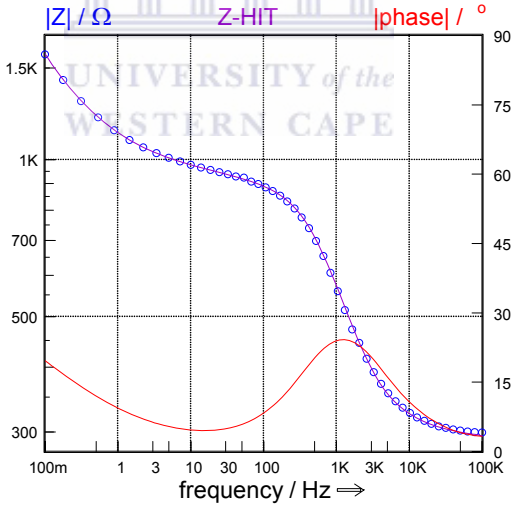

(b)

Figure 6.18 EIS of the immobilised ssDNA probe in $Fe(CN)_6^{3-/4-}$ (a) the Nyquist plot. (b) The Z-HIT check

The impedance parameters in Fig. 6.18a were fitted using the equivalent circuit in Fig. 6.15b and presented in Table 6.4. Upon immobilisation with 2 µM probe

DNA, charge transfer resistance increased by about 290% and the biosensor was stable for over a period of two months when stored at 4 °C. Those stored with the surface moist and tightly covered at room temperature were also stable for this period.

Table 6.4 Fitting results from Fig. 6.18a

Circuit element	GCE	GCE/G1PPI	GCE/G1PPI/ssDNA
Rs (Ω)	254.8	217	293.5
R_{ct} (Ω)	1865	165.4	643
CPE (nF)	460.7	335.3	354.6
Zw (kΩ/$s^{1/2}$)	928.1	593.3	617.9
Phase shift $\lvert\varphi\rvert$	40.36	11.6	24.3

6.7 Hybridisation

Electrochemical impedance spectroscopy was used to monitor the hybridisation with R_{ct} as the analytical parameter. All the impedance measurements passed the Z-HIT test. Fitting of the experimental data was done using the equivalent circuit in Fig. 6.15b and the average error for R_{ct} was less than 2% in all cases.

6.7.1 Blank Hybridisation

The Nyquist plot of the response of the nanobiosensor (GCE/G1PPI/ssDNA) in PBS is presented in Fig. 6.19 and its corresponding fitting values in Table 6.5. The R_{ct} increase observed from blank measurement is termed noise. The first hybridisation gave the highest noise of 49.7 Ω, while

subsequence blank hybridisations were much lower. Nevertheless, noise due to the first blank hybridisation was used in calculating the standard deviation. For 3 samples an average of 28.46 Ω and standard deviation of 16.29 Ω was calculated.

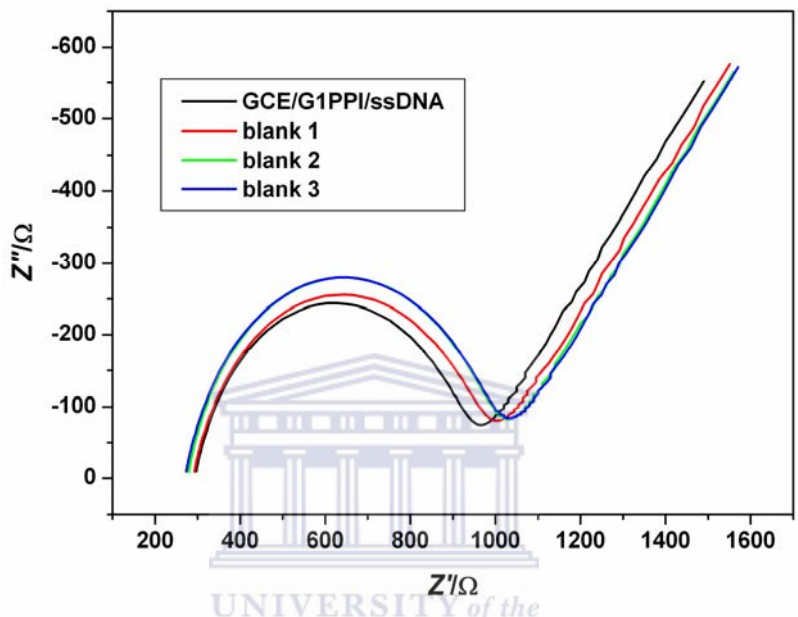

Figure 6.19 Nyquist plot in $Fe(CN)_6^{3-/4-}$ of the response of GCE/G1PPI/ssDNA to blank hybridisation solution of PBS.

Table 6.5 Fitting results of obtained from Fig. 6.19.

Circuit element	Probe	Blank 1	Blank 2	Blank 3
Rs (Ω)	293.5	280.8	276.6	270.6
R_{ct} (Ω)	643	692.7	718.3	728.3
CPE (nF)	354.6	376.5	383.6	367.1
Zw ($\Omega/s^{1/2}$)	617.9	631.9	632.9	640.2

6.7.2 Single stranded DNA target Hybridisation

Charge transfer resistance increased with increase in the concentration of the target ssDNA (Fig. 6.20a). This is due to the increase in the density of the anionic charge of the DNA at the DNA/$Fe(CN)_6^{3-/4-}$ redox probe interface. The more the dsDNA formed as a result of hybridisation, the more the density of the anionic phosphate backbone. This increases the barrier for interfacial electron transfer of the anionic reporter (i.e. the $Fe(CN)_6^{3-/4-}$ redox probe) onto the electrode surface [82, 155, 245]. To obtain a calibration curve (Fig. 6.20b), the R_{ct} was normalised by subtracting 28 Ω (the average obtained from the blank) from each hybridisation value. Using the equivalent circuit in Fig. 6.15b, the fitted values obtained are presented in Table 6.6. A linear range of 0.01 to 10 nM was obtained. The detection limit was calculated using

$$3\sigma/slope \qquad \textbf{eqn. 6.12}$$

The slope (also called sensitivity) was obtained from the linear range while σ is the standard deviation of the noise.

$3\sigma = 3 \times 16.29 = 48.87\,\Omega$ and $slope = 7.4 \times 10^{10}\,\Omega M^{-1}$. Therefore

Detection limit = $3\sigma/slope = 6.6 \times 10^{-10}\,M$

This value falls within the average of the lowest limit reported for impedimetric biosensor.

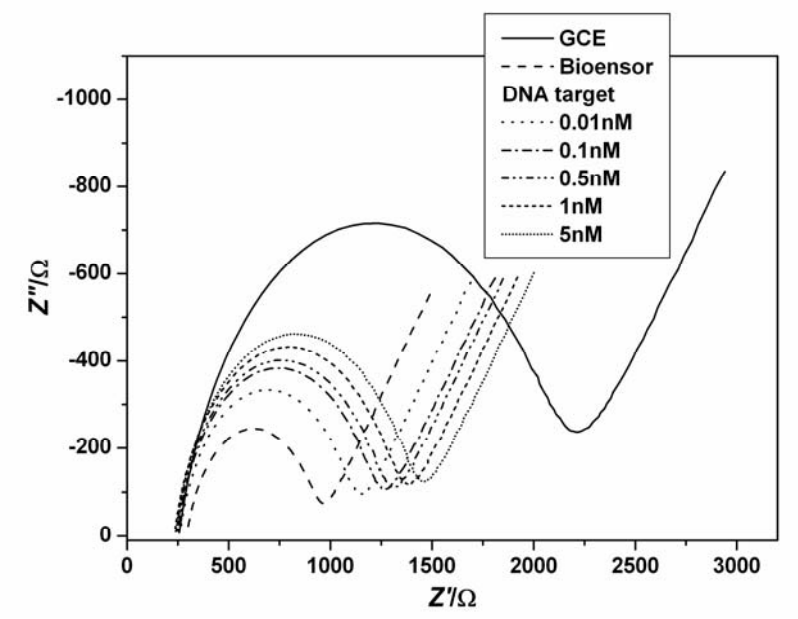

(a)

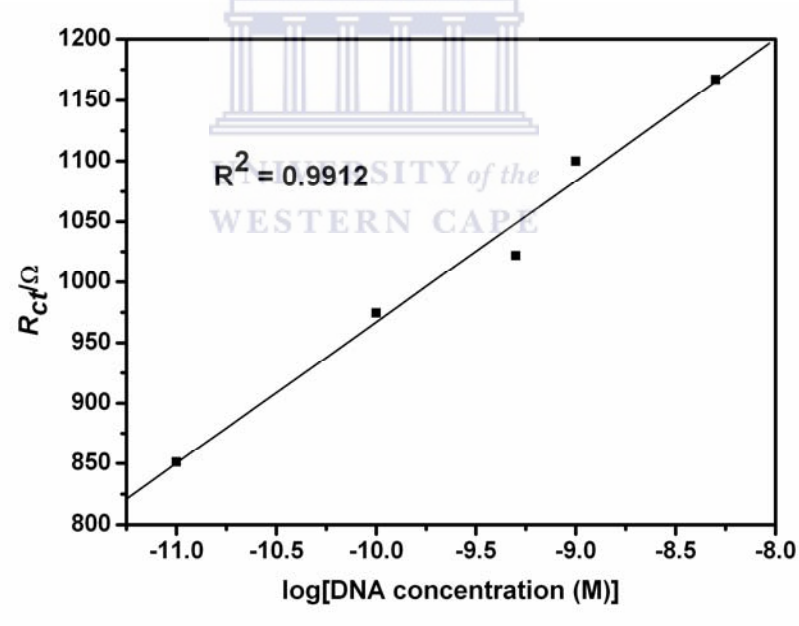

(b)

Figure 6.20 (a) Hybridisation response of the GCE/G1PPI/ssDNA (Biosensor) to target DNA. (b) Linear plot of normalised R_{ct} versus log of target ssDNA concentration

Table 6.6 Fitting results obtained from Fig. 6.20a

Target DNA conc. (nM)	0.01	0.1	0.5	1	5
R_{ct} (Ω)	851.1	974.4	1022	1100	1167
Error % (Rct)	1.27	1.4	1.21	1.52	1.63
R_s (Ω)	258.9	246.4	240.4	232.3	237.7
CPE (nF)	385.5	387.8	391.5	395.8	400.8
Z_w	647.2	658.8	657.5	660.3	670.6

6.7.3 Denaturation of the hybridised nanobiosensor

The EIS result of the denaturation experiments using 6 M urea is presented in Fig. 6.21. The values of R_{ct} obtained after fitting is presented in Table 6.7. Ideally, the R_{ct} should return to a value very close to that of the biosensor (GCE/G1PPI/ssDNA). Because denaturation is just a process of unwinding the double stranded DNA that was formed during the biorecognition event. At high pH, the hydrogen bond between the target ssDNA and probe ssDNA (the dsDNA) is broken leaving the anchored probe ssDNA on the electrode surface. The 5 nM complementary ssDNA hybridised electrode (Hyb 5 nM curve in Fig. 6.21) was immersed in the urea solution with gentle stirring for 10 minutes after impedance measurement and a charge transfer resistance value of 719 Ω (Denature 1 curve) was obtained. The denaturation step was repeated again for 15 min and a value of 665.6 Ω (Denature 2) was recorded. The biosensor was re-hybridised again (Rehyb 5 nM curve) but repeated attempts to denature was not successful (Denature 3). Denaturing on fresh electrodes was done numerous times with inconsistent results. This indicates that the nanobiosensor may be more suitable for single use.

The failure to regenerate the nanobiosensor, from the author's perspective, is not really a disadvantage if the electrochemical DNA biosensor is seen from the view point of commercialisation and the end user. Firstly, a cheap material such as screen printed carbon electrode which can be disposed after use is envisaged and thus regeneration is not necessary if saving cost is the challenge. Secondly, regeneration opens door to the contamination of the biosensor. Thirdly, regeneration takes the user back to time consuming experimental routine, which defeats the purpose of the biosensor. Attempts to regenerate DNA biosensor is more of academic than commercial practicability.

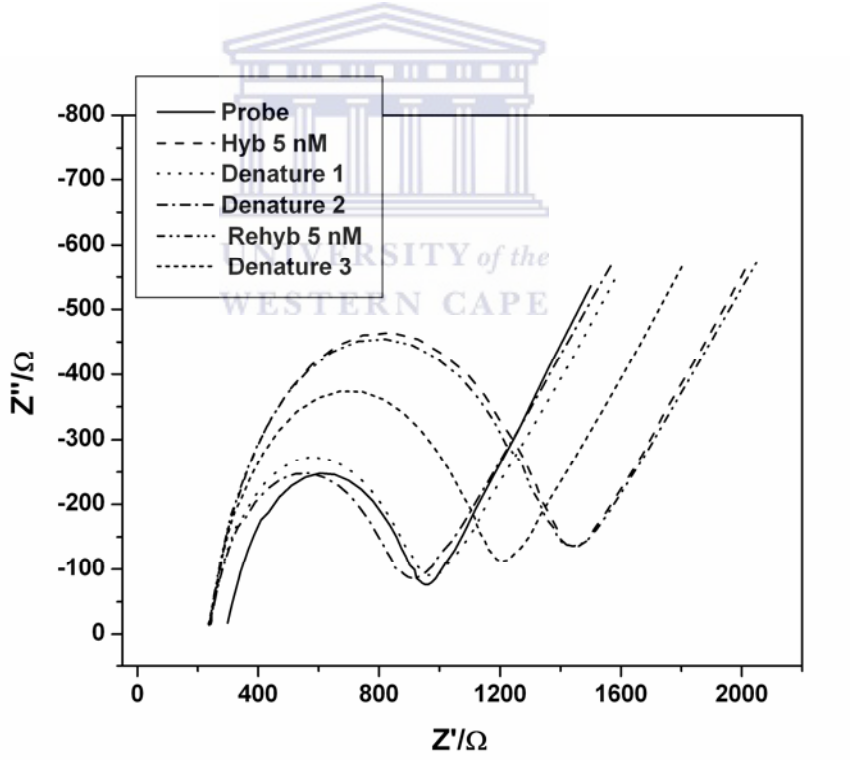

Figure 6.21 Nyquist plot of response of the hybridised biosensor to denaturation

Table 6.7 Charge transfer resistance values obtained from fitting Fig. 6.21

Circuit element	Probe	Hyb 5 nM	Denature 1	Denature 2	Rehyb 5 nM	Denature 3
R_{ct} (Ω)	643	1167	719	665.6	1170	946

6.7.4 Selectivity of the nanobiosensor

The nanobiosensor's responses to 0.5 nM non complementary, three base mismatch and fully complementary target ssDNA are presented in Fig. 6.22. Percentage increase in charge transfer resistance was calculated using

$$\frac{R_{ct}^{HYB} - R_{ct}^{PROBE}}{R_{ct}^{PROBE}} \times 100 \qquad \textbf{eqn. 6.13}$$

R_{ct}^{PROBE} is the charge transfer response of the probe before hybridisation and R_{ct}^{HYB} after hybridisation. The biosensor showed good selectivity.

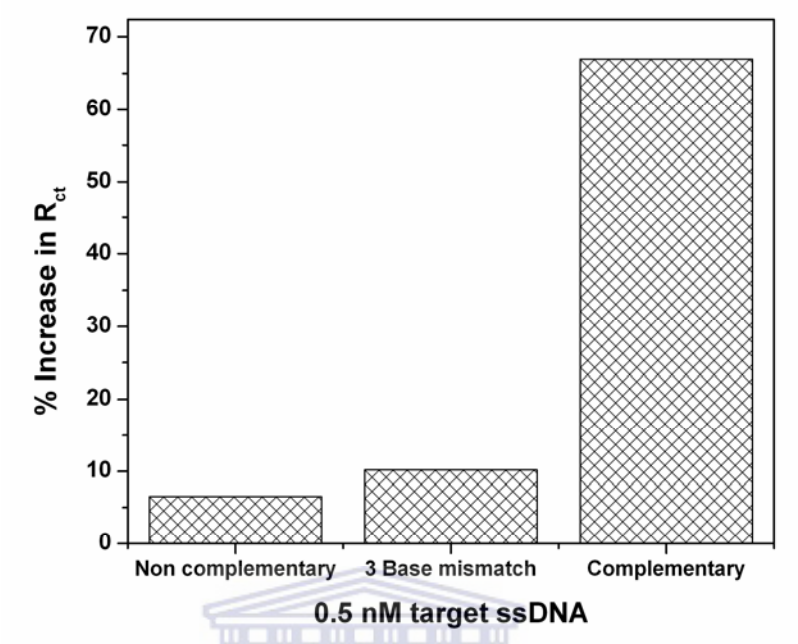

Figure 6.22 A chart showing comparing the response of GCE/G1PPI/ssDNA nanobiosensor to different 21mer DNA targets sequence

6.8 Sub conclusion

A novel simple method of electrodepositing poly(propylene imine) dendrimer on glassy carbon electrode was again established using generation 1 to 3. A size of ca 50 nm observed for the G1 PPI shows that a nanocomposite platform was prepared. G1 PPI exhibited reversible electrochemistry both in solution and when used as platform on GCE in PBS solution and was catalytic towards the electrochemistry of $Fe(CN)_6^{3-/4-}$. Prior to this study, redox properties of pristine poly(propylene imine) dendrimer have not been reported Rather, PPI which have been functionalised with redox molecules such as pyridines [241] and ferrocynyl [260] are those reported as electroacive. PPI has only been studied at liquid-liquid interface [261] and in fact was refereed to as non redox active. The

dendrimer platform was suitable for probe DNA immobilisation and the developed biosensor gave a good detection limit as compared to other reported values based on impedance detection [111, 157]. The PPI based nanobiosensor also able to discriminate non complementary and base mis matches target DNA.

CHAPTER 7

CONCLUSIONS AND RECOMMENDATIONS

7.1 Summary of Findings

The novel salicylaldimine nickel (II) metallodendrimer, generation 4 poly(propylene imine) – gold nanocomposite and pristine G1 poly(propylene imine) dendrimer showed reversible electrochemistry in phosphate buffer solutions at pH of 7.4. These nanomaterials demonstrated catalytic properties towards Fe^{2+} / Fe^{3+} electrochemistry. Electrodeposition of generation one to four PPI dendrimers and PPI-gold nanocomposite was achieved with nano scale sizes. The nano platforms acted as suitable immobilisation layer and their electrochemical impedance behaviours were modelled. A good stability and detection limit in the 10^{-10} M region was obtained in the detection of DNA target. The discrimination towards non complementary DNA was also achieved using the PPI platform.

7.2 Conclusions and Summary of Contributions

As a direct check on my thesis statement, this work has shown that poly(propylene imine) dendrimeric nanomaterials or nanocomposite possess suitable electrochemical properties that make them applicable in the development of an electrochemical DNA nanobiosensor.

Novel electrochemical DNA nanobiosensors based on dendrimeric poly(propylene imine) were successfully developed. The electrochemical DNA biosensor development followed a simple method of drop coating or

electrodeposition, immobilisation and label free hybridisation. The simplicity of this design is seen by the absence of complicated surface modifications or immobilisation chemistries and hybridisation labels. The detection limits obtained were in the range of 10^{-10} M. Though lower detection limits up to 10^{-12} M have been reported, the limits obtained in this work fall within the lower limit in electrochemical DNA biosensor especially for those based on impedance DNA biosensor [111, 157]. Owing to the discrepancies in the results of denaturation, the DNA biosensor is only suitable for single use (disposable), which is a preferable protocol for DNA biosensors. The application of the developed biosensor to real sample is not reported in this thesis. However, the suitability of the design using randomly selected oligonucleotide sequences was proved. Based on this success, quantitative and qualitative application is feasible using a definite ssDNA probe depending on the analyte of interest. The low detection limit achieved may not necessitate the use of PCR for gene amplification.

This work has shown that poly(propylene imine) dendrimers can be used to modify glassy carbon electrode by electrodeposition. The method produced very stable monolayer that was very difficult to remove from the electrode surface. The electrodeposition of PPI dendrimers and co-electrodeposition with gold nanoparticles on glassy carbon electrode is novel and has not been reported to the best of my knowledge elsewhere. The method is very simple and reproducible and hence lends itself to mass production because current and potential are controllable variables.

The electrochemical studies of the poly(propylene imine) dendrimeric materials carried out in phosphate buffer and $Fe(CN)_6^{3-/4-}$ indicated that they are

electroactive nanomaterials. Prior to this electroactive discovery, no redox properties of pristine PPI have been reported. Also, the electrochemical response after immobilisation and hybridisation showed that PPI aided charge transport from the buffer through DNA molecules effectively to the transducer surface. This charge transport phenomenon adds to the repertoire of knowledge on the charge transport ability of DNA molecule in compatibility with nanomaterials.

Some electrochemical data generated such as diffusion coefficient of PPI in solution, Warburg coefficient, redox potentials etc can serve as reference for further dendrimer studies.

7.3 Future Work and Recommendations

1. My thesis opens up an entirely new view of the electrochemistry of poly(propylene imine) dendrimer. Though I used PPI from different renowned chemical manufacturers, to erase suspicion and ensured the reproducibility of my results, future works to further establish the electrochemistry of these dendrimers will be worthwhile
2. Surface studies such as X -ray photoelectron spectroscopy should be investigated so as to have better clue to the surface chemistry of the electrodeposited dendrimer.
3. The electrodeposition variables can be manipulated or optimised to vary the size of the nanomaterials on the platform
4. One of my ultimate objectives is to develop a simple method that can be applied on site, produced on large scale and commercialised. While this may seem distant, the following are of immediate necessity:

- Further optimisation of this method and its application to real sample
- Miniaturisation of the novel electrodeposition method on screen printed electrode and micro array electrodes as a pilot for field use and mass production.
- Immobilisation of a definite ssDNA probe related to a disease strain, pathogen or pollutant and application of the biosensor to samples containing the suspected targets. This can be either qualitative, semi quantitative or quantitative.

5. Dendrimers have been shown to be very compatible with biomolecules. Since this dendrimer modified nanoplatform method worked for DNA, which is not an intrinsically redox molecule, application for other molecules such as enzymes and biochemical analytes such as H_2O_2 may even yield better performance.

References

1. Clark, L.C.; Lions, C. Electrode system for continuous monitoring in cardiovascular surgery. *Annals of the New York Academy of Sciences* **1962,** *102*, 29-45.
2. Drummond, T.G.; Hill, M.G.; Barton, J.K. Electrochemical DNA sensors. *Nature Biotechnology* **2003,** *21*, 1192-1199.
3. Research and markets. *www.researchandmarkets.com* **21, May 2008**.
4. Market Research. *http://www.marketresearch.com/product/display.asp?productid=974421&g=1* **21. May 2008**.
5. Luong, J.H.T.; Male, K.B.; Glennon, J.D. Biosensor technology: Technology push versus market pull. *Biotechnology Advances* **2008,** *26*, 492-500.
6. Somerset, V.S.; Klink, M.J.; Baker, P.G.L.; Iwuoha, E.I. Acetylcholinesterase-polyaniline biosensor investigation of organophosphate pesticides in selected organic solvents *Journal of Environmental and Health Part B* **2007,** *42*, 297-304
7. Smith, R.G.; D'Souza, N.; Nicklin, S. A review of biosensors and biologically-inspired systems for explosives detection. *Analyst* **2008,** *133*, 571 - 584.
8. Luckarift, H.R.; Greenwald, R.; Bergin, M.H.; Spain, J.C.; Johnson, G.R. Biosensor system for continuous monitoring of organophosphate aerosols. *Biosensors and Bioelectronics* **2007,** *23*, 400-406.
9. LaGier, M.J.; Fell, J.W.; Goodwin, K.D. Electrochemical detection of harmful algae and other microbial contaminants in coastal waters using hand-held biosensors. *Marine Pollution Bulletin* **2007,** *54*, 757-770.
10. Teles, F.R.R.; Fonseca, L.P. Trends in DNA biosensors. *Talanta* **2008,** *77*, 606-623.
11. Mikkelsen, S.R. Electrochemical Biosensors for DNA Sequence Detection. *Electroanalysis* **1996,** *8*, 15-19.

12. Xu, Z.; Chen, X.; Dong, S. Electrochemical biosensors based on advanced bioimmobilization matrices. *Trends in Analytical Chemistry* **2006,** *25*, 899-908.

13. Brett, A.M.O.; Paquim, A.M.C.; Diculescu, V.; Oretskaya, T.S. Synthetic oligonucleotides: AFM characterisation and electroanalytical studies. *Bioelectrochemistry* **2005,** *67*, 181-190.

14. Boas, U.; Heegaard, P.M.H. Dendrimers in drug research. *Chemical Society Review* **2004,** *33*, 43-63.

15. Dufes, C.; Uchegbu, I.F.; Schatzlein, A.G. Dendrimers in gene delivery. *Advanced Drug Delivery Reviews* **2005,** *57*, 2177-2202.

16. Majoros, I.J.; Williams, C.R.; Baker Jr, J.R. Current dendrimer applications in cancer diagnosis and therapy. *Current Topics in Medicinal Chemistry* **2008,** *8*, 1165-1179.

17. Gao, Y.; Gao, G.; He, Y.; Liu, T.; Qi, R. Recent advances of dendrimers in delivery of genes and drugs. *Mini-Reviews in Medicinal Chemistry* **2008,** *8*, 889-900.

18. Santhakumaran, L.M.; Thomas, T.; Thomas, T.J. Enhanced cellular uptake of a triplex-forming oligonucleotide by nanoparticle formation in the presence of polypropylenimine dendrimers. *Nucleic Acids Research* **2004,** *32*, 2102-2112.

19. Mulchandani, A.; Bassi, A.S. Principles and applications of biosensors for bioprocess monitoring and control. *Critical Reviews in Biotechnology* **1995,** *15* 105-124.

20. Updike, S.J.; Hicks, G.P. The enzyme electrode, a miniature chemical transducer using immobilised enzyme activity. *Nature* **1967,** *214*, 986-988.

21. D'Orazio, P. Biosensors in clinical chemistry. *Clinica Chimica Acta* **2003,** *334*, 41-69.

22. Updike, S.J.; Shultz, M.; Ekman, B. Implanting the glucose electrode: problem, progress, and alternative solutions. *Diabetes Care* **1982,** *5*, 207-212.

23. Iwuoha, E.I.; Smyth, M.R. Reactivities of organic phase biosensors: 6. Square-wave and differential pulse studies of genetically engineered

cytochrome $P450_{cam}$ (CYP101) bioelectrodes in selected solvents. *Biosensors and Bioelectronics* **2003,** *18*, 237-244.

24. Iwuoha, E.; Ngece, R.; Klink, M.; Baker, P. Amperometric responses of CYP2D6 drug metabolism nanobiosensor for sertraline: a selective serotonin reuptake inhibitor. *IET Nanobiotechnology* **2007,** *1*, 62 - 67.
25. Zejli, H.; Cisneros, J.L.H.H.d.; Rodriguez, I.N.; Liu, B.; Temsamani, K.R.; Marty, J.L. Phenol biosensor based on Sonogel-Carbon transducer with tyrosinase alumina sol–gel immobilization. *Analytica Chimica Acta* **2008,** *612*, 198-203.
26. Gore, M.R.; Szalai, V.A.; Ropp, P.; Yang, I.V.; Silverman, J.S.; Thorp, H.H. Detection of Attomole Quantitites of DNA Targets on Gold Microelectrodes by Electrocatalytic Nucleobase Oxidation *Analytical Chemistry* **2003,** *75*, 6586-6592.
27. Owino, J.H.O.; Ignaszak, A.; Ahmed, A.A.; Baker, P.G.L.; Alemu, H.; Ngila, J.C.; Iwuoha, E.I. Modelling of the impedimetric responses of an aflatoxin B1 immunosensor prepared on an electrosynthetic polyaniline platform. *Analytical and Bioanalytical Chemistry* **2007,** *388*, 1069.
28. Lucarelli, F.; Tombelli, S.; Minunni, M.; Marrazza, G.; Mascini, M. Electrochemical and piezoelectric DNA biosensors for hybridisation detection. *Analytica Chimica Acta* **2008,** *609*, 139-159.
29. Bontidean, I.; Mortari, A.; Leth, S.; Brown, N.L.; Karlson, U.; Larsen, M.M.; Vangronsveld, J.; Corbisier, P.; Csöregi, E. Biosensors for detection of mercury in contaminated soils. *Environmental Pollution* **2004,** *131*, 255-262.
30. Nakamura, H.; Karube, I. Current research activity in biosensors. *Analytical and Bioanalytical Chemistry* **2003,** *377*, 446-468.
31. Carrascosa, L.G.; Moreno, M.; Álvarez, M.; Lechuga, L.M. Nanomechanical biosensors: a new sensing tool. *TrAC Trends in Analytical Chemistry* **2006,** *25*, 196-206.
32. McKendry, R.; Zhang, J.; Arntz, Y.; Strunz, T.; Hegner, M.; Lang, H.P.; Baller, M.K.; Certa, U.; Meyer, E.; Guntherodt, H.-J.; Gerber, C. Multiple label-free biodetection and quantitative DNA-binding assays on a

nanomechanical cantilever array. *Proceedings of the National Academy of Sciences USA* **2002,** *99*, 9783-9788.

33. Raiteri, R.; Grattarola, M.; Butt, H.-J.; Skládal, P. Micromechanical cantilever-based biosensors. *Sensors and Actuators B: Chemical* **2001,** *79*, 115-126.
34. Fuji-Keizai USA Inc. Biosensor Market, R&D and Commercial Implication. *http://www.researchandmarkets.com/reportinfo.asp?cat_id=0&report_id=63374&q=biosensor&p=,* **05. Nov. 2008**.
35. Alocilja, E.C.; Radke, S.M. Market analysis of biosensors for food safety. *Biosensors and Bioelectronics* **2003,** *18*, 841-846.
36. Lin, C.T.; Wang, S.M. Biosensor commercialization strategy - A theoretical approach. *Frontiers in Bioscience* **2005,** *10*, 99-106.
37. Patel, P.D. Overview of affinity biosensors in food analysis. *Journal of AOAC International* **2006,** *89*, 805-818.
38. Newman, J.D.; Setford, S.J. Enzymatic biosensors. *Molecular Biotechnology* **2006,** *32*, 249-268.
39. Long, E. *Fundamentals of Nucleic Acids in Bioorganic Chemistry: Nucleic Acids*; Oxford University Press: NewYork, 1996.
40. Watson, J.D.; Crick, F.H.C. Molecular Structure of Nucleic Acids. *Nature* **1953,** *171*, 737-738.
41. Watson, J.D.; Crick, F.H.C. Genetical implications of the structure of deoxyribonucleic acid. *Nature* **1953,** *171*, 964-967.
42. Genetics Home Reference. What is DNA? *http://ghr.nlm.nih.gov/handbook/basics/dna,* **15. Nov. 2008**.
43. Curran, T. Forensic DNA analysis: Technology and Application. In *http://www.parl.gc.ca/information/library/PRBpubs/bp443-e.htm*; Library of Parliament Research Publications, 1997.
44. Southern, E.M. Detection of specific sequences among DNA fragments separated by gel electrophoresis. *Journal of Molecular Biology* **1975,** *98*, 503-517.

45. Alwine, J.C.; Kemp, D.J.; Stark, G.R. Method for detection of specific RNAs in agarose gels by transfer to diazobenzyloxymethyl-paper and hybridization with DNA probes. *Proceedings of the National Academy of Sciences USA* **1977,** *74*, 5350-5354.

46. Borresen, A.L.; Hovig, E.; Brogger, A. Detection of base mutations in genomic DNA using denaturing gradient gel electrophoresis (DGGE) followed by transfer and hybridization with gene-specific probes *Mutation Research* **1988,** *202*, 77-83.

47. Schena, M.; Shalon, D.; Davis, R.W.; Brown, P.O. Quantitative monitoring of gene expression patterns with a complementary DNA microarray. *Science* **1995,** *270*, 467-470.

48. Feynman, R.P. "There's Plenty of Room at the Bottom". *Engineering and Science* **1960,** *23*, 22-36.

49. Balzani, V.; Credi, A.; Venturi, M. Molecular devices and machines. *nanotoday* **2007,** *2*, 18-25.

50. LaBean, T.H.; Li, H. Constructing novel materials with DNA. *nanotoday* **2007,** *2*, 26-35.

51. Joachim, C.; Gimzewski, J.K.; Aviram, A. Electronics using hybrid-molecular and mono- molecular devices. *Nature* **2000,** *408*, 541-548.

52. Wada, Y.; Tsukada, M.; Fujihira, M.; Matsushige, K.; Ogawa, T.; Haga, M.; Tanaka, S. Prospects and problems of single molecule information devices. *Japanese Journal of Applied Physics* **2000,** *39*, 3835-3849.

53. Seeman, N.C. DNA in a material world. *Nature* **2003,** *421*, 427-431.

54. Sekiguchi, H.; Komiya, K.; Kiga, D.; Yamamura, M. A design and feasibility study of reactions comprising DNA molecular machine that walks autonomously by using a restriction enzyme. *Natural Computing* **2008,** *7*, 303-315.

55. Beissenhirtz, M.K.; Elnathan, R.; Weizmann, Y.; Willner, I. The aggregation of Au nanoparticles by an autonomous DNA machine detects viruses. *Small* **2007,** *3*, 375-379.

56. Beissenhirtz, M.K.; Willner, I. DNA-based machines. *Organic & Biomolecular Chemistry* **2006,** *4*, 3392-3401.

57. Nishikawa, A.; Yaegashi, S.; Tanaka, F.; Ohtake, K.; Hagiya, M. Multi-fueled approach to DNA nano-robotics. *Natural Computing* **2008,** *7*, 371-383.

58. Tabata, H.; Cai, L.T.; Gu, J.H.; Tanaka, S.; Otsuka, Y.; Sacho, Y.; Taniguchi, M.; Kawai, T. Toward the DNA electronics. *Synthetic Metals* **2003,** *133-134*, 469-472.

59. Kelly, S.O.; Barton, J.K. Electron transfer between bases in double helical DNA *Science* **1999,** *283*, 375-381.

60. Kelley, S.O.; Boon, E.M.; Barton, J.K.; Jackson, N.M.; Hill, M.G. Single-base mismatch detection based on charge transduction through DNA *Nucleic Acids Research* **1999,** *27*, 4830-4837.

61. Boon, E.M.; Pope, M.A.; Williams, S.D.; David, S.S.; Barton, J.K. DNA-mediated charge transport as a probe of MutY/DNA interaction *Biochemistry* **2002,** *41*, 8464-8470.

62. Boon, E.M.; Barton, J.K. Charge transport in DNA. *Current Opinion in Structural Biology* **2002,** *12*, 320-329

63. Flink, H.W.; Schoenenberger, C. Electrical conduction through DNA molecules. *Nature* **1999,** *398*, 407-410.

64. Berlin, Y.A.; Burin, A.L.; Ratner, M.A. Charge Hopping in DNA *Journal of the American Chemical Society* **2001,** *123*, 260-268.

65. Cohen, H.; Nogues, C.; Naaman, R.; Porath, D. Direct measurement of electrical transport through single DNA molecules of complex sequence. *Proceedings of the National Academy of Sciences USA* **2005,** *102*, 11589-11593.

66. Giese, B.; Amaudrut, J.; Köhler, A.K.; Spormann, M.; Wessely, S. Direct observation of hole transfer through DNA by hopping between adenine bases and by tunnelling *Nature* **2001,** *412*, 318-320.

67. Boon, E.M.; Ceres, D.M.; Drummond, T.G.; Hill, M.G.; Barton, J.K. Mutation detection by electro catalysis at DNA-modified electrodes *Nature Biotechnology* **2000,** *18*, 1096-1100.

68. Ikeura-Sekiguchi, H.; Sekiguchi, T. Attosecond Electron Delocalization in the Conduction Band through the Phosphate Backbone of Genomic DNA. *Physical Review Letters* **2007,** *99*, 228102.

69. Kerman, K.; Kobayashi, M.; Tamiya, E. Recent trends in electrochemical DNA biosensor technology. *Measurement Science and Technology* **2004,** *15*, R1-R11.

70. Mascini, M.; Palchetti, I.; Marrazza, G. DNA electrochemical biosensors. *Fresenius' Journal of Analytical Chemistry* **2001,** *369*, 15-12.

71. Millan, K.M.; Mikkelsen, S.R. Sequence-selective biosensor for DNA based on electroactive hybridization indicators. *Analytical Chemistry* **1993,** *65*, 2317-2323.

72. Boal, A.K.; Barton, J.K. Electrochemical Detection of Lesions in DNA *Bioconjugate Chemistry* **2005,** *16*, 312-321.

73. Erdem, A.; Kerman, K.; Meric, B.; Akarca, U.S.; Ozsoz, M. Novel hybridization indicator methylene blue for the electrochemical detection of short DNA sequences related to the hepatitis B virus. *Analytica Chimica Acta* **2000,** *422*, 139-149.

74. Rohs, R.; Skelenar, H.; Lavery, R.; Röder, B. Methylene blue binding to DNA with alternating GC base sequence: A modeling study. *Journal of the American Chemical Society* **2000,** *122*, 2860-2866.

75. Sakata, T.; Miyahara, Y. Detection of DNA recognition events using multi-well field effect devices. *Biosensors and Bioelectronics* **2005,** *21*, 827-832.

76. Kobayashi, M.; Mizukami, T.; Morita, Y.; Murakami, Y.; Yokoyama, K.; Tamiya, E. Electrochemical gene detection using microelectrode array on a DNA chip. *Electrochemistry* **2001,** *69*, 1013-1016.

77. Ahmed, M.U.; Idegami, K.; Chikae, M.; Kerman, K.; Chaumpluk, P.; Yamamura, S.; Tamiya, E. Electrochemical DNA biosensor using a disposable electrochemical printed (DEP) chip for the detection of SNPs from unpurified PCR amplicons. *Analyst* **2007,** *132*, 431-438.

78. Zhang, Y.; Kim, H.H.; Heller, A. Enzyme-amplified amperometric detection of 3000 copies of DNA in a 10-uL droplet at 0.5 fM concentration. *Analytical Chemistry* **2003,** *75*, 3267-3269.

79. Zhang, Y.; Pothukuchy, A.; Shin, W.; Kim, Y.; Heller, A. Detection of ~10^3 copies of DNA by an electrochemical enzyme-amplified sandwich assay with ambient O_2 as the substrate. *Analytical Chemistry* **2004,** *76*, 4093-4097.

80. Wong, E.L.S.; Gooding, J.J. Charge Transfer through DNA: A Selective Electrochemical DNA Biosensor. *Analytical Chemistry* **2006,** *78*, 2138-2144.

81. Daniels, J.S.; Pourmand, N. Label-Free Impedance Biosensors: Opportunities and Challenges. *Electroanalysis* **2007,** *19*, 1239 - 1257.

82. Arotiba, O.A.; Ignaszak, A.; Malgas, R.; Al-Ahmed, A.; Baker, P.G.L.; Mapolie, S.F.; Iwuoha, E.I. An electrochemical DNA biosensor developed on novel multinuclear nickel(II) salicylaldimine metallodendrimer platform. *Electrochimica Acta* **2007,** *53*, 1689-1696.

83. Palecek, E.; Fojta, M.; Tomschik, M.; Wang, J. Electrochemical biosensors for DNA hybridization and DNA damage. *Biosensors and Bioelectronics* **1998,** *13*, 621-628.

84. Palecek, E. Oscillographic polarography of highly polymerized deoxyribonucleic acid. *Nature* **1960,** *188*, 656-657.

85. Oliveira-Brett, A.M.; Piedade, J.A.P.; Silva, L.A.; Diculescu, V.C. Voltammetric determination of all DNA nucleotide. *Analytical Biochemistry* **2004,** *332*, 321-329.

86. Pividori, M.I.; Merkoci, A.; Alegret, S. Electrochemical genosensor design: immobilisation of oligonucleotides onto transducer surfaces and detection methods. *Biosensors and Bioelectronics* **2000,** *15*, 291-303.

87. Oliveira, S.C.B.; Corduneanu, O.; Oliveira-Brett, A.M. In situ evaluation of heavy metal-DNA interactions using an electrochemical DNA biosensor. *Bioelectrochemistry* **2008,** *72*, 53-58.

88. Oliveira, S.C.B.; Diculescu, V.C.; Palleschi, G.; Compagnone, D.; Oliveira-Brett, A.M. Electrochemical oxidation of ochratoxin A at a glassy

carbon electrode and in situ evaluation of the interaction with deoxyribonucleic acid using an electrochemical deoxyribonucleic acid-biosensor. *Analytica Chimica Acta* **2007,** *588*, 283-291.

89. Brett, A.M.O.; da Silva, L.A.; Fujii, H.; Mataka, S.; Thiemann, T. Detection of the damage caused to DNA by a thiophene-S-oxide using an electrochemical DNA-biosensor. *Journal of Electroanalytical Chemistry* **2003,** *549*, 91-99.
90. Abreu, F.C.; Goulart, M.O.F.; Oliveira Brett, A.M. Detection of the damage caused to DNA by niclosamide using an electrochemical DNA-biosensor. *Biosensors and Bioelectronics* **2002,** *17*, 913-919.
91. Mascini, M.; Bagni, G.; Di Pietro, M.L.; Ravera, M.; Baracco, S.; Osella, D. Electrochemical biosensor evaluation of the interaction between DNA and metallo-drugs. *BioMetals* **2006,** *19*, 409-418.
92. Lisdat, F.; Schafer, D. The use of electrochemical impedance spectroscopy for biosensing. *Analytical and Bioanalytical Chemistry* **2008,** *391*, 1555-67.
93. Li, D.; Zou, X.; Shen, Q.; Dong, S. Kinetic study of DNA/DNA hybridization with electrochemical impedance spectroscopy. *Electrochemistry Communications* **2007,** *9*, 191-196.
94. Kang, J.; Li, X.; Wu, G.; Wang, Z.; Lu, X. A new scheme of hybridization based on the Aunano–DNA modiWed glassy carbon electrode. *Analytical Biochemistry* **2007,** *364*, 165-170.
95. Ma, H.; Zhang, L.; Pan, Y.; Zhang, K.; Zhang, Y. A Novel Electrochemical DNA Biosensor Fabricated with Layer-by-Layer Covalent Attachment of Multiwalled Carbon Nanotubes and Gold Nanoparticles. *Electroanalysis* **2008,** *20*, 1220 -1226.
96. Bonanni, A.; Esplandiu, M.J.; Pividori, M.I.; Alegret, S.; Valle, M. Impedimetric genosensors for the detection of DNA hybridization. *Analytical Bioanalytical Chemistry* **2006,** *385*, 1195-1201.
97. Bonanni, A.; Pividori, M.I.; del Valle, M. Application of the avidin-biotin interaction to immobilize DNA in the development of electrochemical

impedance genosensors. *Analytical and Bioanalytical Chemistry* **2007,** *389*, 851-61.

98. Bonanni, A.; Esplandiu, M.J.; del Valle, M. Signal amplification for impedimetric genosensing using gold-streptavidin nanoparticles *Electrochimica Acta* **2008** *53* 4022-4029.
99. Peng, H.; Soeller, C.; Travas-Sejdic, J. Novel Conducting Polymers for DNA Sensing. *Macromolecules* **2007,** *40*, 909-914.
100. Kafka, J.; Pänke, O.; Abendroth, B.; Lisdat, F. A label-free DNA sensor based on impedance spectroscopy. *Electrochimica Acta* **2008,** *53*, 7467-7474.
101. Keighley, S.D.; Estrela, P.; Li, P.; Migliorato, P. Optimization of label-free DNA detection with electrochemical impedance spectroscopy using PNA probes. *Biosensors and Bioelectronics* **2008,** *23*, 1291-1297.
102. Bart, M.; Stigter, E.C.A.; Stapert, H.R.; de Jong, G.J.; van Bennekom, W.P. On the response of a label-free interferon-γ immunosensor utilizing electrochemical impedance spectroscopy. *Biosensors and Bioelectronics* **2005,** *21*, 49-59.
103. Ma, K.-S.; Zhou, H.; Zoval, J.; Madou, M. DNA hybridization detection by label free versus impedance amplifying label with impedance spectroscopy. *Sensors and Actuators B: Chemical* **2006,** *114*, 58-64.
104. Weng, J.; Zhang, J.; Li, H.; Sun, L.; Lin, C.; Zhang, Q. Label-free DNA sensor by boron-doped diamond electrode using an ac impedimetric approach. *Analytical Chemistry* **2008,** *80*, 7075-83.
105. Hong, J.; Yoon, D.S.; Park, M.-I.; Choi, J.; Kim, T.S.; Im, G.; Kim, S.; Pak, Y.E.; No, K. A Dielectric Biosensor Using the Capacitance Change with AC Frequency Integrated on Glass Substrates. *Japanese Journal of Applied Physics* **2004,** *43*, 5639-5645.
106. Berney, H.; West, J.; Haefele, E.; Alderman, J.; Lane, W.; Collins, J.K. A DNA diagnostic biosensor: development, characterisation and performance. *Sensors and Actuators B: Chemical* **2000,** *68*, 100-108.
107. Hassen, W.M.; Chaix, C.; Abdelghani, A.; Bessueille, F.; Leonard, D.; Jaffrezic-Renault, N. An impedimetric DNA sensor based on

functionalized magnetic nanoparticles for HIV and HBV detection. *Sensors and Actuators B: Chemical* **2008,** *134*, 755-760.

108. Rechnitz, G.A.; Kobos, R.K.; Riechel, S.J.; Gebauer, C.R. A bio-selective membrane electrode prepared with living bacterial cells. *Analytica Chimica Acta* **1977,** *94*, 357-365.
109. Owino, J.H.O.; Arotiba, O.A.; Hendricks, N.; Songa, E.A.; Jahed, N.; Waryo, T.T.; Ngece, R.F.; Baker, P.G.L.; Iwuoha, E.I. Electrochemical Immunosensor Based on Polythionine/Gold Nanoparticles for the Determination of Aflatoxin B1. *Sensors* **2008,** *8*, In Press, Accepted Manuscript.
110. Cloarec, J.P.; Chevolot, Y.; Laurenceau, E.; Phaner-Goutorbe, M.; Souteyrand, E. A multidisciplinary approach for molecular diagnostics based on biosensors and microarrays. *ITBM-RBM* **2008,** *29*, 105-127.
111. Sassolas, A.; Bouvier, B.D.L.; Blum, L.J. DNA Biosensors and Microarrays. *Chemical Reviews* **2008,** *108*, 109-139.
112. Zhang, W.; Yang, T.; Huang, D.; Jiao, K.; Li, G. Synergistic effects of nano-ZnO/multi-walled carbon nanotubes/chitosan nanocomposite membrane for the sensitive detection of sequence-specific of PAT gene and PCR amplification of NOS gene. *Journal of Membrane Science* **2008,** *325*, 245-251.
113. Lo, P.-H.; Kumar, S.A.; Chen, S.-M. Amperometric determination of H_2O_2 at nano-TiO_2/DNA/thionin nanocomposite modified electrode. *Colloids and Surfaces, B: Biointerfaces* **2008,** *66*, 266-273.
114. Ghanbari, K.; Bathaie, S.Z.; Mousavi, M.F. Electrochemically fabricated polypyrrole nanofiber-modified electrode as a new electrochemical DNA biosensor. *Biosensors and Bioelectronics* **2008,** *23*, 1825-1831.
115. Teles, F.R.R.; Fonseca, L.P. Applications of polymers for biomolecule immobilization in electrochemical biosensors. *Materials Science and Engineering: C* **2008,** *28*, 1530-1543.
116. Songa, E.A.; Somerset, V.S.; Waryo, T.; Baker, P.G.L.; Iwuoha, E.I. Amperometric nanobiosensor for quantitative determination of glyphosate

and glufosinate residues in corn samples. *Pure and Applied Chemistry* **2009,** *81*, 39-55.

117. Díaz-González, M.; de la Escosura-Muñiz, A.; González-García, M.B.; Costa-García, A. DNA hybridization biosensors using polylysine modified SPCEs. *Biosensors and Bioelectronics* **2008,** *23*, 1340-1346.
118. Tencaliec, A.M.; Laschi, S.; Magearu, V.; Mascini, M. A comparison study between a disposable electrochemical DNA biosensor and a Vibrio fischeri-based luminescent sensor for the detection of toxicants in water samples. *Talanta* **2006,** *69* 365-369.
119. Oliveira-Brett, A.M.; Silva, L.A.d. A DNA-electrochemical biosensor for screening environmental damage caused by s-triazine derivatives. *Analytical and Bioanalytical Chemistry* **2002,** *373*, 717-723.
120. Wang, J.; Jiang, M.; Fortes, A.; Mukherjee, B. New label-free DNA recognition based on doping nucleic-acid probes within conducting polymer films. *Analytica Chimica Acta* **1999,** *402*, 7-12.
121. Xu, Y.; Jiang, Y.; Cai, H.; He, P.G.; Fang, Y.Z. Electrochemical impedance detection of DNA hybridization based on the formation of M-DNA on polypyrrole/carbon nanotube modified electrode. *Analytica Chimica Acta* **2004,** *516*, 19-27.
122. Riccardi, C.d.S.; Yamanaka, H.; Josowicz, M.; Kowalik, J.; Mizaikoff, B.; Kranz, C. Label-Free DNA Detection Based on Modified Conducting Polypyrrole Films at Microelectrodes. *Analytical Chemistry* **2006,** *78*, 1139-1145.
123. Thompson, L.A.; Kowalik, J.; Josowicz, M.; Janata, J. Label-Free DNA Hybridization Probe Based on a Conducting Polymer. *Journal of the American Chemical Society* **2003,** *125*, 324-325.
124. Cowan, J.A. Role of metal ions in promoting DNA binding and cleavage by restriction endonucleases. *Nucleic Acids and Molecular Biology* **2004,** *14*, 339-360.
125. Wang, J.; Fernandes, J.R.; Kubota, L.T. Polishable and Renewable DNA Hybridization Biosensors. *Analytical Chemistry* **1998,** *70*, 3699-3702.

126. Akinyeye, R.O.; Michira, I.; Sekota, M.; Al Ahmed, A.; Tito, D.; Baker, P.G.L.; Brett, C.M.A.; Kalaji, M.; Iwuoha, E. Electrochemical synthesis and characterization of 1,2-naphthaquinone-4-sulfonic acid doped polypyrrole. *Electroanalysis* **2007,** *19*, 303-309.

127. Ye, Y.; Ju, H. DNA Electrochemical Behaviors, Recognition and Sensing by Combining with PCR Technique. *Sensors* **2003,** *3*, 128-145.

128. Cooper, M.A. Label-free screening of bio-molecular interactions. *Analytical and Bioanalytical Chemistry* **2003,** *377*, 834-842.

129. Lucarelli, F.; Marrazza, G.; Turner, A.P.F.; Mascini, M. Carbon and gold electrodes as electrochemical transducers for DNA hybridisation sensors. *Biosensors and Bioelectronics* **2004,** *19*, 513-530.

130. Arora, K.; Prabhakar, N.; Chand, S.; Malhotra, B.D. Ultrasensitive DNA hybridization biosensor based on polyaniline. *Biosensors and Bioelectronics* **2007,** *23*, 613-620.

131. Nakajima, N.; Ikada, Y. Mechanism of amide formation by carbodiimide for bioconjugation in aqueous media. *Bioconjugate Chemistry* **1995,** *6*, 123-130.

132. Teh, H.F.; Gong, H.; Dong, X.D.; Zeng, X.; Tan, A.L.K.; Yang, X.; Tan, S.N. Electrochemical biosensing of DNA with capture probe covalently immobilized onto glassy carbon surface. *Analytica Chimica Acta* **2005,** *551*, 23-29.

133. Steel, A.B.; Herne, T.M.; Tarlov, M.J. Electrochemical Quantitation of DNA Immobilized on Gold. *Analytical Chemistry* **1988,** *70*, 4670-4677.

134. Herne, T.M.; Tarlov, M.J. *Journal of the American Chemical Society* **1997,** *119*, 8916-8920.

135. Park, S.; Brown, K.A.; Hamad-Schifferli, K. Changes in Oligonucleotide Conformation on Nanoparticle Surfaces by Modification with Mercaptohexanol. *Nano Letters* **2004,** *4* 1925-1929.

136. Li, F.; Chen, W.; Zhang, S. Development of DNA electrochemical biosensor based on covalent immobilization of probe DNA by direct coupling of sol–gel and self-assembly technologies. *Biosensors and Bioelectronics* **2008,** *24*, 787-792.

137. Erdem, A. Nanomaterial-based electrochemical DNA sensing strategies. *Talanta* **2007,** *74*, 318-325.

138. Wang, J. Nanoparticle-based electrochemical DNA detection *Analytica Chimica Acta* **2003,** *500*, 247-257.

139. Iijima, S. Helical microtubules of graphite carbon. *Nature* **1991,** *354*, 56-58.

140. Arya, S.K.; Datta, M.; Malhotra, B.D. Recent advances in cholesterol biosensor. *Biosensors and Bioelectronics* **2008,** *23*, 1083-1100.

141. Agui, L.; Yanez-Sedeno, P.; Pingarron, J.M. Role of carbon nanotubes in electroanalytical chemistryA review. *Analytica Chimica Acta* **2008,** *622*, 11-47.

142. Daniel, S.; Rao, T.P.; Rao, K.S.; Rani, S.U.; Naidu, G.R.K.; Lee, H.-Y.; Kawai, T.; 672. A review of DNA functionalized/grafted carbon nanotubes and their characterization. *Sensors and Actuators B: Chemical* **2007,** *122* 672-682.

143. Wang, J. Nanoparticle-based electrochemical DNA detection *Perspectives in Bioanalysis* **2005,** *1*, 369-384.

144. Rosi, N.L.; Mirkin, C.A. Nanostructures in Biodiagnostics *Chemical Reviews* **2005,** *105*, 1547-1562.

145. DiScipio, R.G. Preparation of colloidal gold particles of various sizes using sodium borohydride and sodium cyanoborohydride. *Analytical Biochemistry* **1996,** *236*, 168-170

146. Esumi, K.; Matsumoto, T.; Seto, Y.; Yoshimura, T. Preparation of gold-, gold/silver-dendrimer nanocomposites in the presence of benzoin in ethanol by UV irradiation. *Journal of Colloid and Interface Science* **2005,** *284*, 199-203.

147. Esumi, K.; Suzuki, A.; Aihara, N.; Usui, K.; Torigoe, K. Preparation of Gold Colloids with UV Irradiation Using Dendrimers as Stabilizer. *Langmuir* **1998,** *14*, 3157-3159.

148. Feng, Y.; Yang, T.; Zhang, W.; Jiang, C.; Jiao, K. Enhanced sensitivity for deoxyribonucleic acid electrochemical impedance sensor: Gold

nanoparticle/polyaniline nanotube membranes. *Analytica Chimica Acta* **2008,** *616*, 144-151.

149. Zhang, L.; Jiang, X.; Wang, E.; Dong, S. Attachment of gold nanoparticles to glassy carbon electrode and its application for the direct electrochemistry and electrocatalytic behavior of hemoglobin. *Biosensors & Bioelectronics* **2005,** *21*, 337-345.
150. Daniels, M.C.; Astruc, D. Gold Nanoparticles: Assembly, Supramolecular Chemistry, Quantum-Size-Related Properties, and Applications toward Biology, Catalysis, and Nanotechnology *Chemical Reviews* **2004,** *104*, 293-346.
151. Guo, S.; Wang, E. Synthesis and electrochemical applications of gold nanoparticles. *Analytica Chimica Acta* **2007,** *598*, 181-192.
152. Willner, I.; Baron, R.; Willner, B. Integrated nanoparticle–biomolecule systems for biosensing and bioelectronics. *Biosensors and Bioelectronics* **2007,** *22*, 1841-1852.
153. Liu, S.; Leech, D.; Ju, H. Application of Colloidal Gold in Protein Immobilization, Electron Transfer, and Biosensing. *Analytical Letters* **2003,** *36*, 1-19.
154. Shulga, O.; Kirchhoff, J.R. An acetylcholinesterase enzyme electrode stabilized by an electrodeposited gold nanoparticle layer. *Electrochemistry Communications* **2007,** *9*, 935-940.
155. Katz, E.; Willner, I. Probing Biomolecular Interactions at Conductive and Semiconductive Surfaces by Impedance Spectroscopy: Routes to Impedimetric Immunosensors, DNA-Sensors, and Enzyme Biosensors. *Electroanalysis* **2003,** *15*, 913-947.
156. Lucarelli, F.; Marrazza, G.; Mascini, M. Enzyme-based impedimetric detection of PCR products using oligonucleotide-modified screen-printed gold electrodes *Biosensors and Bioelectronics* **2005,** *20*, 2001-2009.
157. Pingarrón, J.M.; Yáñez-Sedeño, P.; González-Cortés, A. Gold nanoparticle-based electrochemical biosensors. *Electrochimica Acta* **2008,** *53*, 5848-5866.

158. Zhao, J.; Zhu, X.; Li, T.; Li, G. Self-assembled multilayer of gold nanoparticles for amplified electrochemical detection of cytochrome c. *Analyst* **2008,** *133*, 1242-1245.

159. Ovádeková, R.; Jantová, S.; Letašiová, S.; Labuda, I.Š.J. Nanostructured electrochemical DNA biosensors for detection of the effect of berberine on DNA from cancer cells *Analytical and Bioanalytical Chemistry* **2006,** *386*, 2055-2062.

160. Li, M.; Huang, S.; Zhu, P.; Kong, L.; Peng, B.; Gao, H. A Novel DNA Biosensor Based on ssDNA/Cyt c/L-Cys/GNPs/Chits/GCE. *Electrochimica Acta In Press, Corrected Proof* DOI:10.1016/j.electacta.2008.10.040.

161. Zhang, Y.; Ma, H.; Zhang, K.; Zhang, S.; Wang, J. An improved DNA biosensor built by layer-by-layer Covalent Attachment of Multi-Walled Carbon Nanotubes, Gold Nanoparticles. *Electrochimica Acta In Press, Corrected Proof* DOI:10.1016/j.electacta.2008.10.052.

162. Liang, C.; Frechet, M.J. Applying key concepts from nature: transition state stabilization, preconcentration and cooperativity effect in dendritic biomimetics. *Prog. Polym. Sci.* **2005,** *30*, 385-402.

163. Boas, U.; Christensen, J.B.; Heegaard, P.M.H. Dendrimers: design, synthesis and chemical properties. *J. Mater. Chem.* **2006,** *16*, 3785-3798.

164. Frontier Scientific inc. "Newkome" Dendrons and Dendrimers. *http://www.frontiersci.com/i/ntreon-dendrimer.htm,* **8. Nov. 2008**.

165. Flory, P.J. Molecular Size Distribution in Three Dimensional Polymers. I. Gelation. *Journal of the American Chemical Society* **1941,** *63*, 3083-3090.

166. Buhleier, E.; Wehner, W.; Vogtle, F. "Cascade"- and "Nonskid-Chain-Like" Syntheses of Molecular Cavity Topologies. *Synthesis* **1978**, 155-158.

167. Newkome, G.R.; Yao, Z.; Baker, G.R.; Gupta, V.K. Cascade Molecules: A New Approach to Micelles. A [27]-Arborol. *The Journal of Organic Chemistry* **1985,** *50*, 2003-2004.

168. Tomalia, D.A.; Baker, H.; Dewald, J.; Hall, M.; Kallos, G.; Martin, S.; Roeck, J.; Ryder, J.; Smith, P. A new class of polymers: starburst dendritic macromolecules. *Polymer Journal (Tokyo, Japan)* **1985,** *17*, 117-32.

169. Hawker, C.J.; Fréchet, J.M.J. Preparation of Polymers with Controlled Molecular Architecture. A New Convergent Approach to Dendritic Macromolecules. *Journal of the American Chemical Society* **1990,** *112*, 7638-7647.

170. de Brabander-van den Berg, E.M.M.; Meijer, E.W. Poly(propylenimine) dendrimers: large-scale synthesis via heterogeneously catalyzed hydrogenation *Angewandte Chemie International Edition English* **1993,** *32*, 1308-1311.

171. Worner, C.; Mulhaupt, R. Polynitrile- and Polyamine-Functional Poly(trimethylene imine) Dendrimers. *Angewandte Chemie International Edition* **1993,** *32*, 1306-1308.

172. Campagna, S.; Denti, G.; Sabatino, L.; Serroni, S.; Ciano, M.; Balzani, V. A New Hetero-tetrametallic Complex of Ruthenium and Osmium: Absorption Spectrum, Luminescence Properties, and Electrochemical Behaviour. *Journal of the Chemical Society, Chemical Communications* **1989**, 1500-1501.

173. Hudson, R.H.E.; Damha, M.J. Nucleic Acid Dendrimers: Novel Biopolymer Structures. *Journal of the American Chemical Society* **1993,** *115*, 2119-2124.

174. Fréchet, J.M. Functional polymers and dendrimers: reactivity, molecular architecture, and interfacial energy. *Science* **1994,** *263*, 1710-1715.

175. Hawker, C.; Frechet, M.J. A new convergent approach to monodisperse dendritic macromolecules. *Chemical Communications* **1990,** *15*, 1010-13.

176. Kojima, C.; Kono, K.; Maruyama, K.; Takagishi, T. Synthesis of Polyamidoamine Dendrimers Having Poly(ethylene glycol) Grafts and Their Ability To Encapsulate Anticancer Drugs. *Bioconjugate Chemistry* **2000,** *11*, 910-917.

177. Krasteva, N.; Guse, B.; Besnard, I.; Yasuda, A.; Vossmeyer, T. Gold nanoparticle/PPI-dendrimer based chemiresistors: Vapor-sensing

properties as a function of the dendrimer size. *Sensors and Actuators B: Chemical* **2003,** *92*, 137-143.

178. Esumi, K.; Hayakawa, K.; Yoshimura, T. Morphological change of gold-dendrimer nanocomposites by laser irradiation. *Journal of Colloid and Interface Science* **2003,** *268*, 501-506.

179. Hwang, S.-H.; Shreiner, C.D.; Moorefield, C.N.; Newkome, G.R. Recent progress and applications for metallodendrimers. *New Journal of Chemistry* **2007,** *31*, 1192-1217.

180. Denti, G.; Serroni, S.; Campagna, S.; Ricevuto, V.; Balzani, V. Directional energy transfer in a luminescent tetranuclear ruthenium(II) polypyridine complex that contains two different types of bridging ligands. *Inorganica Chimica Acta* **1991,** *182*, 127-129.

181. Denti, G.; Campagna, S.; Serroni, S.; Ciano, M.; Balzani, V. Decanuclear homo- and heterometallic polypyridine complexes: syntheses, absorption spectra, luminescence, electrochemical oxidation, and intercomponent energy transfer. *Journal of the American Chemical Society* **1992,** *114*, 2944-2950.

182. Serroni, S.; Denti, G. New procedures for the synthesis of mixed-metal and/or mixed-ligand ruthenium(II) and osmium(II) polypyridine supramolecules and the use of these procedures in the preparation of hexanuclear species. *Inorganic Chemistry* **1992,** *31*, 4251-4255.

183. Newkome, G.R.; Moorefield, C.N.; Baker, G.R.; Johnson, A.L.; Behera, R.K. Chemistry of micelles. 11. Alkane cascade polymers with a micellar topology: micelle acid derivatives. *Angewandte Chemie International Edition* **1991,** *30*, 1176-1178.

184. Newkome, G.R.; Cardullo, F.; Constable, E.C.; Moorefield, C.N.; Thompson, A.M.W.C. Metallomicellanols: incorporation of ruthenium(II)-2,2':6',2"-terpyridine triads into cascade polymers. *Journal of the Chemical Society, Chemical Communications* **1993**, 925-927.

185. Hendricks, N.R.; Waryo, T.T.; Arotiba, O.; Jahed, N.; Baker, P.G.L.; Iwuoha, E.I. Microsomal cytochrome P450-3A4 (CYP3A4) nanobiosensor for the determination of 2,4-dichlorophenol - an endocrine disruptor

compound. *Electrochimica Acta* **2008,** *In Press, Corrected Proof.* DOI:10.1016/j.electacta.2008.09.073

186. Iwuoha, E.I.; Joseph, S.; Zhang, Z.; Smyth, M.R.; Fuhr, U.; Ortiz de Montellano, P.R. Drug metabolism biosensors: electrochemical reactivities of cytochrome P450cam immobilised in synthetic vesicular systems. *Journal of Pharmaceutical and Biomedical Analysis* **1998,** *17*, 1101-1110.
187. Perutz, M.F.; Rossmann, M.G.; Cullis, A.; Muirhead, H.; Will, G.; North, A.C.T. Structure of Hæmoglobin: A Three-Dimensional Fourier Synthesis at 5.5-Å. Resolution, Obtained by X-Ray Analysis. *Nature* **1960,** *185*, 416-422.
188. Bosman, A.W.; Jansse, H.M.; Meijer, E.W. About Dendrimers: Structure, Physical Properties, and Applications. *Chemical Reviews* **1999,** *99*, 1665-1688.
189. Newkome, G.R.; He, E.; Moorefield, C.N. Suprasupermolecules with Novel Properties: Metallodendrimers. *Chemical Reviews* **1999,** *99*, 1689-1746.
190. Al-Jamal, K.T.; Ramaswamy, C.; Florence, A.T. Supramolecular structures from dendrons and dendrimers. *Advanced Drug Delivery Reviews* **2005,** *57*, 2238- 2270.
191. Astruc, D.; Chardac, F. Dendritic Catalysts and Dendrimers in Catalysis. *Chemical Reviews* **2001,** *101*, 2991-3023.
192. Astruc, D.; Blais, J.-C.; Cloutet, E.; Djakovitch, L.; Rigaut, S.; Ruiz, J.; Sartor, V.; Valério1, C. The First Organometallic Dendrimers: Design and Redox Functions *Topics in Current Chemistry* **2000,** *210*, 229-259.
193. He, D. STUDIES OF PPI DENDRIMERS STRUCTURES, PROPERTIES, AND POTENTIAL APPLICATIONS. In *Chemistry*; Marshall University West Virginia, 2002;Vol. MSc, 129.
194. Newkome, G.R.; Shreiner, C.D. Poly(amidoamine), polypropylenimine, and related dendrimers and dendrons possessing different 1 → 2 branching motifs: An overview of the divergent procedures. *Polymer* **2008,** *49*, 1-173.

195. Svenson, S.; Tomalia, D.A. Dendrimers in biomedical applications - reflections on the field. *Advanced Drug Delivery Reviews* **2005,** *57*, 2106-2129.

196. Guillot-Nieckowski, M.; Eisler, S.; Diederich, F. Dendritic vectors for gene transfection. *New Journal of Chemistry* **2007,** *31*, 1111-1127.

197. Thomas, M.; Klibanov, A.M. Non-viral gene therapy: polycation-mediated DNA delivery. *Applied Microbiology and Biotechnology* **2003,** *62*, 27-34.

198. Pearson, S.; Jia, H.; Kandachi, K. China approves first gene therapy. *Nature Biotechnology* **2004,** *22*, 3-4.

199. Cloninger, M.J. Biological applications of dendrimers. *Current Opinion in Chemical Biology* **2002,** *6*, 742-748.

200. Parker, A.L.; Newman, C.; Briggs, S.; Seymour, L.; Sheridan, P.J. Nonviral gene delivery: techniques and implications for molecular medicine. *Expert Reviews in Molecular Medicine* **2003,** *5*, 1-15.

201. Dauty, E.; Behr, J.P.; Remy, J.S. Development of plasmid and oligonucleotide nanometric particles. *Gene Therapy* **2002,** *9*, 743-748.

202. Chen, A.M.; Santhakumaran, L.M.; Nair, S.K.; Amenta, P.S.; Thomas, T.; He, H.; Thomas, T.J. Oligodeoxynucleotide nanostructure formation in the presence of polypropyleneimine dendrimers and their uptake in breast cancer cells. *Nanotechnology* **2006,** *17*, 5449-5460.

203. Dutta, T.; Garg, M.; Jain, N.K. Poly(propyleneimine) dendrimer and dendrosome mediated genetic immunization against hepatitis B. *Vaccine* **2008,** *26*, 3389-3394.

204. Benters, R.; Niemeyer, C.M.; Wohrle, D. Dendrimer-activated solid supports for nucleic acid and protein microarrays. *ChemBioChem* **2001,** *2*, 686-694.

205. Benters, R.; Niemeyer, C.M.; Drutschmann, D.; Blohm, D.; Wohrle, D. DNA microarrays with PAMAM dendritic linker systems. *Nucleic Acids Research* **2002,** *30*, e10.

206. Li, A.; Yang, F.; Ma, Y.; Yang, X. Electrochemical impedance detection of DNA hybridization based on dendrimer modified electrode. *Biosensors and Bioelectronics* **2007,** *22*, 1716-1722.

207. Wei-Jie, S.; Shi-Yun, A.; Jin-Huan, L.; Lu-Sheng, Z. Electrochemical Biosensor Based on Dendrimer Immobilized Deoxyribonucleic Acid. *Chinese Journal of Analytical Chemistry* **2008,** *36*, 335-338.

208. Zhang, H.; Hu, N. Assembly of myoglobin layer-by-layer films with poly(propyleneimine) dendrimer-stabilized gold nanoparticles and its application in electrochemical biosensing. *Biosensors and Bioelectronics* **2007,** *23*, 393-399.

209. Mascini, M. Affinity electrochemical biosensors for pollution control. *Pure and Applied Chemistry* **2001,** *73*, 23-30.

210. Bagni, G.; Osella, D.; Sturchio, E.; Mascini, M. Deoxyribonucleic acid (DNA) biosensors for environmental risk assessment and drug studies. *Analytica Chimica Acta* **2006,** *573-574*, 81-89.

211. Berganza, J.; Olabarria, G.; Garcıa, R.; Verdoy, D.; Rebollo, A.; Arana, S. DNA microdevice for electrochemical detection of Escherichia coli 0157:H7 molecular markers. *Biosensors and Bioelectronics* **2007,** *22*, 2132-2137.

212. Simonsen, M. Expanding clinical role is seen for nucleic diagnostics. *Diagnostic Update* **2000,** *3*, 1-8.

213. Pournaghi-Azar, M.H.; Hejazi, M.S.; Alipour, E. Developing an electrochemical deoxyribonucleic acid (DNA) biosensor on the basis of human interleukine-2 gene using an electroactive label. *Analytica Chimica Acta* **2006,** *570*, 144-150.

214. Pozo, M.V.d.; Alonso, C.; Pariente, F.; Lorenzo, E. DNA Biosensor for Detection of Helicobacter pylori Using Phen-dione as the Electrochemically Active Ligand in Osmium Complexes. *Analytical Chemistry* **2005,** *77*, 2550-2557.

215. GeneOhm Sciences. *Inc. http://www.geneohm.com/,* **01. Nov. 2008**.

216. Patel, P.D. (Bio)sensors for measurement of analytes implicated in food safety: a review. *Trends in Analytical Chemistry* **2002,** *21*, 96-115.

217. Gáspár, C.S.; Leth, S.; Niculescu, M.; Mortari, A.; Bontidean, I.; Soukharev, V.; Dorneanu, S.A.; Ryabov, A.D.; Csöregi, E. Biosensors for

life quality: Design, development and applications. *Sensors and Actuators B: Chemical* **2004,** *102*, 179-194.

218. Viveros, L.; Paliwal, S.; McCrae, D.; Wild, J.; Simonian, A. A fluorescence-based biosensor for the detection of organophosphate pesticides and chemical warfare agents. *Sensors and Actuators B: Chemical* **2006,** *115*, 150-157.
219. BASi. Electrochemical Electrodes. *http://www.bioanalytical.com/products/ec/faqele.php#Carbon,* **05. Nov. 2008**.
220. Kounaves, S.P. Voltammetric Techniques. In *Handbook of Instrumental Techniques for Analytical Chemistry*; Department of Chemistry, Tufts University, 2008.
221. Bard, A.J.; Zoski, C.G. Voltammetry retrospective. *Analytical Chemistry* **2000,** *72*, 346A-352A.
222. Heyrovsky, J.; Shikata, M. Researches with the dropping mercury cathode. II. The polarograph. *Recueil des Travaux Chimiques des Pays-Bas et de la Belgique* **1925,** *44*, 496-498.
223. Kolthoff, I.M.; Laitinen, H.A. Voltammetric determination of oxygen. *Science* **1940,** *92*, 152-154.
224. Bard, A.J.; Faulkner, L.R. *Electrochemical methods: Fundamentals and Application*, 2 Ed.; Wiley: NJ USA, 2001.
225. Monk, P.M.S. *Fundamentals of Electroanalytical Chemistry*; Wiley: England, 2005.
226. Barker, G.C.; Jenkins, I.L. Square-wave polarography. *Analyst* **1952,** *77*, 685-696.
227. Osteryoung, J.; O'Dea, J.J. Square-wave Voltammetry. In *Electroanalytical Chemistry: A Series of Advances*; A.J. Bard, Ed.; Marcel Dekker: New York, 1986;Vol. 14, 209-308.
228. Macdonald, D.D. Reflections on the history of electrochemical impedance spectroscopy. *Electrochimica Acta* **2006,** *51*, 1376-1388.
229. Macdonald, D.D. Review of mechanistic analysis by electrochemical impedance spectroscopy. *Electrochimica Acta* **1990,** *35*, 1509-1525.

230. Pejcic, B.; De Marco, R. Impedance spectroscopy: Over 35 years of electrochemical sensor optimization. *Electrochimica Acta* **2006,** *51*, 6217-6229.

231. Kramers, H.A. *Phys. Zeit* **1929,** *30*

232. Kronig, R.d.L. The theory of dispersion of x-rays. *Journal of the Optical Society of America* **1926,** *12* 547-557.

233. Bode, H.W. *Network Analysis and Feedback Amplifier Design*; Van Nostrand: New York, 1945.

234. Urquidi-Macdonald, M.; Real, S.; Macdonald, D.D. Applications of Kramers-Kronig transforms in the analysis of electrochemical impedance data. III. Stability and linearity. *Electrochimica Acta* **1990,** *35*, 1559-1566.

235. Lasia, A. Electrochemical Impedance Spectroscopy and Its Applications. In *Modern Aspects of Electrochemistry*; B.E. Conway, J. Bockris, R.E. White, Eds.; Kluwer Academic/Plenum: New York, 1999;Vol. 32, 143-248.

236. Ehm, W.; Kaus, R.; Schiller, C.A.; Strunz, W. New Trends in Electrochemical Impedance Spectroscopy and Electrochemical Noise Analysis. F. Mansfeld, F. Huet, O.R. Mattos, Eds.; Electrochemical Society Inc: Pennington NJ, 2001;Vol. 2000-24, 1.

237. Macdonald, J.R. *Impedance Spectroscopy Emphasizing Solid Materials and Systems*; Wiley: New York, 1987.

238. Malgas, R.; Mapolie, S.F.; Ojwach, S.O.; Smith, G.S.; Darkwa, J. The application of novel dendritic nickel catalysts in the oligomerization of ethylene. *Catalysis Communications* **2008,** *9*, 1612-1617.

239. Iwuoha, E.I.; Saenz-de-Villaverde, D.; Garcia, N.P.; Smyth, M.R.; Pingarron, J.M. Reactivities of organic phase biosensors. 2. The amperometric behavior of horseradish peroxidase immobilized on a platinum electrode modified with an electrosynthetic polyaniline film. *Biosensors and Bioelectronics* **1997,** *12*, 749-761.

240. Mathebe, N.G.R.; Morrin, A.; Iwuoha, E.I. Electrochemistry and scanning electron microscopy of polyaniline/peroxidase-based biosensor *Talanta* **2004,** *64*, 115-120.

241. Abruna, D.H. Redox and photoactive dendrimers in solution and on surfaces. *Analytical Chemistry* **2004,** *76*, 310A-319A.

242. Housecroft, C.E.; Sharpe, A.G. *Inorganic Chemistry, 2nd ed.*; Pearson Education Limited England, 2005.

243. Gu, H.; Su, X.d.; Loh, K.P. Electrochemical Impedance Sensing of DNA Hybridization on Conducting Polymer Film-Modified Diamond. *Journal of Physical Chemistry B* **2005,** *109*, 13611-13618.

244. Yang, W.; Butler, J.E.; Russell, J.N.; Hamers, J.R. Interfacial Electrical Properties of DNA-Modified Diamond Thin Films: Intrinsic Response and Hybridization-Induced Field Effects. *Langmuir* **2004,** *20*, 6778-6787.

245. Arotiba, O.; Owino, J.; Songa, E.; Hendricks, N.; Waryo, T.; Jahed, N.; Baker, P.; Iwuoha, E. An Electrochemical DNA Biosensor Developed on a Nanocomposite Platform of Gold and Poly(propyleneimine) Dendrimer. *Sensors* **2008,** *8*, 6791-6809.

246. Barbier, B.; Pinson, J.; Desarmot, G.; Sanchez, M. Electrochemical bonding of amines to carbon fiber surfaces toward improved carbon-epoxy composites *Journal of the Electrochemical Society* **1990,** *137*, 1757-1764.

247. Deinhammer, R.S.; Ho, M.; Anderegg, J.W.; Porter, M.D. Electrochemical Oxidation of Amine-Containing Compounds: A Route to the Surface Modification of Glassy Carbon Electrodes. *Langmuir* **1994,** *10*, 1306-1313.

248. Downard, A.J. Electrochemically assisted covalent modification of carbon electrodes. *Electroanalysis* **2000,** *12*, 1085-1096

249. Speiser, B. Linear Sweep and Cyclic Voltammetry. In *Encyclopedia of Electrochemistry*; A.J. Bard, M. Stratman, P.R. Unwin, Eds.; WILEY-VCH Verlag GmgH & Co. KGaA: Weinheim, 2003;Vol. 3, Ch 2.

250. Kabanov, V.A.; Zezin, A.B.; Rogacheva, V.B.; Gulyaeva, Z.G.; Zansochova, M.F.; Joosten, J.G.H.; Brackman, J. Polyelectrolyte Behavior

of Astramol Poly(propyleneimine) Dendrimers *Macromolecules* **1998,** *31*, 5142-5144.

251. van-Duijvenbode, R.C.; Borkovec, M.; Koper, G.J.M. Acid-base properties of poly(propylene imine)dendrimers. *Polymer* **1998,** *39*, 2657-2664.
252. Ferreira, V.; Tenreiro, A.; Abrantes, L.M. Electrochemical, microgravimetric and AFM studies of polythionine films Application as new support for the immobilisation of nucleotides. *Sensors and Actuators B: Chemical* **2006,** *119*, 632-641.
253. Koper, G.J.M.; vanGenderen, M.H.P.; Elissen-Roman, C.; Baars, M.W.P.L.; Meijer, E.W.; Borkovec, M. Protonation Mechanism of Poly(propylene imine) Dendrimers and Some Associated Oligo Amines *Journal of the American Chemical Society* **1997,** *119*, 6512-6521.
254. Cheng, W.; Dong, S.; Wang, E. Gold Nanoparticles as Fine Tuners of Electrochemical Properties of the Electrode/Solution Interface. *Langmuir* **2002,** *18*, 9947-9952.
255. Tasdelen, M.A.; Demirel, A.L.; Yagci, Y. Poly(propylene imine) dendrimers as hydrogen donor in Type II photoinitiated free radical polymerization. *European Polymer Journal* **2007,** *43*, 4423-4430.
256. Liu, J.; Tian, S.; Nielsen, P.E.; Knoll, W. In situ hybridization of PNA/DNA studied label-free by electrochemical impedance spectroscopy. *Chemical Communications* **2005**, 2969 - 2971.
257. Kabanov, V.A.; Sergeyev, V.G.; Pyshkina, O.A.; Zinchenko, A.A.; Zezin, A.B.; Joosten, J.G.H.; Brackman, J.; Yoshikawa, K. Interpolyelectrolyte Complexes Formed by DNA and Astramol Poly(propylene imine) Dendrimers. *Macromolecules* **2000,** *33*, 9587-9593.
258. Li, M.; Deng, C.; Xie, Q.; Yang, Y.; Yao, S. Electrochemical quartz crystal impedance study on immobilization of glucose oxidase in a polymer grown from dopamine oxidation at an Au electrode for glucose sensing. *Electrochimica Acta* **2006,** *51*, 5478-5486.

259. Cakara, D.; Borkovec, M. Microscopic protonation mechanism of branched polyamines: poly(amidoamine) versus poly(propyleneimine) dendrimers. *Croatica Chemica Acta* **2007,** *80*, 421-428.

260. Nijhuis, C.A.; Boukamp, B.A.; Ravoo, B.J.; Huskens, J.; Reinhoudt, D.N. Electrochemistry of ferrocenyl dendrimer - β -cyclodextrin assemblies at the interface of an aqueous solution and a molecular printboard. *Journal of Physical Chemistry C* **2007,** *111*, 9799-9810.

261. Berduque, A.; Scanlon, M.D.; Collins, C.J.; Arrigan, D.W.M. Electrochemistry of Non-Redox-Active Poly(propylenimine) and Poly(amidoamine) Dendrimers at Liquid-Liquid Interfaces. *Langmuir* **2007,** *23*, 7356-7364.